Investigation into Human Erythrocyte Peroxiredoxin 2: S-Nitrosation and interaction with Haemoglobin

Submitted by

Robert James Kalibala

Of the University of Exeter Medical School as a thesis for the degree of Master of Philosophy in Medical Science

December, 2017

I certify that all material in this thesis which is not my own work has been identified and that no material has been previously submitted and approved for award of a degree by this or any other university.

Signature: **RJKalibala** Date:20-11-2019

Abstract

The most abundant intracellular protein in erythrocytes is haemoglobin (Hb) and the third most abundant protein is peroxiredoxin 2 (Prx2). Prx2 exists in both dimeric and decameric form; its dimeric form has two cysteines (Cys) redox active sites. The presence of the two redox-active Cys sites means that Prx2 possesses free thiols, which can react with reactive nitrogen species to form S-nitrosothiols. The function of Prx2 is not completely understood, although it is thought to be an antioxidant by virtue of its peroxidase activity. Prx2 may play a central role in protecting Hb against oxidative damage and mediating some of the key functions of Hb. Nitric oxide (NO) exerts numerous important physiological functions in biological systems including vasodilation in humans. Because of the short-lived nature of NO, S-nitrosothiols (RSNOs) are believed to act as stable NO carriers.

This study hypothesises a model highlighting possible interactions between NO and Hb, and the HbNO complex and Prx2. In this model, NO is produced upon nitrite reduction by deoxyHb, NO equivalents are transferred to the Cys residues of Prx2 forming S-nitrosoperoxiredoxin (Prx2-SNO). The proximity of Prx2 to Hb promotes S-nitrosothiol formation in Prx2 and avoids the scavenging of NO by Hb itself.

This study also describes the purification of the native hPrx2, and the over-expression and purification of hPrx2 in various forms, as well as the subsequent crystallisation and X-ray diffraction studies. The calibrated gel filtration column confirmed that hPrx2 is mainly produced in the decameric form. Purification of native hPrx2 isolated from human red blood cells (RBCs) was successfully achieved using FFQ Sepharose and gel filtration chromatography (Superdex 200). The recombinant hPrx2 DNA cloned in pET28q was transformed into a competent *E.coli* Rosetta Gami 2 cell line. The purified recombinant hPrx2 protein was achieved using nickel affinity and gel filtration column chromatography. S-nitrosated Prx2 (Prx2-SNO) was achieved by incubation of Prx2 with S-nitrosoglutathione (GSNO) under differing experimental conditions. The mixing of hPrx2 and Hb in various molar ratios, demonstrated a significant specific protein-protein interaction between a Prx2 decamer with an Hb tetramer. The complex binding results

from size exclusion chromatography showed that decameric Prx2 bound to Hb in a 1:1 ratio.

This study also describes the post-modification of hPrx2 cysteine residues, and the nitration of tyrosine residues attained by the incubation of protein with GSNO. The incubation of the recombinant hPrx2 protein with GSNO altered the oligomeric state of hPrx2 into a dimer formation. The gas-phase chemiluminescence, gel filtration chromatography, Saville assay, Western-blot, UV-vis spectrophotometry and LC-MS/MS, confirmed the post-modifications of the protein residues.

This research reports the purification and characterization of the stable; native hPrx2, recombinant hPrx2, hPrx2-SNO, and SNO-Hb proteins necessary to perform the hypothesised interactions, to allow us to understand the transnitrosation process that could occur between hPrx2 and Hb. The study also describes the crystallisation conditions for hPrx2-Hb complex and the co-crystallisation conditions for hPrx2-SNO and [hPrx2-SNO]Hb complex.

Acknowledgements

I would like to thank my supervisory team; Professor Paul Winyard, Professor Jenny Littlechild, Dr Misha Isupov for the continue support towards this achievement. I am so grateful for your collaboration throughout this project and opportunities offered to me to learn different techniques. I also like to thank Professor Lorna Harries for your mentoring, guidance and encouragement you gave me when I needed you most, thank you ever so much. I am also grateful to Dr Kate Heesorn in the department of Biochemistry at Bristol University, for your help with MS work in this project.

I would like to thank body from in the lab past and present especially Miranda Smallwood, Annie Knight, Latizia, Kata and Paul James who were always available for scientific discussion and other help when needed.

I would like to thank my family and friends for their continued love and support. Thank you; Mrs. Josepha Blay, Mr. Fred Treverton, Fr Chris Cutler, Mrs. Tamisa, Mr. Byron Tabula, Mrs. Debbie Manson, Mrs. Kate Gledhill and all those who have been there for me in the most challenging moments in my life.

Abbreviations

3D	3-dimensional
APS	Ammonium persulfate
APC	antigen presenting cell
ATP	Adenosine triphosphate
BAM	Benzamidine
BSA	bovine serum albumin
DNA	Deoxyribonucleic acid
DMSO	dimethyl sulfoxide
DTNB	5,5'-dithiobis-(2-nitrobenzoic acid)
DTT	Dithiothreitol
DTH	delayed type hypersensitivity
EC	Enzyme commission
EDTA	ethylene diamine tetraacetic acid
EGTA	ethylene glycol tetraacetic acid
ELISA	enzyme-linked immunosorbent assay
EM	Electron microscopy
ESI-MS	Electrospray ionization mass spectrometry
FAD	Flavin adenine dinucleotide
FFQ	Fast flow Q Sepharose
GF	Gel filtration
GSH	glutathione
H_2O_2	hydrogen peroxide
Hb	haemoglobin
HEPES	4-(2-hydroxyethyl)-1-piperazineethanesulfonic acid
His-tag	Poly histidine tag
IPTG	Isopropyl-1-thio-β-D-galactopyranoside
LB	Luria-Bertani
MW	molecular weight
MWCO	Molecular weight cut off
NADPH	Nicotinamide adenine dinucleotide phosphate
NOD	nucleotide-binding oligomerization-domain protein

NFKB	nuclear factor _B
NK cells	natural killer cells
NKT cells	natural killer T cell
PDB	Protein data bank
PEG	Polyethylene glycol
PAGE	polyacrylamide gel electrophoresis
PBMC	peripheral blood mononuclear cell
PBS	phosphate buffered saline
PMSF	phenylmethylsulfonyl fluoride
Prx	peroxiredoxin
RF	rheumatoid factor
ROS	reactive oxygen species
SDS	sodium dodecyl sulphate
Srx	sulfiredoxin
TCR	T cell receptor
TEMED	N,N,N',N'-Tetramethyl-1-,2-diaminomethane
T_M	Melting temperature
TNB	5-thiobis-(2-nitrobenzoic acid)
TNF	tumor necrosis factor
Trx	thioredoxin
TrxR	Thioredoxin reductase
UV	Ultraviolet
PBS	phosphate-buffered saline
MS/MS	Tandem mass spectrometry
GSH	reduced glutathione
GSSG	glutathione disulfide

Table of Contents

Chapter 3:

Synthesis and stability of SNO-Hb and hPrx2-SNO

Chapter 5:

Crystallization and X-ray diffraction studies of hPrx2-Hb and hPrx2-SNO complexes

List of Tables

List of Equations

Chapter 1

General introduction

1.1 Introduction

The discovery of the biological functions of nitric oxide (NO) and its role in vascular biology in the late 1980's came by surprise. Later, NO was named 'Molecule of the Year' in 1992 by the journal Science. Furthermore, in 1998, Murad, Furchgott, and Ignarro shared the Nobel Prize for Physiology and Medicine for their work, demonstrating that NO generated by endothelial cells relaxes smooth muscle through activation of guanylate cyclase (Murad, 1986). Increasingly, the diverse cellular activities of NO, one of which is a gaseous signaling molecule, began to be appreciated. Early findings suggested that NO was a freely diffusible secondary messenger, with a promiscuous sphere of influence, functioning predominantly through the regulation of guanylate cyclase (Lancaster, 1994). Recent evidence, however, has resulted in a critical reassessment of this initial model, as NO signaling was increasingly found to occur independently of this key regulatory enzyme. The pioneering work of Stamler (1994) highlighted that the rich redox and additive chemistry of NO facilitates its interactions with centres of iron-sulphur clusters and haem, present in a wide variety of proteins, impacting their activities which is found to be controversial by our research group and others.

1.1.1 General physicochemical properties of NO

NO is a small gaseous molecule consisting of nitrogen (N) and oxygen (O) covalently bound together. The steady-state concentration of NO is determined by its rate of formation and its rate of decomposition. A proper knowledge of the metabolism of NO is a requisite for our understanding and evaluation of its biological effects, and also for the development of reliable analytical methods to assess the production of NO in biological systems.

Nitrogen, one of the elements forming NO, is a unique among the elements in forming no fewer than seven molecule oxides, three of which are paramagnetic, all of which normally are unstable with respect to decomposition into N_2 and O_2 (Greenwood and Earnshaw, 1984). NO is a colourless gas that is sparingly soluble in water under

standardized temperature, pressure, dryness (STPD) conditions. The paramagnetic NO molecule contains odd numbers of electrons, which explains its high reactivity and radical nature. Apart from its reaction with O_2, NO principally may react by electron gain to form the nitroxyl anion (NO^-), and by electron loss to form the nitrosonium ion (NO^+) (Heslop and Jones, 1976). The major breakdown product of NO in aqueous solution is nitrite and the kinetics of autoxidation of NO in aqueous solutions is dependent on the concentration of NO (Ford *et al.*, 1993). Along its migration path, in particular at higher concentration, NO can interact with molecular oxygen, thiols, and reduced haemoproteins (reactions of NO with thiols and haemoproteins will be discussed in details in later sections) (see section 1.4.1). The extent of either of these outcomes largely depends on the microenvironmental conditions under which NO is released, most importantly, the concentration of other bioreactants (Kelm *et al.,* 1997). This explains the large variation in early reports published about the half-life of NO (seconds to minutes) using different bioassays and analytical techniques (Kelm and Schrader, 1990; Borland, 1991). The reaction of NO with O_2 within the hydrophobic regions of membranes is approximately 300 times more rapid than in the surrounding aqueous medium (Liu *et al*., 1998). This implies that biological membranes and hydrophobic tissue compartments are important sites for the disappearance of NO along its travel from being generated to the target cell.

Apart from molecular mechanisms, several reactive oxygen derived species (ROS), such as the superoxide anion radical ($O_2^{\bullet-}$), hydrogen peroxide (H_2O_2) and hydroxyl radical (•OH) are suggested to be involved in the breakdown of NO (Sies, 1991). The basic chemistry of these ROS is described in more detail in section 1.3. The different kinetics of the reactions of NO with these oxygen-derived radicals and their varying concentrations in different cells and organs may account for the slight inconsistency of the reported data (Ignarro, 2010) on *in vivo* degradation of NO. It has been shown that all three ROS compounds are produced by the cells from mammalian species, especially from the endothelial cells and macrophages, both of which also are capable of synthesizing NO.

In biological systems, the mode and the rate of NO metabolism is dependent on its own concentrations, its ability to diffuse, and the surrounding concentrations of the other bioreactants. At room temperature, the diffusion rate of NO in water is 50 m^2s^{-1}

(Loscalzo and Vita, 2000). The half-life of NO *in vivo* is about 10 seconds and NO has a limited reactivity (Ignarro, 2010). NO reacts with O_2 to form nitrogen dioxide (NO_2) (Williams, 2003). Nitrogen dioxide can undergo a further reaction with NO to form dinitrogen trioxide (N_2O_3). The latter molecule is believed to be one of the main nitrosating agents *in vivo,* modulating NO-mediated thiol modifications (Jacob and Winyard, 2009). NO undergoes both oxidation and reduction to form a large number of nitrogen oxide species (NO_x), due to the high number of valence states (from -3 to +5) that the nitrogen atom can acquire (Loscalzo and Vita, 2000; Jacob and Winyard, 2009).

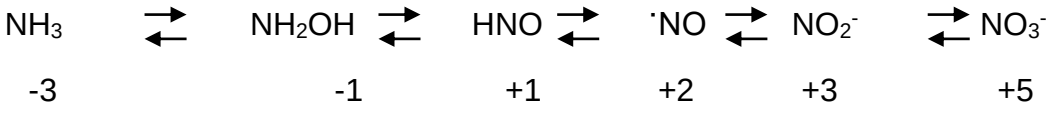

Figure 1.1 Valences of nitrogen and nitrogen oxides. The scheme presents diverse types of nitrogen oxide species (NO_x) with the relative valence state for the nitrogen atom. Ammonia (NH_3), hydroxyl amine (NH_2OH), nitroxyl (HNO), nitric oxide (NO), nitrite (NO_2^-), nitrate (NO_3^-). The scheme is adapted from Loscalzo and Vita (2000).

Diffusion is essential for understanding the ability of NO to act as local modulator and major determinant of biological life time (Lancaster, 1994). The charge neutrality of NO presumably facilitates its free diffusion in aqueous solutions and across cell membranes. The diffusion coefficient of NO at 37^{o}C in aqueous solutions, is 1.4-fold larger than the diffusion coefficient of oxygen. The capacity of NO to diffuse long distances in tissues has been demonstrated using aqueous standards of authentic NO infused into coronary circulation of saline perfused hearts. In the absence of haemoglobin, NO rapidly diffuses along the vasculature and reaches vascular smooth muscle cells and mitochondria of cardiomyocytes in sufficiently bioactive amounts to affect coronary blood flow and left ventricular function (Kelm *et al*., 1995, Kelm *et al*., 1997).

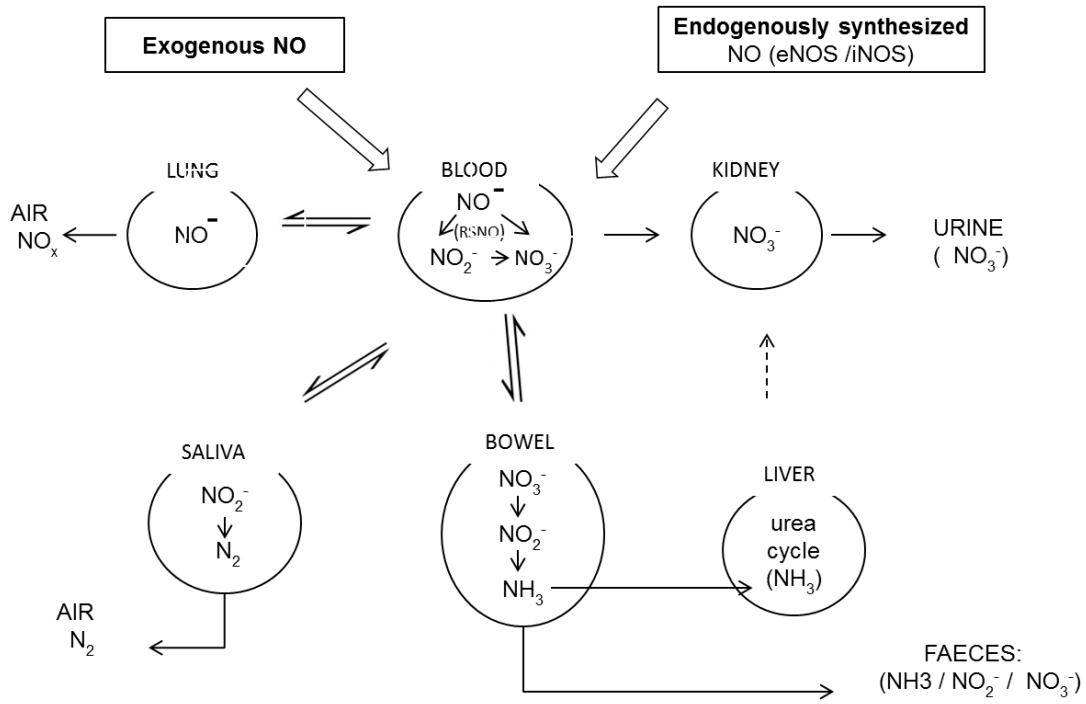

Figure 1.2. Biotransformation of NO and its related N-oxides in mammalian organisms. NO metabolism and breakdown in mammalian organisms is critically determined not only by its rate of formation, but its rate of decomposition can be useful. Yoshida and co-workers in this diagram studied the metabolic pathways of inhaled ^{15}NO and combined ^{15}NO blood injections in male Wister rats monitoring nitrogen excretion in urine and faeces to examine the biotransformation of NO and related N-oxides. Adapted from Kelm (1999).

1.1.2 NITRIC OXIDE PHYSIOLOGY

NO is a biological messenger and homeostatic regulator, which is a key regulator of cardiovascular function by inducing vasodilatation, inhibition of platelet aggregation, and leukocyte adhesion (Moncada and Higgs, 1993). Moreover reduced bioavailability of endothelium-derived NO is closely associated with development of metabolic diseases as well as several cardiovascular diseases including atherosclerosis, ischemia-reperfusion injury, and hypertension (Moncada and Higgs, 1993).

In the cardiovascular system the NO-dependent effects are mostly cytoprotective and anti-atherogenic, including dilatation, inhibition of vascular smooth muscle proliferation, and blockade of leukocyte recruitment and anti-platelet activity (Pacher *et al*., 2007 and Ignorrow, 2010). These characteristics make NO one of the most important cardiovascular protective molecules. Despite the fact NO has the cytoprotective effects its production can be detrimental for tissues. NO has been shown to have both pro-inflammatory and anti-inflammatory properties (Ignorrow, 2010). NO triggers apoptosis (Borutaite and Brown, 2003), regulating lymphocyte function (Liew, 1999), and regulating protein degradation via the N-end rule pathway (Hu *et al.*, 2005). The balance between the two processes depends on “where” and “how much” NO is produced. NO appears to have some biological characteristics in common with other gasotransmitters such as hydrogen sulfide. Low amounts of NO derived from eNOS are thought to be anti-inflammatory, i.e., they inhibit the adhesion and migration of inflammatory cells (Laroux *et al*., 2001; De Caterina and Libby, 2007). In contrast, large amounts of NO produced by iNOS upon stimulation by bacterial products or inflammatory cytokines, for example IL-1β and TNF-α, are thought to contribute to inflammation by causing increased vascular permeability and infiltration of leukocytes to the inflamed tissues (Nagy *et al*., 2007).

Additionally, the major function of NO during inflammation is microbial killing via the generation of reactive nitrogen species (RNS) like peroxynitrite (Eq.1.1).

NO^- + O_2^- ⟶ $ONOO^-$

Nitric oxide Superoxide Peroxynitrite

Equation 1.1

But the excessive NO and $ONOO^-$ levels produced during inflammation may equally be responsible for tissue injury, either directly through damage to proteins, lipids and DNA (Radi *et al*., 1991; Grisham *et al.,* 1991; Nagy *et al*., 2007 and Freeman *et al*., 2008) or indirectly (e.g. through the modulation of leukocyte activity (Caterina and Libby, 2007).

In the nervous system, NO is involved in: neuroprotection (Fernandez-Tome *et al*., 1999), male sexual function (Bulter and Nicholson, 2003) and in synaptic signaling (Bulter and Nicholson, 2003).

As an anti-tumor agent NO is involved in DNA damage (Bulter and Nicolson 2003), and cell death (Umensky and Schirrmacher, 2001) as it increases the sensitivity to radiotherapy (AL- Waili and Butler, 2007). NO has anti-microbial properties which are involved in the immune response (Bulter and Nicolson, 2003). NO is known to cause nitrative stress which results in DNA damage (Akuta *et al*., 2006). NO inhibits pathogenic enzymes such as haem containing enzymes, enzymes with Fe-S clusters including aconitase, NADH dehydrogenase and succinate dehydrogenase, the non-haem metalloenzymes, ribonucleotide reductase and DNA (Venturine *et al*., 2000; Salvati *et al*., 2001), reducing the expression of viral proteins such as Dengue viruses (NS1, NS2A, NS2B, NS3, NS4A, NS4B and NS5), rabies virus, influenza virus and Encepathalomyocarditis virus (Simon *et al*., 2006).

NO chemical reactivity makes its physiology quite diverse due to the number of cellular targets the gas possesses (Zhang *et al.,* 1998). NO can also signal via indirect pathways which involve its main metabolites (NO_3^-, NO_2^-, and RSNO). Especially because of their potential therapeutic applications, nitrite (NO_2^-) and S-nitrosothiols (RSNOs) (Fig 1.3) are of particular interest. These will be introduced and described in the next sections. In the respiratory system, NO is involved in bronchodilation (Belvisi *et al*., 1992), and involved in the release of oxygen from haemoglobin (Lipton, 2001).

1.2 Nitric oxide pathways:

There are two pathways in which NO can be generated namely:

1. The L-arginine / NOS pathway described by Ignarro, Murad and Furchgott in 1998 (Ignarro *et al*., 1998) (Fig 1.1)

2. The nitrite-NO pathway which is a newly discovered pathway by our research group and others (Benjamin *et al.,* 1994 (Fig 1.3).

1.2.1 The NOS pathway

Conventionally, all NO generated in human tissues has been assumed to result from an enzymatic reaction whereby oxygen, arginine and NADPH are the substrates for the enzymatic generation of NO, which also produces citrulline and $NADP^+$ (Fig 1.1). This reaction is catalysed by NO synthase (NOS), a family of three human enzymes: neuronal NOS (nNOS), inducible NOS (iNOS) and endothelial NOS (eNOS). The NOS enzymes are haem-containing enzymes (Alderton *et al*., 2001; Shuehr *et al*., 2004), which use several co-factors, i.e. NADPH, flavin adenine dinucleotide (FAD) and tetrahydrobiopterin (BH_4), to catalyse NO production (Fig 1.1). The oxygenase domain presents the binding sites for BH_4, the haem group and the L-arginine substrate. The reductase domain binds FAD, NADPH and FMN (flavin mononucleotide) (Ravi *et al*., 2004). The NO is produced in the oxygenase domain by a two-step reaction that causes L-Arg oxidation at the haem site (Ravi *et al*., 2004). The NOS first hydroxylates the guanidino nitrogen on L-Arg and then oxidises the N-hydroxy-arginine intermediate to NO and L-citrulline (Stuehr *et al* 2004). The reductase domain, through its flavoprotein co-factors, provides a flow of electrons to the ferric haem during the first step of the reaction. The Fe^{3+} is reduced to Fe^{2+} which reacts with O_2 to form a ferric-haem superoxide species, which is responsible for the reaction with the substrate. In order to hydroxylate L-Arg the ferric-haem superoxide species receives an electron from BH_4 (Channon, 2004). The electron flow from BH_4 prevents futile $O_2^{\bullet-}$ release from the protein (phenomenon otherwise known as NOS uncoupling) and induces the first step in L-Arg oxidation. The N-hydroxy-L-arginine is then oxidised to L-citrulline and $^{\bullet}NO$ in the second step of the reaction.

The NOS enzymes are known to work as homodimers and their function is modulated by Ca^{2+}/Calmodulin (CaM) binding (Alderton *et al*., 2001; Ravi *et al*., 2004). For all three

isoforms the binding of CaM functions as a redox modulator, as it appears to be required for efficient electron transfer between the two domains of the protein (Loscalzo and Vita 2000; Ignarro, 2010). The nNOS and eNOS bind CaM reversibly in a Ca^{2+}-dependent manner, while iNOS binds avidly to CaM even at low intracellular Ca^{2+} concentrations characteristic of resting cells (Loscalzo and Vita, 2000). As the name indicates, iNOS is highly induced in a variety of cells, often as a result of immune stimulation for example lipopolysaccharide and cytokines. Both eNOS and nNOS are regulated primarily by Ca^{2+} via the actions of calmodulin and give rise to pico-nanomolar concentration of NO. In contrast, iNOS is not regulated by Ca^{2+} and may produce high (micromolar) levels of NO (Huang, 2009). Therefore iNOS activation appears to be largely independent of changes in the intracellular Ca^{2+} concentration and its principal form of regulation appears to be at the mRNA level (Loscalzo and Vita, 2000). This is the reason why iNOS is commonly considered an inducible enzyme, while eNOS and nNOS are constitutive enzymes, as they are often found expressed at stable levels in cells and tissues (Ignarro, 2010). The NOS enzymes are critically dependent on the molecular oxygen concentration as a co-substrate to produce the free-radical gas NO. The K_m values for oxygen are around 4 μM for eNOS, 130 μM for iNOS and 350 μM for nNOS (Stuehr *et al*., 2004) which is generally higher than normal oxygen tension in the tissues that ranges from as low as 3 μM in contracting muscles (Richardson *et al.,* 1999) up to 60-100 μM in some tissues under resting conditions (Buerk 2007; Faassen *et al*., 2009).

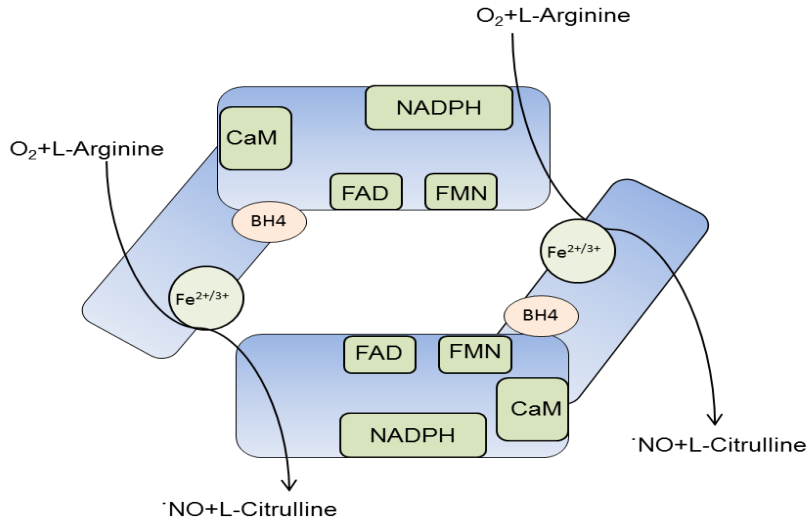

Figure 1.3 A schematic representation of the NOS dimer. The figure presents a schematic representation of the NOS dimer. Every monomeric unit presents two domains: the oxygenase domain and the reductase domain. The former presents the binding site for BH4 and the haem group (here indicated as $Fe^{2+/3+}$). The latter presents the binding site for several co-factors: CaM, FAD, FMN and NADPH. L-arginine oxidation takes place at the haem site in the oxygenase domain. Adapted from Channon (Channon, 2004).

However, the discovery of a separate new pathway of NO formation, starting with ingested nitrate (Duncan *et al*., 1995) provides an important alternative mechanism for NO generation in human tissues, which is independent of NOS. A decrease in NO formation may result from either reduced expression of eNOS or from changes in the concentrations of its substrates / co-factors such as L-arginine or BH4.

1.2.2 The nitrite-nitric oxide pathway

Nitrite is maintained within a narrow range *in vivo* (Lundberg *et al*., 2008) with steady state plasma basal concentrations ranging from 100 to 600 nM in most mammals including humans (Kleinbongard *et al*., 2003). Conversely, nitrite is more concentrated within cells and tissues compared to plasma (Bryan *et al*., 2004; Dejam *et al*., 2005). *In vivo* the half-life of exogenously administered nitrite is relatively short and can range

between 18 and 54 min (Hunault *et al*., 2009) which is likely due to its rapid equilibration with tissues (Bryan *et al*., 2005;Kevil *et al*., 2011) and reaction with oxy-haems to form nitrate. The *in vivo*, half-life of NO_2^- in human blood is only about 110 seconds mainly due to its fast reaction with oxy-haemoglobin (Kelm, 1999).

In the past decade also, it has become apparent that nitrite is an important mediator of physiological responses particularly during hypoxia. In 1995 Zweier *et al*. described a NOS-independent nitrite reduction in the ischaemic and acidic heart and some years later, a physiological role for nitrite in hypoxic and metabolic vasoregulation was suggested (Gladwin *et al*., 2000; Modin *et al*., 2001). In a subsequent study infusion of sodium nitrite into the forearm brachial artery of healthy volunteers increased blood flow even at near physiological blood concentrations producing substantial vasodilation (Cosby *et al.*, 2003). The nitrite is reduced to bioactive NO along a physiological and pathological pH and oxygen gradient by several mechanisms including the increment of haemoglobin (Cosby *et al.*, 2003; Nagababu *et al*., 2003), myoglobin (Shiva *et al*., 2007; Rassaf *et al*., 2007), xanthine oxidoreductase (XOR) (Fig 1.2) (Zhang *et al*., 1998; Millar *et al*., 1998; Godber *et al*., 2000) aldehyde oxidase, (Li *et al*., 2008), components of the mitochondrial electron transport chain (Kozlov *et al.,* 1999; Castello *et al.,* 2006;) CYP (Duthu and Shertzer, 1979; Li *et al*., 2006), carbonic anhydrase (Aamand *et al*., 2009), ascorbate (Carlsson *et al*., 2001), and even NOS itself (Vanin *et al.,* 2007). The generation of NO by these pathways is greatly enhanced during hypoxia and acidosis, thereby ensuring NO production in situations for which the oxygen-dependent NOS enzymes activities are compromised (Giraldez *et al*., 1997; Gladwin *et al*., 2009). Nitrite reduction to NO and NO modified proteins during physiological and pathological hypoxia appear to contribute to the physiological hypoxic signaling, vasodilation, modulation of cellular respiration, cellular response to ischaemic stress (Gladwin *et al*., 2000; Modin *et al*., 2001; Cosby *et al.*, 2003; Durnski *et al.*, 2005; Shiva *et al*., 2007).

The NO can be “stabilized” in blood and tissues by oxidation to nitrite (NO_2^-) and nitrate (NO_3^-) (see section 1.2.6). The NO_2^- in turn can be reduced back to bioactive NO, through different enzymatic and non-enzymatic pathways, with NO_2^- thereby acting as an endocrine molecule, which complements the L-arginine/NOS pathway along the physiological and pathological oxygen and proton gradient. This is a system which brings about regulation of vascular tone, blood pressure control, oxygen supply to

tissues, regulation of mitochondrial oxygen consumption, and cytoprotection against ischaemic reperfusion (I/R) injuries.

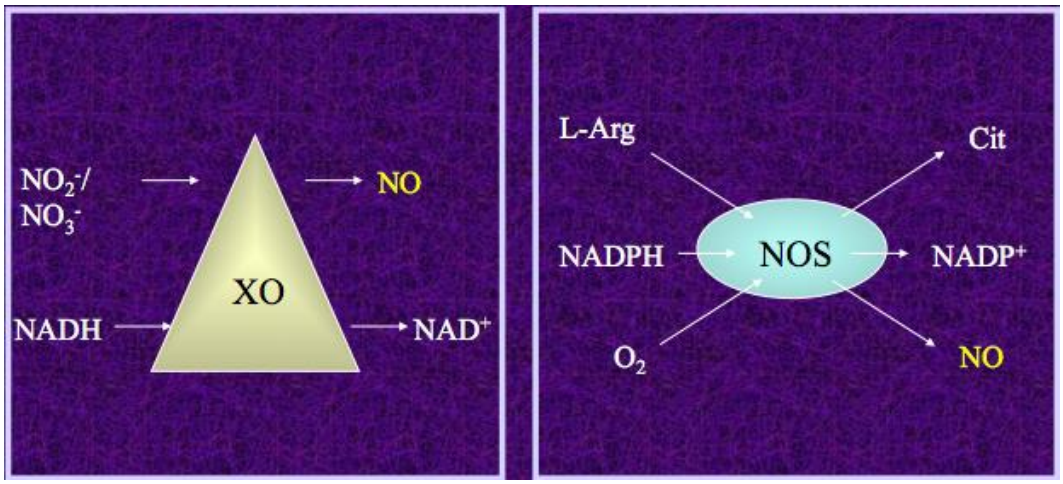

Figure1.4. Schematic representation for the comparison of NO production from xanthine oxidoreductase and NOS as discussed by Zhang *et al.,* 1998.

Zhang *et al*. (1998) – showed that XO could reduce nitrite to NO. Recently, Gladwin (2008) has suggested an alternative nitrite reductase - deoxyHb. Once NO is formed, physiological effects such as an increase of blood pressure were observed (Gladwin 2008).

Humans are exposed to nitrate (NO_3^-) and nitrite (NO_2^-) through dietary sources such as leafy green vegetables and beetroots; NO_3^- and NO_2^- are reduced to NO via several mechanisms (Benjamin *et al.,* 1994) (Fig 1.5). Benjamin *et al.* (1994) were the first to describe the NOS-independent generation of NO in the stomach. Endogenous or ingested NO_3^- is reduced to NO_2^- by commensal bacteria located on the tongue, and NO is produced in the stomach via the protonation of the NO_2^- molecules swallowed with the saliva (Benjamin *et al.,* 1994; Lundberg *et al*., 2004, and Lundberg and Weitzberg, 2010). The production of NO in the human stomach is pH-dependent and it is thought to be one of the main mechanisms in gastric host defence (Bjorne *et al*.,

2004 and Lundberg *et al*., 2008). Therefore, the ingestion of an oral bolus of nitrate in the form of either sodium nitrate or beetroot juice, results in a marked increase in plasma nitrite concentrations in human subjects as recently shown by our research group and others (Lundberg *et al*., 2005; Bailey *et al.,* 2009; Gilchrist *et al.,* 2010; Vanhatalo *et al.*, 2010; Gilchrist *et al*., 2013).

Dose response studies in mice suggest a broad efficacy for a safety range of nitrite of three orders of magnitude, with doses as low as 0.1 µg/l to 100 µg/l providing significant production of nitrite (Duranski *et al*., 2005). Interestingly, the protective effect against nitrite in mice was evident at very low plasma concentrations and an increase of plasma nitrite by approximately 40%, reduced liver and heart infections by 50% (Duranski *et al*., 2005). The maximum protective effect of nitrite was achieved at a dose of 48 nmol nitrite and declined at higher doses. This supports the idea that cytoprotection is reached already at small elevations in NO concentrations, whereas higher non-physiologic NO fluxes may lead to cellular apoptosis and necrosis (Duranski *et al*., 2005). The nitrite-mediated protective effect is independent of the classical L-arginine/NO pathway and abolished by co-administration of the NO scavenger carboxy-PTIO (cPTIO) suggesting a role of NO as one final mediator of nitrite bioactivity (Duranski *et al*., 2005). Interestingly, while the L-arginine/NOS pathway is oxygen dependent the nitrite-NO pathway is gradually activated as oxygen tension falls.

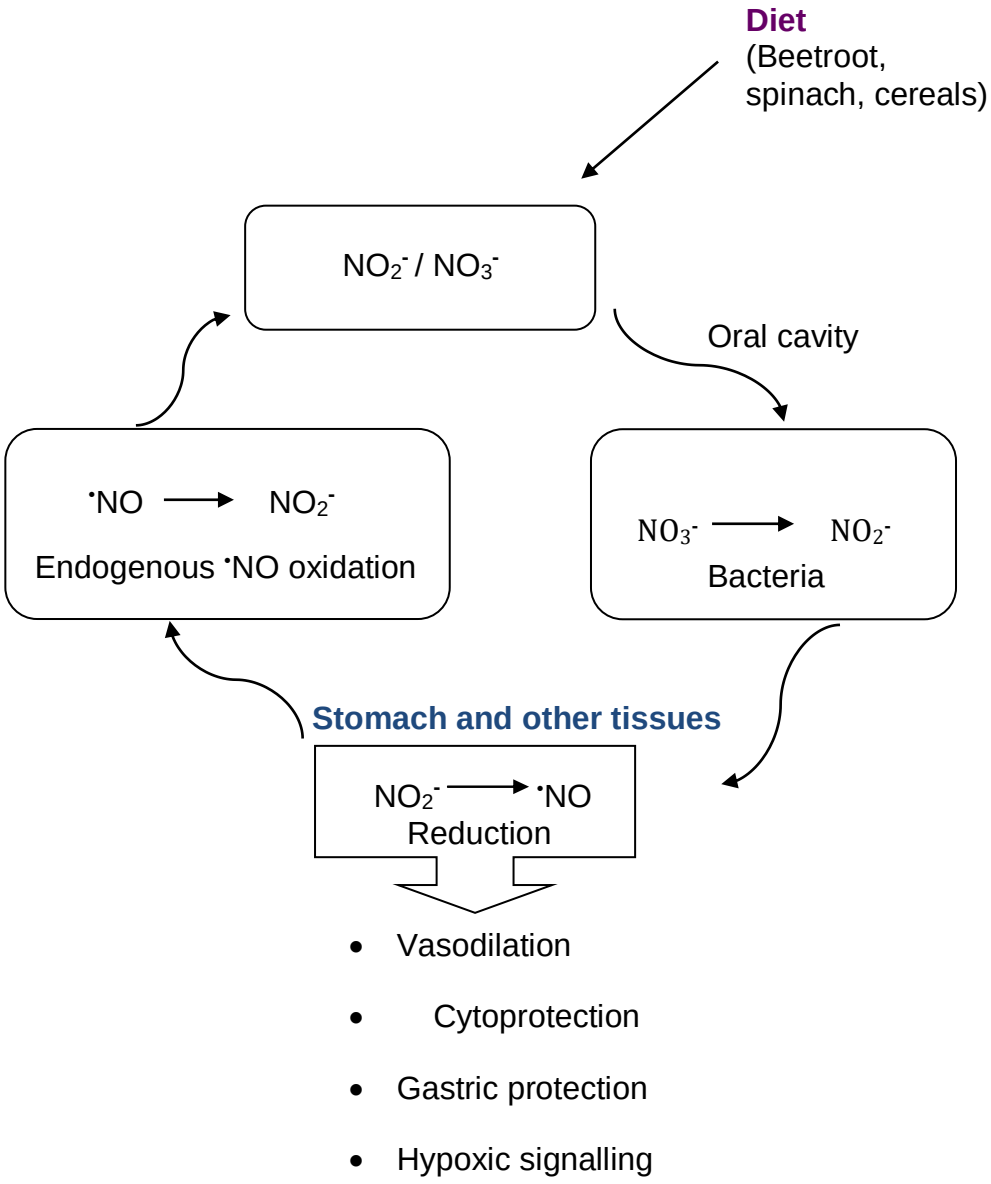

Figure 1.5. The nitric oxide cycle. The two main sources of NO_2^- and NO_3^- are diet and endogenous NO oxidation. In the oral cavity, NO_3^- ingested from dietary sources like beetroot or green leafy vegetables, is reduced to NO_2^- by commensal bacteria. The NO_2^- is then ingested and reaches the stomach and other tissues where it reduced to NO (Benjamin *et al*., 1994).

1.2.3 Roles of NO in the cardiovascular system

NO is known to have other roles in the cardiovascular system, which includes: regulation of vascular smooth proliferation (Heller *et al*., 1999), regulation of endothelium cell growth and apoptosis, antioxidant properties and leukocytes adhesion (Walford and Loscolzo, 2003; Schulz *et al*., 2005). Apoptosis is a mechanism of cell death which is executed to safely dispose of cell corpses and fragments. The NO is a biological messenger and homeostatic regulator, which is a key regulator of cardiovascular function by inducing vasodilatation, inhibition of platelet aggregation, and leukocyte adhesion (Moncada and Higgs, 1993). Moreover reduced bioavailability of endothelium-derived NO is closely associated with the development of metabolic diseases as well as several cardiovascular conditions including atherosclerosis, ischaemia-reperfusion injury, and hypertension. The blood stream NO has an important effect on platelets. Platelets are small cell fragments found in blood and are involved in the formation of blood clots when platelets aggregate together or adhere to the endothelium (Bulter and Nicolson, 2003). The NO activates platelet soluble guanylate cyclase (sGC) to produce guanosine 3',5'-cyclic monophosphate (cGMP), which prevents platelet adhesion, aggregation and activation. The NO-controlled regulation of platelet activity is crucial in the prevention of thrombosis during disease and surgery.

The most likely mechanism for endothelial dysfunction is that of a reduced bioavailability of NO and as a result its interaction with oxygen-derived species, in particular the superoxide ($O_2^{\bullet-}$). Therefore, the inactivation of NO by $O_2^{\bullet-}$ contributes to oxidative stress, a term used to describe an imbalance between excessive formation of reactive oxygen species (ROS) or the oxidants derived from NO and limited antioxidant defences (Buerk, 2007). Oxidative stress has been implicated in established clinical conditions such as dyslipidaemia, diabetes, coronary artery diseases and hypertension (Moncada and Higgs, 2006). Protection against a decrease in the generation of constitutive NO in the vasculature can prevent the development of vascular and metabolic diseases. This may be achieved by the use of either antioxidants such as superoxide dismutase (SOD), or alternatively, nitric oxide synthase (NOS) independent sources of NO, such as red blood cells (RBC's), also known as erythrocytes (Cortese and Kelm 2014).

Remarkably, while the low concentrations of NO generated by eNOS protect against atherosclerosis, higher concentrations of NO generated for example by inflammatory stimuli and iNOS induction are cytotoxic and can promote atherosclerosis either directly or via the formation of NO adducts, such as peroxynitrite (Cortese *et al*., 2012). Inhibition of mitochondrial respiration is an important component of NO-induced tissue damage (Cortese *et al*., 2012). The inhibition becomes persistent as a result of oxidative stress. This is consistent with the dual role of NO as a protective molecule at low concentration and as a toxic molecule at persistently high concentrations (Moncada and Erusalimsky, 2002).

1.2.4 Metabolic products of Nitric Oxide

As mentioned in section 1.1.1, in relation to how the steady state concentration of NO is maintained, a good understanding of the metabolic products of NO is vital.

The NO reacts very rapidly with the superoxide radical to form the reactive peroxynitrite, which can isomerize to nitrate or can be protonated to form peroxynitrous acid. The peroxynitrous acid in turn can split into a hydroxyl and a nitrogen dioxide radical (see Eq.1.3). The NO is also rapidly oxidised by oxy-haems like haemoglobin in red cells to form methaemoglobin, which in turn is reduced to haemoglobin free of oxygen by the enzyme methaemoglobin reductase. This reaction contributes significantly to the endogenous pools of nitrate in the body (see Eq.1.1).

The NO is rapidly metabolized by reactions involving oxy-haemoglobin, multi-copper oxidase, reactive oxygen derived species and other radicals. Oxidative and nitrosative products of NO reactions can provide a storage pool for bio-available NO throughout the body. The NO is stabilized in blood and tissues in the form of nitrate (NO_3^-), nitrite (NO_2^-) and as a quantitatively lower nitros(yl) species S-nitrosothiols (RSNO), N-nitrosamines (RNNO) and NO-haem (Bryan *et al*., 2004).

Auto-oxidation of NO:

Auto-oxidation of NO (Eq.1) is dependent on the concentration of NO itself (second order reaction in NO concentration). Consequently, the speed of this reaction becomes

higher as NO becomes more concentrated. Nitrite formation via auto-oxidation of NO produced by NOS might contribute to the endogenous pool of nitrite in the body.

Nitrite formation in the body via oxidation of NO to NO^+ by the multicopper oxidase ceruloplasmin found in plasma also contributes significantly to the endogenous pool of nitrite in the body (Eq.6).

$$2\ NO + O_2 \longrightarrow 2\ NO_2$$

Equation 1.2

$$NO_2 + NO \longrightarrow N_2O_3$$

Equation 1.3 (Dinitrogen trioxide)

Reaction of NO with superoxide:

The NO contrasts with most intercellular messengers because it diffuses rapidly and isotopically through most tissues with little reaction, but cannot be transported through the vasculature to cause rapid destruction by oxyhaemoglobin (Beckman and Koppenol, 1996). The direct toxicity of NO is modest, but greatly enhanced by reacting with superoxide to form peroxynitrite ($ONOO^-$) (Eq.1.1), can undergo re-arrangement to form (NO_3^-) (Eq. 1.4) and lastly be reduced to nitrogen dioxide and hydroxyl radical (Eq.1.5).

$$ONOO- \longrightarrow NO_3^-$$

Equation 1.4

$$ONOO^- + H^+ \longrightarrow HONOO \longrightarrow {}^{\bullet}OH + NO_2$$

Peroxynitrous acid — nitrogen dioxide

Equation 1.5

Oral nitrate lowers the diastolic/systolic blood pressure, oxygen-cost of exercise and also inhibits platelet aggregation (Rocks *et al*., 2005; Bailey *et al*, 2009; Vanhatalo *et al.*, 2010), presumably *via* nitrite and NO formation. Originally, our group suggested (Zhang *et al*., 1998) that the formation of NO, involves the reduction of plasma nitrite, perhaps involving the xanthine oxidase-catalysed reduction of nitrite. However, other mammalian mechanisms (Luisa *et al*., 2011) of nitrite reduction have since been suggested and this is still an area of controversy.

1.2.5 Sources of nitrite

In mammalian physiology there are at least three sources of nitrite that contribute significantly to the endogenous nitrite pool. One of them is the oxidation of endogenous NO to form nitrite (see Eq. 1.6 to Eq.1.8). *In vivo*, the oxidation of NO is accelerated by at least two mechanisms. The first step, involves polar molecules such as NO or oxygen partition preferably into lipid of protein fractions of low polarity.

The second mechanism involves the copper-storage plasma protein ceruloplasmin. This protein catalyzes the oxidation of NO to nitrosonium ion (NO^+), which is rapidly hydrolyzed to nitrite (Eq. 1.6). Kleinbongard *et al* (2003) highlighted the importance of this route for NO_2^- generation in eNOS knockout mice. The circulating nitrite levels were reduced by up to 70% in eNOS knockout mice, and nitrite levels were also lower in mice lacking caeruloplasmin (Wang *et al*., 2006).

$$NO + Cu^{2+} \longrightarrow NO^+ + Cu^+$$ (Reaction of NO with multi-copper_oxides)

Multicopper protein — Nitrosonium ion — reduced copper

Equation 1.6

$$NO^+ + H_2O \longrightarrow HNO_2 + H^+$$

Equation 1.7 — Nitrous acid

Equation 1.8

Finally, a third important source of the nitrite comes from the reduction of endogenous or dietary-derived sources by nitrate reductase enzymes found in commensal bacterial as previously discussed see section 1.2.2 (Spiegelhalder *et al*., 1976 Lundeberg *et al*., 2004). In humans, nitrites contribute a big percentage to our day-to-day meals i.e. in processed cured meats ~39% of the product is NO_2^- and in baked goods and cereals ~34% of the final product is NO_2^- (Machha and Shechter, 2011). Bacon and ham contain about 9 mg/kg nitrite (Hord *et al*., 2009).

The above studies underline the importance of the NO_2^-/ NO pathway, especially in hypoxic conditions (for example, ischaemia) when the bioavailability of NO is low (Van Faassen *et al*., 2009). Additionally to being an important hypoxia signaling molecule (Gladwin, 2005; Van Faassen *et al*., 2009), though NO_2^- is now also recognized as a very interesting therapeutic agent in the treatment of (IR) injury conditions and hypertension (Lundberg *et al*., 2008). So far all the beneficial effects attributed to NO_2^- are mostly dependent on its ability to release NO (Lundberg *et al*., 2008). For example, in the stomach, upon acidification, NO_2^- releases NO and this mechanism is the basis of bacterial killing and mucus generation (to support gastric mucosal integrity). But it is also the basis of vasodilatory effects in the circulation (Bjorne *et al.,* 2004 and Lundberg *et al*., 2009).

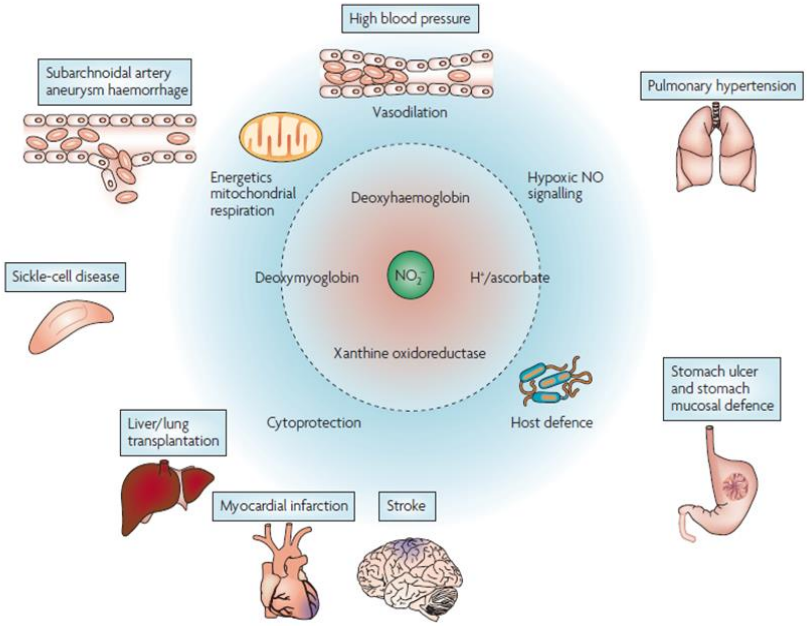

Figure 1.6. Representation of potential beneficial effects of NO_2^- reduction to NO. The reduction reactions of NO_2^- to NO are greatly enhanced in hypoxic conditions. Once NO_2^- is reduced to NO, it can exert beneficial effects of potential therapeutic value: cytoprotection in ischaemic conditions host defense and cytoprotection in the stomach; vasodilation in systemic hypertension and cerebral vasospasm. NO_2^- can also modulate NO-signaling and, for example, it can have effects on the mitochondrial respiratory chain by inhibiting complex I activity (see section 1.2.1). Figure reproduced from Lundberg (Lundberg *et al.,* 2008).

1.2.6 Sources of nitrate

There are two sources of inorganic nitrate in the body. An exogenous source, which is linked mainly to the diet and an endogenous source, which is linked to the oxidation of NO produced by NOS such as the reaction of NO with oxy-haem (see Eq. 1.4 and 1.9).

$$NO + Fe^{2+}O_2 \longrightarrow Fe^{3+} + NO_3^-$$

Oxy-haem reduced-haem

Equation 1.9

In relation to the endogenous source of NO_3^-, NO is rapidly oxidised by oxy-haems like haemoglobin in red blood cells to form methaemoglobin, which in turn is reduced to haemoglobin by the enzyme methaemoglobin reductase. This reaction contributes significantly to the endogenous pool of nitrate in the body.

In relation to exogenous sources of NO_3^-, vegetables like lettuce, spinach, and beetroot contain more than 2.5 g/kg nitrate and can reach levels up to 7.4 g/kg (Hord *et al*., 2009). Drinking water, fish and dairy products such as cheese also contain small quantities of nitrate. Cigarette smoke and car exhausts are one of the other environmental sources of nitrate (Lundberg *et al*., 2004).

Under normal conditions, the contribution of nitrate from the diet versus endogenous sources is almost equal but, with a diet rich in vegetables, dietary NO_3^- becomes more dominant (Hord *et al*., 2009). On average, the dietary nitrate intake ranges from 53 to 300 mg per day and intake is greater in people adhering to the typical Mediterranean diet or the traditional Japanese diet (Machha and Schechter 2011). Under basal conditions the endogenous part of nitrate comes mainly from eNOS in vessels (Fig.1.2) (Lundberg *et al*., 2004 and Hord *et al*., 2009) and some also from the neuronal nNOS, but under inflammatory conditions the inducible isozyme iNOS produces large quantities of NO with a considerable increase in the concentrations of nitrate in the plasma (Benjamin *et al*., 1996).

1.2.7 Role of nitric oxide in maintenance of vascular tone

The endothelium is a single-celled layer of specialised cells which was once considered as a simple barrier between the blood and vessel wall. The endothelium is now regarded as a dynamic organ which lines the entire vascular system (Galley and Webster 2004; Klabounde, 2005). Endothelial cells are located on the intima – which is the inner lining of the vasculature and they control vascular function by responding to various hormones, neurotransmitters and vasoactive factors. In the human vasculature, the function of the cardiovascular system is to supply the correct amount of oxygen to tissues, depending on the demands of different tissues for oxygen. This is achieved by controlling blood pressure and flow *via* contraction and relaxation of smooth muscle cells, which are part of blood vessel walls (Lundberg *et al*., 2008). This balance of

constriction and relaxation of vessels is referred to as vascular tone. The control of vascular tone is complex. There is a wide range of chemical stimuli that can promote muscle contraction and relaxation. Chemical species involved in vasoconstriction are: noradrenalin, myognictone, endothelin, angiotension II, arginine, vasopressin and serotonin from the central nervous system of the gastrointestinal tract. Vasodilation is triggered by the following chemical species: adrenomedullin, NO, calcitonin-gene related peptide (CGRP), atrial natriuretic peptide (ANP), and bradykinin (Kelm *et al*., 1995; Moncada *et al.,* 2002; Lundberg *et al*., 2008). These chemicals act either directly on the smooth muscle cells or trigger response pathways in other parts of the vessel wall such as the endothelial layer which in turn affects the activity of the smooth muscle cells. These chemicals either originate from the neighboring tissues such as connecting nerves or originate from the other parts of the blood vessel wall such as from the endothelium (Moncada *et al.,* 2002). Also those chemical species mentioned initially originate from the blood stream through diffusion into the vessel wall.

The most important vasoconstrictor is noradrenalin (NA), which is released from sympathetic nerves and the most important vasodilator is NO synthesised in the endothelium. The NO and NA are involved in the control of vascular tone whereby NA briefly binds to receptors on the smooth muscle cell which triggers binding of myosin to act within the cell by increasing the level of intracellular calcium, which results in muscle contraction. This effect causes the blood pressure to increase (Camm *et al*., 2006).

Vasodilation (a decrease in blood pressure) can be initiated by the release of NO from the endothelium. Exposure of endothelial cells to contain chemicals (acetylcholine, L-arginine, insulin) or to shear stress, results in increased production and release of NO (via a calcium-dependent activation of eNOS (Walford and Loscalzo, 2003; Klabunde, 2005). The NO diffuses into the smooth muscle cells, where it activates guanosine triphosphate (GTP) to form cyclic guanosine monophosphate (cGMP) (Fig 1.5). Finally, cGMP is a signaling molecule, which then triggers the inhibition of calcium uptake or release in the smooth muscle cells, thus preventing vasoconstriction (Walford and Loscalzo, 2003; Klabunde, 2005) (Fig 1.7). Recent evidence suggests that it is not only NO from the endothelium that is important for vasodilation, but also NO from the red blood cells (RBCs) is important. According to the mechanism described by Gladwin and

colleagues (Gladwin *et al.,* 2012), nitrite-induced hypoxic vasodilation involves at least three steps: first, the reaction of nitrite with deoxyHb; secondly, the escape of the NO produced from RBCs and thirdly, the induction of vasodilation by activation of soluble guanylate cyclase in smooth muscle cells, resulting in cGMP production (Jensen, 2009). However, the mechanism by which NO is able to escape from RBCs despite a local environment containing high concentrations of haemoglobin (Hb) is still an open issue. In fact, there is so much Hb in the blood (10 mM in haem) (Lancaster, 1994), the ability of NO to function as the endothelial-delivered relaxing factor (EDRF), diffusing to smooth muscle without being scavenged by Hb, is seen as a paradox.

Oxygenated Hb (OxyHb) will react very fast with NO to form nitrate and methaemoglobin. This reaction, is rate-limited by the time it takes for the NO to diffuse to the haem pockets of Hb ($k= 10^7 – 10^8$ $M^{-1}s^{-1}$), thus destroying the ability of NO to signal, as nitrate is relatively inert (Doyle and Hoekstra, 1981; Eich *et al*., 1996; Herold et al., 2001). On the other hand, NO can also reversibly bind very tightly to the vacant deoxygenated haem of Hb, whereby even when the NO does come off, it is still likely to be inactivated by its reaction with OxyHb (Cassoly and Gibson, 1975). Therefore, Hb effectively scavenges NO, and according to the work done by Chen *et al.* (2013), who demonstrated that the amount of NO that would be capable of diffusing to the smooth muscles when there is much Hb in blood cannot be sufficient to effect vasodilation, which leaves an open issue as to how NO could function as the EDRF.

An alternative approach has looked into encapsulated Hb and non-encapsulated to explain the paradox of how NO can function to effect vasodilation without being scavenged by Hb (Chen *et al.,* 2013). When Hb is encapsulated inside the RBC, it scavenges NO up to 1000 times slower than when it is cell-free Hb (not encapsulated) (Coin and Olson, 1979; Butler *et al*., 1998; Liu *et al*., 1998; Vaughn *et al*., 1998; Liao *et al*., 1999; Vaughn *et al*., 2000; Vaughan *et al*., 2001; Huang *et al.,* 2001; Liu *et al.,* 2002; Han and Liao, 2005).

A proposed mechanism thought to account for the reduced rate of NO scavenging by the cell-free Hb compared to when it is free in solution is the formation of a cell-free zone (Butler *et al*., 1998; Liao *et al*., 1999). This results into flow within the blood vessel, where the RBCs is pushed inwards away from the endothelium, forming a cell-free zone

next to the endothelium. However, this does not address the problem of OxyHb which will react very fast with NO anyway to make it inactive as mentioned beforehand.

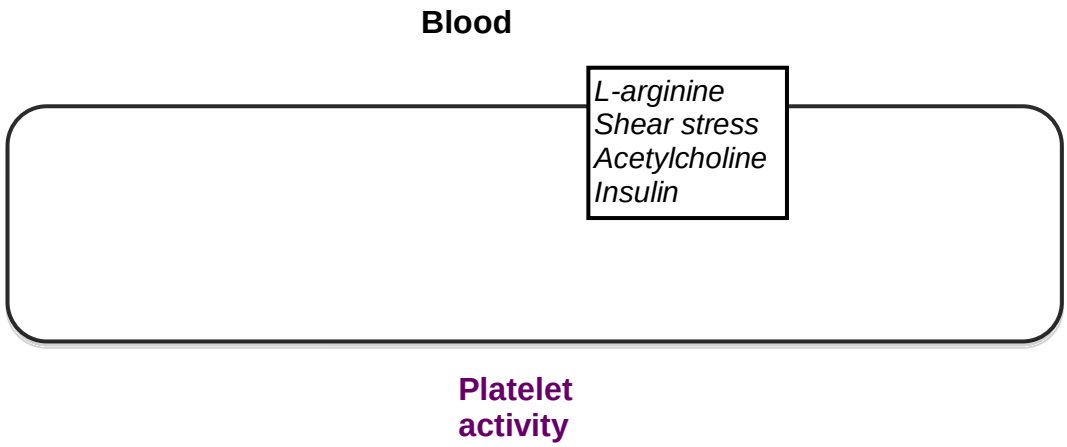

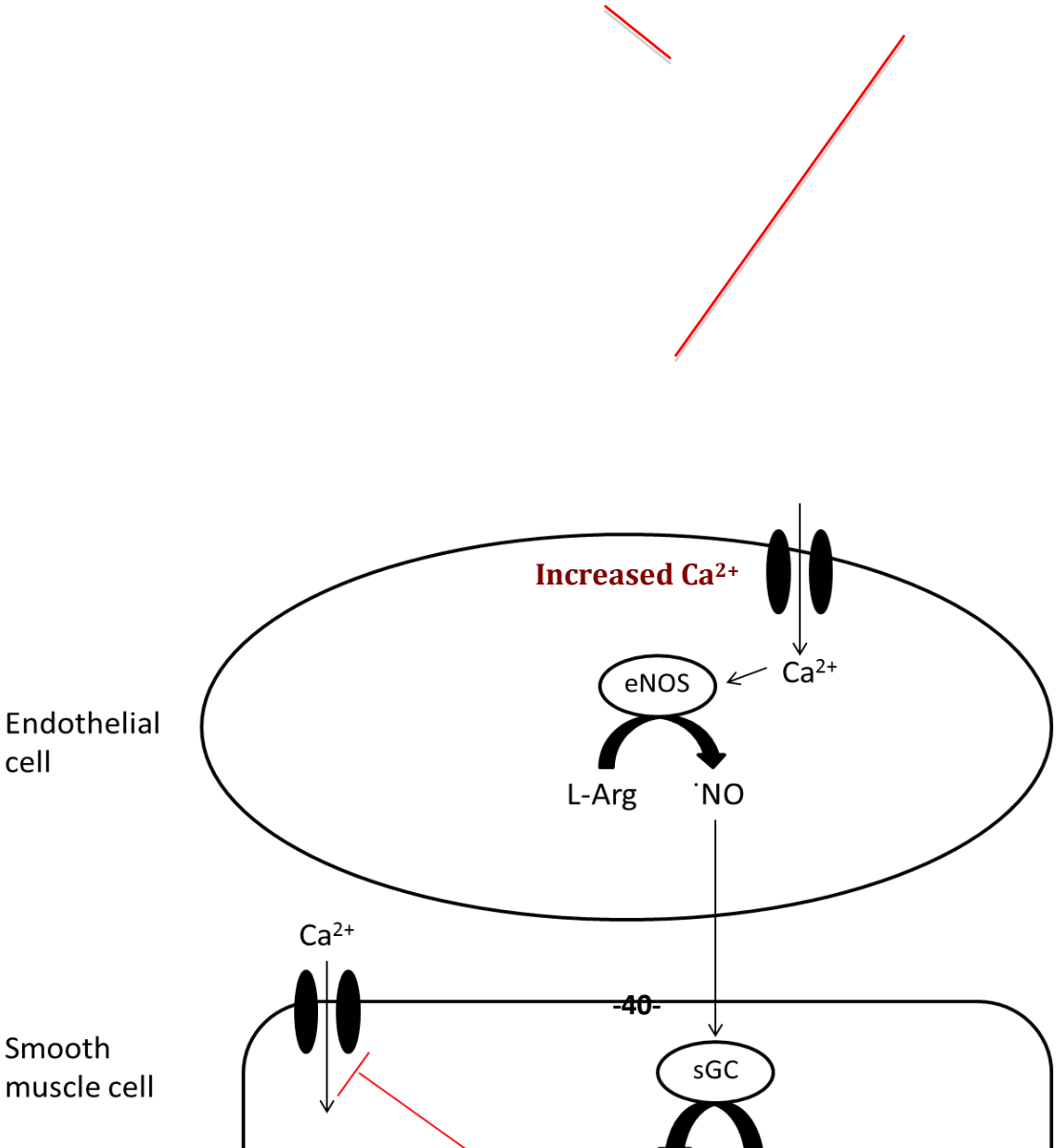

Figure 1.7. The mechanism of vasoconstriction demonstrating how nitric oxide is involved in the maintenance of vascular tone. The increase of intracellular Ca^{2+} concentrations in endothelial cells causes the activation of eNOS and the production of ˙NO from L-arginine (L-Arg). The produced ˙NO translocates to the smooth muscle cells where it activates soluble guanylate cyclase (sGC) to produce cGMP from guanosine triphosphate (GTP). cGMP activates cGMP-dependent kinase (PKG) which blocks (red lines) smooth muscle cell Ca^{2+} uptake and release from the sarcoplasmic reticulum, ultimately blocking activation of myosin light chain kinase (MLCK), myosin phosphorylation and contraction. The blue arrows indicate the pathway inducing contraction of smooth muscle tissue.

1.3 Reactive oxygen species

As mentioned in the early part of the introduction (section 1.1), reactive oxygen species (ROS) are products of normal metabolism and can be beneficial or harmful to cells and tissues depending on their concentration. Gerschman *et al*. (1954) came up with an idea that oxygen may be toxic to cells and that partially reduced forms of oxygen were responsible for this toxicity. The next breakthrough in the identification of ROS occurred when a weak electron paramagnetic resonance signal was attributed to the presence of oxygen free radicals in a number of lyophilized biological materials (Commoner *et al*., 1954). The next major leap forward came in the discovery of the antioxidant enzyme superoxide dismutase (SOD), which provided conclusive evidence for the presence, and importance of ROS in biological systems (McCord and Fridovich, 1969).

This research has led to a vast number of papers that have shown biological systems are not only able to coexist with ROS but use them to their advantage for a number of

biological processes. ROS are molecules containing oxygen that are highly reactive due to the presence of unpaired valence shell electrons that are highly reactive (Halliwell and Cross, 1994). ROS can be split into two groups: the first is the O_2-derived free radicals, $O_2^{\bullet-}$, $HO^{\bullet}$, peroxyl ($RO_2^{\bullet}$) and alkoxyl ($RO^{\bullet}$) radicals etc. The second group is the O_2-derived non-radical species such as hydrogen peroxide (H_2O_2) (Halliwell and Cross, 1994).

ROS species can have beneficial effects on biological systems, usually in low concentrations, as they can take part in cellular signaling and in the defence response to infectious agents (Valko *et al*., 2006). The harmful effects of ROS will be discussed in length in the subsections of this section.

1.3.1 Superoxide anion radical

The $O_2^{\bullet-}$ radical is generated by the reduction of molecular oxygen (O_2). A one-electron addition to molecular oxygen is used to create this free radical species (Eq 1.10) (Raha and Robinson, 2000). Despite being a free radical, the species is thought to be relatively unreactive as it is unable to penetrate lipid membranes and so is localized to the place in which it was produced. The superoxide anion radical is mainly produced in mammals by the mitochondrial electron transport chain. The main locations of this in the mitochondria are at complex I, where superoxide is generated in the matrix, and complex III, where it is produced on both sides of the inner membrane (St-Pierre *et al*., 2002).

$$O_2 + e^- \longrightarrow O_2^{\bullet-}$$

Equation 1.10

The major enzyme involved in catalyzing the reduction of the superoxide anion is SOD, an enzyme which catalyses the disproportionation of the superoxide anion to hydrogen peroxide and oxygen (equation 1.2).

$$2O_2^{\bullet-} + 2H^+ \longrightarrow H_2O_2 + O_2$$

Equation 1.11

1.3.2 Hydrogen peroxide

The major source of hydrogen peroxide in the cell is the dismutation of superoxide (Eq 1.11). Hydrogen peroxide is thought to be much more reactive than the superoxide anion radical because of its ability to move through biological membranes. Although hydrogen peroxide is thought to pass freely across biological membranes this movement is regulated by the lipid and protein composition of the membranes, as well as the presence of hydrogen peroxide carriers such as aquaporins (Bienert *et al*., 2007). Although it is not a radical species it does play a large role in radical formation, reacting to form more reactive ROS such as the hypochlorous acid (HOCl) and the •OH. The H_2O_2 is removed by at least three antioxidant systems: catalases (Alfonso-Prieto *et al*., 2009), glutathione peroxidases (Battin and Brumaghim, 2009) and the peroxiredoxins (Chae *et al*., 1999). Hydrogen peroxide is a very good electrophile and participates in substitution reactions.

1.3.3 Hydrogen peroxide redox signaling

Hydrogen peroxide is able to modify specific and important amino acid side chains residues of proteins. Three of the amino acid side chains (Trp, Tyr, and Phe) contribute significantly to the UV absorption of a protein at 280 nm. The chemical reactivity of the side chains is important in understanding the properties of the proteins. Many of the side chains are nucleophiles. These modifications are usually reversible and form the basis of the redox signaling abilities. The redox signaling either occurs by the direct modification of amino acid residues or indirectly through the products of their reactions blocking important residues that will inhibit the protein function (Salemeen *et al*., 2003; van Montfort *et al*., 2003). Hydrogen peroxide has also been shown to induce conformational changes in target proteins that can also affect protein function (Storz *et al*., 1990). Cysteine is the most easily oxidised especially reactive cysteines in active sites of enzymes.

1.3.4 The hydroxyl radical

The hydroxyl radical is thought to be the most reactive and therefore the most damaging of all the ROS. The hydroxyl radical is produced by the reduction of hydrogen peroxide, which is catalyzed by the presence of transition metal ions such as iron (Fe^{2+}) and copper (Cu^{+}) ion in a reaction known as the Fenton reaction (Eq 1.12) (Winterbourn, 1995).

$$H_2O_2 + Fe^{2+}/ Cu^{+} \longrightarrow \bullet OH + HO^{-} + Fe^{3+}/ Cu^{2+}$$

Equation 1.12

Hydrogen peroxide undergoes a redox reaction producing a hydroxyl anion and a hydroxyl free radical in the presence of a metal catalyst.

1.3.5 Production sites of reactive oxygen species in the body

Within the eukaryotic cell there are a number of different producers of ROS: of the total O_2 consumed by mitochondria 2% is converted to ROS (Turrens, 2003). The mitochondria are the most common site for the dismutation of the superoxide anion radical and the breakdown of hydrogen peroxide in the Fenton reaction. Peroxisomes form the major source of cytosolic hydrogen peroxide. Peroxisomes are a single membrane organelle present in eukaryotic cells that play a major role in lipid metabolism and the metabolism of many other organic substrates (Wanders *et al*., 2010).

1.4 Antioxidant enzymes

Cells have developed a number of mechanisms such as interacting enzyme networks for the detoxification of ROS. The first ROS-metabolizing enzyme that was discovered was the previously discussed zinc and copper ion containing SOD (Dougherty *et al*., 1978). This enzyme is able to catalyse the reaction of two molecules of the superoxide anion radical together with two hydrogen ions converting them into molecular oxygen and hydrogen peroxide (Liochev and Fridovich, 2010) (Eq 1.13).

Catalase, another antioxidant enzyme, contains a haem group and will catalyse the dismutation of hydrogen peroxide to water and molecular oxygen (Deisseroth and Dounce, 1970) (Eq 1.14).

$$2O_2^{\bullet -} + 2H^+ + e^- \longrightarrow H_2O_2 + O$$

Equation 1.13

$$2H_2O_2 \longrightarrow 2H_2O + O_2$$

Equation 1.14

Selenocysteine containing enzymes such glutathione peroxidases (GPx) have been found to detoxify organic hydroperoxides (ROOH) by their conversion to alcohols while forming a glutathione disulfide (GSSG) (Eq 1.15) (Epp *et al*., 1983).

$$ROOH + 2GSH \longrightarrow ROH + GSSG + H_2O$$

Equation 1.15

The system that this study focuses on is the peroxiredoxin system. The peroxiredoxin system contains a number of enzymes (four enzymes: thioredoxin reductase (TrxR), thioredoxin (Trx), peroxiredoxin 2 (Prx2), sulfiredoxin and a cofactor; nicotinamide adenine dinucleotide (NADH)) that interact to reduce peroxide substrates using redox active cysteine residues (Hofmann *et al*., 2002).

1.4.1 The biological redox chemistry of cysteine

Cysteine (Cys) is an amino acid that contains a side chain thiol (SH) group (Fig1.8). Cysteine can play an important role in the folding (and therefore structure) and stability of some proteins through the formation of disulfide bonds

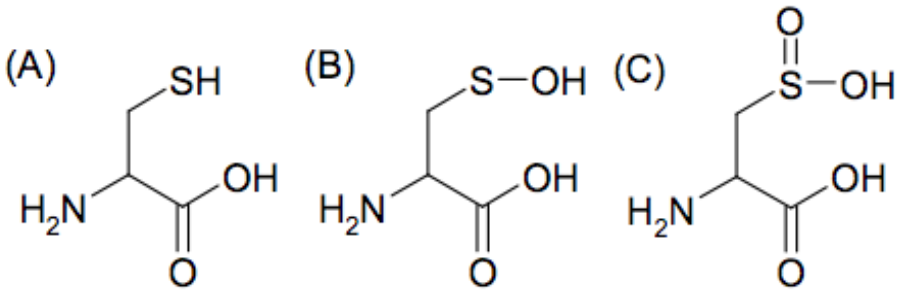

Figure 1.8. The chemical structure of the amino acid cysteine in the thiol (A), sulfenic acid (B) and sulfinic acid form (C).

The thiol group is important in the detection of hydrogen peroxide (Jackubowski, 2013). The rate of reaction between the protein thiol group and hydrogen peroxide is very important in redox signaling. The two most important factors in the reactivity of the thiol group are the ability of the cysteine residue to be deprotonated to the thiolate anion, as shown in equation 1.16, and how accessible this thiol group is.

$$\text{Protein-S-H} \rightleftharpoons \text{Protein-S}^- + \text{H}^+$$

Equation 1.16

The cysteine residue thiol group is nucleophilic and has a p*K*a of 8.5. This p*K*a is close to neutral in the cell and so the thiol group is often seen in its reactive thiolate (S^-) form, which is highly nucleophilic often found in active site of dehydrogenase (GAPDH) enzymes (Bulaj *et al*., 1998). The reactivity of the thiol for example group is highly linked to pH, which shows the importance of the thiolate form in the reactivity of the cysteine residue (Jocelyn, 1972).

The structural environment in which the thiol group is located can also play a large role in the reactivity of the group (Friedman, 1973) as the environment will usually provide a positively charged residue to stabilize the negative charge on the thiol group. The structural environment will also play a large role in the accessibility of the thiolate anion. As well as the thiol, there are three other species involving the sulfur atom of the cysteine side chain that are of interest in this project. These are the sulfenic acid (R-SOH), sulfinic acid (R-S (O) OH) and the disulfide form (R-S-S-R). There is a switch in the oxidation state of sulfur between the thiol (-2), sulfenic acid (0) and sulfinic acid (+2) states.

1.4.2 Reaction of thiol with hydrogen peroxide

As mentioned earlier, the reaction of the thiol group usually proceeds through the thiolate ion produced depending on the environment of the cysteine residue. This thiolate ion is a highly reactive nucleophile and its oxidation reaction with hydrogen peroxide (H_2O_2) produces a sulfenic acid as well as a molecule of water, as illustrated in equation 1.17 (Jacob *et al*., 2004). The thiolate ion formation is not the only

prerequisite for the reaction with H_2O_2. It was discovered by studying the rates of different thiol containing enzymes (Stone, 2004) that the reaction also requires residues around the active site cysteine that are able to stabilize the reaction intermediate (Tosatto *et al*., 2008).

$$\text{Protein-S}^- + H_2O_2 + H^+ \longrightarrow \text{Protein-SOH} + H_2O$$

Equation 1.17

1.5 What are S-nitrosothiols (RSNOs)?

The RSNOs are endogenous NO donors which are comprised of NO bound to the amino acid cysteine. The RSNO can be formed either via the reaction of thiols with N_2O_3, or NO-derived reactive intermediates, or through direct combination of NO and thiyl radicals. In addition, transnitrosation between RSNOs and thiols forms other RSNOs (Broniowska and Hogg, 2012; Thomas and Jourd'heuil, 2012). Probably the most important reaction of an S-nitrosothiol inside a cell or in a biological fluid is transnitrosation (Amelle and Stamler, 1995). The S-nitroso functional group can be transferred to a thiolate in a reversible reaction, as shown in (Eq 1.21) (RSNO can sometimes transfer directly NO^+ to another thiol). Stamler *et al.* (1996) have suggested that NO circulates in plasma mainly as S-nitroso (SNO) proteins; the majority of which is SNO albumin. It has been suggested that the relatively stable RSNOs serve as reservoirs or carriers of NO with which the biological action of NO can be regulated in a sustained manner (Stamler *et al* 1992 and 1994). With the advancement in bioanalytical methods, various RSNOs have been detected and identified in biological systems (Grisham *et al*., 2000; Paige *et al.,* 2008) and the *S*-nitrosoproteome has recently received much attention in the fields of proteomics and nitric oxide research (Chen *et al*., 2010; Doulias *et al*., 2010; Seth and Stamler 2011; Foster, 2011). While we support the principle advanced by Stamler and colleagues that NO circulates in plasma mainly as S-nitroso their proposed mechanisms have been challenged by multiple laboratories: Neil Hogg, Mark Gladwin and Rakesh Patel, strongly disagree with Jonathan Stamler.

Hogg 2002 criticised the methodological flaws and the experimental techniques applied: characterization, measurement and tissue localization of RSNOs which are difficult. The importance of S-nitrosothiols for NO storage and long-distance transport under some circumstances (i.e. pharmacological application of NO or NO donor drugs) is now widely accepted (Rassaf *et al.*, 2002). However, there is a lot of controversy with the suggested concept of RSNO-based NO stores to explain the reports of low concentrations of S-nitrosothiols in normal human plasma ranging from 10 nM to 20 nM (Giustarini *et al*., 2007). Nitrite (Bryan *et al*., 2005) and nitrated fatty acids (Baker *et al*., 2005 and Schafer *et al*., 2005) are increasingly considered as the alternative to NO reservoirs (Wang *et al*., 2004), since these species can also induce NO-like vasodilation (Morin *et al.,* 2001; and Lima *et al*., 2005). Gladwin *et al*, say that NO circulates in plasma mainly as NO_2^- (Gladwin *et al*., 2006). A major challenge facing the nitrite-reductase hypothesis is the question of how does NO escape the red cell following nitrite reduction? As discussed earlier (see section 1.1.1), the half-life of NO in a red cell is estimated to be less than 2 microseconds. Calculations suggest that any NO formed in a red cell could never escape the scavenging reactions of deoxy- and Hb (see section 1.2.7). Despite these theoretically insurmountable obstacles, recently sulfhydryl (SH) containing macromolecules were reported as possible NO carriers (Chen *et al*., 2012) that control the delivery of NO. In theory, virtually all proteins with free cysteine SH groups can be chemically modified into RSNOs. *In vivo* however, most of the efforts have been dedicated to developing macromolecular NO systems using the most abundant plasma protein –albumin (Chen *et al*., 2012). The main product from the reaction of RSH and NO under anaerobic conditions are RSOH and N_2O whilst under aerobic conditions a redox S-nitrosation reaction occurs (DeMaster *et al.,* 1995) (Eq 1.20).

1.5.1 Formation of S-nitrosothiols

S-nitrosation of thiols *in vivo* can be via acidified nitrite in the gut (Foster *et al*., 2003; Giustarini *et al*., 2007), via a radical mechanism (Gow *et al.,* 1997; Kolberg *et al*., 2002), or via transnitrosation or through the reaction of cysteine with dinitrogen trioxide (N_2O_3) (Schrammel *et al*., 2003; Miersch and Mutus 2005) (see Eq 1.18 to 1.20) below.

S-nitrosation of protein thiols

$$2NO + O_2 \longrightarrow 2NO_2$$

Equation 1.18

$$NO + NO_2 \longrightarrow N_2O_3$$

Equation 1.19

$$N_2O_3 + RSH \longrightarrow RSNO + NO_2^- + H^+$$

Equation 1.20

$$RS^*H + RSNO \rightleftharpoons RS^*NO + RSH$$

Equation 1.21

The occurrence of the pathway of S-nitrosation of protein thiols described in (Eq1.18 to 1.20) above, has been generally defied because the oxidation of NO radical in aqueous solution is slow compared to that in a polar environment (Giustarini *et al*., 2007) but this is being reconsidered following the change of approach i.e. after the development of the concept of the molecular lens effect (Chen *et al*., 2012). The concept states that NO radical and oxygen concentrate in hydrophobic areas such lipid membranes and hydrophobic pockets of proteins for example Hb, hence resulting in the increase of nitrosating species (Herold and Rock, 2005).

Now a number of methods (Chen *et al*., 2012; Majmudar and Martin, 2014) are available for the *in vivo* synthesis of RSNOs, including the use NO gas, acidified nitrite and transnitrosation.

1.5.2 S-nitrosation as a post-translational modification of proteins

As mentioned formerly in section 1.1, the discovery of the biological functions of NO in the late 1980s (Murad, 1986) came as a surprise. This raised controversy over the biological mechanisms of NO transport, from its place of production to its multiple effectors, to explain the endocrine properties of NO. It is now recognized that NO and its related species can introduce posttranslational modifications of proteins using different routes. The metabolic half-life of NO is known to be short, in the region of seconds (Beckman and Koppenol 1996). In nature, S-nitrosothiols (RSNOs) act as stable NO carriers (Ssu-Han *et al*., 2012). *In vivo,* NO is enzymatically formed in reactions catalysed by various types of nitric oxide synthases (NOS) (Alderton *et al.,* 2001) and by nitrite reductases (as described earlier in section 1.2.1). Once formed, the gaseous free-radical molecule acts through direct and indirect pathways (Wink and Mitchell, 1998). The direct mechanism involves direct binding of NO to the haem iron of soluble guanylyl cyclase (sGC), thereby resulting in enzyme activation. The indirect pathway requires reactions of NO with multiple molecular targets (e.g., oxygen, superoxide), which transforms NO into various reactive (unstable) intermediates, *i.e.*, reactive nitrogen and oxygen species (Alderton *et al*., 2001). S-nitrosation, the covalent attachment of the NO moiety to a cysteine, is established as a key post-translational modification of native peptides in animals (Yigin *et al.,* 2006). The term nitrosation indicates an electrophilic reaction involving attack by NO^+ or a carrier of NO^+ at a nucleophilic centre (like amine, thiol, or hydroxyl residues). It should not be interchanged with the term nitrosylation, which indicates an addition of NO without change in the formal charge of the substrate, e.g., addition of NO to haem proteins. According to Lancaster (1994), NO was a freely diffusible second messenger, with a loose sphere of influence, functioning mostly through the regulation of guanylate cyclase. Most recently, however, evidence has resulted in a critical reassessment of this initial archetype, as NO signaling was increasingly found to occur independently of this key regulatory enzyme. The rich redox and additive chemistry of NO facilitates its interactions with centres of iron-sulphur clusters and haem, present in a wide variety of proteins, impacting their activities (Stamler, 1994). Over the last decade, S-nitrosation has been demonstrated to regulate an increasing number of signaling systems, structural proteins, and metabolic processes in animals (Hess *et al*., 2005). There is also a developing appreciation of the precise spatial and temporal regulation of SNO

formation, which confers an exquisite specificity of NO signaling (Stamler *et al*., 1997). S-nitrosation has now become established as the prototypic, redox-based, post-translational modification within the animal sciences.

The NO moiety required for S-nitrosation can be derived from a diversity of sources in addition to NO, including other NO_x species, metal-NO complexes, peroxynitrite, nitrite, or SNOs. At the moment, specific enzymatic mechanisms responsible for S-nitrosation have not been identified; however, several enzymes are known to promote S-nitrosation reactions. Caeruloplasmin for example catalyses the S-nitrosation of the proteoglycan, glypican and it can also promote the formation of S-nitrosoglutathione (GSNO) from NO (Inoue *et al.,* 1999).

1.5.3 Biological functions of RSNOs

S-nitrosothiols are known to be involved in regulating vasodilatation, platelet aggregation and cell signaling (Longford *et al.*, 1994; Emery, 1995; Ceron *et al*., 2001 and Orie *et al*., 2005). Various RSNOs are known to cause blood-vessel dilation via cGMP dependent (Kwak *et al*., 2006) (Fig 1.9) and independent pathways (Gupta *et al*., 1995; Travis *et al.*, 2000 and Ceron *et al*., 2001).

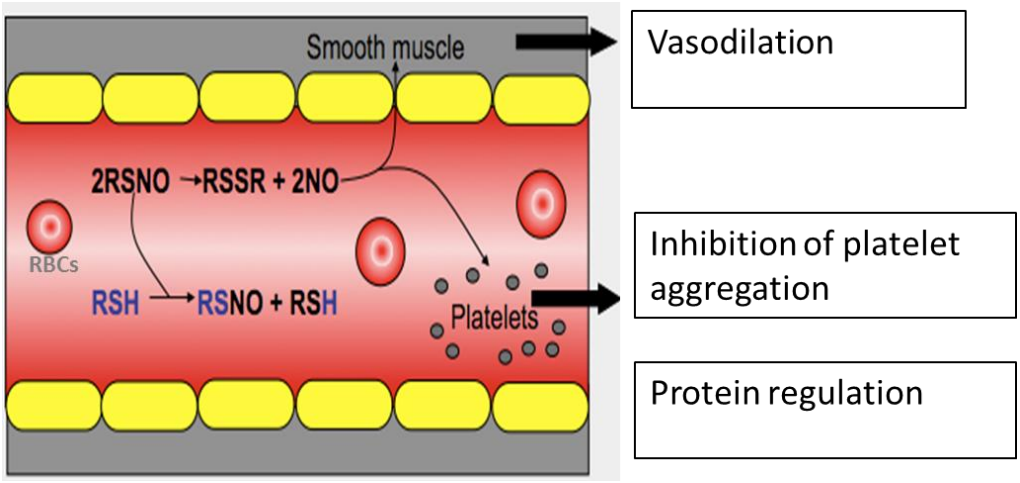

Figure 1.9 A diagram showing some of the biological activities of RSNO. The diagram was modified from Sarr, M*. et al*, 2005.

Another controversial link between RSNOs and control of vascular function involves the rate of S-nitrosohaemoglobin (Hb-SNO) in controlling oxygen delivery (Jia *et al*., 1996; Stamler *et al*., 1997; Guistarini *et al*. 2004; Zhang and Hogg, 2004b). Stamler *et al* (1998) suggested that Cys93 of the haemoglobin beta-chain is the key residue responsible for binding NO. At a low pressure of oxygen, such as in a constricted or respiring blood vessels, Hb undergoes a conformational change during which it releases NO as well as oxygen. Then NO induces smooth muscle relaxation and the blood flow is increased to meet the high oxygen demand. Protein-SNO such as S-nitrosoalbumin and nitroso-derivatives of haemoglobin, were proposed to act as a stable reservoir of NO, which can be used when needed (Stamler *et al*., 1992a; Stamler *et al*., 1992b). However, the evidence from Gladwin *et al* (2002b) and Salvati *et al* (2001) disagreed with the proposed mechanism. They demonstrated that Hb-SNO degraded rapidly independently of oxygen saturation.

1.5.4 Decomposition of RSNOs

On the decomposition of RSNOs, either nitric oxide as NO, or NO^+, or NO^- is released *via* the dissociation of the S-N bond (either a homolytic or heterolytic break, as shown in equations 1.22 – 1.24 (Stamler and Tone, 2002; Wang, 2002).

$$RSNO \longrightarrow RS + NO \text{ (hemolytic)} \quad \textbf{Equation 1.22}$$

$$RSNO \longrightarrow RS^{+} + NO^{-} \text{ (heterolytic)} \quad \textbf{Equation 1.23}$$

$$RSNO \longrightarrow RS^{-} + NO^{+} \text{ (heterolytic)} \quad \textbf{Equation 1.24}$$

RSNO is decomposition induced by temperature (Shishido *et al.,* 2003): light (Shishido *et al.,* 2003), pH (Williams, 2004), metal ions (such as copper, mercury and iron) (Williams, 1996; Noble and Williams, 2000, free thiols (Scorza *et al*., 1997). The presence or the absence of the above mentioned species may play an important role in the release of NO from RSNOs *in vivo*.

1.5.4.1 Thermal decomposition and photolysis of RSNOs

As discussed in section 1.5.4, RSNOs decomposition is dependent on temperature. Shishido *et al*. (2003) reported the release of NO from gel-incorporated RSNOs to be higher at 37°C than lower temperatures. The reaction products from this reaction are NO and RSSR as the bond breaks in a hemolytic fashion (Eq. 1.22) (Williams, 1999). It is also true that the homolytic decomposition of RSNOs can occur when the compounds are irradiated at 335 nm or 540 nm (Williams, 1999).

The exposure of RSNOs to the increased temperature and light forms the basis of controlled delivery of NO from RSNOs (Shishido *et al*., 2003). Therefore, it is a common practice to store RSNOs in the dark below 4°C (Tullett *et al.,* 2001).

1.5.4.2 Effect of metals on the stability of RSNOs

A range of metal ions catalyses the decomposition of RSNO, these include: mercury (Hg^{2+}), copper (Cu^{+}) and iron (Fe^{2+}) cations (Cook *et al*., 1996). Hg^{2+} catalyses the rapid and specific decomposition of RSNOs to nitrite (Eq. 1.25), with reaction yield of 100% RSNO decay. Therefore, Hg^{2+} is often used in the detection of RSNOs (for example in the Saville reaction described by Saville, 1958) in order to distinguish between RSNOs and NO metabolites such as nitrite.

$RSNO + Hg^{2+} + H_2O \longrightarrow RSHg^{+} + HNO_2 + H^{+}$ (**Equation 1.25**)

RSNO decomposition is also induced by copper. However, unlike mercury, copper acts as a catalyst and causes the release of NO rather than nitrite (Eq. 1.26-1.28) (Stubauer *et al*., 1999). The inconsistent stability of RSNOs both *in vitro* and *in vivo* is attributed by the intrinsic Cu^{2+} in the samples. It has been reported that the presence of Cu^{2+} increases RSNO-induced vasorelaxation, and their absence may be responsible for the lack of RSNO-vasorelaxation during pre-eclampsia (Gandley *et al*., 2005).

$Cu^{2+} + 2RS^{-} \longrightarrow Cu^{+} + RSSR$ (**Equation 1.26**)

$Cu^{+} + RSNO \longrightarrow Cu^{2+} + RS^{-} + NO$ (**Equation 1.27**)

$2RS^{-} \longrightarrow RSSR$ (**Equation 1.28**)

Some evidence suggests that iron also has a major effect on the stability of RSNOs (Vanin *et al*., 2002). However, irrespective of the metal species, metal-induced RSNO decomposition can be stopped by the addition of metal ion chelators, such as EDTA to RSNO samples.

1.6 Transnitrosation of protein thiols

The RSNOs can directly transfer NO^{+} to another thiol (see Eq. 1.21 in section 1.5.1) (transnitrosation). Previous work on the physiological chemistry of *S*-nitrosothiols indicates that they can release NO in the presence of cuprous ion (Dicks and Williams 1996), ascorbate (Masato *et al*., 1996), or thiols (Scorza *et al*., 1997).

The S-nitrosothiols serve as a possible source of nitroxyl (NO^{-}) ions (Oae *et al.,* 1978) and can undergo transnitrosation reactions (Barnett *et al*., 1994; Dicks and Williams 1996) (see Eq. 1.21 in section 1.5.1).

The transnitrosation reaction involves the nucleophilic attack of a thiolate anion on the nitroso nitrogen. Since the products of this reaction are an S-nitrosothiol and a thiol, a similar reaction in reverse will yield the original reactants. If one of the species in

Eq.1.20 is a protein, then this reaction represents a mechanism of S-nitrosation or S-denitrosation of protein. The equilibrium position of (Eq.1.21) will depend on the ratio of the forward and reverse-rate constants (Hogg, 1999). The reaction in (Eq.1.20) does not require a separate redox partner as 2005 demonstrated by the direct reaction of SNOG with mitochondria aldehyde dehydrogenase (Moon *et al*., 2005). The rate of the reaction is second order and depends on the pKa of the thiol group and the accessibility of the thiol group (Rossi *et al.*, 1997; Gladwin *et al.,* 2002b).

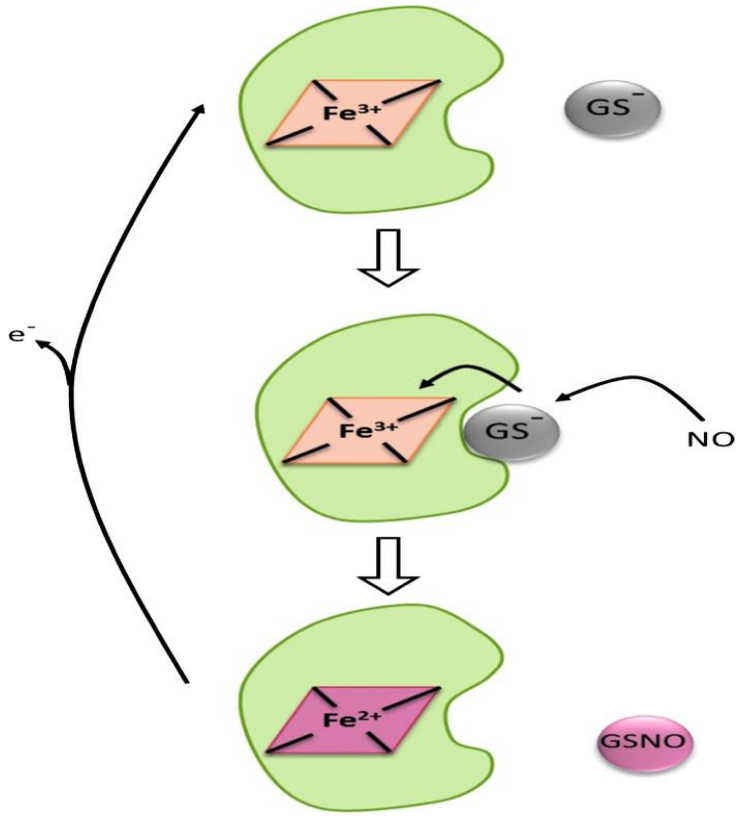

Figure 1.10 Cytochrome c-dependent S-nitrosothiol formation. Ferric cytochrome c weakly binds glutathione, and forms a complex which reacts with NO to form GSNO and ferrous cytochrome c. The process becomes catalytic when cytochrome c is further oxidised by, for example, mitochondrial complex IV (the scheme was taken from Katarzyna *et al.,* 2012).

Transnitrosation is also dependent on the pKa and the accessibility of the reactive groups. For example the rate constant for the reactions of HSA and cysteine with GSNO are 1.15 and 57 $M^{-1}s^{-1}$ respectively, according to a number of studies conducted with samples treated with N-ethylmaleimide (NEM) to improve the stability of RSNO (Orie *et al*., 2005). The job of NEM is to prevent the transnitrosation reaction from taking place by reacting with the sulfur of free thiols. Transnitrosation reactions are not particularly fast and can vary between about 0.1 and 500 $M^{-1}s^{-1}$(Rossi *et al*., 1997; Patel *et al.,* 1999), depending on the nature of the reactants. In the absence of all other factors, the distribution of S-nitrosothiols within a cell will depend on the kinetics and equilibria of such reactions, and while the catalysis of transnitrosation by enzymes such as thioredoxin (Mitchell and Marletta, 2005) may change the kinetics of this reaction, it will not change the equilibrium position. There are many examples of studies of isolated proteins that show preferential S-nitrosation of a single site on the protein after exposure to a low-molecular-mass S-nitrosothiol. A classic example is human Hb that is relatively selectively S-nitrosated on the cysteine residue (as discussed in section 1.5.3) on exposure to S-nitrocysteine (Wolzt *et al.*, 1999) or GSNO (Stamler *et al.,* 1996).

1.6.1 Detection of RSNOs

A number of techniques are available for the detection of RSNOs *in vitro* and *in vivo* and has been thoroughly reviewed by (Giustarini *et al*., 2007). These include: spectroscopic techniques, EPR spectrometry chemiluminescence, fluorescence, electrochemistry and the biotin switch antibody method. However, there is a great variation given in the quantification of RSNO *in vivo*, an indication that no method for the detection of RSNOs is yet perfect (Giustarini *et al*., 2007).

1.6.2 Haemoglobin

The main function of red cells is oxygen transport to tissues and that is possible thanks to a metalloprotein, haemoglobin, firstly described from Perutz in 1960 (Perutz, 1960). A mature RBC contains about 270 million Hb molecules, which comprise over the 95 % of cytoplasmic proteins. Hemoglobin (Hb) has an oxygen binding capacity of 1.34 ml O_2 per gram (Dominguez *et al*., 1981), which increases the total blood oxygen capacity seventy-fold compared to dissolved oxygen in blood.

Hb is the most abundant red blood cells (RBC's) protein, making up 96% of the RBC's dry content (by weight), and around 35% of the total content (including water) (Wead *et al*., 1963), and is the iron containing oxygen-transport metalloprotein in the RBC's and vertebrates (Hopkins, 1993). Hb is made up of four protein subunits (globulin chains) that interact together. The normal adult Hb molecule contains two α-globulin chains and two β-globulin chains. In fetuses and infants, β-chains are not common and the Hb molecule is made up of two α chains and two gamma (γ) chains (Jean Hopkins, 1993). As the infant grows, the γ-chains are gradually replaced by β-chains, forming the adult Hb structure, which is a tetramer with four haem iron centres. The haem is vital in transporting oxygen and carbon dioxide in our blood. The iron contained in Hb is also responsible for the red color of blood (Wead *et al*., 1963). The Hb also plays an important role in maintaining the shape of the RBC's. In their natural shape, RBC's are round with narrow centres resembling a donut without a hole in the middle (Kessel *et al*., 2003). Abnormal Hb structure can, therefore, disrupt the shape of RBC's and impede their function as seen in sickle cell anaemia and flow through blood vessels.

When oxygen binds to the iron complex, it causes the iron atom to move back towards the center of the plane of the porphyrin ring (Chou, 1989). At the same time, the imidazole side-chain of the histidine residue interacting at the other pole of the iron is pulled toward the porphyrin ring. This interaction forces the plane of the ring sideways toward the outside of the tetramer, and also induces a strain in the protein helix containing the histidine as it moves nearer to the iron atom (Chou, 1989). This strain is transmitted to the remaining three monomers in the tetramer, where it induces a similar conformational change in the other haem sites such that binding of oxygen to these sites becomes easier. This is called co-operativity. The binding of oxygen in a normal adult Hb is a cooperative process (Chou, 1989). Therefore, the binding affinity of Hb for oxygen is increased by the oxygen saturation of the molecule, with the first oxygens bound influencing the shape of the binding sites for the next oxygens, in a way favorable for binding. This positive cooperative binding is achieved through steric conformational changes of the Hb protein complex as discussed above; i.e., when one subunit protein in Hb becomes oxygenated, a conformational or structural change in the whole complex is initiated, causing the other subunits to gain an increased affinity for oxygen.

1.6.3 The interactions of nitric oxide and haemoglobin

In the last decade, the interactions of NO and Hb have become the subject of much interest. The NO reacts very vigorously with Hb to form a stable complex of either Hb[Fe-NO] (nitrosylated) or Cys93(SNO-Hb) (nitrosated). Understanding the interactions of NO with RBC's is vital to elucidating the metabolic fate of NO in the vasculature. Hb is the most abundant intraerythrocytic protein, and reacts rapidly with NO. The interaction of NO with Hb has been studied extensively (Tae *et al*., 2002). The NO reaction with RBCs is nearly 1,000-fold slower than the reaction with cell-free Hb (Tae *et al*., 2002). However, the reaction rate of NO with cell-free Hb and RBC's is different (Tae *et al*., 2002) (explained in section 1.6.3).

Hb denotes both oxygenated and deoxygenated Hb. The reactions of NO with cell-free Hb, and red blood cell-encapsulated Hb have been investigated extensively for many years. The physiological importance of these reactions was established with the identification of NO as the endothelium-derived relaxation factor (Ignorro *et al.,* 1987; Palmer *et al*., 1987). The NO biology in the specific realm of the cardiovascular system has been predicted in two classic views: (1) NO binding to deoxygenated haem is noncooperative and effectively irreversible (Eq. 1.29), and (2) that NO reaction with oxyhaemoglobin yields methemoglobin and nitrate (Eq. 1.30). However, the NO interaction with RBC-encapsulated Hb is still a problem of considerable controversy, adding to the existing controversy in relation to how NO from RBC's cause vessel dilation. NO is inactivated by oxyHb at an extremely high rate ($k \approx 10^7$ $M^{-1} \cdot s^{-1}$) (Doyle and Hoekstra, 1981; Eich *et al*., 1996; Herold *et al*., 2001). How is NO bioactivity preserved in the cardiovascular system? Liao *et al*. (1999) demonstrated experimentally that an RBC-free zone near the vessel wall reduces the consumption of NO by RBC's. In addition, NO does not react with RBC-encapsulated Hb as rapidly as it does with cell-free Hb (Lancaster, 1994) because of an extracellular diffusion limitation (Liu *et al.,* 1998) and a sub-membrane diffusion barrier consisting of the RBC cytoskeleton and other comparatively NO-inert proteins such as MetHb (Vaughn *et al*., 2000; Huang *et al*., 2001).

Parallel with the diffusion barrier model of NO preservation, another model has been proposed which involves new chemistry to explain the preservation of NO bioactivity in

the vasculature (Gow and Stamler, 1998). The model suggested by Stamler and colleagues supports the nitrosation mechanism whereby, NO is transported on haemoglobin by binding to the highly reactive and conserved β-chain cysteine 93 residue, forming a stable complex, S-nitrosohaemoglobin (SNO-Hb) (Stamler *et al.,* 1996; Stamler *et al.,* 1997; Gow and Stamler, 1998; Bonaventura et al., 1999). One stipulation of this theory is that nitrosylated haemoglobin Hb[Fe(II)]NO is produced from the cooperative binding of NO to the minor population of free haem on normoxic Hb (≈99% oxyHb and 1% deoxyHb), thereby avoiding degradation of NO to nitrate. The formation of Hb[Fe(II)]NO in high concentrations is contrary to the original findings of Doyle and Hoekstra (Doyle and Hoekstra, 1981) and a later paper by Eich *et al.* (Eich *et al*., 1996). More recently, the formation of Hb[Fe(II)]NO has been investigated further by multiple laboratories (Gladwin *et al.*, 2001; Joshi *et al*., 2002). Another stipulation of this theory is that NO, is carried on haemoglobin β-chain cysteine 93, and is delivered from the lungs to the microvasculature where, on deoxygenation in the tissues, the S-nitroso linkage is weakened. This allows the NO molecules, to be freed from small thiols, to diffuse through the erythrocytes to the vascular walls to explain the endocrine role of NO.

The only evidence to date *in vivo,* of SNO-Hb measurements, was performed in the Sprague-Dawley rat. Therefore, the physiological significance in humans is questioned. The reaction of NO with haemoglobin, to form SNO-Hb, is additional to two other well-characterised NO reactions namely: with oxyhaemoglobin to form methaemoglobin (FeIII) and nitrate ion, and with deoxyhaemoglobin to form Hb[Fe(II)]NO. The Hb[Fe(II)]NO reaction was recently subjected to great research interest. Kosaka and colleagues (1997) have demonstrated that Hb[Fe(II)]NO is a six-coordinate species whereby iron binds four nitrogens, a proximal histidine and NO. Hb[Fe(II)]NO is reported to demonstrate an enhanced Bohr effect, promoting oxygen release and increasing sensitivity to tissue acidosis (Yonetani *et al*., 1998).

According to Bohr's effect, haemoglobin's oxygen binding affinity is inversely related both to acidity and to the concentration of carbon dioxide. The loss of the oxygen binding site which is replaced by NO, may explain why Hb[Fe(II)]NO may therefore effectively deliver oxygen than pure oxyhaemoglobin to regions with very low oxygen

tensions (Kosaka and Seiyama, 1997). The amount of Hb[Fe(II)]NO formation in the body is unclear. The sensitivity of electron paramagnetic resonance spectrometry is limited as the primary method for measuring the interactions of NO with Hb. Different approaches have been applied using *in vitro* NO-oxyhaemoglobin reactions, using relatively physiological conditions of oxygen saturation, ionic strength, and molar ratios (Gow *et al.*, 1999). Gow *et al* approaches suggested that the pathway might be equal in magnitude to the long-studied reaction of NO oxidation of ferrous to ferric haem (Gow *et al.*, 1999). The *in vitro* measured results of Hb[Fe(II)]NO; SNO-Hb and FeIII were found comparable. The level of nitrosylation of haemoglobin in the human circulation is very low. A very sensitive technique with sensitivity levels of $1X10^{-5}$ (0.001%) mol of NO bound to haemoglobin per mol of haem subunit, (0.004% with respect to haemoglobin tetramer) is needed in order to detect the interaction (Gladwin *et al.,* 2000).

$$Hb[Fe(II)] + NO \rightleftharpoons Hb[Fe(II)]NO \qquad \textbf{Equation 1.29}$$

$$Hb[Fe(II)O_2 + NO \longrightarrow Hb[Fe(III)] + NO_3^- \qquad \textbf{Equation 1.30}$$

1.6.4 The effect of cell-free haemoglobin on the bioavailability of NO

Experimental evidence (Reiter *et al*., 2002; Torres *et al.*, 2005) and theoretical modelling (Kavdia *et al.,* 2002; Jeffers *et al.*, 2006) have established that the presence of cell-free haemoglobin in blood significantly reduces NO bioavailability of enzymatically generated NO. However, the possibility of NO release in the reaction of cell-free Hb with nitrite (Chen *et al*., 2008) made scientists ask whether cell-free Hb could serve as a NO producer, rather than being a scavenger, under hypoxic conditions, in which the enzymatically generated NO level is greatly moderated. According to simulations (Chen *et al*., 2008), this scenario is unlikely; the results demonstrated that under typical haemolytic conditions in which 20 µM cell-free haemoglobin is present in the lumen, only approximately 0.02 pM NO reaches smooth muscles. The results suggested that although the nitrite reduction by cell-free haemoglobin can occur close to the vascular wall, the NO delivered was still negligible (Chen *et al*., 2008). Under such conditions, the NO production rate from nitrite reduction is low and thus presumably cannot significantly contribute to the steady state of NO concentration. The results from Chen *et al.*, 2008) further confirmed that a higher level

of cell-free Hb can enhance the NO release from the RBC source, but also increases the scavenging rate of NO by haemoglobin, leading to a plateau in the NO concentration profile. Thus, a more concentrated cell-free Hb presence does not result in more net NO from the source; instead, it strengthens the scavenging effect of NO from other endocrine and paracrine sources.

1.7 The problem of NO escape from erythrocytes

As a result of the combination of the reduction of dietary nitrate and the oxidation of NO derived from NOS, nitrite concentrations in healthy human plasma and RBC's are about 100-300 nM (Crawford *et al*., 2006). Nitrite in the plasma can reversibly diffuse into RBC's (Dejam *et al.*, 2005). Thus RBC nitrite is a "storage form" of NO, and NO is released under hypoxic conditions (Crawford *et al.*, 2006; Feelisch *et al*., 2008; Gladwin *et al*., 2006; Pinder *et al*., 2009; Van Faassen *et al*., 2009). As mentioned (section 1.2.2) the identity of the nitrite reductase(s) is controversial. We previously showed that xanthine oxidoreductase has nitrite reductase activity Zhang *et al.* (1998) and several other groups such as Li *et al* (2003) and others confirmed this observation. It was also recently shown in our laboratory (Lo Faro *et al*, 2010) that hydrogen sulfide (H_2S) - a gasotransmitter, which exerts physiological effects similar to NO – can reduce nitrite and S-nitrosothiols to NO.

However, many of the latter experiments were done using isolated RBC's, the assumption having been made that the observed nitrite reductase activity in these cells was due to deoxyHb. The potential role in NO formation of the abundant RBC enzymes such as Prx2 (described in section 1.9.1), was apparently not considered. According to the mechanism described by Gladwin and colleagues (Gladwin *et al.,* 2012), nitrite-induced hypoxic vasodilatation involves at least three steps: first, the reaction of nitrite with deoxyHb; secondly, the escape of the NO produced from RBC's and, thirdly, the induction of vasodilatation by activation of soluble guanylate cyclases in smooth muscle cells, resulting in cGMP production (Jensen, 2009). The hypothesis we present that peroxiredoxin 2 facilitates the transfer of NO from RBCs to smooth muscle cells within the human vasculature:- provides a potential molecular pathway, which may explain how NO, is able to escape RBC's and how NO is able to exert functional effects at sites that are remote from RBCs.

1.8 The human erythrocyte

Erythrocytes, or red blood cells (RBCs), are anucleated cells with a typical biconcave shape; they are the major means of transport for O_2 in the body, O_2 being taken up from the lungs and delivered while moving through capillaries (Engelhardt and Arnold, 1975). Erythrocytes are thought to be exposed to oxidative stress from a wide range of different sources. Erythrocytes have been shown to possess large amounts of O_2 and Hb as part of their function, both of which are producers of the ROS, $O_2^{\bullet-}$ and H_2O_2 (Halliwell and Gutteridge, 1999; Alayash *et al*., 2001). Erythrocytes have a 120-day life span and are unable to produce new protein so they require robust antioxidant pathways to detoxify ROS before any damage can occur to the proteins contained within erythrocytes (Halliwell and Gutteridge, 1999; Alayash *et al*., 2001).

1.9 Peroxiredoxin

Peroxiredoxins (Prxs) are a family of multi-functional enzymes that protect against oxidative stress (Hofmann *et al*., 2002). Prxs are antioxidant enzymes that use the redox active cysteine residues to reduce an O-O bond present in hydrogen peroxide and a range of organic hydroperoxides (ROOH) (Peshenko and Shichi, 2001). Prxs are located mainly in the cytosol but have also been found in mitochondria, chloroplasts and peroxisomes (Hofmann *et al*., 2002). This is expected, as these are also the major sites of ROS production. Prxs can be produced at very high levels and are found to be the third most abundant protein in erythrocytes (Moore *et al*., 1991), and in the top ten most produced proteins in *Escherichia coli (E. coli)* (Link *et al*., 1997). The protein is also thought to form between 0.1 and 0.8% of the total soluble protein in other types of mammalian cells (Chae *et al*., 1999).

The Prxs are a ubiquitous family of enzymes that have been identified in yeast (Morgan and Veal, 2007), plant (Dietz, 2003) and animal cells (Miranda-Vizuete *et al*., 2000) as well as in bacteria and archaea (Dubbs and Mongkolsuk, 2007) and have been seen to increase levels of expression under oxidative stress conditions (Halliwell, 1999)

Prxs are split into two categories, the 1-Cys and 2-Cys Prx, based upon the number of redox active cysteines they possess. With further structural and mechanistic data

available the 2-Cys Prx were then further split into two sub- classes, the typical and atypical 2-Cys Prx. The typical 2-Cys Prx are homodimers than contain two identical active sites (Hirotsu *et al*., 1999a; Schroder *et al*., 2000; Alphey *et al*., 2000) (Fig. 1.9).

The atypical 2-Cys Prx are thought to behave in the same way, but are functionally monomeric with the redox active cysteines located on the same protein (Seo *et al*., 2000). It is thought that all of the different classes of Prx have the same first step in the mechanism and it is the recycling of the oxidised sulfenic acid form back to the reduced thiol state that differs.

Prx, thioredoxin, thioredoxin reductase and sulfiredoxin make up the peroxiredoxin system enzymes. There are six different sub forms of Prx (PrxI – VI) discovered in mammals. PrxI – IV are all typical 2-Cys Prx, PrxV is an atypical 2-Cys Prx and PrxVI is a 1-Cys Prx. The different sub forms of Prx differ in length (ranging from 198 – 271 amino acids), cellular location and the location on the human chromosome (Wood *et al*., 2003b). Prx I, II, III and V are reduced solely by thioredoxin (coupled with thioredoxin reductase and NADPH). Prx IV is able to use thioredoxin and glutathione, where-as Prx VI is only able to use glutathione.

Prxs have been shown to have catalytic efficiencies of ~10^{7} M^{-1} s^{-1} (Akerman and Muller, 2005). This catalytic efficiency is comparable to those of catalase, haem peroxidase and selenium-containing glutathione reductase (Wood *et al*., 2003b).

1.9.1 Peroxiredoxin 2 from human erythrocytes

Peroxiredoxin 2 from human erythrocytes (hPrx2) (EC 1.11.1.15) over the years has been known as thiroredoxin peroxidase B, natural killer enhancing factor-B (Shau *et al.*, 1994), thioredoxin-linked peroxidase (Chan and Kim, 1995). The gene encoding Prx2 is located on chromosome 19 (19p13.2).

The hPrx2 protein consists of 198 residues with a molecular weight of approximately 22 kDa (Moore and Shriver, 1994). In human erythrocytes, Hb is the most abundant intracellular protein in RBC, and peroxiredoxin 2 (Prx2) is the 3rd most abundant protein (Matte *et al*., 2012). The hPrx2 is thought to exist mainly in the reduced state under

native conditions due to the reductive environment within the erythrocyte. The hPrx2 is shown to have a high sensitivity towards H_2O_2 and is shown to result in formation of the disulfide intermediate (Low *et al*., 2007). It is believed that the recycling of the disulfide intermediate is relatively slow in the erythrocyte due to the relatively low amounts of thioredoxin reductase present, which can lead to the accumulation of disulfide hPrx2. The Prx2 is thought to be very important in the protection of the erythrocyte from H_2O_2 produced by Hb as mice deficient in Prx2 suffer from hemolytic anaemia (Low *et al*., 2008) whereas mice deficient in catalase or glutathione peroxidase do not (Johnson *et al*., 2000; Ho *et al*., 2004). The high abundance of Prx2 in RBCs raises questions, could it be that Prx2 plays a central role in protecting Hb against oxidative damage, and in mediating some of the key functions of Hb such as NO mobilisation from nitrite?

The presence of the two redox-active cysteines (Cys) (Fig. 1.9) means that Prx2 possesses free thiols, which can react with reactive nitrogen species to form S-nitrosothiols (Stamler *et al*., 1996). The function of Prx2 is not completely understood, although it is thought to be an antioxidant by virtue of its peroxidase activity (Han *et al*, 2012). Together with the Trx-TrxR (thioredoxin-thioredoxin reductase) system, Prx2 contributes to peroxide detoxification in RBCs (Low *et al*., 2007; Low *et al*., 2008). Due to the role of RBCs as carriers of oxygen (O_2), they are exposed to highly oxidising conditions. The Prx2 thus protects the cells as a crucial part of the RBC antioxidant defence system (Han *et al*, 2012). But possibly Prx2 has other functions which support the biological functions of Hb pertaining to NO metabolism, (this will be discussed in more detail in sections 1.10.1 – 1.10.3 and in sections 1.11- 1.13).

Figure 1.11. Protein sequence for hPrx2

1.9.2 The structure of hPrx2

A three dimensional crystal structure of purified human RBC Prx2 has been solved by Prof Littlechild's research group in Exeter (Schroder *et al*, 2000). The crystal structure of the decameric hPrx2 was solved to a resolution of 1.7 A. They have combined the decameric crystallographic structure of Prx2 with cryoelectron microscopy (Harris *et al.*, 2001). The crystal structure of hPrx2 showed to be in a decameric structure, is made up from five dimers linked end-on through predominantly hydrophobic interactions to form a toroid (Fig. 1.12), with point symmetry 52 (Schroder *et al*, 2000) with a maximal diameter of about 130 Å, an inside diameter of about 60 Å and thickness of about 50 Å. The Prx2 is proposed to represent an intermediate in the *in vivo* reaction cycle. The decameric structure of this protein had been observed previously using electron microscopy (Harris *et al*., 1969).

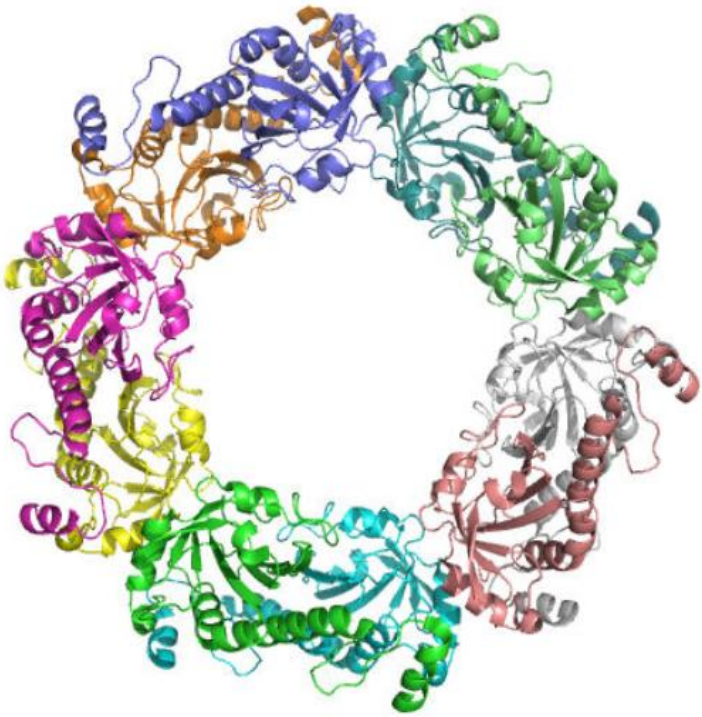

Figure 1.12 Cartoon representation of the decameric structure of hPrx2 from human erythrocytes (PDB: 1QMV) with each individual chain within the 5 homodimers being shown in a different colour (figure taken from Dr. Paul James' PhD thesis, 2010).

It was discovered that the monomeric structure could split into two domains (Dr. Paul James' PhD thesis, 2010). Domain I (residues 2-169) consists of five α helices, two 3_{10} helices and an extended seven-stranded β sheet. The second domain is the C-terminal arm (residues 170-198) and is made up of one α helix. The hPrx2 contains a thioredoxin fold, which consists of four β strands (β3, β4, β6 and β7) and four α helices (α1, α2, α4 and α5) (Schroder *et al*., 2000)

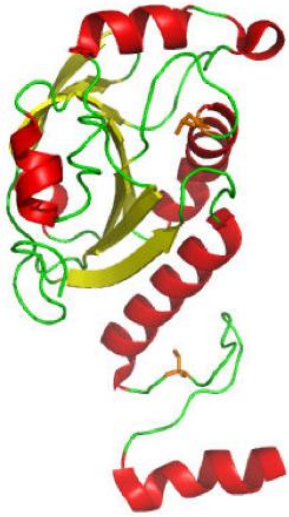

Figure.1.13 Cartoon representation of the monomeric unit from the decameric structure of hPrx2 from human erythrocytes (PDB: 1QMV). The redox active cysteines are shown in orange sticks with the loop regions shown in green, α helices shown in red and β sheets shown in yellow. Dr. Paul James (PhD thesis 2010) used PyMol DeLano Scientific computer software to create this image.

hPrx2 is thought to be functionally as a dimeric and the dimer within the decameric structure reveals an active site where the Cys_P and Cys_R, which are brought by different members of the homodimer and each dimer contains two redox active sites (Schroder *et al*, 2000). The dimer has an ellipsoidal shape with dimensions 52 Å x 53 Å x 60 Å. The dimer interface buries 2109 $Å^2$ (21 %) of solvent-accessible surface area per monomer. The dimer is held together by hydrogen bonds and hydrophobic interactions between the C-terminal arm of one monomer and domain I of the other monomer (Fg.1.13repres).

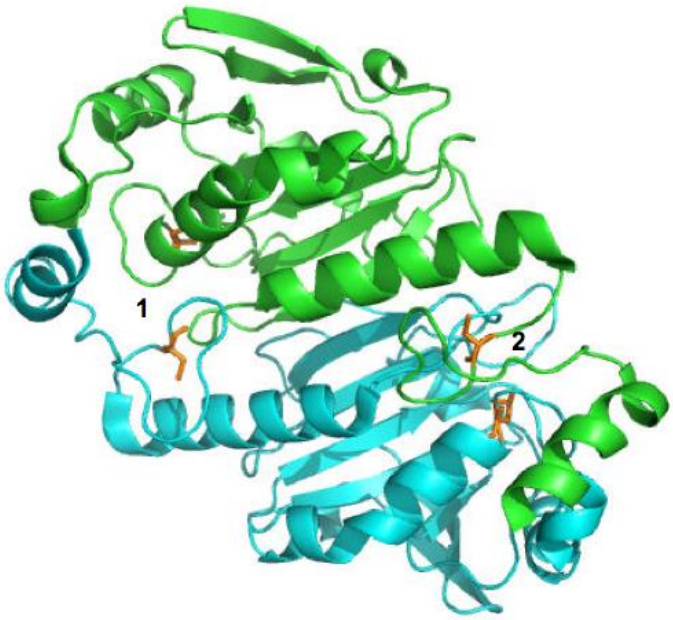

Figure 1.14 Cartoon representation of the homodimeric structure of hPrx2 from human erythrocytes (PDB: 1QMV) the two monomers are coloured differently one is coloured in green and the other coloured in blue. The dimer contains two redox active sites indicated by the numbers 1 and 2. The redox active cysteines are shown in orange in stick mode (PyMol DeLano Scientific computer software was used to create this image) (Dr. Paul James, PhD thesis, 2010).

1.9.3 The active site of hPrx2

The active site of hPrx2 is a homodimer with two active sites. Each active site is made up of two redox active cysteines; the Cys_P is located on the N-terminus of one chain and the Cys_R, which is located on the C-terminus of the other chain. In the crystal structure presented in Schroder *et al*., (2000), the Cys_P is shown to be in the hyper-oxidised sulfinic acid form that was thought to leave the protein inactive until the discovery of sulfiredoxin (Srx). The Cys_P is located in a hydrophobic pocket made up of residues Tyr43, Pro44, Thr48, Val50, Glu54, 34Trp86, Arg127, Arg150 and Val171 from the other subunit (Fig. 1.13) and from these residues both Thr48 and Arg127 have been confirmed as essential for activity through mutagenetic studies (Montemartini *et al*., 1999; Flohe *et al*., 2002; Dr. Paul James' PhD thesis, 2010). The Arg127 residue is essential as it lowers the p*K*a of the Cys_P during the first step of the reaction mechanism, which breaks the salt bridge (Montemartini *et al*., 1999).

The Cys_R (Cys172) is located in a polar environment that has limited solvent accessibility that could account for why the Cys_R does not undergo hyper- oxidation and is preserved in its thiol status (Dr. Paul James' PhD thesis, 2010). There is a ~10 Å gap between the Cys_P and the Cys_R which is too far away for an interaction between the two, meaning there must be a structural rearrangement that must occur to allow the two to interact (Schroder *et al*., 2000).

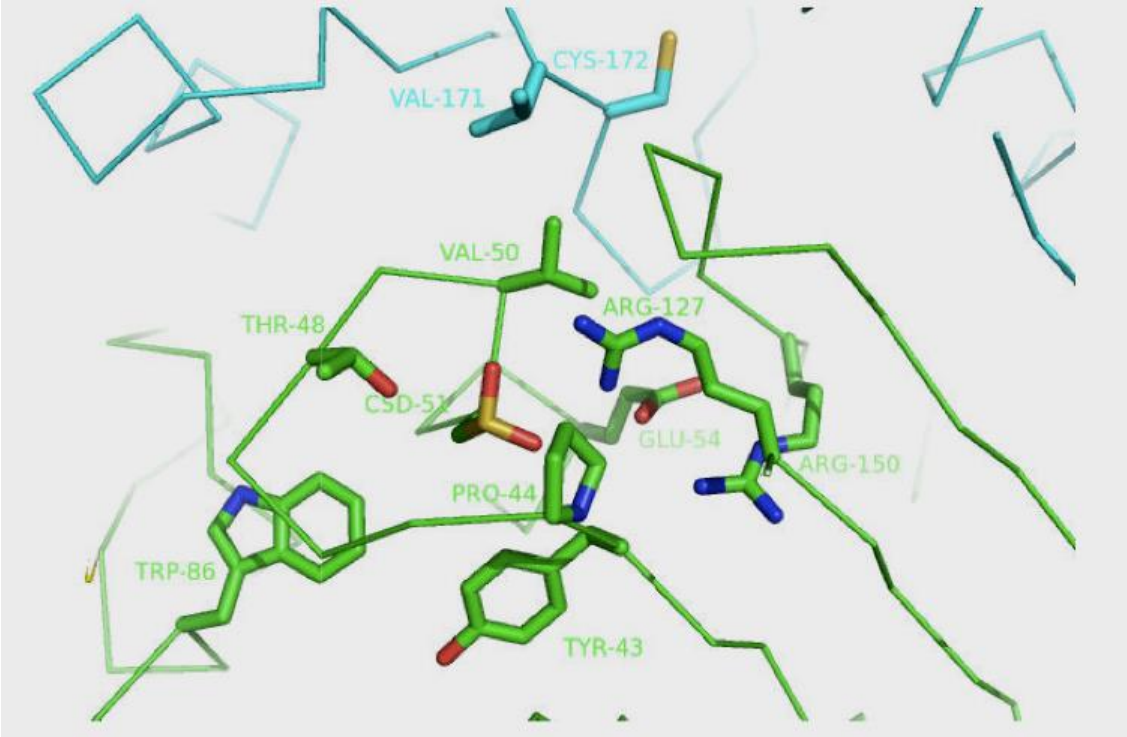

Figure 1.15 Ribbon and stick representation for the structure of the active site of hPrx2 from human RBCs, the hydrophobic region around the active site Cys_P (CSD51) of hPrx2 (PDB: 1QMV). The different subunits of the hPrx2 homodimer are shown in green and cyan (Dr. Paul James, PhD thesis, 2010).

1.9.4 Mechanism

The presence of the two redox-active cysteines (Cys) means that Prx2 possesses free thiols, which can react with reactive nitrogen species to form S-nitrosothiols (Jonathan Stamler *et al*., 1996). The function of Prx2 is not completely understood, although it is thought to be an antioxidant by virtue of its peroxidase activity (Han *et al*, 2012).

1.9.5 Oligomerisation state of hPrx2

Although proteins are known to be homodimeric, there was evidence for the oligomerisation of the protein to the decameric form as early as the 1960's when Torin now known to be hPrx2, a protein from human erythrocytes, showed complexes with tenfold symmetry when studied using transmission electron microscopy (TEM) (Harris, 1969; Harris *et al*., 2002). The decameric form seen in the TEM was confirmed by the crystal structure of hPrx2 (Schroder *et al*., 2000). The decameric form has also been observed for Rat PrxI (Matsumura *et al*., 2008). Bovine Prx2 (Cao *et al*., 2005) can exist in a dodecameric form and when crystallised a novel structure was revealed.

This crystal structure showed that two dodecamers are interconnected forming a two-ring catenane (Cao *et al*., 2005). This oligomerisation of the Prx is thought to be affected by a number of different factors. The oligomeric properties of the Prx have been studied using a number of different biophysical techniques such as gel filtration (Logan and Mayhew, 2000), dynamic light scattering (Wood *et al*., 2002a) and analytical ultracentrifugation (Schroder *et al*., 2000). The factors shown to affect the oligomeric state of the protein are ionic strength (Schroder, 1998), pH (Kristensen *et al*., 1999) and changes in the redox active cysteines (Wood *et al*., 2002). It has also been shown that the histidine (his) tag attached and used for purification may affect the oligomeric state of the protein. Size exclusion studies of the PrxIII protein showed that the presence of the poly histidine tag stabilized the formation of the dodecamer and may be a source of bias when working with recombinant Prxs (Cao *et al*., 2007).

It is believed that the change in oligomeric state of Prxs can link its redox state to its function. A study by Barrano-Medina *et al*., (2008) showed that the formation of decameric Prx occurs at a critical concentration (1 – 2 μM) that is similar for a range of Prxs. It is believed that this critical concentration is not affected by the presence of any poly histidine tag. A study of Prx from pea (Bernier-Villamor *et al*., 2004) and barley (Konig *et al*., 2002; Konig *et al*., 2003) revealed that the decameric form of the protein is preferred under reducing conditions. The decameric form was also preferred when the pH was reduced (8.0 – 7.5), suggesting a protonatable amino acid could aid decamer formation (Barranco-Medina *et al*., 2009). The hPrx2 decamer has been shown to break

down at pH less than 7.8 and in the presence of high concentrations (2.5 M) of urea (Kristensen *et al*., 1999).

It was proposed by Schroder *et al*. (2000), that the intermolecular disulfide state would find it difficult to form or stay in the decameric structure due to the structural rearrangements that would need to take place for the disulfide to form. The interconversion between the oxidised (Matsumura *et al*., 2008) and the disulfide form of rat PrxI (HBP23) (Hirotsu *et al*., 1999a) led to a breakdown from the decamer to the dimer (Matsumura *et al*., 2008), respectively, and it is noted that this could also occur with the hPrx2 (Schroder *et al*., 2000).

A further study by Alphey *et al.* (2000) postulated that the nucleophilic attack of Cys_R upon Cys_P would cause the structural rearrangements that break the decameric structure during disulfide formation. It is believed that the dimer-decamer switch in Prx is dynamic and *in vivo* there is continuous inter-conversion between the species. Decameric Prx2 has also been shown to aggregate together to form higher molecular weight forms (HMW). A dodecameric form of Prx has been observed and is believed to have a chaperone function (Moon *et al*., 2005) and presence in the human erythrocyte has been postulated (Meissner *et al*., 2007).

1.9.6 The cell signaling activity of Prx2

One theory put forward to explain the hyper-oxidation of Prx2 to the sulfinic acid state is the ability of Prx2 to take part in cell signaling. It is well documented that higher eukaryotic organisms are able to use higher concentrations of peroxide in the cell to mediate cell signaling (Rhee *et al*., 2006). The “floodgate” hypothesis suggests that Prx2 is responsible for removing H_2O_2 before it is able to reach the peroxide sensitive targets. When the H_2O_2 concentration increases and Prx2 becomes hyperoxidised, the peroxide is able to break through the Prx2 barrier enabling the peroxide to interact with peroxide sensitive targets (Wood *et al*., 2003a).

A second hypothesis suggests Prx2 is used as a measuring tool for the amount of peroxide the cell is exposed to. In this theory hyperoxidised Prx2 is the oxidative stress signal and this signal can be turned off when the sulfinic acid is reduced and can be used to signal apoptosis (Jonsson and Lowther, 2007).

1.9.7 Prx enzyme activity

The Prxs utilise Trx as a reducing substrate to catalyse the removal of peroxides. Thus Prxs are effectively thioredoxin peroxidases. Human Trx is a 12-kDa protein with a strongly reducing couple of two cysteine residues within its active site. The peroxidase reaction mechanism of Prxs is a two-step process: first, the conserved site peroxidatic cysteine attacks the peroxide. The cysteine residue is oxidised to cysteine sulfenic acid (Cys-SOH). It is subsequently reduced back to the thiol (Cys-SH) form in the second step of the reaction, when the resolving cysteine (Cys-SH) of one subunit attacks the peroxidatic cysteine (Cys-SOH) of the other subunit, forming an intersubunit disulfide bond, which is then reduced by Trx.

As mentioned earlier (section 1.9), there are six mammalian Prx isoforms which are currently known, and all these isoforms share the first step of the catalytic mechanism, where the peroxidatic cysteine is oxidised to sulfenic acid (Cys-SOH) by a peroxide substrate – such as hydrogen peroxide (H_2O_2) or peroxynitrite (ONOO-) (Manta *et al*., 2008). In the latter case, Prx functions as a peroxynitrite reductase (Dubuisson *et al.,* 2004). The reduction of the sulfenic acid back to thiol (Cys-SH), however, divides the six isoforms into three distinct classes: typical 2-Cys-Prxs (Prx 1, 2, 3, 4), atypical 2-Cys Prxs (Prx 5) and 1-Cys Prxs (Prx 6). Typical 2-Cys-Prxs, such as Prx2, are obligate homodimers. The reactive cysteines in the active site of Prx2 are also able to form S-nitrosothiols, presumably through the reaction of the Cys residues with NO-related species (e.g. N_2O_3 and/or ONOO-) (Fang *et al*., 2007). Thus cellular Prx2-SNO formation has been described (Yang and Loscalzo, 2005; Fang *et al*., 2007), although RBCs were not studied. It was shown by Fang *et al*. (2007) that Prx2-SNO, in turn, transnitrosated cysteine residues in other proteins. Preliminary enzyme activity assays using mixtures containing isolated human RBC Prx2, Trx, TrxR, NADPH and nitrite were conducted by Maria Letizia Lo Faro in our research group have shown that Prx2 appears to have nitrite reductase activity (Manta *et al*., 2008). Nevertheless, it remains

to be demonstrated whether Prx2 is actually a nitrite reductase *in vivo*, or whether it simply receives NO equivalents from Hb, in a mechanism by which Hb acts as the nitrite reductase.

1.9.8 Interactions of haemoglobin with ligands

Besides the oxygen ligand, which binds to Hb in a cooperative manner, Hb ligands also include competitive inhibitors such as carbon monoxide (CO) and NO and allosteric ligands such as carbon dioxide (CO_2). The CO_2 is bound to amino groups of the globin proteins as carbaminohaemoglobin and is thought to account for about 10% of carbon dioxide transport in mammals (Jensen, 2009).

As discussed earlier (section 1.6.1), in contact with NO, Hb forms a stable complex [HbFe(II)NO], which can dissociate into free NO and HbFe(II) again, as the Hb releases NO from its haem site. Also it can be S-nitrosated at Cys93 to form S-nitrosohaemoglobin (SNO-Hb) (Stamler *et al.*, 1996).

1.9.9 S-nitrosation of peroxiredoxin

The peroxiredoxins (Prx) family of proteins is made up of important antioxidant enzymes (see section 1.9); they limit the accumulation of intracellular peroxides. Prx2 is one of the antioxidant Prx enzymes, and is the most abundant in mammalian RBC's and neurons (Moore *et al*., 1991), making it a prime candidate to defend against oxidative stress.

The S-nitrosation targets the redox-active Cys-51 and Cys-172 residues, which are both critical for Prx2 activity (see section 1.9.3) (Chae *et al.*, 1994), thus inhibiting its neuroprotective functions against oxidative stress (Fang *et al*., 2007). SNO-Prx2, was generated (Fang *et al*., 2007) by the reaction of GSNO with Prx2 at the two critical cysteine residues, resulting in Prx2 dysfunction. Therefore Prx2 S-nitrosation provides a mechanistic link between nitrosative and oxidative stress (Fang *et al*., 2007). The cysteine motifs are conserved in all Prx containing dual–thiol active sites enzymes (Prx1-4). It was hypothesized by Fang *et al*., (2007) that each of them could be a target of S-nitrosation, and that NO therefore regulates metabolism of intracellular peroxides

through S-nitrosation of their active sites. All present evidence suggests that, Prx2 activity is regulated by NO *in vitro* and *in vivo* by S-nitrosation of redox-active cysteines residues in Prx2, forming SNO-Prx2 (Fang *et al*., 2007). S-nitrosation of Prx2 inhibits its protective properties against oxidative stress-induced neuronal cell death. Data from Fang *et al*. (2007) demonstrated a previously unrecognised relationship between NO and oxidative stress in neurodegenerative disorders, showing that Prx2 is S-nitrosated *in vitro* in cell-based models. Protein nitrosation has attracted considerable interest in biomedical research as a biomarker of NO-dependent oxidative stress (Radi, 2004) and because it can alter catalytic activity and interfere with cellular signaling processes (Greenacre and Ischiropoulos, 2001; Schopfer *et al*., 2003). Koech *et al.* (2001) demonstrated that protein nitrosation is a reversible and selective process that can also interfere with signaling processes associated with protein Tyr phosphorylation, either keeping the protein from performing the normal task of the phosphorylated form or mimicking the structural changes imposed by protein phosphorylation (Klotz *et al*., 2002). It is now recognised that NO and its ROS species can introduce posttranslational modifications of proteins using different routes. In additional to its capability to bind metal ions of haem groups, as reported in animals for guanylate cyclase activation (Denninger and Marletta, 1999), NO performs important S-nitrosation and nitration, which are major NO-dependent protein modifications, which were later investigated by Zaninotte *et al*., 2006).

The observed links of S-nitrosation to the transduction of NO and ROS-mediated signaling events suggests that the nitrosation of proteins regulates and fine-tunes the effects of its own radicals, such as ONOO-, through the S-nitrosation of crucial components of the antioxidant defence machinery, such as Prx2. This concept reinforces the model of NO / ROS crosstalk, and sheds light on the combined action of reactive oxygen, and nitrogen species, paving the way for studies of the modification of cysteine residues in proteins to yield SNO-Prx2, which improves the interactions of Prx2 with other metalloproteins such as haemoglobin in particular.

1.9.10 Interactions between haemoglobin and peroxiredoxin 2

There is evidence that Hb can interact with some peroxiredoxins (James, 2010; Szabo-Taylor *et al.,* 2011 and James *et al*., 2014, manuscript in preparation), the form of interaction between Hb and hPrx2 is yet to be confirmed. Further work recently performed in our group (James, 2010 and Szabo-Taylor *et al.,* 2011) suggested that Prx2 may be physically associated with Hb: during hPrx2 purification from human RBC it was possible to separate fractions containing either just Prx2 or Hb, but each protein was invariably contaminated with the other, and it was difficult to further purify either protein to the extent of fully removing the other. This implies the formation of a complex between the two proteins (Szabo-Taylor, 2011). According to the literature, Prxs 1 and 2 may interact with haem, and Prx1 originally had the name “Haem Binding Protein (HBP)” (Iwahara *et al*., 1995; De Franceschi *et al.*, 2011).

For the first time, Ying *et al*. (2012) demonstrated that the binding of Prx2 to Hb is effective for stabilizing Hb against excessive oxidative damage in mouse and human RBCs. Upon oxidative stress, ROS and Heinz body formation were significantly increased in Prx2 knockout RBCs compared to wild-types, which ultimately accelerated the accumulation of hemosiderin and haem-oxygenase 1 in the Prx2 knock-out livers (Ying *et al*., 2012). In addition, ROS-dependent Hb aggregation was significantly increased in Prx2 knockout RBCs. Interestingly, Prx2 interacted with Hb in mouse RBCs, and their interaction, in particular, was severely impaired in RBCs of patients with thalassemia and sickle cell anemia (Ying *et al*., 2012). Hb was bound to the decameric structure of Prx2, by which Hb was protected from oxidative stress (Ying *et al*., 2012).

It might be suggested that determining the binding status between Prx2 and Hb could provide a diagnostic marker and a target for designing therapeutic strategies for hemolytic anemia patients, including thalassemia.

1.10 How NO might escape from erythrocytes

Considering the high concentration of Hb in the RBC and the binding affinity of NO for Fe^{2+} within haem, it is doubtful that the NO produced could be exported as "free" NO simply by diffusion (Jensen, 2009). In addition to NO needing to not be scavenged by the vast excess of Hb within RBC's, NO also needs to escape oxidation to nitrate by oxyHb (Gladwin and Kim-Shapiro, 2012). However, Jensen (2009) suggested that the association of deoxyHb with the RBC membrane could help the release of NO by the formation of intermediate N_2O_3 and subsequent S-nitrosothiol formation. We speculate that the interaction between Prx2 and Hb facilitates a transnitrosation mechanism (discussed in section 1.13), which mediates the release of NO. In addition to interaction of Prx2 with Hb, there is evidence that Prx2 also has the capacity to associate with the RBC membrane (Cha *et al*., 2000; Matte *et al*., 2012) and appears to be localised on the exofacial surface of the RBC membrane (Morocco *et al*., 2012). It has have also recently demonstrated in our laboratory using natural killer cells that Prx2 is localised to the exofacial surface of human blood lymphocytes (Szabo-Taylor, 2011).

1.11 Suggested model for the escape of NO from RBC

We suggest a model whereby NO escapes from RBCs as NO equivalents, in the form of Prx2-SNO, this is further facilitated by the association of Prx2 with the cell membrane and the relocalisation of Prx2 to the exofacial surface of the RBC. The NO reacts with Hb to form a nitrosylHb adduct [HbNO]. The NO equivalents are transferred to the Cys residues of Prx2 forming S-nitrosoperoxiredoxin (Prx2-SNO). The proximity of Prx2 to Hb promotes S-nitrosothiol formation in Prx2 and this avoids the scavenging of NO by Hb itself as illustrated in the figure 1.16.

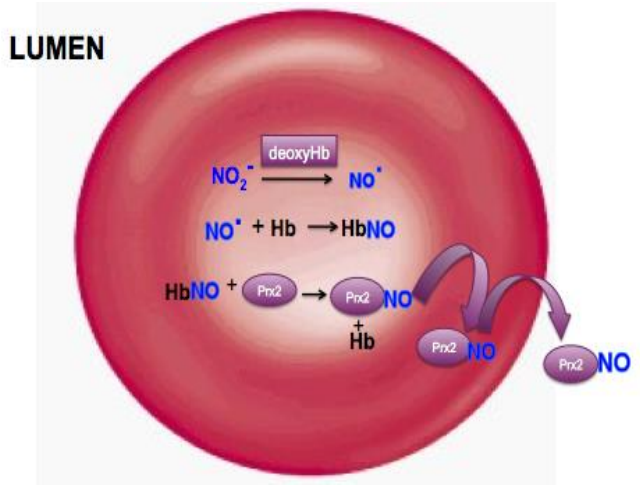

Figure 1.16 Diagram of a RBC, showing the proposed model for the escape of NO from RBC. The model demonstrates the hypothesis of the research that Prx2 facilitates a transnitrosation mechanism (discussed in section 1.13), highlighting possible interactions between NO and Hb, and the HbNO complex and Prx2. In this model, NO is produced upon nitrite reduction by deoxyHb. The NO reacts with Hb to form a nitrosylHb adduct (HbNO). The NO equivalents are transferred to the Cys residues of Prx2 forming S-nitrosoperoxiredoxin (Prx2-SNO). The proximity of Prx2 to Hb promotes S-nitrosothiol formation in Prx2 and avoids the scavenging of NO by Hb itself.

1.12 Transnitrosation between hPrx2 and Hb

As described in section 1.6, the transnitrosation reaction involves nucleophilic attack of thiolate anion on the nitroso nitrogen (RSNO). Regarding the candidate proteins for such an essential reaction to take place inside a cell or in biological fluids, both proteins must have free thiols, which readily react with reactive nitrogen species. Free thiols were reported both in hPrx2 and Hb (Chin and Chen 2012; Rotem *et al*., 2013). Transnitrosation cannot be discussed without acknowledging protein-protein interactions. Section 1.10.5 earlier presented evidence suggesting a protein-protein interaction between Hb and hPrx2. However, a complete knowledge of all direct and indirect interactions between hPrx2 and Hb in a given cell could represent an important milestone towards understanding how Prx2 could be a novel NO carrier from erythrocytes to smooth muscle cells within the human vasculature. Currently, protein interactions and associations are annotated at various levels of detail in online resources, ranging from raw data repositories to highly formalized pathway databases. For many applications, a global view of all the available interaction data is desirable, including lower-quality data and computational predictions. Publication of the human genome and proteomics based protein profiling studies catalyzed resurgence in protein interaction analysis (Prakash and Raj, 2015).

Approximately 30,000 genes of the human genome are speculated to give rise to $1x10^6$ proteins through a series of post-translational modifications and gene splicing mechanisms (David Waugh, 1954). Although a population of these proteins can be expected to work in relative isolation, the majority are expected to operate via contacts with others proteins in complexes and networks to orchestrate the myriad of processes that impact cellular structures and function. These processes include cell-cycle control differentiation, protein folding, signaling, transcription, translation, post-translational modification and transport.

Equation 1.31 The transnitrosation of protein thiols of hPrx2 and Hb

A possible transnitrosation reaction, as might occur in the case of Hb and Prx2, is demonstrated in figure 1.15. Transnitrosation does not require a separate redox partner as demonstrated by the direct reaction of SNOG with mitochondrial aldehyde dehydrogenase (Moon *et al*., 2005). The rate order of such reactions is second order. The reaction rate depends greatly on the pKa of the thiol group and the accessibility of the thiol group (Rossi *et al.*, 1997; Gladwin *et al.,* 2002b). Transnitrosation is also dependent on the pKa and the accessibility of the reactive groups. Orie *et al.* (2005) presented an example: the rate constant for the reactions of HSA and cysteine with SNOG was discovered to be 1.15 and 57 $M^{-1}s^{-1}$ respectively (Orie *et al*., 2005). A number of studies have been conducted to demonstrate how transnitrosation reactions between protein free thiols can be prevented (Orie *et al*., 2005; Rocks *et al*., 2005). Protein samples in the study were treated with N-ethlmaleimide (NEM) which improved the stability of RSNO, whereby NEM prevented transnitrosation reactions from taking place. Thus, NEM bound onto the sulfur of the free thiols (Orie *et al*., 2005; Rocks *et al*., 2005).

1.13 Aim and Objectives

The main overall objective of this project was:

1. To investigate the interaction between NO, Hb, and hPrx2 to determine whether there is this transfer which involves transnitrosation, whether there is an interaction between nitrosated haemoglobin (NOHb) and hPrx2, which would support that the nitrosated peroxiredoxin 2 (hPrx2-SNO) can actually get outside the RBC, and thereby diffuse to remote sites where it can act as an NO donor molecule to explain the endocrine role of NO.

The specific aims were as follows:

- To isolate Prx2 from red blood cell, to be used to complete the interaction studies of hPrx2 and Hb.

- Over-expression and purification of the recombinant hPrx2. This is also to be used in the interaction studies of Prx2 and Hb, to see if there are there any interaction differences between the two sets of protein samples (native and recombinant).

- To identify reliable gram scale method to synthesis Prx2-SNO and HbNO, using both the native hPrx2 and recombinant hPrx2 protein samples to complete the initial physicochemical characterization of the product to ensure no adverse damage has occurred to the protein structure and its activity, and subsequently crystallization and structural analysis, to be carried out with Dr. Michail Isupov in the group of Prof. Littlechild.

- To study the interactions between hPrx2, NO, Hb, and hPrx2-SNO for both native and recombinant hPrx2 protein samples.

- To characterize the hPrx2 protein samples.
- To test the formation of a complex between hPrx2 and Hb. The complex formation will be then studied using size exclusion, chromatography and surface plasmon resonance, and crystallization attempt to obtain a 3D structure of the complex.

Chapter 2

Isolation and characterisation of human erythrocyte-derived peroxiredoxin 2, and human recombinant peroxiredoxin 2

2.0 Introduction

The abundance of Prx2 in RBCs (section 1.9.1) suggests an important role for this protein in these cells (Low *et al*., 2008). The order of abundance of proteins in RBC base on a recent proteomics study suggests haemoglobin is the most abundant protein in human RBC's, followed by catalase and then Prx2 (Matte *et al*., 2012). Also carbonic anhydrase, spectrin and ankyrin are abundant in these cells (Kakhniashvili *et al*., 2004). Prx2 is important in the antioxidant defense of RBCs as it scavenges H_2O_2 generated via the autoxidation of haemoglobin, the most abundant protein in red blood cells, and probably protects haemoglobin from oxidative damage (Low *et al*., 2008, Alessandro *et al*., 2010, Nagababu *et al*., 2013). Manta *et al*. (2009) anticipated that Prx2 in RBCs could act as an antioxidant for the whole vasculature due to its high reactivity with H_2O_2 and peroxynitrite, its high concentration in RBCs, and the diffusible nature of H_2O_2 and peroxynitrite through membranes.

By forming high molecular weight structures, Prdx2 also acts as a molecular chaperone. Oligomerisation might occur as a result of oxidation, phosphorylation (reviewed by Low *et al*. (2008)) or S-nitrosation (Romero-Puertas *et al*., 2007), and these high molecular weight structures are able to protect proteins from heat-denaturation. Human Prx2 (hPrx2) is also associated with the red blood cell membrane, and plays a role in the activation of the Gárdos-channels, promoting potassium efflux from the red blood cells (Plishker *et al*., 1986). Low *et al*. (2008) proposed that membrane-associated Prx2 might also scavenge lipid hydroperoxides; thereby protecting the membrane from oxidative damage.hPrx2 is highly homologous with Prx1. Although hPrx2 is the third most abundant protein in RBC, little is published about the interactions of Prx2 with Hb or haem. Prx2 was originally described as a 23 kDa haem-binding protein from rat liver cytosol and was termed HBP23 (haem-binding protein 23) (Iwahara *et al*., 1995). The protein was found to be highly expressed in rat liver, and it was upregulated at the mRNA level following haem exposure and partial hepatectomy, which suggests that it might play a role in haem metabolism (Iwahara *et al.*, 1995).

Haem has been recently recognised as a pro-inflammatory signaling molecule (Porto *et al*., 2007). Sites of tissue injury, haemolysis and haemorrhage are characterised by an increased haem concentration, which activates the migration and oxidative burst of

neutrophils (Porto *et al*., 2007). Haem also activates the TLR 4 signaling pathway and induces TNF-α secretion by macrophages, thereby acting as a danger signal for the innate immune system (Figueiredo *et al.*, 2007). Interestingly, haem also acts as a cofactor for immunoglobulins, enhancing and extending their epitope recognition, which may not only act as a defense mechanism against pathogens but may also have pathophysiological functions by promoting autoimmunity (Dimitrov *et al*., 2007). Therefore, potential interactions of Prdx2 with haem may have important implications concerning inflammation.

2.1 Protein purification

In order to study an enzyme it must be isolated from other proteins in the organism in order to remove any inhibitors or proteins with similar functions. This can be achieved by exploiting enzyme properties, such as its charge and size, in order to separate it from other proteins. Different types of purification include ion exchange, affinity and hydrophobic chromatography and gel filtration.

Ion exchange chromatography

Ion exchange chromatography uses a porous resin that is charged with ionised groups on its surface. The resin can be charged with anions or cations depending on the properties of the proteins being purified. Proteins that bind to the column can be eluted by a salt gradient, which alters the number of ions in the buffer and therefore decreases the affinity by competing with the protein for the column media. The protocol is designed so that protein of interest is eluted during the low to high salt gradient.

Gel filtration chromatography

Gel filtration (GF) or size exclusion chromatography separates proteins according to the molecular weight of the native protein. The medium is formed by beads of a cross-linked gel, which contain pores of a known size. Smaller proteins will become caught in the pores and their movement will be retarded, whereas larger proteins will travel around the beads and be eluted first. These columns are calibrated with standard proteins prior to use and can give information as to the overall molecular weight of a

protein which is expressed as a Stokes radius using (Eq 2.1). Partition coefficient, K_{av} is determined by the Stoke's radius (rotational volume) of the molecule, which is proportional to its molecular weight and shape.

$$K_{av} = \frac{V_e - V_0}{V_t - V_0}$$

Equation 2.1. The Stoke's radius. Where V_e = elution volume of the protein, V_o = void volume and V_t = total volume.

Proteins of known molecular weight are used to produce a Log MW *vs*. K_{av} standard curve for a given gel filtration column and this allows the estimation of protein size.

Affinity Chromatography

Affinity chromatography uses a medium that has a ligand bound to it, which will interact specifically with the protein of interest. This is a common method for recombinant protein that can have specific tags added such as a His-tag that will interact with Ni^{2+}. Adding a protease that specifically cleaves the tag or a buffer which competes with the protein / ligand interaction, as it has a greater affinity for the ligand can elute protein. Altering the pH or increasing the ionic strength of the buffer decreases non-covalent interaction between the ligand and protein and will also cause protein to be eluted from the column.

2.2 Aims and objectives

Does the reactive thiol-containing enzyme Prx2 interact with Hb?

In order to test the hypothesis in the later chapters, that the interaction between hPrx2 and Hb involves a transnitrosation (section 1.6) mechanism (which could in turn be involved in transport of NO from RBC's to smooth muscle cells within the human vasculature), we needed purified human Prx2 and recombinant Prx2 for the planned experiments. Therefore, the aim of this chapter was to purify native hPrdx2 from red blood cells and recombinant hPrx2 expressed in *E.coli*. Furthermore, we hypothesised that similar to Prx1, Prx2 may also interact with haem or haemoglobin. Therefore, a subsidiary aim of this chapter was to study the biochemical properties of Prx2 during the purification process, and carry out preliminary experiments to study a potential Prx2 / haemoglobin interaction.

The first step was to extract the hPrx2 protein from human RBC lysates. From this purification, samples of pure hPrx2 and hPrx2 containing traces of Hb were obtained. Samples of hPrx2, containing traces of Hb, were analysed by SDS PAGE and Western Blot to confirm the protein – protein (hPrx2-Hb) interaction.

2.3 Materials and methods

There are different methods of Prx2 purification from RBC's (Moore *et al*., 1990; Shau *et al*., 1993; Schröder *et al*., 1998; Kristensen *et al.*, 1999). RBCs are the most abundant source of native human Prx2. Here, I report a reliable protocol that I used to purify hPrx2 from expired RBC's and from *E.coli* for the recombinant Prx2.

2.3.1 Isolation of hPrx2 from red blood cells

The method used to isolate and purify the native protein was reproduced from (Schröder *et al.*, 1998). The purification of native hPrx2 was achieved from out of date RBC packs, which were purchased and collected from the National Blood Service (Bristol, UK). The University of Exeter of Medical School Research Ethics Committee and the National Blood Service Ethics Committee granted approval for this study (appendix). The lysates were then used for Prx2 purification.

2.3.1.1 Haemolysis and purification buffers

The haemolysis buffer contained: 0.625 mM Tris-HCl pH 7.5, 5 mM EDTA, 20 µM benzamidine (BAM), and 10 µM phenylmethanesulfonylfluoride (PMSF). The native hPrx2 purification buffer (A) contained the following chemicals: 0.625 mM Tris-HCl pH 7.5, 5 mM EDTA, 20 µM BAM, and 10 µM PMSF. Different buffers were used during the native hPrx2 purification. The buffers were: for buffer (B) 20 mM Tris-HCl pH 7.5 was mixed with 5 mM EDTA, 20 µM BAM, 10 µM PMSF, and 2 M NaCl. Then, for the native hPrx2 purification buffer (C) this consisted of: 25 mM Tris-HCl pH 7.5, 1 mM EDTA, 20 µM BAM, 10 µM PMSF, and 0.1 M NaCl.

2.3.1.2 Haemolysis of erythrocytes

Packed RBC's (200 ml) were used for the haemolysis step (Schroder *et al*., 1998). The packed RBC's were centrifuged at 4^{o}C, 1000 g for 40 min. The supernatant was discarded. The centrifugation step was repeated. The pellet was re-suspended in 200 ml of hypotonic lysis buffer (0.625 mM Tris-HCl, 5 mM EDTA, 20 µM BAM, 10µM PMSF, pH 7.5), which disrupted the RBC's. The haemolysate was centrifuged at 4^{o}C, 13700 g for 90 min, in order to pellet the membranes. The supernatant was stored at 4^{o}C (overnight) until the next chromatography step.

2.3.1.3 Ion exchange chromatography of native hPrx2

The pI of Prx2 is 5.66. Therefore, anion exchange chromatography was used to isolate a Prx2 containing fraction from the crude haemolysate. A HiLoad column containing 250 ml of Fast Flow Q Sepharose media (FFQ) (Amersham Q Sepharose Fast Flow medium, GE Healthcare, Buckinghamshire, UK) was equilibrated with three column volumes of buffer A at a flow rate of 3 ml/min. The sample was loaded onto the column under gravity and unbound sample was eluted with buffer A until the flow through ran clear. The column was then connected to an ÄKTA purifier (GE Healthcare, Amersham Buckinghamshire, UK) and an elution was carried out over a six column volume linear gradient of 0–50% buffer B. Fractions were collected throughout the entire protocol and the absorbance measured at 280 nm. Fractions were analysed using SDS-PAGE.

2.4.1.4 Size exclusion chromatography of native hPrx2

The Superdex 200 gel filtration column was calibrated with the protein standards as follows: ferritin (440 kDa), β-amylase (200 kDa), alcohol dehydrogenase (158 kDa), albumin (67 kDa), carbonic anhydrase (29 kDa), cytochrome *c* (12.4 kDa) and a very low molecular weight protein, macrophage inflammatory protein (MIP) (11 kDa). These protein standards were applied to the column pre-equilibrated with 10 mM Tris-HCl, pH 8.0 and eluted with the same buffer. The void volume was determined using the molecular weight standard Blue Dextran (2000 kDa). The elution profile (Fig. 2.5a) on page 21 was used to determine the Stokes radius for the proteins using the calculations in (Eq. 2.1) on page 3.

Calculation of K_{av} (Stoke's radius): Where V_e = elution volume of the protein, V_o = void volume of the column (44 ml), V_t = total volume of the column (122 ml). A rearrangement of the equation of the line from the calibration was used to calculate the log molecular weight from the K_{av} value.

$$\log MW = \frac{1.0185 - Kav}{0.3457}$$

Equation 2.2. Calculation of the log of the molecular weight

A Superdex 200 HiLoad 16/60 (GE Healthcare, Amersham Buckinghamshire UK) gel filtration column (column volume 120 ml) was equilibrated with one column volume of buffer C at a flow rate of 1 ml/min. The sample was loaded and fractions were collected over the elution volume of one column volume and the absorbance measured at 280 nm and 418 nm. Fractions were analysed using SDS-PAGE.

The fractions from the anion exchange chromatography (Fig. 2.2), which contained the purest Prx2, were pooled and concentrated. The concentration step was carried out using an Amicon Millipore regenerated cellulose ultrafiltration membrane (pore size 10000 Da, Millipore, Watford, UK) under Argon pressure. Alternatively, an Amicon 10000 Da cut-off centrifugal filter unit (Millipore, Watford, UK) was used.

A Superdex 200 gel filtration column (GE Healthcare, Buckinghamshire, UK) was equilibrated with a pH 8.0 buffer containing 25 mM Tris-HCl, 1mM EDTA, 20 µM BAM and 10 µM PMSF. Following equilibration, the concentrated Prx2-containing sample was loaded onto the column and eluted using the same buffer. The eluate was collected as fractions, and selected fractions were analysed by SDS-PAGE (Fig 2.7) to reveal the most pure and most concentrated Prx2 fractions. The identity of Prx2 was also confirmed by Western blotting.

2.3.2 Purification of recombinant hPrx2

In order to study hPrx2, it was essential to have a sample of Prx2, which was free from Hb contaminants. A recombinant protein of hPrx2, which could be expressed and purified to high homogeneity, was the decisive solution. A clone of the *hPrx2 gene* in the pET28a expression vector was obtained from Dr Paul James, PhD thesis, 2010. Paul James (2010) reported that the original attempts to purify the enzyme proved problematic because the recombinant enzyme aggregated very easily during purification, dialysis and concentration. The initial cloning work of *hPrx2* was done by Dr Kirsty Line (University of Exeter). The recombinant protein was found to be predominantly produced in a different oligomeric state to that of the native enzyme. Native hPrx2 is seen mainly in the decameric form with a small amount in the dimeric form, but the opposite was observed for the hPrx2 clone (Paul James PhD thesis, 2010). This was due to a point mutation in the DNA sequence, which resulted in a change of the fourth amino acid of the protein from glycine to valine (Paul James, PhD thesis, 2010). Glycine is the smallest amino acid, very flexible, and valine is much larger and hydrophobic. Thus point mutation was correct by site – directed mutagenesis and observed to have the same decameric structure as observed for the native enzyme (Paul James PhD thesis).

2.3.2.1 Expression of recombinant hPrx2

The *hPrx2* gene was cloned (by Paul James, PhD thesis) incorporating an N-terminal His-tag and expressed under the control of the T7 promoter. The recombinant *hPrx2*

gene was transformed into the *E. coli* Rosetta Gami 2 expression cell line and cells (from glycerol stock) containing the pET28a/*hPrx2* construct were used to inoculate 100 ml LB containing kanamycin (50 µg/ml) tetracycline (37.5 µg/ml) and chloroamphenicol (12.5 µg/ml). This starter culture was grown under agitation at 200 rpm overnight at 37ºC and 20 ml were used to inoculate 1 L fresh LB medium containing the appropriate antibiotics for selection, and was grown with agitation at 37ºC until the optical density (OD) at 600 nm was approximately 0.8, when isopropyl-β-D-thiogalactopyranoside (IPTG) was added to a final concentration of 1.0 mM and the culture incubated for a further four hours at 37ºC. The *E. coli* cells were harvested by centrifugation (20,000 x *g*, 20 min, 4ºC) using a Beckman JA-25.50 rotor. The cell pellet was stored at -20ºC until further use.

2.3.2.2 Purification of recombinant hPrx2

***Cell lysis**:*

The cell paste was re-suspended at 10% w/v in 100 mM Tris-HCl, pH 7.5, 0.5 M NaCl. Cells were disrupted by sonication at 10 microns (Soniprep 150, Sanyo) using the setting: 30 sec on, 1 min off (x 6 cycles) and the cell debris removed by centrifugation at 20,000 x *g*, 20 min and 4ºC using a Beckman JA-25.50 rotor.

2.3.2.2 Purification buffers

Buffer A was 100 mM Tris-HCl, pH 7.5 containing 0.5 M NaCl. Buffer B was 100 mM Tris-HCl, pH 7.5 containing 0.5 M NaCl and 1 M imidazole. Buffer C was 100 mM Tris-HCl, pH 7.5 and containing 0.1 M NaCl.

2.3.2.4 Nickel affinity chromatography

A HiLoad (GE Healthcare) column containing 50 ml metal chelating cellulose charged with Ni^{2+} (Bioline) was equilibrated with three column volumes of buffer A at a flow rate

of 3 ml/min. The sample was then applied to the column via an injection “super loop” (GE Healthcare, Amersham Buckinghamshire, UK). Any unbound sample was removed by applying three column volumes of buffer A. Then a six column volume gradient to 100% buffer B was applied to the column, followed by two further column volumes of 100% buffer B. Fractions were collected throughout the entire protocol and the absorbance measured at 280 nm. Fractions were analysed using SDS-PAGE. All columns were run on an ÄKTA Purifier (GE Healthcare).

2.3.2.5 Gel filtration chromatography

A Superdex 200 HiLoad 16/60 (GE Healthcare) gel filtration column (column volume 120 ml) was equilibrated with one column volume of buffer C at a flow rate of 1 ml/min. The sample was loaded and fractions were collected over the elution volume of one column volume and the absorbance measured at 280 nm. Fractions corresponding to protein peaks were analysed using SDS-PAGE.

2.3.3 Protein concentration

The protein was concentrated using an Amicon Ultrafiltration centrifugal concentrator (10 kDa cut-off PES membranes, Millipore, Cork, Ireland) at 4,000 x *g* and 4^{o}C.

2.3.4 SDS-PAGE

Protein was analysed by SDS-PAGE following a modification of the method of (Laemmli, 1970). A gel containing a 6% stacking gel and a 12.5% separating gel was

made and run using a Mini Protean II system (BioRad Labaratories Ltd).

2.3.4.1 Stock solutions

In order to prepare 10 x SDS PAGE running buffer**,** the following chemicals were mixed: 36 g Tris-HCl, pH 8.8 was mixed with 12 g SDS followed by 172.8 g glycine and made up to 2 L with ddH_2O.

Solution A contained acrylamide (30%), and bisacrylamide (0.8%) solution, solution B contained 1.5 M Tris-HCl, adjusted to pH 8.8. Solution C was 0.5 M Tris-HCl, pH 6.8 and lastly, solution D consisted of SDS 10 % w/v.

The SDS PAGE loading buffer was 100 mM Tris-HCl containing 0.2% bromophenol blue w/v, 20% glycerol v/v SDS, merceptoethanol.

2.4.4.2 SDS PAGE non-reducing loading buffer

The non-reducing loading buffer was 100 mM Tris-HCl pH 8.0, containing 8.2% bromophenol blue w/v and 20% glycerol v/v SDS.

2.4.4.3 SDS-PAGE stain and destaining

The staining and destaining of the SDS-PAGE gels was done using a microwave as follows: 1 g coomassie Brilliant Blue was mixed with 1 L methanol, 800 ml ddH_2O, and 200 ml glacial acetic acid for 15 min.

2.4.4.4 Preparation of gels

SDS-PAGE gels (Chrambach and Rodbard, 1971) were prepared using a Mini Protein III rig (Bio-Rad, Hemel Hempstead, UK). The glass plates of the apparatus were

cleaned with 30% ethanol and assembled. Fresh 10% ammonium- persulfate (APS, Thermo Fisher Scientific, Northumberland, UK) was prepared by adding 0.1 g APS to 990 µl distilled water. 15% gels were prepared by mixing the following: 5 ml acrylamide bis-acrylamide 30% (Sigma, Dorset, UK), 2.4 ml distilled water, 2.5 ml 1.5 M Tris-HCl (Thermo Fisher Scientific, Northumberland, UK) pH 8.8 and 62.5 µl 20% SDS (Thermo Fisher Scientific, Northumberland, UK). Following the mixing of these four components, 100µl fresh 10 % APS and 10 µl TEMED (N,N,N',N'-tetramethylethylenediamine) (Thermo Fisher Scientific, Northumberland, UK) were added and mixed. This resolving gel was then poured into the mould between the glass plates, leaving a 2 cm gap on top, sealed with 20 µl isopropanol to ensure smooth setting and prevent air bubbles appearing in the gel, and left to set for 30 minutes or longer. Once the gel had set, the isopropanol was poured off, the top of the gel rinsed with distilled water, and a 5 % stacking gel was poured on top of the resolving gel to complete the gel. To prepare the stacking gel, the following reagents were mixed: 660µl acrylamide bis-acrylamide 30%, 3 ml distilled water, 1260 µl 1 M Tris-HCl pH 6.8 and 25 µl 20% SDS. Once thoroughly mixed, the mixture was supplemented with 20 µl 10% APS and 5µl TEMED. After pouring the stacking gel on top of the resolving gel to fill the glass plates to the top, a plastic 10 or 15 well comb was inserted into the liquid stacking gel. The gel was subsequently left for at least 30 min to set. The set gels were then ready to use.

2.4.5 Sample preparation

2 x SDS-PAGE loading buffer was mixed with the protein samples. The SDS buffer denatures the proteins and also adds a negative charge to the protein molecules that is proportional to mass. The loading buffer also contained β-mercaptoethanol to reduce any disulfide bridges within the proteins. The mixture was heated at 100^{o}C for 5 min to ensure the protein was fully denatured before being loaded onto the gel-stacking layer. Once fully denatured the protein was capable of travelling through the gel at a distance proportional to its individual subunit molecular weight allowing for determination of molecular weight.

Protein samples were prepared in reducing or non-reducing, 2x or 4x sample (loading)

buffer (Laemmli buffer). A more concentrated sample buffer (4x) was used for cell lysate samples. The 4x sample buffer consisted of 1 ml 1 M Tris HCl pH 6.8, 1 ml 40% SDS, 2 ml glycerol, and 200 µl 10% bromophenol blue (50 mg in 500µl) and 800 µl distilled water

2.4.5.1 Sample preparation using non-reducing buffer

2 x non-reducing SDS-PAGE loading buffer was mixed with the protein sample. In this case, the buffer contained no reducing agents and was not heated therefore leaving any disulfide bonds intact. The mixture was left for 5 min at room temperature. The protein was then loaded onto the gel-stacking layer.

2.4.5.2 SDS-PAGE

For all the applications, the in-house made gels were used. The gels were assembled according to the manufacturer's instructions in Mini Protein III tanks (Bio-Rad, Hemel Hempstead, UK), loaded with appropriate volumes of samples. The prepared samples were loaded into the gel wells using a 20 µl Hamilton syringe (Hamilton, Stedim Biotech, Germany). Additionally 5µl of a molecular weight marker (Precision Plus Protein Standard 15–250 kDa, BioRad Laboratories, Appendix 7.2) was loaded as a molecular weight marker. The gel was run at 150 V for 65 min.

2.4.5.3 Native PAGE

For certain applications, 6% native PAGE was used. These gels were prepared in a very similar way to SDS-PAGE gels. However, for native PAGE, no SDS was added either to the gel, the sample buffer or the running buffer. The resolving gel consisted of the following mixture: 1 ml bis-acrylamide 30%, 2.7 ml distilled water, 1.25 ml 1.5 M Tris-HCl pH 8.8, 50 µl 10% APS and 5 µl TEMED. The stacking gel consisted of 330 µl bis-acrylamide 30%, 1.5 ml distilled water, 630µl 1 M Tris-HCl pH 6.8, 10 µl 10% APS and 2.5 µl TEMED. The sample buffer consisted of 4.19 ml distilled water, 2.5 ml 0.75

M Tris-HCl pH 6.5, 1 ml glycerol and 50 µl 1% bromophenol blue. The 10x running buffer used for native PAGE contained 25 mM Tris and 192 mM glycine and was adjusted to pH 8.3 using 1 M HCl.

2.4.5.4 Gel staining procedure

The SDS-PAGE gel was removed from the gel tank apparatus and placed in the microwave stain solution and heated in the microwave on full power for 3 min. The gel was transferred to 1 L of ddH_2O and heated on full power for 20 min to destain.

2.4.5.5 Protein concentration determination using A_{280}

The protein concentration was calculated by measuring the absorbance at 280 nm. A 200µl aliquot of the protein solution was placed in a quartz cuvette with a 1 cm path length. The A_{280} measurement was taken in a Biotech UV1101 Photometer (Shimadzu), blanked against a cuvette containing all buffers and reagents apart from the protein. The Prx2 protein's extinction coefficient of 10,930 m^{-1} cm^{-1} was calculated using the protein sequence and the Protparam online bioinformatics tool (Wilkins *et al*., 1999) (www.expasy.ch/tools/protparam.html). The protein concentration was then calculated using the Beer-Lambert Law (Eq. 2.3).

$$A=\varepsilon.l.c$$

Equation 2.3 Beer-Lambert Law, where: (**A**) is the absorbance at 280 nm, (**ε**) is the extinction coefficient of the protein, (**l**) is the path length and (**c**) is the concentration.

2.4.6 Western-blotting

A Thermo Scientific Pierce G2 Faster Blotter iBind kit was used for Western blotting. For each gel, four sheets of 0.83 mm thick Western blotting filter papers were used and one sheet of nitrocellulose or PVDF membrane cut to the same size. Before starting the blotting process, the filter papers and the membrane were equilibrated in Thermo Scientific™ Pierce™ 1-step transfer for at least 5 minutes. The PVDF membrane was wetted with methanol or ethanol before equilibration with Pierce™ 1-step transfer buffer.

After electrophoresis, the gel(s) were removed from cassette(s) and briefly placed into a tray containing deionized water or transfer buffer. This was to ensure even wetting, facilitate proper gel placement and to improve gel contact with the membrane. Assembly of the kit was done using a sandwich type set up; cathode (-) at the top, anode (+) at the bottom. The connections were: from the top two sheets of pre-wet filter papers of the similar thickness, followed by the gel, then a membrane. After the membrane, two sheets of pre-wet filter papers of similar thickness were added then connected to the anode. After repeated washing in washing buffer, (25 mM Tris, 0.15M NaCl, pH 7.5) the membrane was incubated with the primary antibody overnight at 4^{o}C. This step was followed by washing in washing buffer and incubation with the secondary antibody in blocking buffer for 1 hour at room temperature under agitation. After extensive washing (5-6 times, 5-10 min in washing buffer), the membrane was imaged using the LI-COR system (LI-COR Biosciences, Ltd, UK), using high sensitivity detection and an image setting of 5 seconds starting exposure time, 800 seconds total exposure time.

2.4.6 **LCMS analysis**

This was carried out at the University of Bristol mass spec service by Dr. Kate Heesom. Gel slices were subjected to in-gel tryptic digestion using a DigestPro automated digestion unit (Intavis Ltd). The resulting peptides were fractionated using an Ultimate 3000 nanoHPLC system in line with an LTQ-Orbitrap Velos mass spectrometer (Thermo Scientific). Peptides in 1% (vol/vol) formic acid were injected onto an Acclaim PepMap C18 nano-trap column (Thermo Scientific). After washing with 0.5 % (vol/vol) acetonitrile 0.1% (vol/vol) formic acid peptides were resolved on a 250 mm × 75 µm

Acclaim PepMap C18 reverse phase analytical column (Thermo Scientific) over a 150 min organic gradient, using 7 gradient segments (1-6% solvent B over 1min., 6-15% B over 58 min., 15-32% B over 58min., 32-40% B over 3min., 40-90% B over 1min., held at 90% B for 6min and then reduced to 1% B over 1min.) with a flow rate of 300 nl min^{-1}. Solvent A was 0.1% formic acid and Solvent B was aqueous 80% acetonitrile in 0.1% formic acid. Peptides were ionized by nano-electrospray ionization at 2.1 kV using a stainless steel emitter with an internal diameter of 30 µm (Thermo Scientific) and a capillary temperature of 250°C. Tandem mass spectra were acquired using an LTQ-Orbitrap Velos mass spectrometer controlled by Xcalibur 2.1 software (Thermo Scientific) and operated in data-dependent acquisition mode. The Orbitrap was set to analyze the survey scans at 60,000 resolution (at m/z 400) in the mass range m/z 300 to 2000 and the top twenty multiply charged ions in each duty cycle selected for MS/MS in the LTQ linear ion trap. Charge state filtering, where unassigned precursor ions were not selected for fragmentation, and dynamic exclusion (repeat count, 1; repeat duration, 30s; exclusion list size, 500) were used. Fragmentation conditions in the LTQ were as follows: normalized collision energy, 40%; activation q, 0.25; activation time 10ms; and minimum ion selection intensity, 500 counts.

The raw data files were processed and quantified using Proteome Discoverer software V1.4 (Thermo Scientific) and searched against the SwissProt Human database using the Mascot search engine (Matrix Science). Peptide precursor mass tolerance was set at 10ppm, and MS/MS tolerance was set at 0.8Da. Search criteria included carbamidomethylation of cysteine (+57.0214), modification of cysteine and oxidation of methionine (+15.9949) as variable modifications. Searches were performed with full tryptic digestion and a maximum of 1 missed cleavage was allowed. The reverse database search option was enabled and all peptide data was filtered to satisfy false discovery rate (FDR) of 5%.

2.4.8 Matrix-assisted laser desorption and ionisation time-of-flight mass spectrometry (MALDI-TOF MS) analysis

This was carried out at the University of Bristol mass spec service by Dr. Kate Heesom. Protein bands were cut into 1mm^2 pieces and digested with sequencing grade trypsin (Promega) using a DigestPro automated digestion unit (Intavis Ltd.). The resulting peptides were analysed by mass spectrometry. Mass spectra were recorded in positive ion mode on an Applied Biosystems 4700 MALDI-TOF mass spectrometer. MS spectra were recorded in reflector mode. For MSMS analysis the top 5 most intense, non-tryptic, precursors were selected for fragmentation by collision-induced dissociation. Neither baseline subtraction nor smoothing was applied to recorded spectra.

MS and MSMS data were analysed using GPS Explorer 3.5 (Applied Biosystems). MS peaks were selected between 800-4000 Da and filtered with a signal to noise ratio greater than 15, to exclude masses derived from trypsin autolysis. MSMS peaks were selected on the basis of a signal to noise ratio greater than 10 over a mass range of 50 Da to 20 Da below the precursor mass.

Data was analysed using the MASCOT 1.9 search engine (Matrix Science) to search against the human NCBInr protein database. Search parameters allowed for one missed tryptic cleavage site, the carbamidomethylation of cysteine, and the possible oxidation of methionine; precursor ion mass tolerance was 100 ppm and fragment ion mass tolerance was 0.25 Da. All identified proteins had a Mascot score greater than 64 (the default MASCOT threshold for such searches), corresponding to a statistically significant ($p < 0.05$) identification.

2.5 Results

2.5.1 Purification of native hPrx2

2.5.1.1 Ion exchange chromatography of native hPrx2

Native human Prx2 was purified from RBCs as described in section 2.4.1.3. The haemolysate was prepared from packed RBCs and the haemolysate was loaded onto a Sepharose anion exchange column using a 20 mM Tris-HCl buffer (pH 7.5) as described in the methods section 2.4.1.3 producing the trace seen in figure 2.1. The protein was subsequently eluted using the same buffer with a continuous salt gradient. The fractions were analysed using SDS-PAGE as described in section 2.4.1.4 (Fig. 2.2). The fractions containing the largest amount of Prx2 (in Fig. 2.2), with the least amount of contaminating protein as detected by SDS-PAGE (fractions C11–D7, Fig. 2.2.) were pooled and concentrated and they were used in a gel filtration chromatography step.

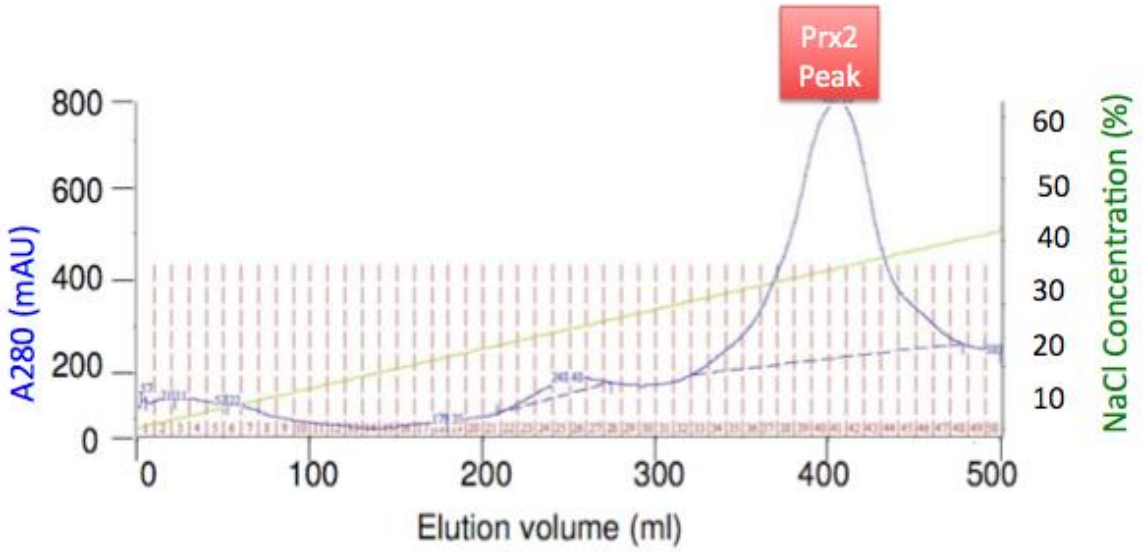

Figure 2.1. Elution profile of native hPrx2 (blue line) from ion exchange chromatography.

250 ml haemolysate was obtained by treating human packed RBC's with a hypotonic buffer and the haemolysate was applied to the column as described in the Methods section 2.4.1.2, then 15 ml fractions were collected throughout the entire elution. The red box indicates fractions that showed a band of the correct size of 22 kDa on SDS-PAGE. The third peak showed protein on a gel, but the protein was not hPrx2. The X axis represents the elution volume (ml), and the Y axis represents the absorbance at 280 nm (mAU). The blue curve represents the absorbance and the green line represents the increasing salt gradient.

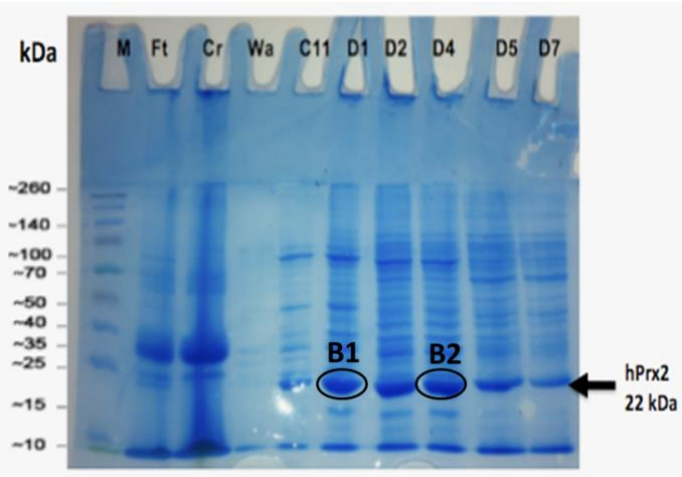

Figure 2.2. SDS-PAGE analysis of the elution from the hPrx2 ion exchange chromatography.

The SDS-PAGE was prepared in the presence of SDS and in the presence of beta mercaptoethanol. Lane (M), molecular weight marker (**appendix 1**), (Cr) = Crude sample, (Ft) = Flow-through, (Wa) Wash, and (Ft) =Flow-through. (Wa) = Wash samples collected from washing the column with 450 ml of buffer and C11 to D7 are the elution fractions which were collected. The protein hPrx2 in fractions D1 and D4 marked “B1” and “B2” were identified by **MALDI–TOF–MS** analysis (table 2.3a and 2.3b)**.**

In order to confirm that the purified protein was Prx2, the samples were analysed by mass spectrometry and Western blotting. Purified putative Prx2 samples were resolved on SDS-PAGE under reducing and non-reducing conditions. The gel bands, which were thought to correspond to Prx2, were cut out and a trypsin digest was carried out on the samples. Following this, MALDI-TOF-MS analysis was carried out on the samples using the facilities at the University of Bristol in Dr. Kate Heesom’s laboratory.

(a)

Protein name	Number of peptides	Sequence coverage [%]	MW [kDa]	Score
Catalase	9	21.40	59.70	521.48
Aldehyde dehydrogenase	5	13.60	54.80	232.61
Thiol-specific antioxidant protein (a.k.a.Prx2)	8	8.60	21.80	41.13

(b)

Protein name	Number of peptides	Sequence coverage [%]	MW [kDa]	Score
Catalase	9	21.40	59.70	521.48
Aldehyde dehydrogenase	5	13.60	54.80	232.61
Thiol-specific antioxidant protein (a.k.a.Prx2)	8	8.60	21.80	41.13

Table 2.3. MS results for band 1 (B1) and band 2 (B2) as obtained by cutting out the bands from the SDS-PAGE shown in figure 2.2.

The table shows all the statistically significant identifications ($p<0.05$) resulting from a Mascot search of the MALDI MS data against the NCBI Human database as shown in appendix 3. **Area**

In order to determine the oxidation status of the active site of the isolated protein, non-reducing SDS-PAGE was performed as shown in figure 2.4 below. The gel samples were prepared in a non-reducing manner as described in the Methods section 2.4.5.1. The non-reduced hPrx2 samples were found to run as a dimer (44 kDa) on the SDS-PAGE and as a monomer (22 kDa) for the reduced samples.

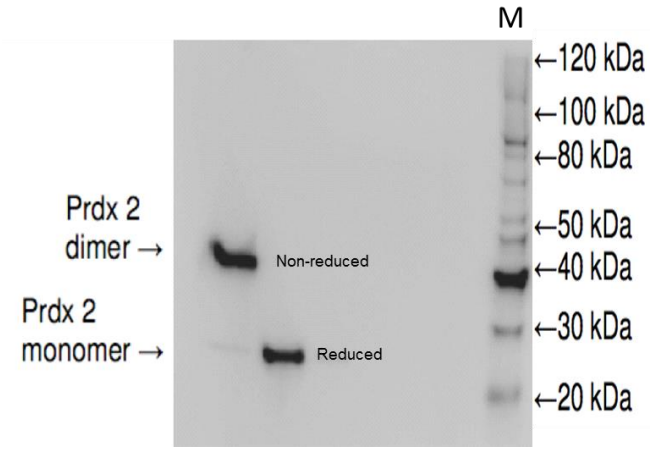

Figure 2.4 Reducing and non-reducing SDS-PAGE of the purified native hPrx2.

hPrx2 protein was obtained from haemolysed human packed red blood cells as described in the Methods section 2.4.1.2. The protein sample was treated in either a reducing or non-reducing manner as described in the Methods sections 2.4.5.1 or 2.4.5.2. Known molecular weight standards (M) were used to estimate the molecular size of the protein.

2.5.1.2 Calibration of Superdex 200 with known standards

The gel filtration column was calibrated with the known protein standards as described in the Methods section 2.2.1.4.

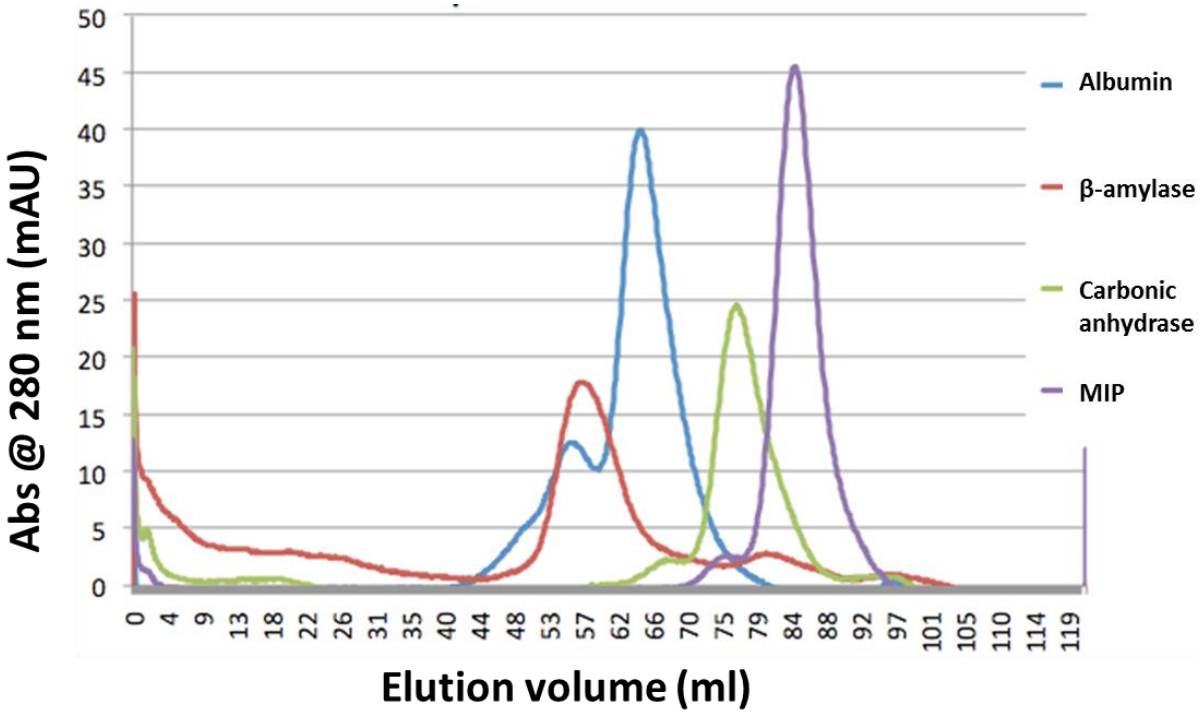

(a)

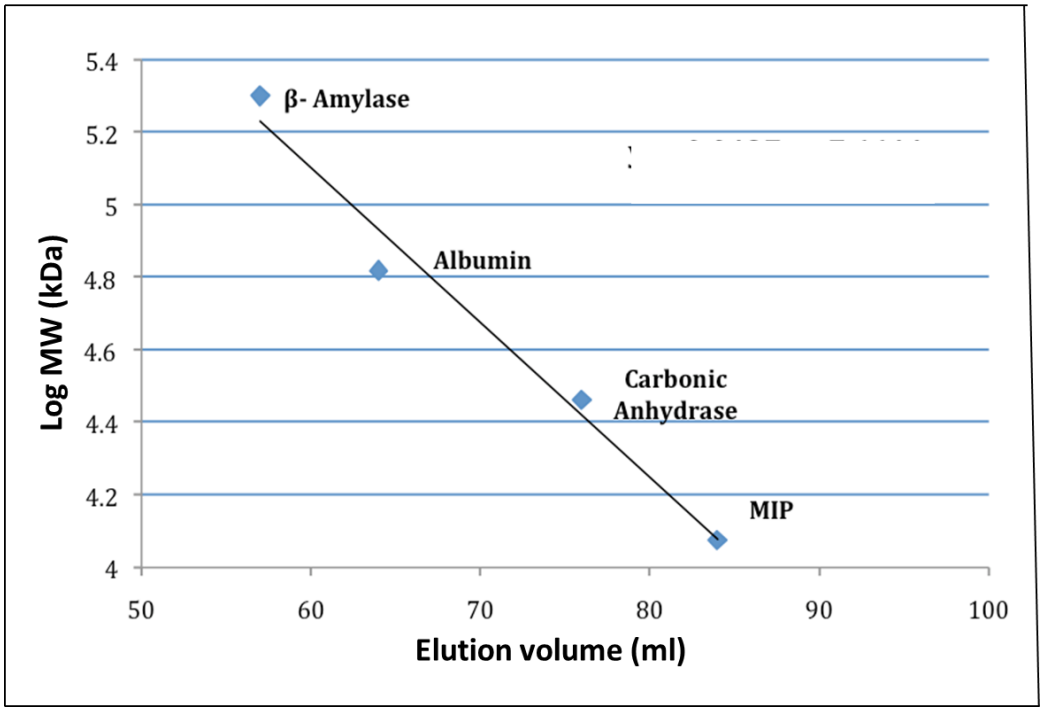

(b)

Figure 2.5. Calibration of Superdex 200 with known molecular weight standards using 20 mM Tris-HCl pH 8.0, 5 mM EDTA buffer.

The following molecular weight standards were used: albumin (66 kDa), carbonic anhydrase (29 kDa), β-amylase (200 kDa) and MIP (11 kDa). From the calibration curve, molecular weights of the unknown proteins were able to be determined. I carried out this work from Prof. Littlechild's lab.

2.3.1.3 Gel filtration chromatography of native hPrx2

Gel filtration chromatography was used as a final step of the purification and as a tool for estimation of the oligomeric state of the protein. A concentrated protein sample was loaded onto an equilibrated and calibrated HiLoad 16/60 Superdex 200 (GE Healthcare) and run as described in method section 2.4.1.4.

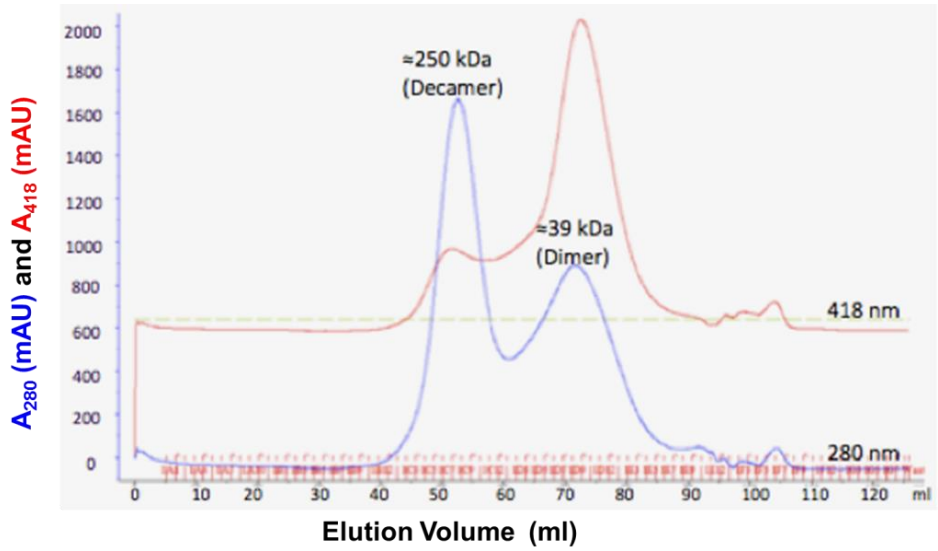

Figure 2.6. The elution profile for native hPrx2 from gel filtration chromatography.
The void volume of the column was about 36 ml. Peak 1 (50 ml) corresponds to the decameric form of the protein (~250 kDa); Peak 2 (75 ml) corresponds to the dimeric form of the protein (~48 kDa).

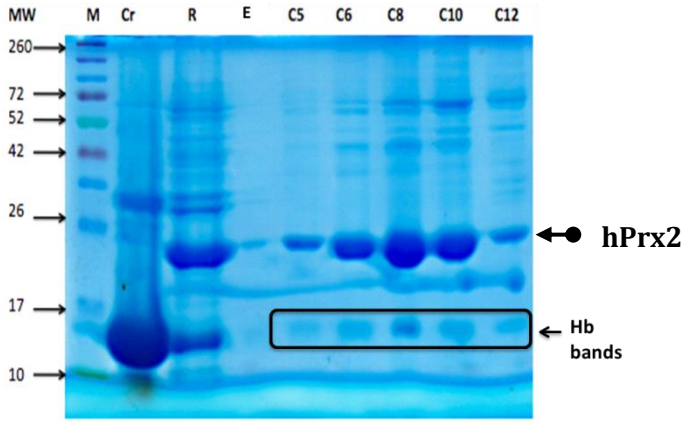

Figure 2.7 SDS-PAGE for the dimeric peak fractions of the gel filtration chromatography for native hPrx2.

Lane 1 (M) molecular weight marker; Lane 2 crude sample (cr) loaded onto the column; Lane 3, flow through sample (R); Lane 4, is an empty lane (E), from column elution; C5 to C12 are fractions across the decameric peak (Fig. 2.6). The gel filtration peak 2 was of Prx2 but contaminated with high molecular weight proteins and Hb, confirmed by mass spectrometry.

2.5.1. 4 Overview of purification of native hPrx2 from RBC's

Gel filtration or size exclusion chromatography separates proteins based on their molecular weight: proteins with a high molecular weight elute first, followed by low molecular weight proteins.

The purification of native hPrx2 was successfully achieved using FFQ Sepharose and gel filtration chromatography. The trace from FFQ chromatography produced two peaks with the first containing the native hPrx2 protein. The calibrated gel filtration column confirmed that hPrx2 protein to be mainly produced in the decameric form. Using this method ~20 mg of protein was purified from 500 ml of blood. SDS-PAGE analysis for the elution fractions from the two peaks, confirmed that both peaks were Prx2 but contaminated with higher molecular weight proteins and Hb (Fig. 2.7).

According to the calibration of the column, molecular weight of peak 1 fractions on SDS-PAGE and MS identification results, the elution fractions collected from peak 1 were assumed to contain the decameric form of hPrx2. Using this method, approximately 90 mg of Prx2 protein was purified from 1000 ml of blood.

2.5.2 Purification of recombinant hPrx2

One litre of culture produced 1.95 g of cell pellet and after cell lysis and centrifugation (as described previously in method section 2.4.4.1), the supernatant was purified using nickel affinity chromatography and gel filtration chromatography as described in method sections.

2.5.2.1 Expression of recombinant hPrx2

The pET28a/*hPrx2* construct was transformed into the *E. coli* strain Rosetta Gami 2. Rosetta Gami 2 was chosen as it aids disulfide bond formation through mutations in the thioredoxin B (*trxB*) and glutathione oxidoreductase (*gor*) genes. As the hPrx2 protein contains an intra-molecular disulfide bond in its reaction mechanism, it was thought that the promotion of this oxidation state might aid protein stability. hPrx2 protein expression was under the control of the T7 promoter and was induced by IPTG. The over-expression of hPrx2 was investigated by induction studies to obtain the best conditions

for over- expression. The optimal over-expression was achieved by addition of a final concentration of 1 mM IPTG when the cells had reached an OD600nm of 0.8 with further incubation for 4 hours at 37ºC. The over-expression of hPrx2 resulted in soluble protein being produced at the expected size (~24 kDa) (Fig. 2.8) as reported by Schirmer *et al*., 2010.

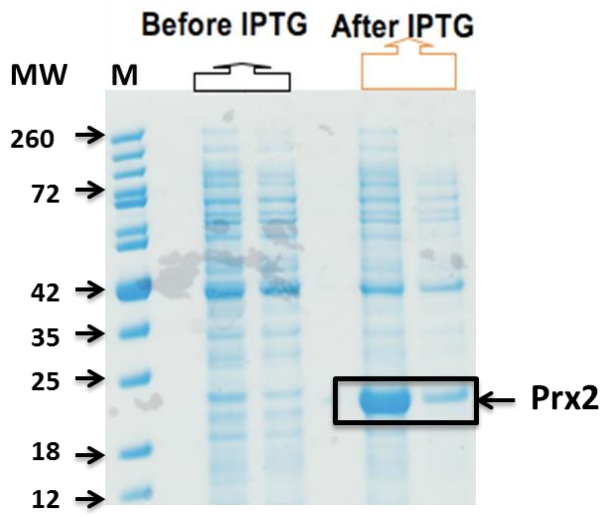

Figure 2.8 SDS-PAGE analysis of the over-expression of hPrx2 in *E.coli*.
Lane 1 (M) molecular weight marker; Lane 2 and 3 protein samples before IPTG addition; Lane 4 and 5, protein samples after IPTG.

Figure 2.9 Sequences analysis of pET28a/hPrx2 construct.

Open reading frames are highlighted in red, which can be used to identify the relative amino acid sequence.

2.5.2.2 Nickel affinity chromatography

The clarified cell extract was applied to a nickel column as described in method section. The fractions were analysed using SDS-PAGE as described in method section. The fractions containing hPrx2 were pooled and concentrated as described in method section for gel filtration chromatography analysis.

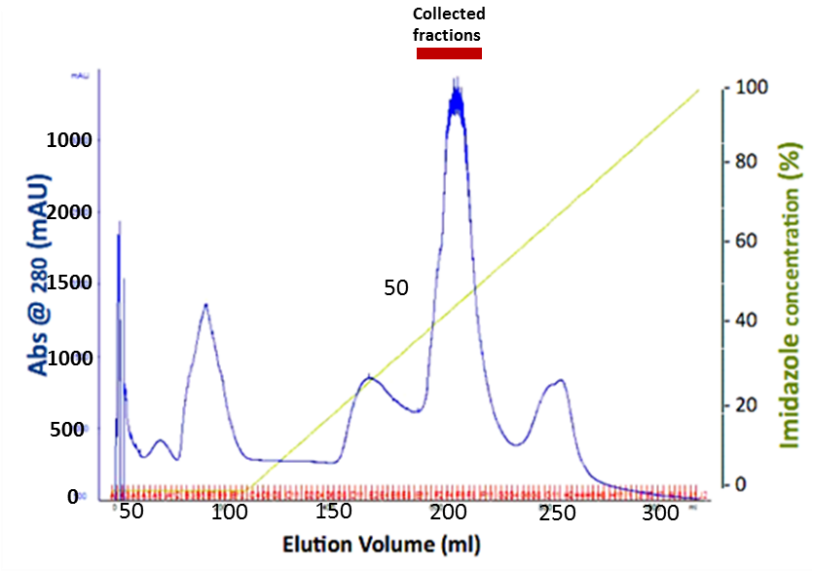

Figure 2.10 Elution profile of hPrx2 from nickel affinity chromatography.

10 ml fractions were collected throughout the entire elution. The blue line shows the % imidazole concentration. A red bar indicates the fractions that showed a band of the correct size (24 kDa) on SDS-PAGE (Fig. 1.11).

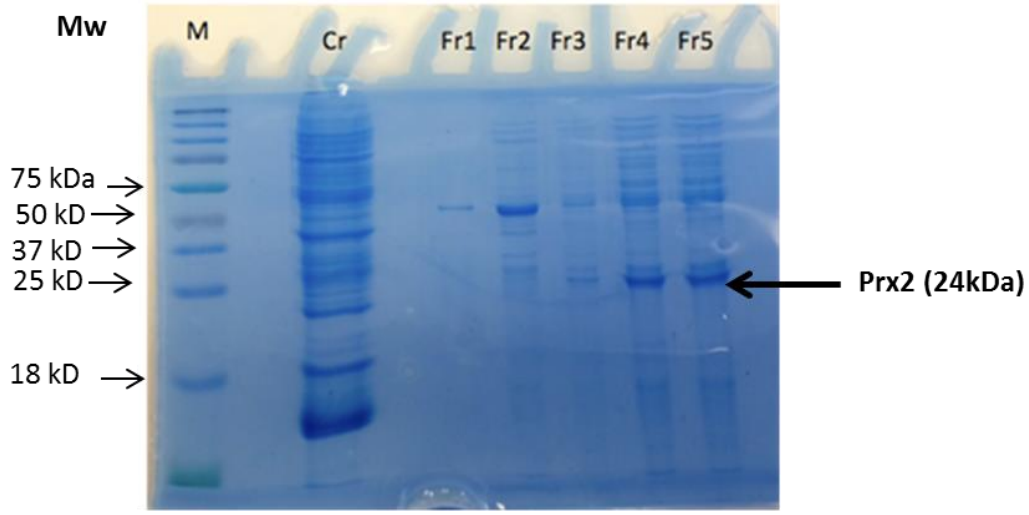

Figure 2.11 SDS-PAGE analysis of the hPrx2 nickel affinity column elution.

Lane 1 (M), molecular weight marker; Lane 2 (Cr), sample after IPTG; Lane 4(Fr1), sample from 160 ml; Lane 5, sample from 170 ml; Lane 6, sample from 180 ml; Lane 7, sample from 210 ml; Lane 8, sample from 220 ml. Fractions correspond to the fractions 1-5 shown on which chromatography in (Fig. 2.10).

2.5.2.3 Gel filtration chromatography

Gel filtration chromatography was used as a final step of the purification and as a tool for the estimation of the molecular weight of the protein. The concentrated protein sample was loaded onto an equilibrated HiLoad 16/60 Superdex 200 and run as described in method section 2.4.4.4. The gel filtration elution profile for the recombinant hPrx2 is shown in figure 2.12 below. The peak fractions were analysed by SDS-PAGE and protein fractions, which contained hPrx2, were pooled and concentrated for further experimental use.

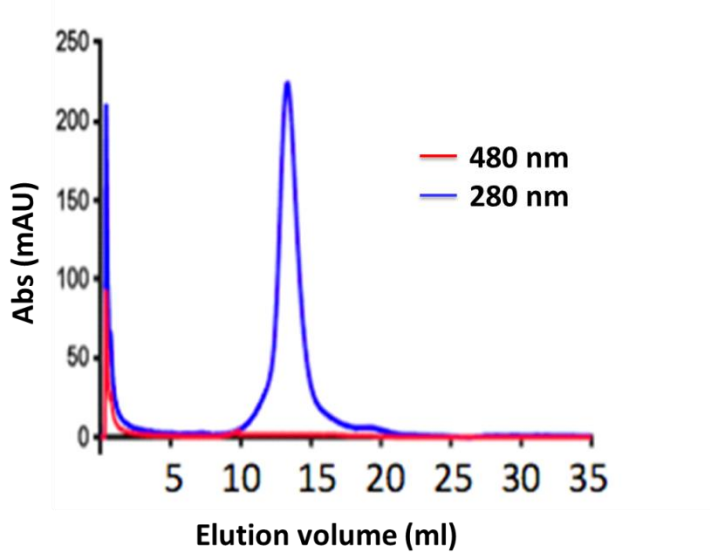

Figure 2.12. The elution profile from the Superdex 200 gel filtration column for recombinant hPrx2.

Red line absorbance at 418 nm (absorbance for haemoglobin), blue line absorbance at 280 nm (absorbance for hPrx2). Fractions were collected at 1 ml intervals throughout the elution volume. A single peak protein, which corresponds to the decameric form of hPrx2, was formed. The oligomeric state was determined using a calibrated Superdex 200 column (Fig. 2.5b).

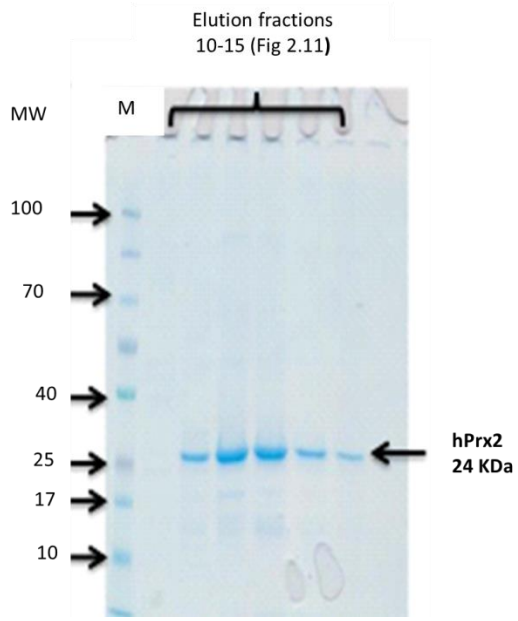

Figure 2.13 SDS-PAGE analysis of peaks from gel filtration chromatography of recombinant hPrx2. Lane 1, molecular weight markers (M) and lanes 2 to 6 are protein fractions 10-15 collected across the elution peak (Fig. 2.11).

2.6 Discussion

In order to confirm that the purified protein was Prx2, the samples were analysed by mass spectrometry and Western blotting. Purified putative Prx2 samples were resolved on SDS-PAGE under reducing and non-reducing conditions (Fig. 2.4). The gel bands, which were thought to correspond to nature Prx2, were cut out and we then carried out a trypsin digest on the samples. Finally, MALDI-TOF-MS analysis was performed on the samples using the facilities at the University of Bristol. The results confirmed the presence of Prx2 but contaminated with other proteins.

From our findings (table 2.3a and b), catalase and aldehyde dehydrogenase both had higher scores compared to Prx2, but we choose to study Prx2 this is because both catalase and aldehyde dehydrogenase enzymes havea well-known roles in RBC. Catalase is a common enzyme found in nearly all living organisms exposed to oxygen

(such as bacteria, plants, and animals). It catalyzes the decomposition of hydrogen peroxide to water and oxygen. It is a very important enzyme in protecting the cell from oxidative damage by reactive oxygen species (ROS)

During the early studies on native hPrx2 a number of difficulties were encountered during purification and concentration. It was discovered that most of the protein was being lost on the centrifugal ultrafiltration membranes (see section 2.4.1.4). Therefore, the best non-sticky ultrafiltration membranes were established. The Centricon plus-70 non-sticky centrifugal ultrafiltration units of 10,000 mw cut off (Merck Millipore) were used to concentrate hPrx2 protein. To get pure Prx2 from RBCs was problematic: hPrx2 failed to be completely separated from Hb as demonstrated from: MALDI–TOF–MS analysis report (tables 2.3), and gel filtration (Fig. 2.6). hPrx2 is known to have an affinity for Hb (Prx2 was sometimes been called haem-binding protein) (Shoko *et al*., 1999).

Using an anion exchange column followed by gel filtration chromatography, we purified native human Prx2 from packed RBCs. Without any reducing treatment, Prx2 was present in the haemolysate in decameric and dimeric forms, from which the decameric form was isolated.

Studying the spectral properties of purified Prx2, we found that the preparation displayed a peak at 418 nm, which is indicative of the Soret band. This suggested that the purified Prx2 was contaminated by haem or haemoglobin. Since Prx2 is known to interact with haem (Iwahara *et al*., 1995), we considered whether this contamination of Prx2 by haem or haemoglobin might be due to protein-protein interactions similar to those reported (Iwahara *et al*., 1995). Therefore, we concluded that native human haemoglobin may contain contamination, due to Prx2 binding (this hinted at a potential interaction between Prx2 and Hb). Hence, as a next step, the recombinant hPrx2 content, expected to be free of haemoglobin was analysed using gel filtration chromatography and Western blotting. What was observed was that, and as expected recombinant hPrx2 samples were free of haemoglobin contamination as demonstrated in Fig. 2.11 and Fig. 2.12.

In order to confirm if there was indeed a Prx2–Hb interaction and to answer why it had been impossible to separate the two proteins (Prx2 and Hb), the following experiments were carried out:

- To the native hPrx2 samples, we carried out a repeat of purification using the two chromatographic columns (ion exchange chromatography, and gel filtration chromatography) freshly re-packed. The same problem of haemoglobin Prx2-Hb contamination still remained.
- We turned to the use of recombinant hPrx2 as a control i.e. (we chromatographed recombinant hPrx2 on its own on Superdex 200 gel filtration, then ran Hb down the same column on its own and ran a mixture of recombinant hPrx2 + Hb. We measured the absorbance at both 280 nm and 418 nm. The chromatograph for the recombinant hPrx2 had a strong absorbance at 280 nm and the chromatograph for Hb had a strong absorbance at 418 nm due the sole band of haem. When hPrx2 + Hb were loaded onto the column, mixtures of peaks appeared: hPrx2 with a strong absorbance at 280 nm was found to co-elute with Hb with a strong absorbance at 418. This indicated a protein-protein interaction was taking place between these two proteins as discussed in chapter 4.

Chapter 3:

Synthesis and stability of SNO-Hb and Prx2-SNO

3.0 Introduction to some of key methods available for the synthesis and detection of S-nitrosated proteins

In order to study the structural and functional consequences of the S-nitrosation of hPrx2 and Hb, it was necessary to first synthesise the S-nitrosated forms of these two proteins. There are no reports that human Prx2-SNO has previously been synthesised however, Stamler and co-workers (Stamler *et al.* 1992) reported several general methods for the nitrosation of protein thiols including exposing the protein to NO gas, acidified nitrite, use of S-nitrosoglutathione and endothelial cells secreting NO. Other methods comprise the use of NO other donors (transnitrosation) such as S-nitroso-N-acetylpencillamine (SNAP) (Christen *et al.,* 2007) and the use of alkyl nitrite.

As discussed in section 1.5, RSNOs can be low molecular weight species such as: S-nitrosocysteine, S-nitrosoglutathione (GSNO), and (SNAP) or protein-species such as S-nitrosohaemoglobin (Wang *et al*., 2002). Under anaerobic conditions, the main products from the reaction of RSH and NO are RSOH and N_2O and under aerobic conditions a redox S-nitrosation reaction occurs (DeMaster *et al*., 1995). S-nitrosothiols *in vivo* could also occur via metal catalysed reactions (reviewed by Foster *et al*., 2003; Giustarini *et al*., 2007), in addition to what has been described in section 1.5.1 and demonstrated in Eq 1.2, 1.3 and 1.20. The existence of this pathway has been challenged because the oxidation of NO in aqueous solution is low (Giustarini *et al*., 2007), but it has been reconsidered following the development of the concept of the molecular lens effect: according to this concept, NO and O_2 concentrate in hydrophobic areas such as lipid membranes and hydrophobic pockets of proteins, for example Hb. This results in an increased production of nitrosating species (Nedospasov *et al.,* 2000; Kalyanaraman, 2004; Herold and Rock, 2005). As discussed at the beginning of this chapter a number of methods are available for the *in vivo* synthesis of RSNOs, including the use of: NO gas, acidified nitrite and transnitrosation. There are advantages and disadvantages with each method, thus influencing the decision which needed to be made about which method to use.

3.0.1 Via acidified nitrite

S-nitrosated proteins can be prepared by exposing the native proteins to acidified nitrite. NO_2^- itself does not nitrosate proteins (Marley *et al*., 2001; Orie *et al*., 2005 and Ishima *et al*., 2010). However, under acidic conditions, NO_2^- is converted to HNO_2 (Eq. 3.0), which in turn is converted into a number of nitrosating species, which include: NO^+, N_2O_3 and NOCl (Williams, 2004).

$$NO_2^- + H^+ \rightarrow HNO_2$$

Equation 3.0

N_2O_3 is the predominant nitrosating agent (Kharitonov *et al*., 1995). It is the main species present in equilibrium with nitrous acid according to its equilibrium constant (K). N_2O_3 also reacts with thiols faster than other HNO_2/H^+ -delivered species such as NOCl.

Treatment of protein thiols with acidified nitrite is the most common method for the production of S-nitrosated proteins as it is simple and relatively inexpensive. Thus it has scope to be completed on an industrial scale. However, the two main problems associated with this method are the denaturation of the protein and non-specific nitrosation (Katsumi *et al.,* 2004).

3.0.2 Synthesis by use of alkyl nitrites (RONO)

Protein thiols can be nitrosated by exposing them to RONO (such as *t*-butyl nitrite) diluted in a hydrophobic solvent such as chloroform for 30 min at room temperature and neutral pH (Hughes, 1999; Nedospasov *et al*., 2000) (Eq.3.1). This method is simple and the reagents are readily accessible. However, the method can cause denaturation of the protein. Using a less reactive RONO such as isoamyl nitrite can solve the problem of protein denaturation but it is a very expensive reaction.

$$C(CH_3)O\text{-}NO + RS^- \rightarrow RSNO + C(CH_3)O^-$$

Equation 3.1

3.0.3 Synthesis by use of NO gas

RSNO's can be prepared by bubbling NO gas through proteins in helium-deoxygenated sodium phosphate buffer (Wright *et al*., 2005). The presence of an electron acceptor allows the NO to attack the thiol group; the nitrosation species formed in this method is dinitrogen trioxide (N_2O_3). The method involves the oxidation of NO gas (see Eq 1.18 – 1.20). In aqueous solutions, N_2O_3 is converted into nitrous acid (HNO_2) from which other nitrosation agents can be derived. The process is done under anaerobic conditions to prevent the formation of higher oxides of nitrogen such as dinitrogen tetroxide (N_2O_4) which can destroy the protein (Wright *et al*., 2005) and cause nitration of amine residues (Williams, 2004).

The advantage of this technique is that it is completed at physiological pH ensuring the structure of the protein is retained. However, pure NO gas is expensive and this has implications if the assay is to be adapted to (a large) industrial scale: this can be prevented by dialysing the reaction mixture after nitrosation (Herold and Rock, 2005) or further bubbling with an inert gas (Palmerini *et al*., 2002).

3.0.4 Synthesis by use of NO donors

There are a wide range of NO donors used for the nitrosation of thiols: for example SNAP (Christen *et al*., 2007), diazeniumdialates and S-nitrosoglutathione. Many of these are low molecular weight RSNOs which nitrosate protein thiols via a transnitrosation reaction. This occurs under gentle conditions. Thus no adverse damage to the protein should occur. The disadvantage of using NO donors in the synthesis of RSNOs is that some of the donor molecules are expensive. If an RSNO-based NO donor is used, it is likely that the thiol group will be released as a by-product from the donor. For example glutathione will be released from SNOG, which may undergo a disulfide formation with free thiols of the protein preventing the nitrosation of the targeted sites.

3.1 Detection of S-nitrosothiols, in order to confirm that proteins have been successfully S-nitrosated

There are a number of techniques available for the detection of RSNOs *in vitro* and *in vivo,* which were reviewed a decade ago by Giustarini *et al*. (2007). They include spectroscopic techniques such as EPR spectrometry. Other methods include chemiluminescence, fluorescence, electrochemistry and the 'biotin switch' antibody method. There is great variation in the reported concentrations of RSNOs in specific bio-fluids and this suggests that no method for the detection of RSNOs is as yet preferred (Giustarini *et al*., 2007). In this part of the project, three different methods were used in order to confirm that target proteins had been successfully S-nitrosated: spectrophotometry (see section 3.1.1), gas phase chemiluminescence (see section 3.1.2) and the Saville assay (see section 3.1.3).

3.1.1 Spectrophotometric detection of RSNOs

RSNOs absorb light at 334 nm and 350 nm (Feelisch and Stamler, 1996). Therefore, it is possible to detect some RSNOs such as GSNO by UV-vis absorbance. However, this is not always possible for other RSNOs such as nitrosated albumin (SNOA) due to its low extinction coefficient. There are some other chemical groups such as RNNO, which absorb light around 335 nm which might be present in addition to RSNO (Kirsch *et al.*, 2003). However many studies use UV-vis spectrophotometry to monitor the synthesis of RSNOs because it is easy to use for an initial indication as to whether nitrosation has occurred without any time consuming preparation. Moreover, the analysed samples can be recovered.

The Saville assay (as described in section 3.8.6.1) was selected as the primary assay for the quantification of S-nitrosothiols in this study as it is simple and quick to perform although it has a detection limit of 0.2 μM, which is not low enough for the detection of RSNOs formed *in vivo*.

3.1.2 The use of gas-phase ozone-based chemiluminescence

NO metabolites such as NO_2^-, NO_3^- and RSNOs in biological samples are commonly detected by gas-phase ozone-based chemiluminescence (Moorcroft *et al*., 2001; Rockets *et al*., 2005; Giustarini *et al*., 2007; Winyard *et al*., 2008 and Bailey *et al*., 2009). The technique is based on the chemical reduction of these molecules to NO (MacArthur *et al*., 2007). The NO produced is carried by a flux of N_2 to the chemiluminescent reaction chamber where it reacts with ozone (O_3) to produce nitrogen dioxide in an excited state (NO_2^*). As the molecule relaxes to its energetic ground state it releases a photon ($h\nu$), which is then detected and transduced to an electric current by a photomultiplier tube (Eq. 3.2 and Fig. 3.0).

$$NO + O_3 \rightarrow NO_2^* + O_2$$

Equation 3.2

$$NO_2^* \rightarrow NO_2 + h\nu$$

Equation 3.3

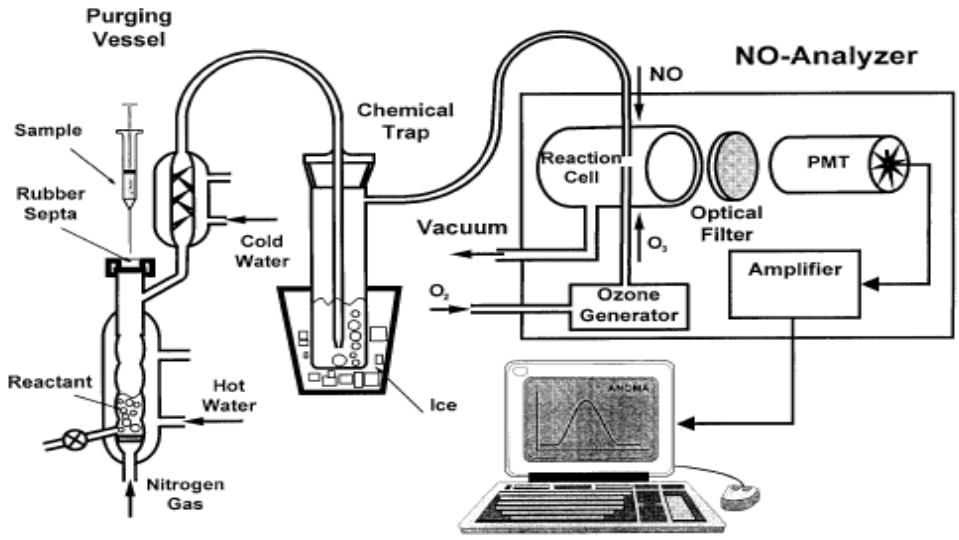

Figure 3.0. A diagram showing the nitric oxide analyser setup. Samples are injected through a rubber septum into the purge vessel (left) containing the reducing agent (reactant). A flux of N_2 carries the NO produced to the reaction cell (right), where the reaction with O_3 takes place. The signal is then detected and amplified. This scheme was obtained from Samouilov and Zweier (1998).

Acidic iodide (I^-) solution (for example 1% NaI w/v in acetic acid) is most commonly used as a reducing agent for many NO-derived metabolites (Giustarini *et al*., 2007). In the study reported in this thesis, the reducing agent used for the detection of NO_2^- consisted of NaI dissolved in deionized water. This solution was then added to the purge vessel of the nitric oxide analyser, containing glacial acetic acid. NO_2^- can be detected using this solution via the reaction in (Eq. 3.2).

$$I^- + NO_2^- + 2H^+ \rightarrow NO + \tfrac{1}{2} I_2 + H_2O$$

Equation 3.3

The same approach is used for the detection of RSNOs, although usually free iodine (I_2,) is added to the reducing agent to form tri-iodide, I_3^-, which will then react with the RSNOs in the sample (MacArthur *et al*., 2007) (Eq. 3.4 to Eq. 3.6).

$$I^- + I_2 \rightarrow I_3^-$$

Equation 3.4

$I_3^- + 2RSNO \rightarrow 3I^- + RSSR + 2NO^+$

Equation 3.5

$2NO^+ + 2I^- \rightarrow 2^{\cdot}NO + I_2$

Equation 3.6

The system functions by: I_3^- reduces RSNO to 20% disulfide (RSSR) and the nitrosonium ion (NO^+) and after reaction with I^-, NO^+ is reduced to NO which is detected by the system (MacArthur *et al*., 2007 and Giustarini *et al*., 2007). The data are reported as chemiluminescence time courses (mV vs. time). The quantification of NO_2^- or RSNO in the samples involves the conversion of the signal peak areas to molar concentrations by using a standard curve prepared with known concentrations of NO_2^-/RSNO.

3.1.3 S-nitrosothiol detection by the Saville assay

The oldest method for the detection of RSNOs was developed by Saville (1958) and involves a spectrophotometric assay. Mercury is used in this technique, which causes the selective decomposition of RSNOs, from which NO is released as nitrite (Swift and Williams, 1997). Nitrite reacts with the Griess reagent (sulfhanilamide) (SULF) and N-(1-napthyl)-ethylenediamine (NED) to form an azo-dye which is detected by its absorbance at 540 nm (E = 50000 $M^{-1}cm^{-1}$). This technique obeys the principle that one mole of S-nitrosothiol produces one mole of chromophore (Feelisch and Stamler, 1996). Therefore, the absorbance at 540 nm is directly related to the amount of RSNO present (change in absorbance between mercury treated and non-mercury treated samples).

$Hg^{2+} + 2\ RSNO \rightarrow Hg(RS)_2 + 2\ NO^+$

Equation 3.7

$NO^+ + H_2O \rightarrow HNO_2 + H^+$

Equation 3.8

$HNO_2 \rightarrow NO_2^- + H^+$

Equation 3.9

3.2 Factors affecting structural and functional properties of proteins

Protein structure is highly complex and is comprised of amino acids as building blocks. Regardless of their origin (e.g., animal, plant, or microbial) proteins contain 20 amino acids (Well, 2004). The amino acids are organic compounds which are composed of an amino group (NH_2), a carboxyl group (COOH), and a side chain (R) as described in Figure 3.1. The side chain distinguishes one amino acid from the other. When two amino acids are bound chemically, a dipeptide is formed. One polypeptide can form a tertiary structure composed of many amino acids are joined together. When numerous polypeptide chains give rise to a unique three-dimensional structure it is known as a protein unit.

The structural and functional properties of proteins are greatly affected by the following factors: the physiological pH, temperature, solvent concentration and the ionic strength of the solution. In the presence of all the mentioned factors, proteins assume a particular preferred folded conformation. It is commonly accepted that both light and metals readily cause decomposition of RSNOs. Treating samples with Chelex resin, and storage in the dark, can increase the lifespan of RSNOs to a certain degree but does not restore the conformational changes in a protein which might be caused by the factors mentioned above. Therefore, after synthesising our RSNOs it was important to test the stability of the proteins.

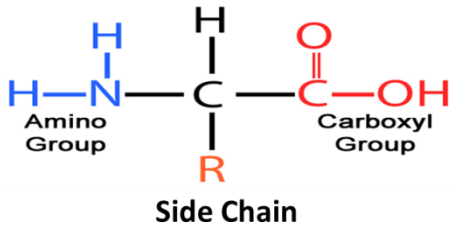

Figure 3.1 A typical amino acid structure

3.2.1 Stability of proteins and ligands

The detection of protein-ligand interactions using differential scanning fluorimetry is a reliable and sensitive technique used to study the stability of the hPrx2 protein under various pH conditions and temperatures.

Proteins bind, with varying affinities, to a diverse range of other molecules from simple ions to other large macromolecules. In many cases, proteins bind to small molecule partners as part of their normal function. For example, a kinase binding to ATP. Other interactions may be unrelated to function, but are experimentally useful as tools (for example, small molecules that stabilize proteins to improve crystallization success or assist in maintaining proteins in solution); whilst small molecules that bind to active sites and allosteric sites of proteins can act as inhibitors, and so modulate the activity of enzymes.

There is a wide range of techniques that can be used to determine the affinity of proteins for partner molecules: for example, isothermal titration calorimetry (Freyer and Lewis 2008), and other label free methods such as surface plasmon resonance or bilayer interferometry (Abdiche *et al*., 2008). Differential scanning fluorimetry (DSF or thermo shift assay) is being increasingly used as a robust method for initial screening of proteins for interacting small molecules, either for identifying physiological partners or for hit discovery (Vivoli *et al*., 2014). DSF was first described in Pantoliano *et al*., (2001) as a method for drug discovery. In this method, proteins are incubated with a fluorescent dye (initially naphthalene-sulfonic dyes), which alters the fluorescence of the dye upon binding to the hydrophobic regions of the proteins. The protein-dye sample is then heated, and the fluorescence monitored as the heat rises. The unfolding of the protein, and exposure of hydrophobic parts of the protein, gives rise to a characteristic pattern in the fluorescence as a function of temperature.

In this project, DSF was used to measure the stability of the synthesised Prx2-SNO and Hb-SNO. DSF is the most cost effective method available, compared to existing methods on the market for the determination of the dissociation constant between a protein and interacting small molecules. Most of the techniques available require access to specialized equipment and expertise to effectively analyse data. The DSF

technique has the advantage that it only requires a PCR machine, a commonly available instrument in almost all laboratories.

3.2.2 The determination of the dissociation constant for the protein

The overall goal for this procedure is to estimate the dissociation constant for a protein-ligand interaction. This is done by first preparing mixtures of the protein with different concentrations of the ligand together with the indicator dye. The second step is to heat the samples while recording the fluorescence of the indicator to monitor the unfolding of the protein. Next the protein unfolding curves are converted into a series of melting temperatures. The final step is, to fit these data onto an appropriate model to estimate the dissociation constant (K_d). Using equations 3.10 and 3.11, the dissociation constant for the protein can be calculated.

$$K_d = c^{\ominus} e^{\frac{\Delta_r G}{RT}} \qquad \Delta G = \Delta H - T\Delta S$$

Equation 3.10 **Equation 3.11**

where c^{θ} is the standard reference concentration, $\Delta_r G$ is the Gibbs free energy change of the reaction, R is the molar gas constant, ΔH is the enthalpy change in the reaction, ΔS is the entropy change in the reaction and T is the temperature (in kelvin or ˚C).

3.3 Aims and objectives

The aim of this chapter was to synthesise both Hb-SNO and hPrx2-SNO. It was necessary to synthesise these nitrosated proteins (Hb-SNO or hPrx2-SNO) in order to study their potential interactions with non nitrosated (Hb or hPrx2), in order to begin to address the question of whether Prx2 might be involved in NO release from RBCs. This is was important because according to Neal *et al*., (2013) evidence suggests that, physical association of NO with a protein determines the specificity of that protein's interactions with other proteins.

The first step was to extract hPrx2 protein from human RBC lysates and to prepare recombinant hPrx2 from *E.coli* to use as a control. From this purification, samples of hPrx2 and hPrx2 containing traces of haemoglobin (Hb) were obtained. Samples of hPrx2 containing traces of Hb were analysed by SDS PAGE and Western blotting to confirm the presence of Hb. SNOPrx2 and SNO-Hb were then chemically synthesised. The interaction of hPrx2 with Hb and a possible formation of a SNOPrx2-Hb complex were studied spectrophotometrically.

3.4 Materials and methods

3.4.1 Materials

Sodium nitrite ($NaNO_2$) was used as a source of NO_2^- (Fisher chemicals, Loughborough, Leicestershire, UK). Sodium acetate/acetic acid (Fisher Chemicals, Loughborough, Leicestershire, UK), 3-(N-morpholino) propanesulfonic acid (MOPS, BDH chemicals, Poole, Dorset, UK) and N-cyclohexyl-3-aminopropanesulfonic acid (CAPS, BDH Chemicals, Poole, Dorset, UK) were used to obtain buffers at pH 4.0 (acetate buffer), 6.0, 7.4 (MOPS) and 10.0 (CAPS). S-nitrosoglutathione (GSNO, Enzo Life Sciences, Exeter, Devon, UK) was used as a standard. For the detection of NO production from NO_2^- gas-phase ozone-based chemiluminescence was used. S-nitrosothiols (RSNOs) determination was carried out with three different techniques: gas-phase ozone-based chemiluminescence, UV-vis spectra and the Saville assay, which is a colorimetric assay (see sections 2.2.2.3 and 2.2.2.5). For the gas-phase ozone based chemiluminescence experiments, the following reagents were used (MacArthur *et al*., 2007): sodium iodide (NaI, Fisher Chemicals, Loughborough, Leicestershire, UK), acetic acid (Fisher Chemicals, Loughborough, Leicestershire, UK), and free iodine (I_2, Sigma Aldrich, Dorset, UK). For the Saville assay the samples were treated with sulfanilamide (Acros Organics, Fisher Chemicals, Loughborough, Leicestershire, UK), mercuric chloride ($HgCl_2$, Fisher Chemicals, Loughborough, Leicestershire, UK) and N-1-napthylethylendiamine dihydrochloride (NED, Acros Organics, Fisher Chemicals, Loughborough, Leicestershire, UK).

All the chemicals purchased were of the highest purity commercially available. All the general laboratory plastic-ware used throughout this project was purchased from Alphalabs (Hampshire, UK) unless otherwise stated. The cell culture plastic-ware was purchased from Greiner Bio-one (Gloucestershire, UK) unless otherwise indicated. All other chemicals were purchased from Sigma Aldrich, UK.

3.4.2 Methods

3.4.2.1 Isolation of hPrx2 from RBCs

Isolation of native hPrx2 from RBCs was carried out as described in chapter 2, sections 2.4.1.1 - 2.4.1.4.

3.4.2.2 Preparation of recombinant hPrx2

Recombinant hPrx2 was prepared as described in chapter 2 (see sections 2.4.2 - 2.4.2.6).

3.4.2.3 Synthesis of hPrx2-SNO using nitrite in acetate buffer pH 4.5

The protocol was modified from (Wright *et al*. 2005). Additionally, Chelex-treated ultra-pure water was used to prepare all reagents except the Prx2 protein sample, to improve the stability of the SNOPrx2 product. Chelex-100 is a resin containing iminodicatate ions, which bind polyvalent metal ions. This was done to remove metal contaminants such as copper and iron which can cause the decay of any nitrosothiols formed (Kirsch *et al*., 2003).

Purified hPrx2 protein samples prepared from RBCs (section 2.4.1) and by recombinant techniques (section 2.4.2) were used in the synthesis of SNO-Prx2. SNOPrx2 was synthesised using acidified NO_2^- as the nitrosating agent. The protocol used for the synthesis had been previously developed by our research group in association with Dr. John More and colleagues at Bio Products laboratory (BPL, Elstree, UK) for the synthesis of SNOA. In this protocol no reducing agents were used to pre-treat the protein (to reduce potentially oxidised Cys residues).

2 ml 5mg Prx2 previously purified from RBCs was added to 2.5 ml 50 mM acetate buffer pH4.5 and 0.5 ml 0.05 M $NaNO_2$. This was incubated for two hours at room temperature. The reaction was then terminated by eluting the reaction mixtures on a gel filtration column. After a 2 h incubation at room temperature, the solutions were applied to a PD10 desalting column (GE Healthcare, Chalfont St Giles, Buckinghamshire, UK) and eluted with phosphate buffer (50 mM, pH 7.4, $Na_2HPO_4(2H_2O)$ and $NaH_2PO_4(H_2O)$

(from Fisher Chemicals, Loughborough, Leicestershire, UK). This allowed the protein to be separated from the excess NO_2^- and to be re-equilibrated in phosphate buffer. Several 1 mL fractions of the eluate were collected and the ones with the highest absorbance at 280 nm (highest protein concentration) were pooled together (absorbance values were read on a Cary 300 UV-Vis spectrophotometer). To additionally remove any residual NO_2^-, the solutions collected were dialysed overnight in 4 L of phosphate buffer (50 mM, pH 7.4), using dialysis cassettes (Slide-A-Lyzer Dialysis Cassette, 10K molecular weight cutoff, Thermo Fisher Scientific, Northumberland, UK). After synthesis and dialysis SNOPrx2, samples were characterised by the Saville assay, to determine the RSNO concentration. Saville assay reagents were prepared as previously described (Section 3.2.2.4). The SNOPrx2 samples (20 µL) were treated with 1% (w/v) sulfanilamide in HCl 0.5 M (20 µL) and 1% sulfanilamide in HCl 0.5 M in the presence of 0.2% $HgCl_2$ (20 µL), in a 96-well plate. After 5 minutes of room temperature incubation (in the dark), NED (0.02%, 40 µL) was added to each treatment, leading to the formation of a purple azo-dye. After 5 minutes the absorbance of the samples was read at 540 nm (on a BMG Labtech Fluostar Optima plate reader, Thermo Fisher Scientific, Northumberland, UK). The amount of RSNO in the samples was derived from the difference in absorbance between the Hg^{2+}-treated sample and the Hg^{2+}-untreated sample. The standard curve was prepared by using solutions of GSNO (Enzo Life Sciences, Exeter, Devon, UK) of known concentrations (0-300 µM).

3.4.2.4 Synthesis of Hb-SNO using nitrite in acetate buffer, pH 4.5

Hb (1 mM) was incubated with a 5-fold excess of $NaNO_2$ (5 mM) in acetate buffer (200 mM, pH 3.7). Control solutions were also prepared: in the first deionized water was added to Hb and in the second, Hb was treated with the same amount of NO_2^-, but at neutral pH (no nitrosation reactions take place in these conditions). All the solutions used for the work were treated with a chelating agent (e.g. Chelex-100) to ensure the stability of the RSNO group in the protein after the synthesis. After 1h of incubation at room temperature, the solutions were eluted from PD10 desalting columns (GE Healthcare, Chalfont St Giles, Buckinghamshire UK) with sodium phosphate buffer (50 mM, pH 7.4) as mentioned. This allowed the protein to be separated from the excess NO_2^- and to be re-equilibrated in phosphate buffer. Several 1 mL fractions of the eluate

were collected and the ones with highest absorbance at 280 nm (highest protein concentration) were pooled together. The absorbance of the fractions was read using a Cary 300 UV-vis spectrophotometer (Agilent Technologies).

To additionally remove any residual NO_2^-, the collected solutions were dialysed overnight in 4 L of sodium phosphate buffer (50 mM, pH 7.4), using dialysis cassettes (Slide-A-Lyzer Dialysis Cassette, 10 kDa molecular weight cutoff, Thermo Fisher Scientific, Northumberland, UK).

3.4.3 Characterisation of RSNOs (hPrx2-SNO and Hb-SNO)

3.4.3.1 S-nitrosothiol detection by the Saville assay

The amount of RSNO in the samples was derived from the difference in absorbance between the Hg^{2+}-treated group and the Hg^{2+}-untreated group. The standard curves used for the experiments in this work were prepared by using solutions of GSNO of known concentration (concentrations of the standards were determined by UV-vis spectrophotometry (Cary 300 UV-Vis spectrophotometer, Agilent Technologies UK Ltd., Stockport, Cheshire, UK) using GSNO absorbance at 540 nm and a molar extinction coefficient (ε) of 767 M^{-1} cm^{-1}) Feelisch and Stamler, 1996).

3.4.3.2 Determination of protein concentration

The Bradford assay is a method used to determine protein concentration. It is based on the change in absorbance from 465 nm to 595 nm of the dye, Coomassie Brilliant Blue, when it binds to proteins (Boyer, 2000).
The protein samples of 4.8 mg were diluted 100-fold. On a 96-well plate, 20 µl of each protein solution was added to 40 µl Bradford reagent and 140 µl water in triplicate. The plate was read at 595 nm by a Dynex MRX plate reader. A standard curve created using known amounts of bovine serum albumin (BSA) (0, 0.05, 0.1, 0.25, 0.5, 0.8 and 1 mg/ml, Sigma Aldrich) was used to calculate the protein concentration.

3.4.3.3 Modification of the protocol for hPrx2-SNO and Hb-SNO synthesis

The degree of nitrosation of hPrx2 and Hb thiols was improved by a change of the buffer conditions: 200 mM acetate buffer pH 3.7 was discovered to yield more nitrosation than 50 mM acetate buffer pH 4.5. The protocol for the synthesis of SNO-Prx2 and SNO-Hb was done as described in sections 3.4.2.5 and 3.4.2.6. The pHs of the mixtures were taken before the nitrite was added and after a 1 h incubation. The reaction products were then eluted from a PD10 column and analysed using the Bradford and Saville assays (with a GSNO standard curve) (Fig. 3.3) as described in section 3.4.3.1. However, there was a problem during the synthesis of SNO-Prx2 and SNO-Hb. The acidic conditions caused denaturation and precipitation of both proteins. Therefore there was a need to establish the optimum pH for the synthesis.

3.4.3.4 Testing for the stability of hPrx2-SNO and Hb-SNO

The stability of Prx2-SNO and Hb-SNO was done by measuring the melting temperature of a protein using thermal shift assay. The protein mixtures contained: 5000X SYPRO Orange (1.78 µl), 0.5 M HEPES pH7.0 (22.2 µl), 5 M NaCl (33.3 µl) and added water to 180 µl final volume, were prepared as detailed in Table 3.0. 18 µl of the protein mixture was aliquoted into eight wells in a qPCR plate. 2 µl of the solvent buffer was added to the first well, and then 2 µl of each member of the ligand dilution series was added. A PCR seal was placed over the plate to prevent evaporation. To achieve a good seal of the plate, a hand applicator was placed in the middle of the plate, smoothing down the seal to one side, and then this process was repeated on the other half of the plate. The plate was centrifuged at 500 x g for two minutes to remove air bubbles. Then the plate was placed in a StepOne qPCR instrument (Thermo Fisher, Thermo Fisher Scientific, Northumberland, UK) the "Melt curve" option was selected using, the ROX filters. The fast ramp speed was chosen (this provides a 2 min pause at 25°C, followed by a ramp to 99°C, over 40 min, and then a 2 min pause). A thermal denaturation programmer was then run. When the denaturing program was completed, the results were analysed using protein thermal shift software. The melting temperature

of the protein was checked in the presence and absence of a solvent buffer. The analysis of the data was done by creating a table of the ligand concentrations and the melting temperatures. A graph of melting temperature (°C) vs ligand concentration (µM) was plotted, and used to approximate the dissociation constant for the protein (hPrx2).

3.4.3.5 GSNO preparation

Freshly prepared GSNO was achieved by mixing an equimolar concentration of 200 mM glutathione (in 0.75N HCl) with the same volume of 200 mM of potassium nitrite (NO_2^-) the mixture was added, incubated for 5 min at room temperature, then neutralised with 1M Tris buffer pH 7.5. The amount of GSNO produced was quantified using the Saville assay.

3.4.3.6 Synthesis of Prx2-SNO using GSNO

Synthesis of Prx2-SNO using GSNO was achieved in two ways:

(a) Incubation of freshly made GSNO of known concentration with purified hPrx2 samples (nitrosation dependent formation of hPrx2 dimer).
(b) Addition of GSNO to the growth medium during the over-expression of hPrx2.

20 µl (200 mM) of freshly made GSNO was mixed with 80 µl (10 mg) hPrx2, and then incubated for 4 h on ice. 10 µl of glycerol was added to the product and kept at -20^{o}C for future use.

Synthesis of Prx2-SNO, *via* the addition of GSNO to the growth medium, was done as follows: the recombinant hPrx2 gene was transformed in *E.coli* as described in section 2.4.2.2, the start culture was grown under agitation at 200 rpm overnight at 37^{o}C and 20 ml were used to inoculate 1 L of fresh growth medium containing the appropriate antibiotics for selection. The culture was grown with agitation at 37^{o}C until the optical density (OD_{600nm}) was approximately 0.8. Then 50 ml of freshly made GSNO (200 mM) was added to the medium and the synthesis of the protein was induced by addition of Isopropyl β-D-1-thiogalactopyranoside (IPTG) to the final concentration of 1.0 mM. The culture was incubated for a further 4 h at the same temperature as before. The *E. coli*

cells were harvested by centrifugation (20,000 x g, 20 min at 4^{o}C) using a Beckman JA-25.50 rotor. The cell pellet was stored at -20^{o}C until further use.

The purification of Prx2-SNO was done by re-suspending the *E.coli* cell pellet in 10% w/v 100 mM Tris-HCl, pH 7.5, 0.5 M NaCl, 20 mM imidazole. The cells were then disrupted by sonication at 10 microns on ice using the setting: 30 sec on and 1 min off for 6 cycles (as described in section 2.4.2.3). The cell debris was removed by centrifugation at 20,000 x g, 20 min at 4^{o}C using a Beckman JA-25.50 rotor. The supernatant was kept for further purification procedures (nickel affinity chromatography followed by gel filtration chromatography) as described in sections 2.4.2.5 and 2.4.2.6.

3.4.3.7 Synthesis of SNO-Hb using GSNO

5 g of Hb were dissolved in 50 ml of buffer (100 mM Tris-HCl, 0.1 M NaCl, pH 7.5). This solution was mixed with a freshly made solution of 200 mM GSNO and incubated for: 4 h, 8 h, 12 h and 24 h at 4^{o}C, followed by the characterisation of the products.

3.4.3.8 Characterisation of hPrx2-SNO and Hb-SNO

After synthesis and dialysis of the protein products (hPrx2-SNO and Hb-SNO), samples were characterised by the Saville assay (as described in the methods section 3.7.5) to determine the RSNO concentration. The DTNB assay was used to determine the residual amount of free thiols, and the final protein concentration produced was determined using the Bradford assay (as described in Methods section 3.7.6). Mass spectrometry and Western blotting was used to confirm the identities of purified proteins (hPrx2-SNO and Hb-SNO).

3.4.3.9 Gel electrophoresis and Western blotting of hPrx2-SNO

Reducing and non-reducing SDS-PAGE was performed as described in Chapter 2. A six percent final concentration of acrylamide was used to prepare gels for native PAGE. Native PAGE was performed as described in Chapter 2 (see section 2.4.5.3).

Western blotting was performed as described in Chapter 2. Monoclonal and polyclonal (Li-COR Biosciences, Ltd UK) anti-Prx2 antibodies were used to detect Prx2-SNO.

3.4.3.10 Peroxidase activity of hPrx2-SNO

The enzyme activity was measured using the protocol from (Engelman *et al*. 2012). 10 µM of Prx2-SNO was diluted in: 25 mM potassium phosphate, 1 mM EDTA buffer pH 7.0. The mixture was incubated with a thioredoxin (Trx) system (5 µM Trx, 0.1 µM TrxR (thioredoxin reductase), and 450 µM NADPH) and 500 µM H_2O_2 at 37^{o}C for 10 min. After 10 min, 20 µl aliquots were taken every minute and each aliquot was transferred into 980 µl of Fox reagent (100 mM sorbitol, 125 µM xylenol orange, 250 µM ferrous ammonium sulfate and 25 mM H_2SO_4). The absorbance was monitored at 560 nm every after 5 min for a duration of 30 min and compared to the readings from the H_2O_2 standard curve. The peroxidase activity of Prx2-SNO was derived from the linear regression of a plot of absorbance vs time.

3.4.3.11 Gel electrophoresis and Western-blotting of hPrx2-SNO

A Bio-Rad Trans-Blot apparatus (iBind ^{TM} Thermo Fisher Scientific, UK) was used for the Western blotting (Burnette, 1981). The apparatus was set up as instructed by the supplier. For each gel, four sheets of 0.83 mm thick Western blotting filter paper and one sheet of nitrocellulose membrane were used, cut to the same size. The filter papers together with the membrane were equilibrated in Thermo Scientific Pierce 1-step transfer buffer for 5 min. After electrophoresis, gels were removed from the cassette and briefly placed into a tray containing deionized water. This was to ensure even wetting of the gel, facilitating proper gel placement and improving gel contact with the membrane.

The apparatus was assembled as shown in Fig. 3.2: the gel was sandwiched between the filter paper and the membrane and placed in the centre of the cassette.

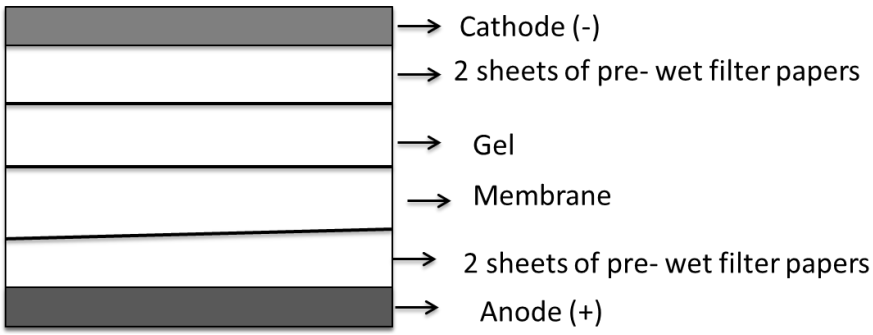

Figure 3.2. iBind apparatus set up for Western blotting

The cassette was locked and placed into the control unit, and then a pre-programmed method was selected in the main menu and the number of gels for the transfer was selected. Finally, the appropriate programme was selected and the transfer was started. The membrane was analysed using LI-COR Odyssey CLX imaging system (LI-COR Biosciences, Ltd, UK).

3.4.3.12 Mass spectrometry characterization of hPrx2-SNO to confirm the modification of Prx2 Cys

Prx2-SNO samples were also characterized by mass spectrometry (MS). By analysing the intact protein it was possible to study the presence of S-nitrosation in the protein. Additionally, after analysis of the peptides derived from the protein tryptic digest, it was also possible to identify the position of the modification.

1cm of each sample was run into a 1D gel and the gel piece then excised and subjected to in-gel tryptic digestion using a DigestPro automated digestion unit (Intavis Ltd, Nottingham, UK). The resulting peptides were fractionated using an Ultimate 3000 nanoHPLC system in line with an LTQ-Orbitrap Velos mass spectrometer (Thermo Scientific Ltd, UK). Peptides in 1% (vol/vol) formic acid were injected onto an Acclaim PepMap C18 nano-trap column (Thermal Scientific, Ltd, UK). After washing with 0.5% (vol/vol) acetonitrile 0.1% (vol/vol) formic acid, peptides were resolved on a 250 mm × 75 μm Acclaim PepMap C18 reverse phase analytical column (Thermo Scientific Ltd,

UK) over a 150 min organic gradient, using 7 gradient segments (1-6% solvent B over 1 min, 6-15% B over 58 min, 15-32% B over 58 min, 32-40% B over 5 min, 40-90% B over 1min, held at 90% B for 6 min and then reduced to 1% B over 1 min.) with a flow rate of 300 nl min^{-1}. Solvent A was 0.1% formic acid and Solvent B was aqueous 80% acetonitrile in 0.1% formic acid. Peptides were ionised by nano-electrospray ionization at 2.1 kV using a stainless steel emitter with an internal diameter of 30 µm (Thermo Scientific Ltd, UK) and a capillary temperature of 250°C. Tandem mass spectra were acquired using an LTQ-Orbitrap Velos mass spectrometer controlled by Xcalibur 2.1 software (Thermo Scientific Ltd, UK) and operated in data-dependent acquisition mode. The Orbitrap was set to analyse the survey scans at 60,000 resolution (at m/z 400) in the mass range m/z 300 to 2000 and the top ten multiply charged ions in each duty cycle selected for MS/MS in the LTQ linear ion trap. Charge state filtering, where unassigned precursor ions were not selected for fragmentation, and dynamic exclusion (repeat count, 1; repeat duration, 30s; exclusion list size, 500) were used. Fragmentation conditions in the LTQ were as follows: normalised collision energy, 40%; activation (q), 0.25; activation time 10 ms; and minimum ion selection intensity, 500 counts.

The raw data files were processed and quantified using Proteome Discoverer software V1.4 (Thermo Scientific) and searched against the SwissProt Human database using the Mascot search engine. Peptide precursor mass tolerance was set at 10 ppm, and MS/MS tolerance was set at 0.8 Da. Search criteria included oxidation of methionine (+15.999) as a variable modification and the following variable modifications of cysteine: carbamidomethylation (+57.021), 3-nitrotyrosine (+44.997), 6-nitrotryptophan (+44.997), sulfinic acid (+31.998), Cys-NO (+28.998). Searches were performed with full tryptic digestion and a maximum of 1 missed cleavage was allowed. The reverse database search option was enabled and all peptide data was filtered to satisfy a false discovery rate (FDR) of 1%.

3.5 Results

3.5.1 Saville assay

There were high levels of colouration observed in Prx2-SNO samples treated with no Hg^{2+}. In one reaction the absorbance at 540 nm was 0.16 absorbance units for the Hg^{2+}-treated Prx2-SNO sample and 0.11 absorbance units for the non-Hg^{2+}-treated samples Fig. 3.2. Zhang *et al*. (1996) reported similar observations with other nitroso groups such as N-nitrosoalbumin in studies of NO release. However, the same observation of high levels colouration was also observed by us with standard solutions of GSNO thus makes this explanation to appear unlikely.

In the non-Hg^{2+}-treated samples, the high colouration is due to the decomposition of RSNO (most commonly caused by metal ions in water) which is independent of that caused by Hg^{2+} (Zhang *et al*.,1996). This problem was solved by treating all reagents with Chelex resin to remove metals that might cause decomposition of Prx-SNO.

Non-Mercury treated					Treated With Mercury				
Concentration of GSNO (µM)	(Expt 1	rans) 2	3	Mean (Abs)	1	2	3	Mean	Mean difference between Hg^{2+} treat and non-treated samples (Abs in nm)
0	0.044	0.063	0.065	0.057	0.064	0.082	0.092	0.079	0.022
50	0.054	0.077	0.122	0.084	0.179	0.207	0.230	0.205	0.121
100	0.059	0.068	0.088	0.072	0.332	0.345	0.397	0.358	0.287
200	0.08	0.076	0.104	0.087	0.574	0.535	0.570	0.559	0.473

Table 3.0 Mean differences obtained from non-mercury treated GSNO samples and corresponding mercury-treated GSNO samples.

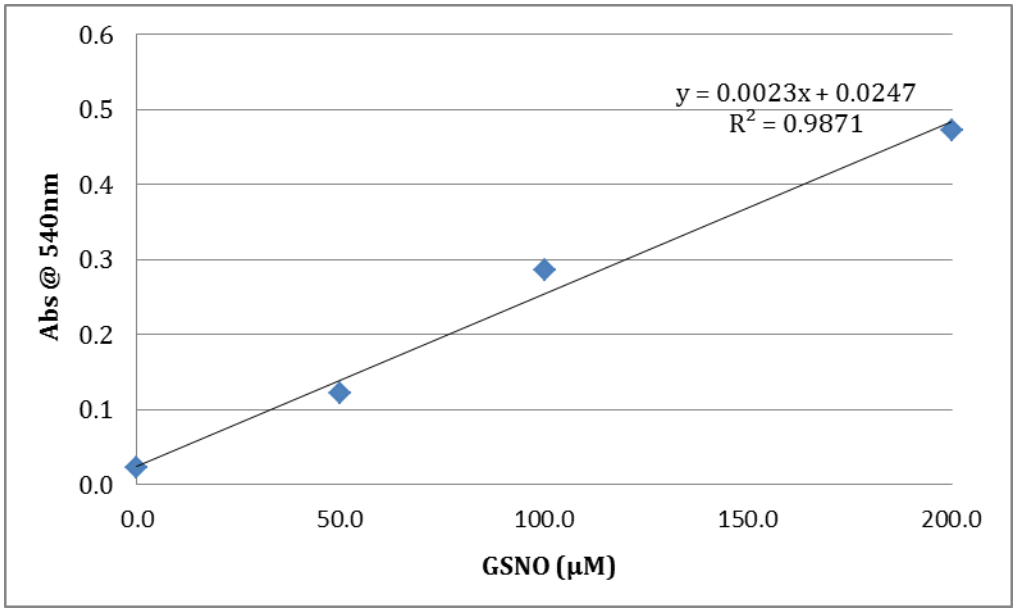

Figure 3.3 The standard curve from the Saville assay employing different concentrations of GSNO. The graph was used to determine the concentrations of the unknown synthesised RSNOs.

3.5.2 Stability of SNO-Hb and Prx2-SNO

The DSF method was used to monitor the stability of SNO-Hb and Prx2-SNO synthesised by various methods. The unfolding of the protein and exposure of hydrophobic parts of the protein, gave rise to a characteristic pattern in the fluorescence as a function of temperature as shown in Fig. 3.4. With the Prx2-SNO synthesised at pH 5.6, there was less absorbance of the fluorescent dye observed with the increasing protein melting temperatures compared to Prx2-SNO synthesised at a lower pH (pH 3.7 – pH 5.6). A similar pattern was observed with the Hb-SNO samples.

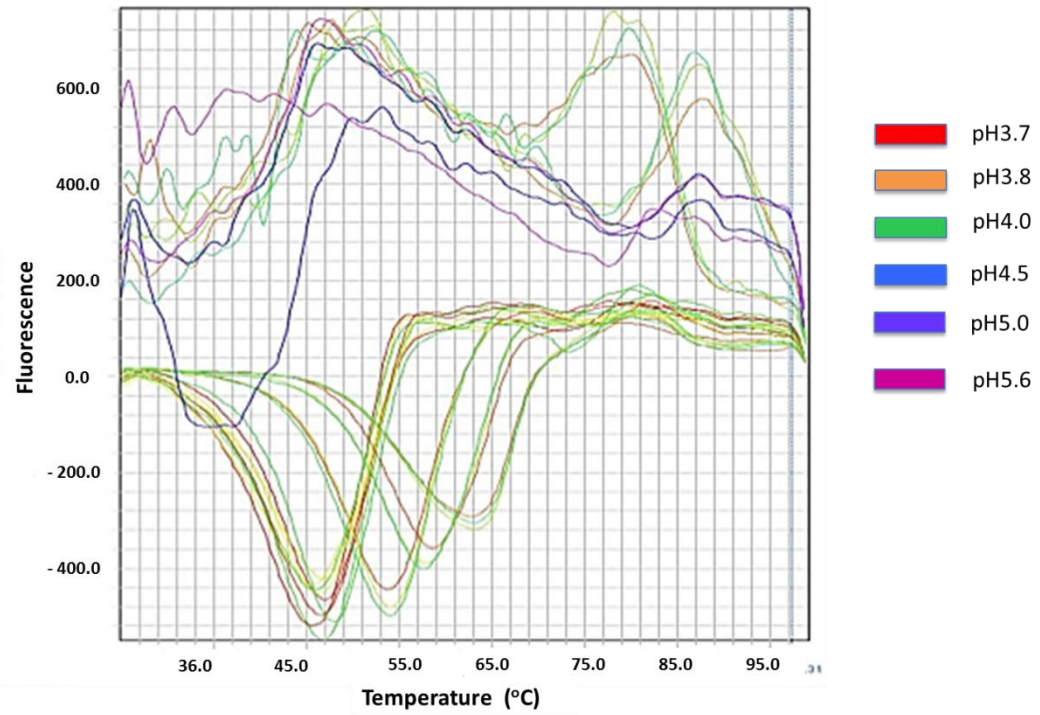

Figure 3.4. Melting curves showing the binary shifts in the melting pattern of hPrx2-SNO under different pHs. According to the DSF method (described in Methods section 3.7.6) when proteins are properly well folded, less fluorescence of the dye is detected by the system. The synthesised Prx2-SNO samples under different acid conditions were analysed for their stability. At low pH (pH's 3.7 – 5.0) a high absorbance of the dye was observed with the increasing melting temperatures. This means that the protein (Prx2-SNO) formed was not folded well (denatured) under the conditions causing the fluorescent dye (naphthalene-sulfonic dye) to bind more to the hydrophobic regions of the protein causing the huge absorbance readings observed.

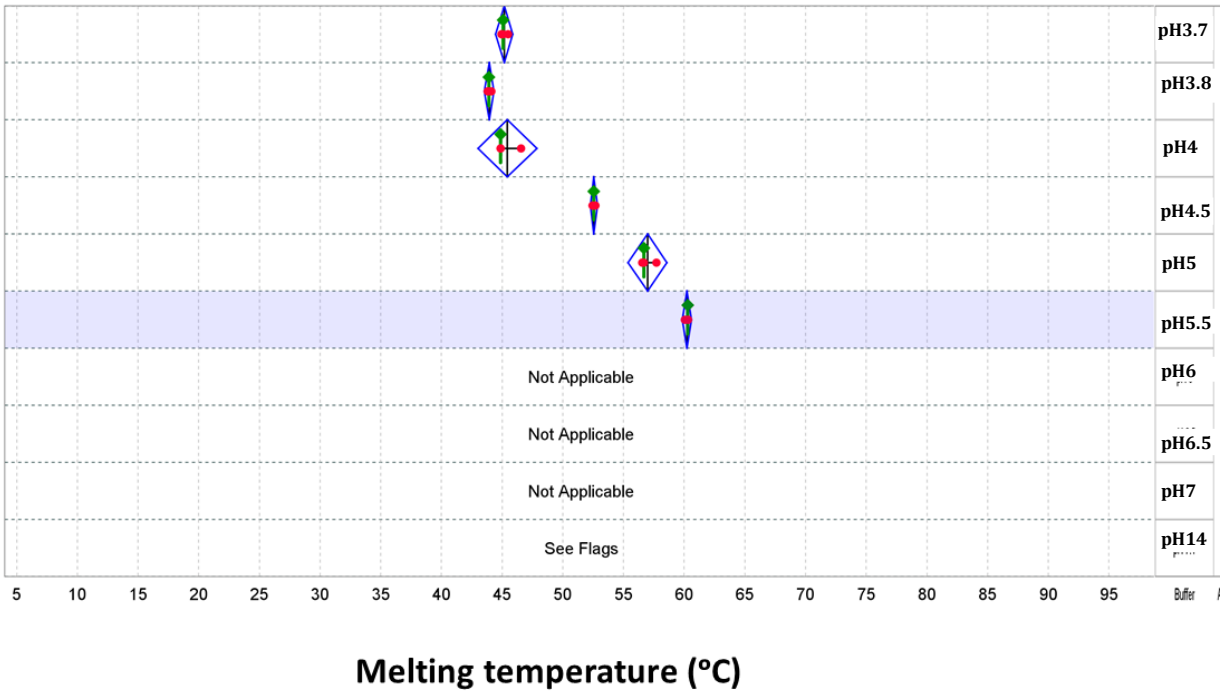

Figure 3.5. The Prx2 pH screening (Boltzmann temperature melting plot) of RSNOs synthesised via the acidified nitrite method. The stability of the synthesised RSNOs was monitored by unfolding of the protein under the increasing temperature. The amount of fluorescent dye detected corresponds to the unfolding of the protein. RSNOs synthesised at pH 3.7 had the highest fluorescent dye detected. The amount of fluorescent dye detected, decreased with the increasing pHs. The best pH at which S-nitrosation was able to take place while the protein was still stable was at pH 5.6. Points on the graph marked 'not application' indicates there were no fluorescent dye detected by the system, indicating well folding of the protein.

Differential scanning fluorimetry demonstrated its power as a robust and versatile method for characterizing proteins, and identifying the optimal pH of buffer for the hPrx2 nitrosation without denaturing the protein. It should be possible to carry out the nitrosation of hPrx2 in acetate buffer at pH 5.6, but with a reduced yield. This is because synthesis of RSNOs in biological systems is known to take place preferably under acidic environment (Zhang *et al*., 1996).

3.5.3 Results from the synthesis of Prx2-SNO using GSNO

(a) GSNO was incubated with purified recombinant hPrx2

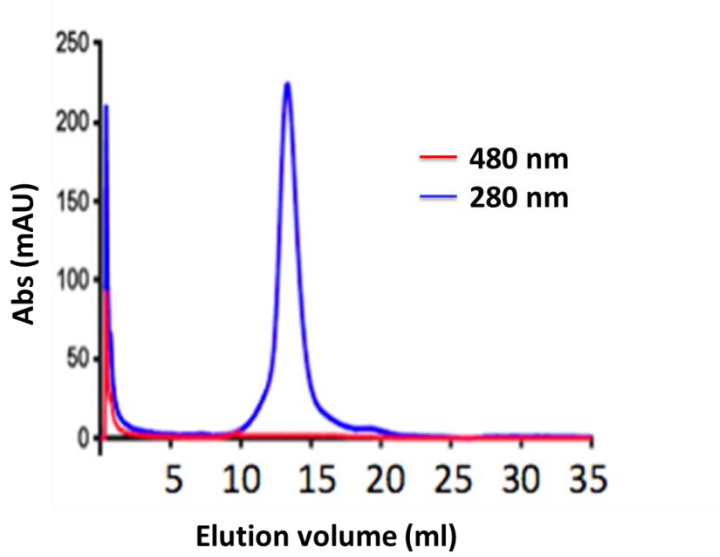

Figure 3.6 The elution profile from the Superose 6 (S6) gel filtration column for recombinant hPrx2. The red line indicates the absorbance at 418 nm (absorbance of the haem group in haemoglobin). The blue line indicates the absorbance at 280 nm (absorbance of the aromatic amino acid residues in both haemoglobin and hPrx2). Fractions were collected at 1 ml intervals throughout the elution volume. A single peak of protein, which corresponds to the decameric form of hPrx2, was observed (~14 ml).

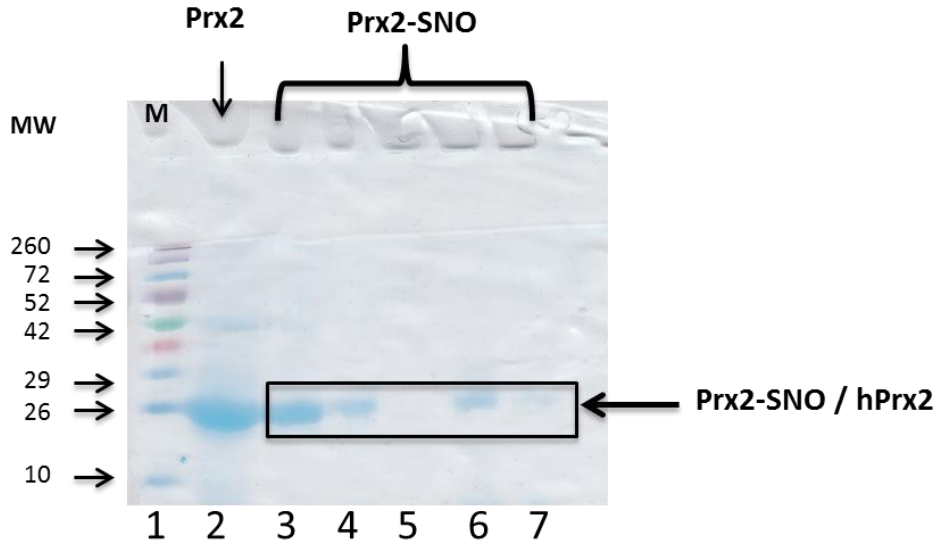

Figure 3.7 SDS-PAGE for the products (Prx2-SNO / hPrx2) when Prx2 was incubated with GSNO, then the fractions collected after gel filtration (Fig. 3.4). Lane 1 (M) molecular weight maker; lane 2, Prx2 sample; and lanes 3 to 6 are Prx2-SNO.

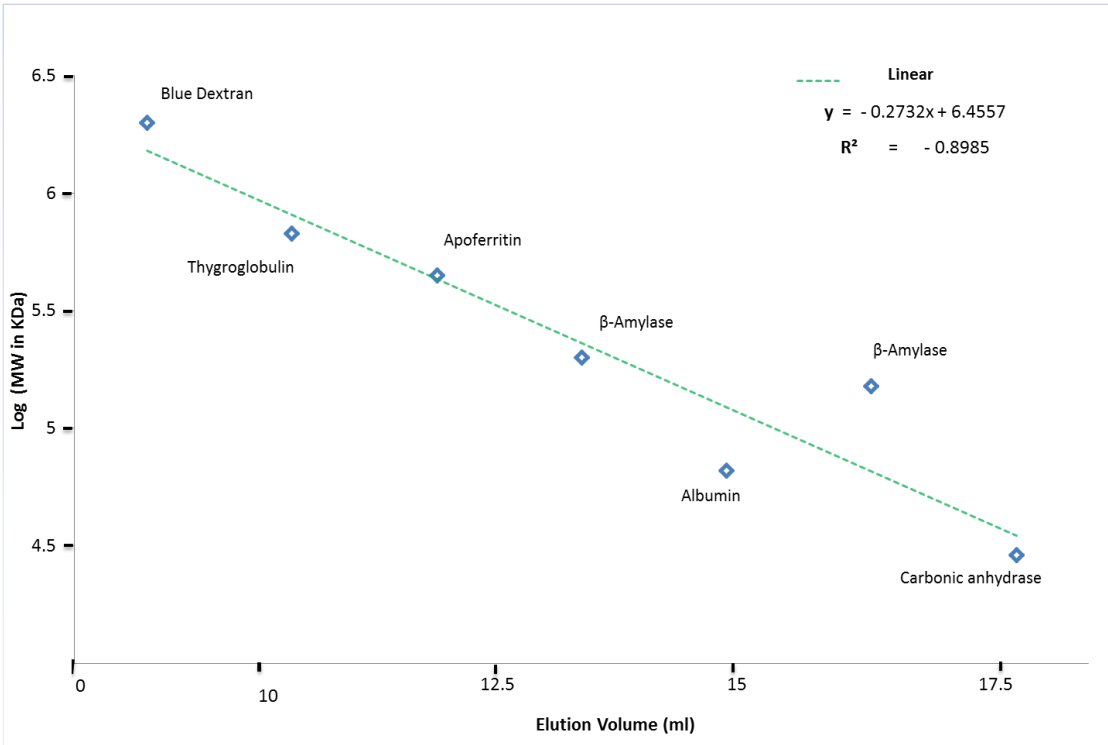

Figure 3.8 Calibration of a Superose 6 gel filtration column with known molecular standards using a mobile phase of 20 mM Tris-HCl, pH 8.0, containing 5 mM EDTA.

The following molecular weight standards were used: β-amylase (200 kDa), alcohol dehydrogenase (150 kDa), carbonic anhydrase (29 kDa), albumin (66 kDa), apoferritin (443 kDa), thyroglobulin (669 kDa) and blue dextran (2000 kDa). Using the calibration curve, the molecular weights of the unknown proteins were estimated.

(b) GSNO added to the growth medium during over-expression of hPrx2 in E.coli

The purification of the recombinant protein (Prx2-SNO) was done following the same procedures described in section 2.4.3.3.

Cells were opened by sonication, and then centrifuged to remove debris. Nickel affinity chromatography as described in methods section 2.4.2.4 was applied to the supernatant of the lysed cells. Fractions from the Ni^{2+} affinity column which were of the expected size for hPrx2 on the SDS-PAGE of about 22 kDa, were collected for the final purification step - the gel filtration chromatography (as described in section 2.4.2.6).

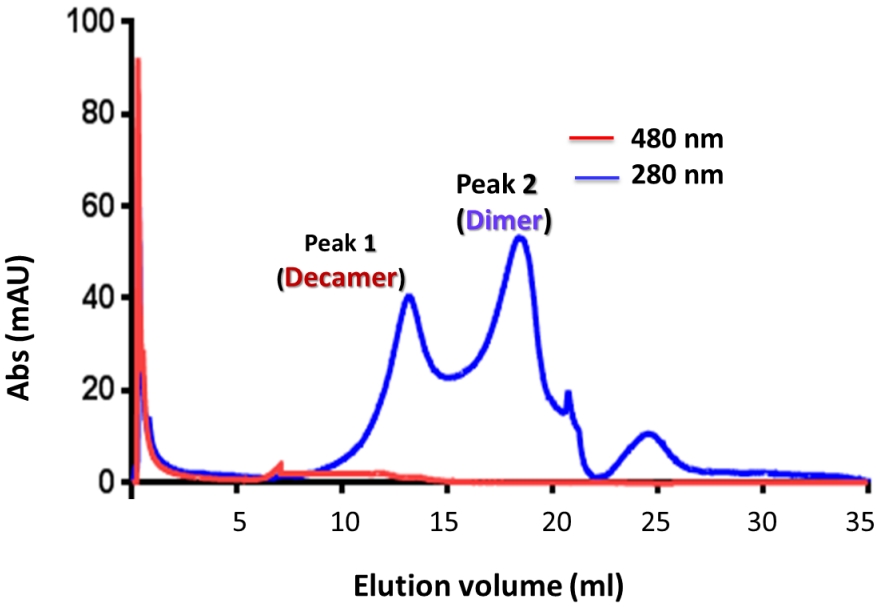

Figure 3.9 Elution profile for the recombinant hPrx2 from gel filtration chromatography, showing the nitrosation dependent formation of the hPrx2 dimer. The chromatogram was obtained using a Superose 6 FPLC column. The fractions were collected at 0.5 ml intervals throughout the elution volume. According to the calibration curve of the column, peak 1 in the chromatograph (~14 ml) corresponds to the decameric form of hPrx2; peak 2 (~18 ml) corresponds to the dimeric form of hPrx2. The oligomeric state was determined using a calibrated S6 column (Fig 3.7).

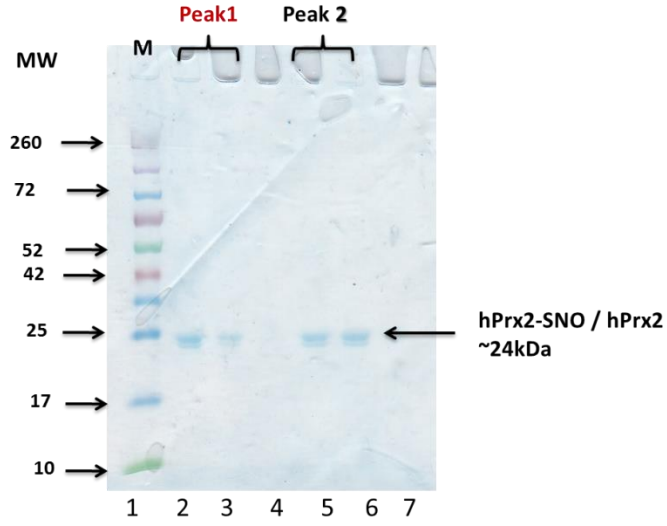

Figure 3.10 SDS-PAGE of the peak fractions from the gel filtration chromatography of the modified hPrx2 (Prx2-SNO). Lane I (M) molecular weight marker; lanes 1 and 2 are samples collected from peak 1 (Fig. 3.6); Lanes 4 and 5 are samples collected from peak 2 (Fig. 3.8).

3.9.4 Western-blotting of hPrx2-SNO results

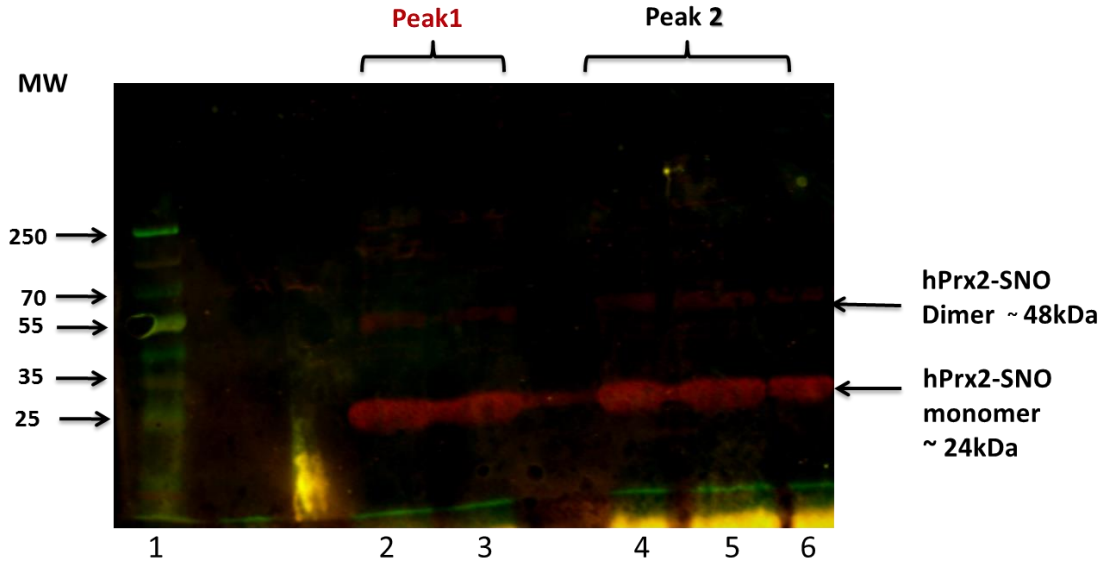

Figure 3.11. Detection of Prx2-SNO / Prx2 in both dimeric and monomeric form by reducing SDS-PAGE followed by Western blotting with an anti-polyhistidine antibody. Lane I, molecular weight markers; lanes 2 and 3, fraction samples collected from peak 1 (Fig. 3.8); lanes 4, 5 and 5, fraction samples collected from peak 2 (Fig. 3.8). The anti-histidine (primary antibody); (IgM) was produced in mouse. The secondary antibody (anti-mouse IgG), was produced in goat and has a covalently complexed chromophore of IRDYE680 (LI-COR) (with a working dilution 1:10,000 – 1:40,000). The dimeric bands were present indicating the presence of the disulfide bonds, indicating the sensitivity of Western blot method over SDS-PAGE (Fig. 3.6). Imaging was carried out using LI-COR Odyssey Imaging system (see Methods section 2.4.7.

3.5.5 Measurement of S-nitrosothiols in the characterised protein samples of Prx2-SNO

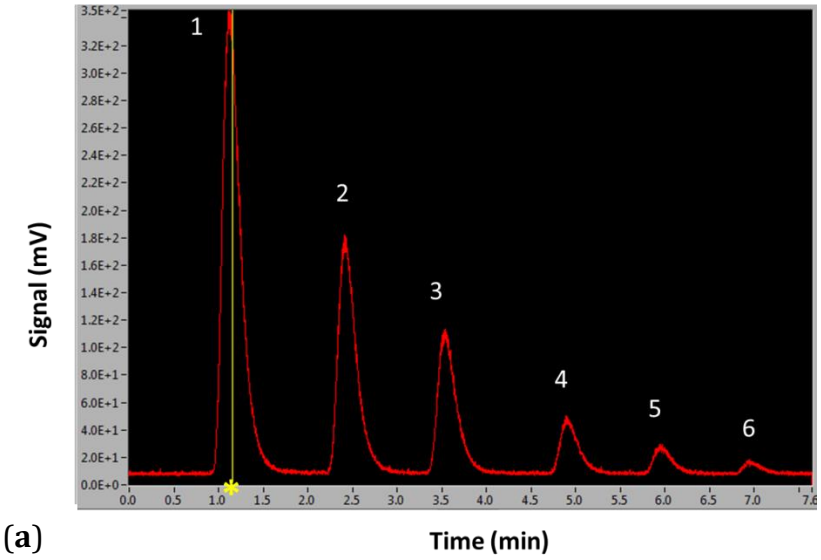

(a)

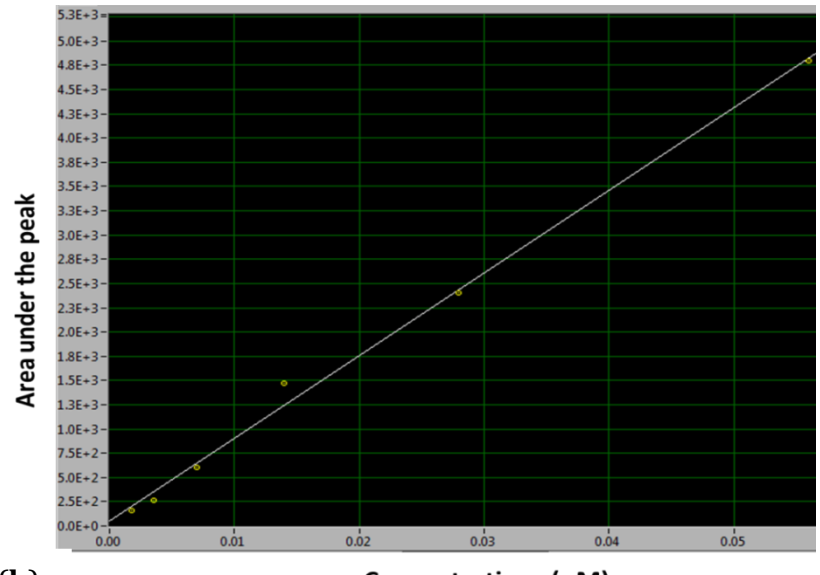

(b)

Figure 3.12. Plot of the signal time-course for the gas-phase chemiluminescence system following multiple injections of various known concentrations of GSNO (a) and the corresponding standard curve (b).

Known concentrations of RSNOs were injected into the NO analyser (Siever 280i nitric oxide analyser); the readings were recorded to generate the graph in (b) above. The dilutions were: peak I, 56 µM GSNO; 4793.6 arbitrary units of area; peak 2, 28 µM GSNO; 2406.2 arbitrary units of area; peak 3, 14 µM GSNO; 1470.1 arbitrary units of area; peak 4, 7 µM GSNO; 608.6 arbitrary units of area; peak 5, 3.5 µM

GSNO; 267.3 arbitrary units of area and peak 6, 1.75 µM GSNO; 156.9 arbitrary units of area. ***** Cursor line associated with the peak tracing function of the software.

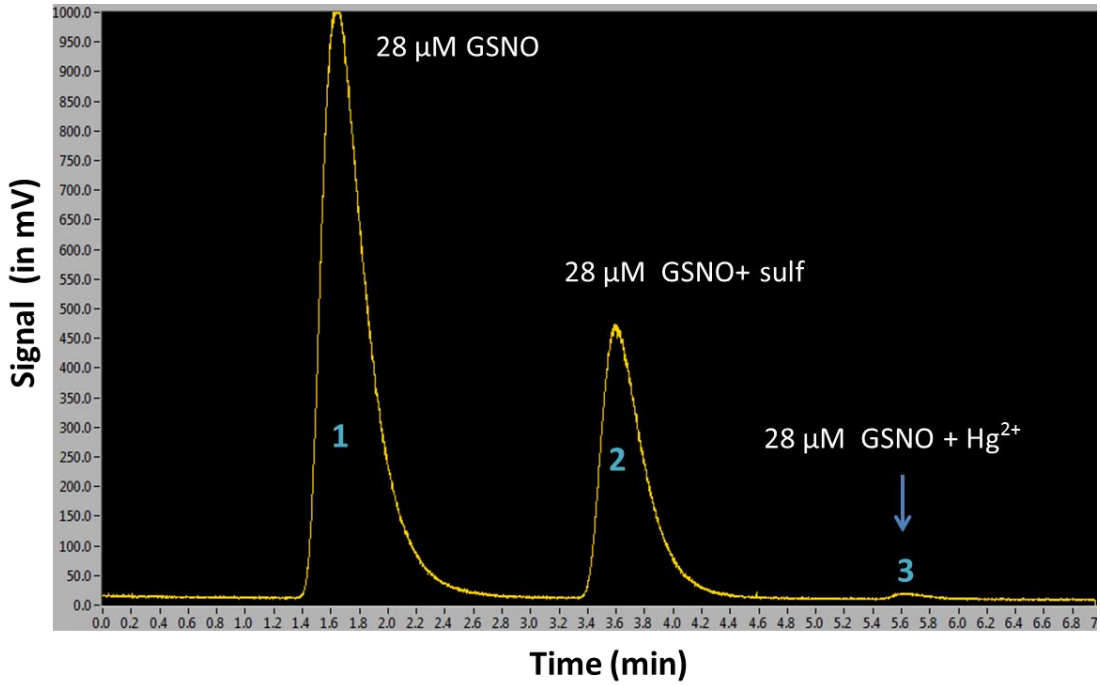

Figure 3.13. Chemiluminescence time-course following injections of GSNO.

Peak 1 represent the signal obtained when 100 µl (28 µM of GSNO) was injected into the NO analyser (Fig. 3.0), the peak had 22565 arbitrary units of area. Peak 2 represent the signal obtained when 100 µl (28 µM of GSNO) treated with sulfanilamide (sulf) was injected; the peak had 9713.3 arbitrary units of area. Peak 3 represents the signal obtained when 100 µl of 28 µM GSNO was treated with mercury Hg^{2+}. The data presented are representative time courses for n=2 independent experiments. Data were collected at room temperature at pH 7.4.

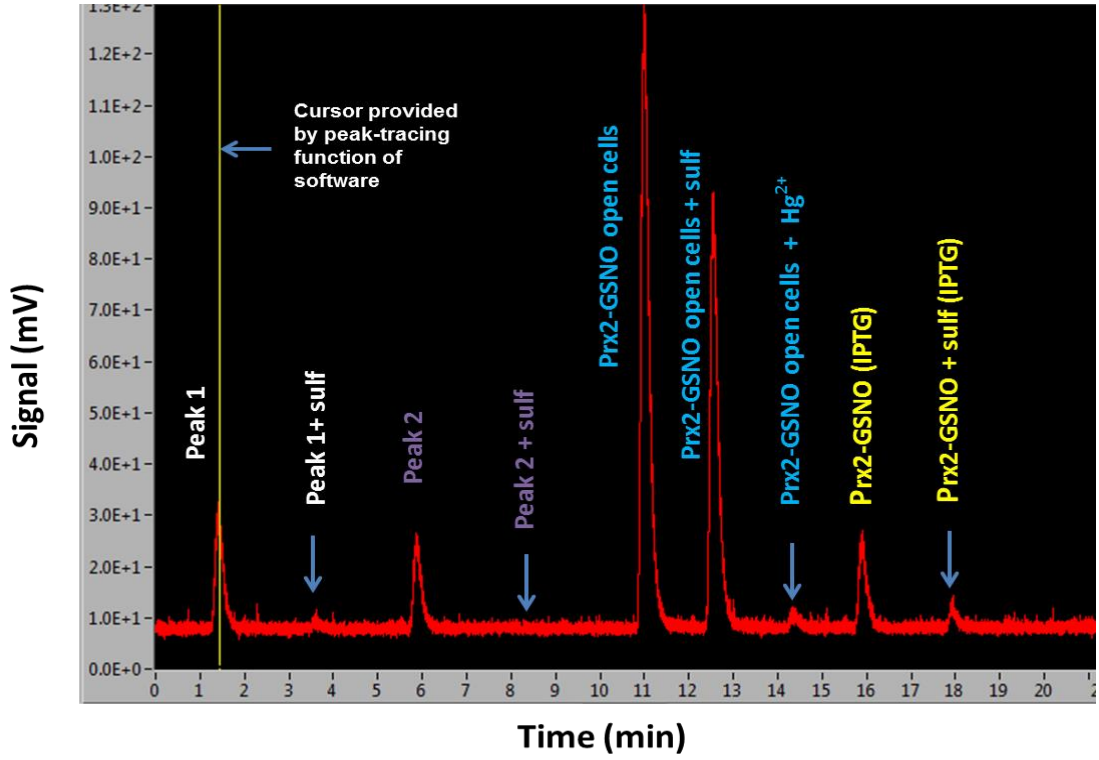

Figure 3.14. Representative chemiluminescence time-course of NO production from multiple injections of S-nitrosated protein samples.

"Peak 1" is the signal obtained when peak 1 fraction from figure 3.8 was injected into the NO analyser; the peak had 237.9 arbitrary units of area. "Peak 1 + sulf" (sulfanilamide) corresponds to the signal obtained when peak 1 from figure 3.8 was mixed with sulfanilamide and then injected into the NO analyser; the peak had 140.9 arbitrary units of area. "Peak 2" is the signal obtained from peak 2 (Fig.3.8) sample when injected into the analyser; the peak had 1412.7 arbitrary units of area. "Peak 2 + sulf" corresponds to the signal obtained when peak 2 samples (Fig. 3.7) were treated with sulf; the peak had 963.5 arbitrary units of area. "Peak (Prx2-GSNO open cells)" corresponds to the signal obtained from samples obtained when GSNO solution was added to the recombinant hPrx2 after sonication; the peak had 147.1 arbitrary of units of area. "Peak (Prx2-GSNO open cells + sulf)", is the signal obtained from samples prepared when hPrx2 open samples were treated with sulfanilamide; the peak had 98 arbitrary units of area. "Peak (Prx2-GSNO – IPTG)" is the signal obtained when samples of hPrx2-SNO when S-nitrosation was obtained by the addition of GSNO to the growth medium during the protein induction (the addition of IPTG) stage; the peak had 267.3 arbitrary units of area. "Peak (Prx2-SNO + sulf)" is the signal obtained when the samples were treated with sulfanilamide; the peak had 156.9 arbitrary units of area. The data presented are representative time courses for n=8 independent experiments. The peak difference between samples treated with or without sulfanilamide, is the amount of nitrite present. From the calculations, about 8 nM RSNO is present in Prx2-GSNO from Open cells.

3.5.6 Mass spectrometry analysis

Confidence level	Sequence	Modifications	Charge	M/Z [Da]	MH+[Da]
High	^{35}GKYVVLFF**Y^{NO2}**PLDFTFV**C^{NO}**PTEIIAFSNR^{61}	3-nitrotyrosine and S-nitrosocysteine	+3	1087.545	3260.621
High	^{62}AEDFRKLG**C^{OO}**EVLGVSVDSQFTHLAWINTPR^{91}	Cys Sulfinic acid	+3	1140.908	3420.710
High	^{62}AEDFRKLG**C^{OO}**EVLGVSVDSQFTHLAWINTPR^{91}	Cys Sulfinic acid	+4	855.934	3420.694
Medium	^{67}KLG**C^{OO}**EVLGVSVDSQFTHLAWINTPR^{91}	Cys Sulfinic acid	+2	1401.719	2802.430
High	^{68}LG**C^{OO}**EVLGVSVDSQFTHLAWINTPR^{91}	Cys Sulfinic acid	+2	1337.666	2674.324
High	^{158}LVQAFQYTDEHGEV**C^{OO}**PAGWKPGSDTIKPNVDDSKEYFSK^{196}	Cys Sulfinic acid	+2	1105.267	4418.065
Medium	^{158}LVQAFQYTDEHGEV**C^{OO}**PAGWKPGSDTIKPNVDDSKEYFSK^{196}	Cys Sulfinic acid	+4	1105.272	4418.065
High	^{158}LVQAFQYTDEHGEVCPAG**W^{NO2}**KPGSDTIKPNVDDSKEYFSK^{196}	Carbamidomethyl and 6-nitrotryptophan	+4	1122.779	4488.095
High	^{158}LVQAFQYTDEHGEVCPAG**W^{NO2}**KPGSDTIKPNVDDSK^{191}	Carbamidomethyl Cys and 6-nitrotryptophan	+3	1278.592	3833.777
High	^{58}LVQAFQ**Y^{NO2}**TDEHGEV**C^{OO}**PAGWKPGSDTIKPNVDDSKEYFSK^{196}	3-nitrotyrosine and Cys Sulfinic acid	+4	1116.522	4463.068
High	^{158}LVQAFQ**Y^{NO2}**TDEHGEV**C^{OO}**PAG**W^{NO2}**KPGSDTIKPNVDDSKEYFSK^{196}	3-nitrotyrosine; Cys Sulfinic acid and 6-nitrotryptophan	+4	1127.773	4508.069
Medium	^{158}LVQAFQ**Y^{NO2}**TDEHGEV**C^{NO}**PAG**W^{NO2}**KPGSDTIKPNVDDSKEYFSK^{196}	3-nitrotyrosine; S-nitrosocysteine and 6-nitrotryptophan	+4	1127.023	4505.069

Table 3.1 Protein modifications detected using LC-MS/MS system, in the primary structure of the untreated Prx2 samples. Samples were prepared as described in the material section 3.4.3.12. Modifications at the cysteine (Cys) residues are marked in bold underlined red letters (C^{OO} and S^{NO}). Modification at the tyrosine residues are marked in bold purple letters (Y^{NO2}). Modification at the tryptophan residues are marked in bold blue letter (W^{NO2}). The like-hood for the modifications mentioned to occur were found to be medium and high.

According to the results in table 3.1 above, 9 peptide modifications were identified with high confidence with various combinations of modification: (nitrotryptophan and nitrosocysteine; nitrotyrosine and cysteine sulfinic; nitrotryptophan, nitrotyrosine and cysteine sulfinic as shown in Fig. 3.1 above. There were 3 nitrotryptophan, 3 nitrotyrosine, 6 cysteine sulfinic acid, and 1 nitrosocysteine. 3 peptides modifications were identified with medium confidence: 2 cysteine sulfinic at Cys71 and at Cys172, nitrotryptophan, nitrotyrosine and cysteine sulfinic at Cys172.

Confidence level	Sequence	Modifications	Charge	M/Z [Da]	MH+[Da]
High	^{62}AEDFRKLG**C^{OO}**EVLGVSVDSQFTHLAWINTPR^{91}	Cys Sulfinic acid	+4	855.932	3420.707
High	^{67}KLGcEVLGVSVDSQFTHLA**W^{NO2}**INTPR^{91} +	Carbamidomethyl Cys and 6-nitrotryptophan	+3	958.156	2872.452
High	^{67}KLGcEVLGVSVDSQFTHLA**W^{NO2}**INTPR^{91} +	Carbamidomethyl Cys and 6-nitrotryptophan	+3	958.154	2872.449
High	^{68}LGCEVLGVSVDSQFTHLA**W^{NO2}**INTPR^{91} +	Carbamidomethyl Cys and 6-nitrotryptophan	+2	1372.684	2744.360
High	^{158}LVQAFQYTDEHGEVcPAG**W^{NO2}**KPGSDTIKPNVDDSK^{191}	Carbamidomethyl and 6-nitrotryptophan	+3	1278.601	3833.788
High	^{158}LVQAFQYTDEHGEVcPAG**W^{NO2}**KPGSDTIKPNVDDSK^{191}	Carbamidomethyl and 6-nitrotryptophan	+4	959.202	3833.786
High	^{158}LVQAFQYTDEHGEV**C^{OO}**PAG**W^{NO2}**KPGSDTIKPNVDDSK^{191}	Sulfinic acid and 6-nitrotryptophan	+4	952.936	3808.724
High	^{158}LVQAFQ**Y^{NO2}**TDEHGEV**C^{OO}**PAGWKPGSDTIKPNVDDSK^{191}	3-nitrotyrosine and Cys Sulfinic acid	+4	952.936	3808.724
High	^{158}LVQAFQYTDEHGEV**C^{OO}**PAGWKPGSDTIKPNVDDSKEYFSK^{196}	Cys Sulfinic acid	+4	1105.269	3808.724
High	^{158}LVQAFQYTDEHGEV**C^{OO}**PAGWKPGSDTIKPNVDDSKEYFSK^{196}	Cys Sulfinic acid	+4	1105.270	4418.058
High	^{156}LVQAFQYTDEHGEV**C^{NO}**PAG**W^{NO2}**KPGSDTIKPNVDDSKEYFSK^{196}	S-nitrosocysteine and 6-nitrotryptophan	+4	1115.771	4460.061

Table 3.2 Protein modifications in the primary structure of the treated Prx2 samples with GSNO, detected by LC-MS/MS system. Modifications at the cysteine (Cys) residues are marked in bold underlined red letters (C^{OO} and S^{NO}). Modification at the tyrosine residues are marked in bold purple letters (Y^{NO2}). Modification at the tryptophan residues are marked in bold blue letter (W^{NO2}). The like-hood for the modifications mentioned to occur were found to be medium and high.

In table 3.2, 11 peptides modifications were identified with high confidence: 7 nitrotryptophan, 1 nitrotyrosine, 1 S-nitrosocysteine and 5 cysteine sulfinic acid. 3 new nitrotryptophan were identified in the Prx2 GSNO treated samples which were not present in the untreated samples.

Table 3.3 MS-MS Recombinant Prx2 peptides of the untreated protein samples. (a) Modified peptides detected in the untreated Prx2 protein samples. (b) Corresponding sequences, as detected by MS-MS of peptides not modified (other than by sample preparation for MS i.e carbamidomethyl derivatives).

(a)

Peptide sequence	Modification	Charge	RT [min]	Precursor Area
^{35}GKYVVLFF**Y^{NO2}**PLDFTFV**C^{NO}**PTEIIAFSNR^{61}	3-nitrotyrosine and S-nitrosocysteine	+3	60.82	-
^{62}AEDFRKLG**C^{OO}**EVLGVSVDSQFTHLAWINTPR^{91}	Cysteine Sulfinic acid	+4	49.94	1.207E7
	Cysteine Sulfinic acid	+4	49.88	1.207E7
	Cysteine Sulfinic acid	+3	49.96	2.567E6
^{67}KLG**C^{OO}**EVLGVSVDSQFTHLAWINTPR^{91}	Cysteine Sulfinic acid	+2	47.44	-
^{68}LG**C^{OO}**EVLGVSVDSQFTHLAWINTPR^{91}	Cysteine Sulfinic acid	+2	52.33	8.673E6
^{158}LVQAFQYTDEHGEV**C^{OO}**PAGWKPGSDTIKPNVDDSKEYFSK^{196}	Cysteine Sulfinic acid	+4	38.94	2.537E6
	Cysteine Sulfinic acid	+2	35.01	-
	Cysteine Sulfinic acid	+4	37.24	4.460E6
^{158}LVQAFQYTDEHGEV**C**PAG**W^{NO2}**KPGSDTIKPNVDDSK^{191}	Carbamidomethyl Cysteine and 6-nitrotryptophan	+3	37.98	-
^{158}LVQAFQYTDEHGEV**C**PAG**W^{NO2}**KPGSDTIKPNVDDSKEYFSK^{196}	Carbamidomethyl Cysteine and 6-nitrotryptophan	+4	34.23	2.126E8
^{158}LVQAFQ**Y^{NO2}**TDEHGEV**C^{OO}**PAG**W^{NO2}**KPGSDTIKPNVDDSKEYFSK^{196}	3-nitrotyrosine; Cysteine Sulfinic acid and 6-nitrotryptophan	+4	41.64	5.934E6

(b)

Peptide sequence	Modification	Charge	RT [min]	Precursor Area
^{35}GKYVVLFFYPLDFTFV**C**PTEIIAFSNR^{61}	Carbamidomethyl Cys	+3	60.86	8.946E8
	Carbamidomethyl Cys	+3	61.94	8.946E8
^{62}AEDFRKLG**C**EVLGVSVDSQFTHLAWINTPR^{91}	Carbamidomethyl Cys	+3	47.29	8.344E8
	Carbamidomethyl Cys	+3	47.63	8.344E8
	Carbamidomethyl Cys	+4	47.27	2.648E9
	Carbamidomethyl Cys	+4	47.81	2.648E9
^{67}KLG**C**EVLGVSVDSQFTHLAWINTPR^{91}	Carbamidomethyl Cys	+3	68.80	-
	Carbamidomethyl Cys	+3	68.00	-
	Carbamidomethyl Cys	+3	60.21	8.946E8
^{68}LG**C**EVLGVSVDSQFTHLAWINTPR^{91}	Carbamidomethyl Cys	+2	64.12	9.808E7
	Carbamidomethyl Cys	+2	65.60	2.029E7
	Carbamidomethyl Cys	+2	57.68	4.359E6
	Carbamidomethyl Cys	+2	57.21	8.463E6
	Carbamidomethyl Cys	+2	59.27	8.485E6
	Carbamidomethyl Cys	+2	68.82	2.781E7
	Carbamidomethyl Cys	+2	51.39	2.899E7
^{158}LVQAFQYTDEHGEV**C**PAGWKPGSDTIKPNVDDSK^{191}	Carbamidomethyl Cys	+3	34.32	4.909E9
	Carbamidomethyl Cys	+3	37.98	-
^{158}LVQAFQYTDEHGEV**C**PAGWKPGSDTIKPNVDDSKEYFSK^{196}	Carbamidomethyl Cys	+4	62.26	-
	Carbamidomethyl Cys	+4	33.71	1.797E7
	Carbamidomethyl Cys	+4	38.94	2.537E8
	Carbamidomethyl Cys	+4	64.87	2.766E6
	Carbamidomethyl Cys	+4	61.41	5.290E5
	Carbamidomethyl Cys	+4	43.07	2.655E6
	Carbamidomethyl Cys	+4	38.21	1.815E7
^{158}LVQAFQYTDEHGEV**C**PAGWKPGSDTIKPNVDDSKEYFSK^{196}	Carbamidomethyl Cys	+4	62.26	-
	Carbamidomethyl Cys	+3	65.14	-
^{158}LVQAFQYTDEHGEV**C**PAGWKPGSDTIKPNVDDSKEYFSK^{196}	Carbamidomethyl Cys	+4	40.60	-
	Carbamidomethyl Cys	+4	62.26	-
	Carbamidomethyl Cys	+4	64.87	2.766E6
	Carbamidomethyl Cys	+4	61.41	5.290E5
	Carbamidomethyl Cys	+4	43.07	2.655E6
	Carbamidomethyl Cys	+4	38.21	1.815E7

Untreated Prx2 protein sample not only contain cysteine sulfinic acid, it contained all other modifications: nitrotryptophan, nitrotyrosine and S-nitrosocysteine. Therefore, Prx2 peptides are highly accepted to nitration.

Table 3.4 MS-MS Report for the Recombinant Prx2 peptides of the treated protein samples with GSNO. (a) Modified peptides detected when Prx2 samples were incubated overnight in the cold-room with GSNO. (b) Corresponding sequences, as detected by MS-MS of peptides not modified (other than by sample preparation for MS i.e carbamidomethyl derivatives). Newly modified peptides that were not present in the untreated samples with GSNO are marked with a plus (+) sign, and peptides also present in the untreated with a star (*) sign.

(a)

Peptide sequence	Modification	Charge	RT [min]	Precursor Area
^{62}AEDFRKLG**C**^{OO}EVLGVSVDSQFTHLAWINTPR^{91} *	Cysteine Sulfinic acid	+4	50.05	-
^{67}KLG**C**EVLGVSVDSQFTHLA**W**^{NO2}INTPR^{91} +	Carbamidomethyl Cys and 6-nitrotryptophan	+3	42.41	-
^{68}LG**C**EVLGVSVDSQFTHLA**W**^{NO2}INTPR^{91} +	Carbamidomethyl Cys and 6-nitrotryptophan	+2	46.20	-
^{158}LVQAFQYTDEHGEV**C**PAG**W**^{NO2}KPGSDTIKPNVDDSK^{191} *	Carbamidomethyl Cys and 6-nitrotryptophan	+3	31.40	-
^{158}LVQAFQYTDEHGEV**C**^{OO}PAG**W**^{NO2}KPGSDTIKPNVDDSK^{191} +	Cysteine Sulfinic acid and 6-nitrotryptophan	+4	32.56	
^{158}LVQAFQ**Y**^{NO2}TDEHGEV**C**^{OO}PAGWKPGSDTIKPNVDDSK^{191} +	3-nitrotyrosine and Cysteine Sulfinic acid	+4	32.56	-
^{158}LVQAFQYTDEHGEV**C**^{OO}PAGWKPGSDTIKPNVDDSKEYFSK^{196} *	Cysteine Sulfinic acid	+4	36.36	1.585E7
^{156}LVQAFQYTDEHGEV**C**^{NO}PAG**W**^{NO2}KPGSDTIKPNVDDSKEYFSK^{196} *	S-nitrosocysteine and 6-nitrotryptophan	+4	39.82	-

(b)

Peptide sequence	Modification	Charge	RT [min]	Precursor Area
* 35GKYVVLFFYPLDFTFVCPTEIIAFSNR61 *	Carbamidomethyl Cys	+2	60.47	6.580E7
	Carbamidomethyl Cys	+3	62.81	1.693E6
62AEDFRKLGCEVLGVSVDSQFTHLAWINTPR91	Carbamidomethyl Cys	+4	47.37	5.542E9
	Carbamidomethyl Cys	+4	47.33	5.542E9
	Carbamidomethyl Cys	+4	64.26	8.421E6
67KLGCEVLGVSVDSQFTHLAWINTPR91	Carbamidomethyl Cys	+3	45.13	2.662E7
	Carbamidomethyl Cys	+3	46.48	-
	Carbamidomethyl Cys	+3	53.23	2.230E7
	Carbamidomethyl Cys	+3	52.72	3.052E7
68LGCEVLGVSVDSQFTHLAWINTPR91	Carbamidomethyl Cys	+2	60.41	1.775E7
	Carbamidomethyl Cys	+2	66.39	8.911E6
	Carbamidomethyl Cys	+2	50.35	-
	Carbamidomethyl Cys	+2	53.32	5.745E7
	Carbamidomethyl Cys	+2	58.58	9.516E6
	Carbamidomethyl Cys	+2	68.95	5.836E7
	Carbamidomethyl Cys	+2	51.90	1.615E8
158LVQAFQYTDEHGEVCPAGWKPGSDTIKPNVDDSK191	Carbamidomethyl Cys	+3	35.11	5.779E8
	Carbamidomethyl Cys	+3	34.53	2.312E10
	Carbamidomethyl Cys	+3	34.39	6.321E9
	Carbamidomethyl Cys	+3	35.78	-
158LVQAFQYTDEHGEVCPAGWKPGSDTIKPNVDDSK191	Carbamidomethyl Cys	+4	34.30	2.312E10
	Carbamidomethyl Cys	+4	40.01	-
158LVQAFQYTDEHGEVCPAGWKPGSDTIKPNVDDSKEYFSK196	Carbamidomethyl Cys	+3	36.07	6.211E9
	Carbamidomethyl Cys	+4	38.84	6.216E7
	Carbamidomethyl Cys	+4	38.59	6.216E7
	Carbamidomethyl Cys	+3	36.07	6.211E9
	Carbamidomethyl Cys	+4	34.81	8.213E7
	No modification at all	+4	35.69	-

4 newly modified peptides were identified in the GSNO treated samples which were not present in the untreated Prx2 samples.

Cys51 in the treated Prx2 samples was not nitrosated as identified in untreated sample table 3.3a, but instead carbamidomethyl cysteine was formed.

Sequence of peptide not modified (other than by sample preparation for MS)	Modification (not related to MS preparation)	Charge of both modified and unmodified peptide	RT of unmodified peptide	RT of modified peptide	Precursor area of modified peptide	Precursor area of unmodified peptide	Precursor area ratio modified / unmodified peptide
^{35}GKYVVLFFYPLDFTFV**C**PTEIIAFSNR^{61}	3-nitrotyrosine; Cys51 NO	+3	60.86	60.82	-	8.946E8	**-**
^{62}AEDFRKLG**C**EVLGVSVDSQFTHLAWINTPR^{91}	Cys71sulfinic acid	+3	47.63	29.96	2.567E6	8.344E8	**3.076E-3**
		+4	47.81	49.88	1.207E7	2.648E9	**4.558E-3**
^{68}LG**C**EVLGVSVDSQFTHLAWINTPR^{91}	Cys71 sulfinic acid	+2	51.39	52.33	8.673E6	2.899E7	**0.299**
^{158}LVQAFQYTDEHGEV**C**PAGWKPGSDTIKPNVDDS KEYFSK^{196}	3-nitrotyrosine Cys173 Sulfinic acid; 6-nitrotryptophan	+4	38.94	41.64	5.934E6	2.537E8	**0.023**
	Cys173 sulfinic acid	+4	38.21	38.94	2.537E6	1.815E7	**0.140**
		+4	34.23	37.24	4.460E6	2.126E8	**0.021**
^{158}LVQAFQYTDEHGEV**C**PAGWKPGSDTIKPNVDDS KEYFSK^{196}	6-nitrotryptophan	+4	38.98	34.23	2.126E8	2.537E8	**0.838**
^{158}LVQAFQYTDEHGEVCPAGWKPGSDTIKPNVDDS K^{191}	6-nitrotryptophan	+3	34.32	37.98	-	4.909E9	**-**

Table 3.5 Calculation of peptide modification using precursor areas (produced by peptides of similar charges, almost similar retention time) for both modified and unmodified peptides for untreated Prx2 samples.

Sequence of peptide not modified (other than by sample preparation for MS)	Modification (not related to MS preparation)	Charge of both modified and unmodified peptide	RT of unmodified peptide	RT of modified peptide	Precursor area of modified peptide	Precursor area of unmodified peptide	Precursor area ratio modified / unmodified peptide
^{67}KLG**C**EVLGVSVDSQFTHLAWNTPR^{91}	6-nitrotryptophan	+3	45.13	42.41	-	2.662E7	-
^{62}AEDFRKLG**C**EVLGVSVDSQFTHLAWINTPR^{91}	Cys71 sulfinic acid	+4	47.37	50.05	-	5.542E9	-
^{68}**LG**C**C**EVLGVSVDSQFTHLAWINTPR^{91}	6-nitrotryptophan	+2	51.90	46.20	-	1.615E8	
^{158}LVQAFQYTDEHGEV**C**PAGWKPGSDTIKPNVDD SK^{191}	6-nitrotryptophan	+3	34.39	31.40	-	6.321E9	-
^{158}LVQAFQYTDEHGEV**C**PAGWKPGSDTIKPNVDD SK^{191}	Cys173 sulfinic acid; 6-nitrotryptophan	+4	34.30	32.56	-	2.312E10	
^{158}LVQAFQYTDEHGEV**C**PAGWKPGSDTIKPNVDD SKEYFSK^{196}	Cys173 sulfinic acid	+4	36.07	36.36	1.585E 7	6.211E9	2.552E-3
	Cys173 NO; 6-nitrotryptophan	+4	38.59	39.82	-	6.216E7	

Table 3.6 Calculation of peptide modification using precursor areas (produced by peptides of similar charges, almost similar retention time) for both modified and unmodified peptides for Prx2 samples incubated overnight in the cold-room with GSNO.

Figure 3.15 Comparison of the protein sequences for Prx2 untreated and Prx2 treated with GSNO.

3.5.7 UV-vis spectrophotometry

Figure 3.15 shows the UV-vis spectrum of 1 ml of GSNO between 200 and 500 nm and figure 3.16 is the spectrum of 1 ml of GSNO between 450 and 650 nm. There were predominant peaks at 334 nm and 540 nm in the two scans which correspond to the absorbance of the SNO group. When the spectrum of the pinkish product visible by eye in Prx2-SNO samples prepared as described in the Methods section 3.8.10 was taken after all the chromatographic protein purification steps, again there was a peak at 330-360 nm and between 500-550 nm. This data suggested nitrosation has occurred.

We got mixed results with modification studies of hPrx2 using LC-MS/MS. Both treated and untreated Prx2 samples were both found to have post-modification at the cysteine residue.

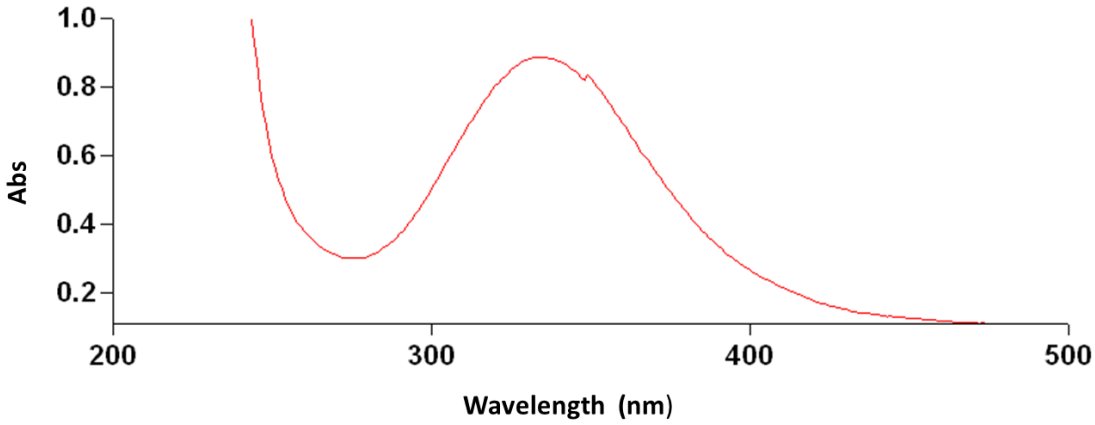

Figure 3.16 UV-Vis spectrum scan of GSNO at 334 nm.

10 µl of GSNO was mixed with 990 µl of ultrapure (Milli-Q) water and placed into a 1.5 ml quartz cuvette and a spectrum scan between 200 nm and 500 nm was taken data at 25°C and pH 7.4.

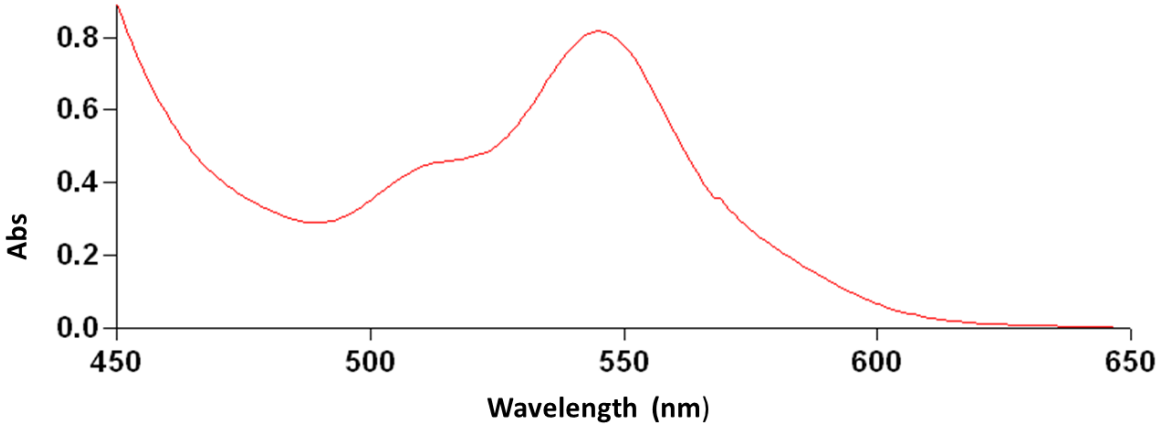

Figure 3.17 UV-Vis spectrum scan of GSNO at 545 nm.

1 ml of 2.0 GSNO (of 0.25 mg/ml concentration) was placed into 1.5 ml quartz cuvette and a spectrum scanned between 450 nm and 650 nm. Data were recorded at 25°C and pH 7.4 as mentioned in Fig. 3.13 above.

3.6 Discussion

The post-modification studies of hPrx2 using LC-MS/MS system produced a mixture of results. Some of the results were in agreement with the literature available about post-modification of Cys residues in proteins (the formation of cysteine sulfinic acid) (Schroder *et al*., 2000), while as others were inconclusive. The inconsistence of the results might be due the absence of repeating the experiment a couple times (n=3). Both treated and untreated hPrx2 samples were found to have post-modification at the cysteine residues. This suggested that Cys51 and Cys172 were readily modifiable. The Cys51 in the untreated samples was found to be nitrosated (S-nitrosocysteine) (Table 3.1), with high confidence level and Cys71 and Cys172 of the same sample were already oxidised to cysteine sulfinic acid with high confidence levels. However, Cys51 in the treated samples (the most active cysteine in the active site) was found to be carbamidomethylated with a high confidence level, a post-modification caused by the sample preparation for MS lather than treatment with GSNO. This was unexpected result depending on the sensitivity and selectivity of NO_x for cysteines with GSNO (David *et al*., 1994). This raised a number of questions such as; the chemistry between the sample preparation buffers used (carbamidomethyl) and the hPrx2 active site, the degree of post-modification caused by GSNO treatment (strong or partial modification) which can be interfered by carbamidomethyl. The cysteine sulfinic acid modification of Cys71 and Cys172 this was expected modification, previously observed (Schroder *et al*., 2000) by X-ray crystallography. Other modifications were observed; the 3-nitrotryrosine modifications and 6-nitrotroptophan modifications, in both treated and untreated samples. These were expected post-modifications commonly to occur in nature.

In blood vessels, tyrosine nitration occurs with increasing nitric oxide concentration (Amirmansour *et al.,* 1999). Endothelial dysfunction plays an important role in the pathogenesis of peripheral vascular diseases such as diabetic microcirculatory disorders, Raynaud's syndrome or chronic leg ulcers (Veves *et al.,* 1998; Herrick, 2005). A main feature of endothelial dysfunction is that vasoconstrictors outweigh the effects of vasodilators in the microcirculation. This vascular dysfunction leads to impaired autoregulation of blood flow and is suggested to be an early event in insulin resistance (Meigs *et al*., 2006).

S-nitrosothiols (RSNOs) such as *S*-nitrosoglutathione (GSNO) have already been identified a dacade ago as endogenous NO carriers and donors in mammals (Hogg, 2000; Zhang and Hogg 2005). RSNOs have been at the centre of several pharmacological studies investigating the importance of NO in living systems and it has already been demonstrated that they are vasodilators and inhibitors of platelet aggregation (as discussed in chapter 1). Seabra *et al*., findings, testing the possible side effects of topical GSNO application, it was discovered that RSNOs can induce nitration of tyrosine residue, which inhibits specific proteins such as the protein transport chain complex (Seabra *et al.,* 2007).

Glutathione (GSH) inhibits the formation of nitrotyrosine (Kirsch *et al*., 2001). However, nitration of tyrosine was observed in all the hPrx2-treated samples at a high degree of confidence level, which is contrary to the X-ray crystal data (Schroder *et al*., 2002). Surprisingly**,** tryptophan nitration modifications were also observed in untreated samples. The modification took place next to the resolving cysteine Cys_R (Cys172). The cysteine sulfinic acid modification at Cys172 was expected, this was present in both treated and untreated as reported previously (Schroder *et al*., 2000) by X-ray crystallography. In Prx2 peptide sequence, the tryptophan residues were surrounded by charged amino acids, which influenced tryptophan residues to be nitrated. This has been previously discussed (Souza *et al.*, 1999; Bayden *et al.*, 2011) suggesting a nearby charge favour nitration though other studies (Seeley and Stevens, 2012) suggest uncharged polar residues are more favourable.

The peptide modification can be quantified by comparing the precursor areas of particular peptides of the same peptide but in different environment (treated or un-treated) (Tables 3.5 – 3.6). We were not able to use this route because; some of the identified peptides did not have precursor areas. This was caused by the overlapping peaks, which made the system not to be able to detect the baseline of the identified peptides to calculate their precursor areas therefore, recorded with no precursor area.

Chapter 4:

Interactions between: hPrx2, NO, Hb and hPrx2-SNO for both native and recombinant hPrx2

4.0 Introduction

Formerly we looked at what are RSNOs and how RSNOs can be formed *in vivo* (sections 1.5 and 1.5.1). However, there is a controversy there is a low nanomolar amount of RSNOs under basal conditions Gladwin and co-workers (Gladwin *et al*., 2001). Both endogenous and exogenous NO react with thiols in proteins to form long-lived RSNOs with vasodilatory activity (Stamler *et al,* 1992). We hypothesised that RSNOs (Prx2-SNO) provides a reservoir of NO bioactivity that might be utilized in states of NO deficiency and that vasodilation thus, providing a realistic mechanism how NO might escape from erythrocytes.

One physiological benefit of RSNOs over NO is their resistance to inactivation by superoxide (O_2^-). In damaged tissues, increased O_2^- can react with NO to produce toxic peroxynitrite. It is therefore noteworthy to think that NO can diffuse through RBC's membrane in an unprotected manner. As discussed earlier in section 1.5.2, RSNO formation provides a stable means by which NO can be transported in the body (Ssu-Han *et al*., 20012). The exchange of NO groups between SNO-Hb and the RBCs membrane is governed by oxygen tension: RBCs dilate blood vessels at low oxygen, (Pawloski *et al*., 2001; McMahon *et al*., 2000), but Prx2 is the 3rd most abundant protein in RBC as described in section 1.9. Therefore, there was a need to demonstrate the existence of intraerythrocytic equilibria between NO bound to the reactive thiol (Cys51) of hPrx2 and reactive thiols (Cysβ93) of Hb. A sensitive and reliable technique: the chemiluminescence was required to detect the presence these important protein species (RSNO) which might be crucial for the escape of NO from RBCs.

4.1 Protein-protein Interaction

Most biochemical reactions and processes are carried out by macromolecular complexes that interact in a reversible manner to form functionally active structures (Alberts B, 1998). Therefore, the quantitative characterization of reversible macromolecular associations, in terms of stoichiometry and strength of the interactions, is essential to our understanding of normal biological processes, pathological aggregation and degradation reactions, and the stability of biological macromolecules with respect to aggregation. For these reasons, there exists a large variety of methods

for studying protein interactions, many of which have been recently reviewed (Phizicky E and Fields S, 1995; Golemis E and Adams P, 2005).

Protein-protein interactions between two proteins can generally be studied using biochemical techniques such as crosslinking, co-immunoprecipitation and co-fractionation by chromatography. The lives of biological cells are controlled by interacting proteins in metabolic and signaling pathways and in complexes such as the molecular machines that synthesize and use adenosine triphosphate (ATP), replicate and translate genes, or build up the cytoskeletal infrastructure (Albert *et al*., 1994; Lodish *et al*., 1995). Our knowledge of protein-protein interactions has been accumulated from biochemical and genetic experiments, including the widely used yeast two-hybrid test (Fields and Song 1989).

The study of protein interactions is vital to the understanding of how proteins function within the cell. Publication of the human genome and proteomics-based protein profiling studies catalysed resurgence in protein interaction analysis. The ~30,000 genes of the human genome are speculated to give rise to 1×10^6 proteins through a series of post-translational modifications and gene-splicing mechanisms. Although a population of these proteins can be expected to work in relative isolation, the majorities are expected to operate in concert with other proteins in complexes and networks to orchestrate the myriad of processes that impact cellular structure and function. These processes include cell-cycle control, differentiation, protein folding, signaling, transcription, translation, post-translational modification and transport.

Traditionally, protein–protein interactions have been identified and characterized using low-throughput biophysical methods such as NMR, crystallography, and a range of spectroscopic and calorimetric methods (Mike and Michael, 2010). Protein interactions fundamentally can be characterized as stable or transient. Both stable and transient interactions can be either strong or weak. Stable interactions are those associated with proteins that are purified as multi-subunit complexes. The subunits of the complex can be identical or different. Hemoglobin and core RNA polymerase are two examples of stable multi-subunit complex interactions. Stable interactions are best studied by co-immunoprecipitation, pull-down or far-Western methods (Mike and Michael 2010).

Transient interactions control the majority of cellular processes (Mike and Michael, 2010).

Over the years, numerous techniques were reported to detect protein complex formation such as silver staining technique (Gallyas, 1971; Allen, 1980, and Guevara *et al.,* 1982), Western blotting, gel filtration chromatography, native SDS-PAGE. However, these techniques were found not to be accurate; they tend to pull-apart the disulfide bonds of the protein. Precise and versatile methods have re-emerged to detect protein complex formation. Monitoring the sedimentation of macromolecules those tool-methods are: cross-linking and mass spectrometry (Julian *et al*., 2004), analytical ultracentrifugation (Jacob *et al.*, 2002; Geoffrey H and Allen M, 2006), SAXs (Cvekl *et al.*, 1994; Andras and Igor, 2001), analytical gel filtration (Paula *et al*., 2012; Bai, 2015), surface plasmon resonance (Cullen *et al*., 1997; Jiri *et al*., 1999; Jiri H, 2008), cryo-electron microscopy, HPLC MALDI-ToF mass spec (Minghui *et al*., 2000; Ze-Young and David H 2001), dynamic light scattering (DLS) (Xiong *et al*., 2008; Hilde *et al*., 2009), and isothermal titration calorimetry (ITC) (Adrian *et al*., 1990; Jan *et al*., 2007). Here we ask if protein-protein interactions can be recognized between hPrx2 and Hb by purely biochemical techniques means.

We applied both old and recently emerged techniques which are precise and versatile methods in the detection of protein complex. The following techniques were applied to detect protein complex formation between hPrx2 and Hb: silver staining technique, Western blotting, gel filtration chromatography, native SDS-PAGE, analytical gel filtration, and by Spectroscopic study.

4.2 Material and methods

4.2.1 Preparation of Superose 6 gel filtration column

Superose 6, column (S6) (GE Healthcare, Amersham Buckinghamshire UK), was cleaned using a reserve flow rate technique as recommended by the manufacturer. Cleaning of the column was performed at low flow rate of 0.2 mL/min with one column volume sodium hydroxide (500 mM NaOH). Then the column was equilibrated with two column volumes of water, then with two column volumes of running buffer (25 mM Tris-HCl pH 7.5, 1 mM EDTA, 20 µM BAM, 10 µM PMSF, and 0.1 M NaCl) after cleaning.

4.2.2 Size exclusion chromatography of native hPrx2 and recombinant Prx2

The S6 analytical gel filtration column was calibrated with the protein standards as follows: Apoferritin (443 kDa), β-amylase (200 kDa), alcohol dehydrogenase (150 kDa), albumin (66 kDa), carbonic anhydrase (29 kDa), thyroglobulin (669 kDa) and Blue Dextran (2000 kDa).

S6 analytical (GE Healthcare, Amersham Buckinghamshire UK) gel filtration column (column volume 120 ml) was equilibrated with one column volume of buffer C (section 2.4.1.1) at a flow rate of 0.5 ml/min. The sample was loaded and fractions were collected over the elution volume of one column volume and the absorbance measured at 280 nm and 418 nm, then the collected fractions were analyzed using SDS-PAGE as described in material section 2.4.1.4.

4.2.3 Titration of peroxiredoxin 2 with haemoglobin

The hPrx2 protein was titrated against Hb in the molecular ratios: 10:1 (4 Prx2 :1 Hb), 10:2 (2 Prx2 decamer : 1 Hb), 10:4 (1 Prx2 : 1 Hb), 10:6 (2 Prx2 : 3 Hb), and 10:8 (1 Prx2 : 2 Hb). 500µl for each molecular ratio mixture were prepared and eluted onto the calibrated S6 column. The sample mixtures were prepared as follows: for 10:1 titration, 5.666 mg/ml Prx2 was mixed with 0.4105 mg/ml Hb and the mixture was incubated in the cold room for 24 h. For 10:2 molar ratio titrations, 5.666 mg/ml Prx2 was mixed with

0.821 mg/ml Hb and the mixture was incubated at 4°C for 24 h. For 10: 4 molar ratio 5.666 mg/ml Prx2 was incubated with 1.648 mg/ml Hb for 24 hr in the cold room. For 10:6 molar ratio, 5.666 mg/ml Prx2 was mixed with 2.463 mg/ml Hb and incubated for 24 h at 4°C in the cold room. For 10:8 molar ratio; 5.666 mg/ml Prx2 was mixed with 3.289 mg/ml Hb and incubated at 4°C in the cold room.

4.2.3.1 Interaction of hPrx2 with haemoglobin

In order to measure the protein-protein interaction of hPrx2 with Hb, known molar concentrations for both proteins were mixed together under a controlled temperature and pH conditions. The interaction was studied using filtration chromatography and SDS-PAGE followed by Western blotting. Purified commercial native haemoglobin human lyophilized powder (SIGMA – ALDRICH) was suspended in PBS pH 7.5 (25 mM Tris-HCl pH 7.5, 1 mM EDTA, 20 µM BAM, 10 µM PMSF, and 0.1 M NaCl). Mixtures of hPrx2 and Hb were prepared without any pre-treatment, at room temperature and at ambient oxygen tension. Mixtures were left to react for 0, 24, 48 or 72 h prior to loading them onto acrylamide gels or a Superose 6 gel filtration column. The gel filtration column was eluted with elution buffer (25 mM Tris-HCl pH 7.5, 1 mM EDTA, 20 µM BAM, 10 µM PMSF, and 0.1 M NaCl) Acrylamide gels and Western blots were prepared as described in Chapter 2.

4.2.3.2 10: 4 molar ratio mix of hPrx2 and Hb (1 mg/ml hPrx2: 1 mg/ml Hb)

625 µl of 1.6 mg/ml Hb stock solution was mixed with 82.2 µl of 36.5 mg/ml Prx2 stock solution. The two proteins were mixed by pipetting the solution up and down gently five times in the Eppendorf tube on ice. The protein mixture was incubated for 24 h at 4°C. After the incubation, the protein mixture was centrifuged at 4000 rpm at 4°C for 10 min to remove any possible debris. The supernatant were collected and loaded onto the equilibrated S6 column with Buffer C (100 mM Tris-HCl, pH 7.5 and containing 0.1 M NaCl). The fractions were collected over the elution volume of one column volume and the absorbance measured at both 280 nm and 418 nm. Fractions corresponding to protein peaks were analysed using SDS-PAGE as the described in previous chapters (chapter 2 and chapter 3).

4.2.3.3 10:2 molar ratio mix of hPrx2 and Hb (2 Decamer hPrx2 with 1 Hb)

500 µl of 5.666 mg/ml Prx2 was mixed with 500 µl of 0.821 mg/ml Hb, mixed well gently by pipetting up and down in the Eppendorf tube on ice, and the protein mixture was incubated for 24 h at 4°C. The samples were loaded onto the analytical gel filtration column as described in material section 4.2.3.2.

4.2.3.4 10:6 molar ratio mix of hPrx2 and Hb (2 hPrx2 with 3 Hb)

500µl of 5.666 mg/ml Prx2 was mixed with 500µl of 2.463 mg/ml Hb; this was done by pipetting the solution up and down gently five times in the tube on ice. The protein mixture was incubated for 24 h at 4°C followed by concentrating the protein mixture to 500 µl, then followed similar procedures for protein analysis as described in material section 4.2.3.2 above.

4.2.3.5 10:8 molar ratios mix of hPrx2 and Hb (1 hPrx2 with 2 Hb)

500 µl of 5.666 mg/ml Prx2 was mixed with 500 µl of 3.289 mg/ml Hb; this was done by pipetting (1 ml) protein mixture up and down gently in the Eppendorf tube five times on ice. The protein mixture was incubated under the same conditions (24 h at 4°C) as described in material section 4.2.3.4. The protein was concentrated to 500 ml, and then loaded onto the S6 column as described in material section 4.2.3.2, followed by the protein-protein interaction analysis.

4.2.3.6 10:1 molar ratios mix of hPrx2 and Hb (4 hPrx2 with 1 Hb)

500µl of 5.666 mg/ml Prx2 was mixed with 500µl of 0.4105 mg/ml Hb in Eppendorf tube on ice then followed exactly the same procedures as described in material sections 4.2.3.2 – 4.2.3.5.

4.2.4 Spectroscopic study of Hb and Prx2-SNO interaction

Observations of changes in the UV-vis absorbance of Hb Soret band were used to detect any potential interaction between Hb and Prx2 or SNOPrx2. Hb (1µM) was incubated with Prx2 (1µM) in PBS (KH_2PO_4 144 mg/L, NaCl 9 g/L, Na_2HPO_4 795 mg/L, Lonza, Verviers, Belgium) at pH 7.4. The UV-vis absorbance spectrum of the mixture was then recorded between 220-520 nm on a Cary 300 UV-vis spectrophotometer (Agilent Technologies UK Ltd., Stockport, Cheshire, UK). Similarly UV-vis spectra were collected for: Hb (1µM) incubated with SNOPrx2 (protein concentration was 1 µM and RSNO concentration was 15 nM) and Hb (1 µM) incubated with albumin (90 nM) or SNOA (90 nM and RSNO concentration 15 nM) as a control. Due to the different moles of RSNO/moles of protein ratios of the synthesised SNOPrx2 and SNOA, it was not possible to simultaneously have the same protein and RSNO concentrations between the SNOPrx2 sample and the SNOA controls. Therefore it was decided to run the controls by incubating Hb with an equal amount of RSNO (which was 15 nM) in the form of SNOA.

4.2.5 hPrx2 activity assay

Prx2 and SNOPrx2 activity was studied by a spectrophotometric activity assay for Prxs described by Kim *et al*. (2005). As previously mentioned in Section 1.1.6 Prx2 works in co-operation with the Trx/TrxR system, and uses NADPH as a source of reducing equivalents. NADPH has a characteristic absorbance maximum at 340 nm, which decreases in intensity if NADPH is oxidised to $NADP^+$. The Prx2 spectrophotometric assay was based on recording NADPH oxidation (decrease in absorbance at 340 nm) as an index of Prx2 activity (Kim et al., 2005). The following mixtures were added to separate wells of a 96-well plate: 20 µL of Prx2 (1 µM) with H_2O_2 (100 µM); 20 µL of SNOPrx2 (1 µM, protein concentration) with H_2O_2 (100 µM); 20 µL of 50 mM HEPES-NaOH buffer (pH 7.0) with H_2O_2 100 µM (control with no Prx2) and 20 µL of 50 mM HEPES-NaOH buffer (pH 7.0) as blank. The Prx2-based reaction was started by injection into each well of 180 µL of a reaction mixture that consisted of: 50 mM HEPES-NaOH buffer (pH 7.0); 1 mM EDTA; 200 µM NADPH; 1.5 µM yeast Trx and 0.8

µM yeast TrxR. The reaction (NADPH oxidation) was followed for 30 minutes at 30˚C at 340 nm in a BMG Labtech Fluostar Optima plate reader.

4.2.6 Silver staining

Mini gel electrophoresis units were purchased from Idea Scientific Company, Corvallis, Oregon. Electrophoresis chemicals and molecular weight markers were from BioRad. Silver nitrate, formaldehyde, sodium carbonate and potassium dichromate were obtained from Mallinckrodt. All solutions were prepared in deionized water. 10% SDS2-polyacrylamide mini gels (75 X 105 X 0.8 mm) or slab gels (100 X 160X 1.5 mm) were prepared according to the method of Laemmli, (1970). The glass plates were acid washed, and handled with gloves to prevent contamination. Samples containing hPrx2 from various stages of purification (manuscript in preparation), molecular weight markers, or proteins of known amino acid composition were loaded into 4-mm-wide wells in the gel. Bromophenol blue was added to the samples as a tracking dye. Gels were electrophoresed at 150 V at 4ºC until the tracking dye had just migrated off the gel.

The silver staining procedure was done in a stepwise method: after electrophoresis, gels were fixed in 10% trichloroacetic acid in a 12-cmdiameter dish for 30 min. For silver staining, the method of Merril *et al*. (Merril *et al*., 1981) was modified. All procedures up to the reducing step were carried out at 30°C with mild agitation in a shaking water bath, under normal lighting. After fixing, gels were washed three times with 10% ethanol-5% acetic acid for a total of 30 min. Then 100 ml of oxidizer solution (0.0034 M potassium dichromate, 0.0032N nitric acid) was added for 5 min, and removed, and the gel was washed twice with deionized water for 10 min. Next, 100 ml 0.012 M silver nitrate was added for 20 min (30 min for 1.5-mmthick gels). The gel was then washed for 1 min with deionized water, and 50 ml of freshly prepared reducing solution (0.28 M sodium carbonate, 0.0185% or 0.037% formaldehyde) was added and removed after 30 s. The reducing solution gives best results if it was no more than 7 days old. The sodium carbonate solution can be prepared and stored indefinitely, and the formaldehyde added just prior to using. Additional reducing solution was added and the dish was placed in a 20, 30, 37, or 42°C water bath for about 5 min. Fresh reducing

solution can be added for an additional 5 min if needed. When development was complete, the reducing solution was removed and 5% acetic acid was added for 5 min to prevent excessive background colour. At this point colour development is complete and the gel background is yellow. Photographic fixer was added to lighten the background when required. The stained gels were stored in deionized water or dried between cellulose acetate sheets.

4.3 Results

4.3.1 Detection of protein complex formation between hPrx2 with Hb using: gel filtration chromatography, native SDS-PAGE, and analytical gel filtration.

After the purification of Prx2 free of heam (recombinant Prx2) as described in Chapter 2, we were in position to study the interaction of hPrx2 with Hb. First of all, we were interested to answer if the native Prx2 preparation was contaminated by haem, as this would be indicative of an interaction.

We also investigated the Prx2 content of commercially available, purified haemoglobin. Purified decameric recombinant Prx2 was eluted on a size exclusion column as described in chapter 2 (see Section 2.3.2.3), and the absorbance was monitored at 280 nm and 418 nm. We found that purified recombinant hPrx2 displayed a sharp absorbance at 280 nm (Fig. 4.2) but not at 418 nm, which corresponds to the Soret band (400-420 nm), characteristic of haem (Trbojevic-Cepe *et al.,* 1992). With the commercial purified Hb, we detected a peak at 280 nm and at 418 nm (Fig 4.1).

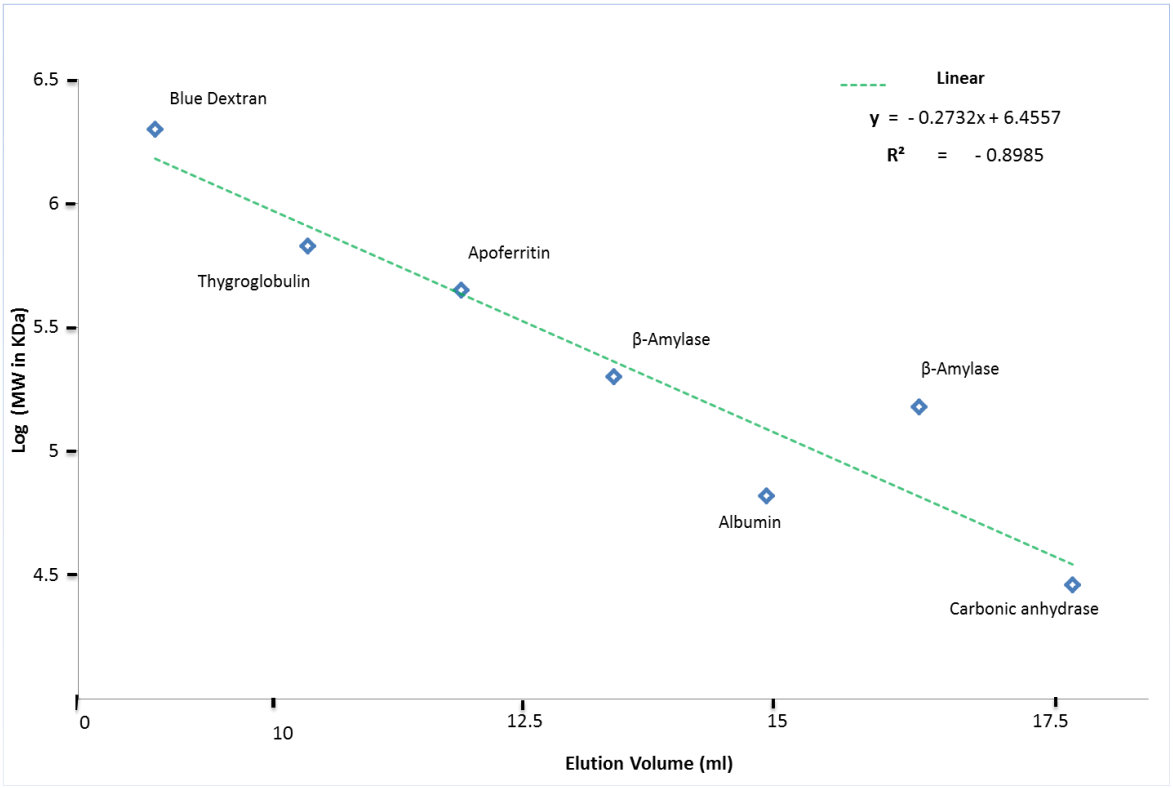

Figure 4.0 Calibration of a Superose 6 gel filtration column with known molecular standards using a mobile phase of 20 mM Tris-HCl, pH 8.0, containing 5 mM EDTA. The following molecular weight standards were used: β-amylase (200 kDa), alcohol dehydrogenase (150 kDa), carbonic anhydrase (29 kDa), albumin (66 kDa), apoferritin (443 kDa), thyroglobulin (669 kDa) and blue dextran (2000 kDa). Using the calibration curve, the molecular weights of the unknown proteins were estimated.

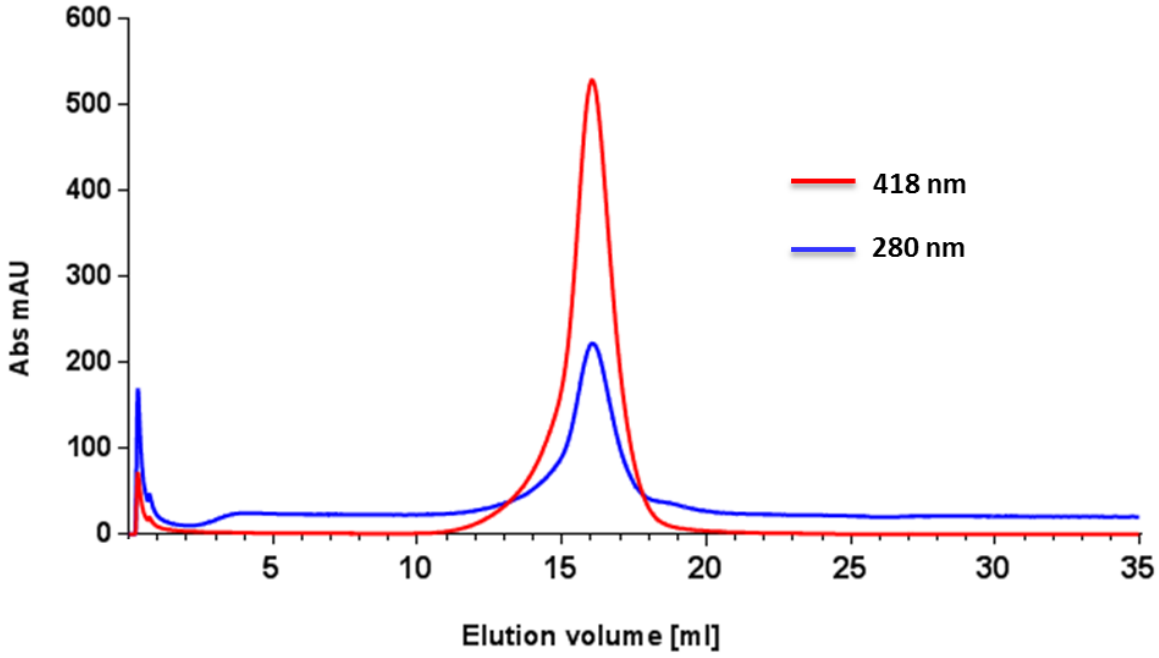

Figure 4.1. The elution profile for Hb from gel filtration (S6) chromatography.
500 ml of 5.1 mg /ml Hb was incubated for 24 h at 4˚C and then loaded onto an equilibrated and calibrated S6 column and run as described in method section 2.4.1.4. Fractions were collected at 0.5 ml intervals throughout the elution volume. A single peak protein which absorbed at 280 nm and 418 nm was formed.

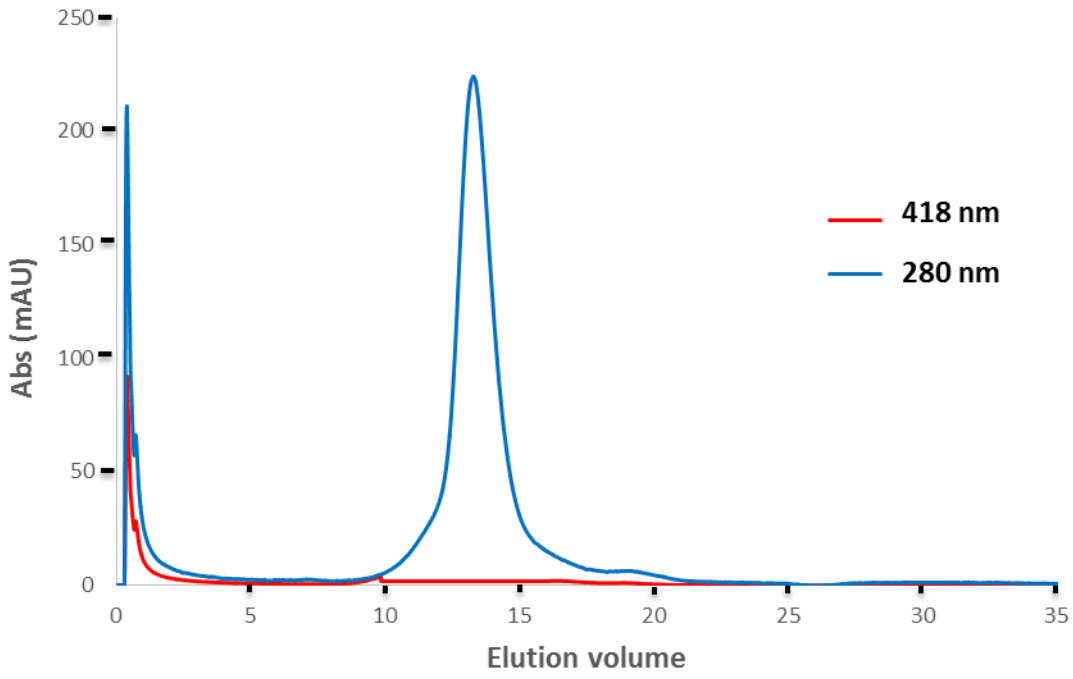

Figure 4.2. The elution profile from S6 gel filtration column for recombinant hPrx2 protein sample after 24 h incubation at 4°C. Fractions of 0.5 ml were collected as described in Fig 4.1. A single peak protein with zero absorbance at 418 nm (the absorbance which corresponds to the haem group), was formed.

When mixtures of Prx2 and Hb (2:1, 1:4, 2:3, 1:2, 4:1 molar ratios of Prx2 and tetrameric Hb) were loaded after; 24, 48 or 72 h incubation at 4°C temperature, on a size exclusion column using a PBS buffer, the pattern of peaks of these mixtures were detected at 280 nm and 410 nm wavelength (see Figures; 4.3, 4.5, 4.7 and 4.9) These were very similar to a combination of the pattern of the Prx2 only and Hb only chromatograms (Fig. 4.1 and 4.2). No peak shift - indicative of complex formation with increased molecular weight - took place either without incubation or after; 24 h, 48 h or 72 h incubation, suggesting that no complex was formed between Prx2 and haemoglobin under the described experimental conditions.

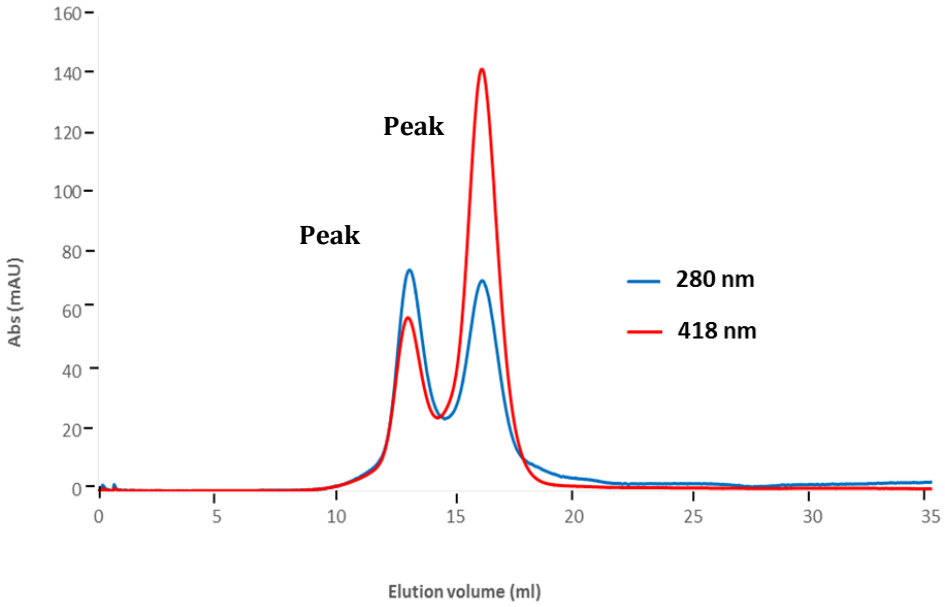

Figure 4.3. The elution profile from S6 gel filtration column for the molar ratio incubation of one mole of hPrx2 with four moles of Hb after 24 h at 4˚C. Fractions were collected at 0.5 ml intervals throughout the elution volume. Two peaks were formed; peak 1 and peak 2. Peak 1 (at 280 nm) had a height of 17.7 cm and was eluted at 13.08 ml which correspond to Mr ~ 251188.6 kDa according to the calibration curve (Fig. 4.0). Peak 2, (at 280 nm) had a height of 11.1 cm eluted at 16.17 ml which corresponds to Mr ~ 56234 kDa according to the calibration curve.

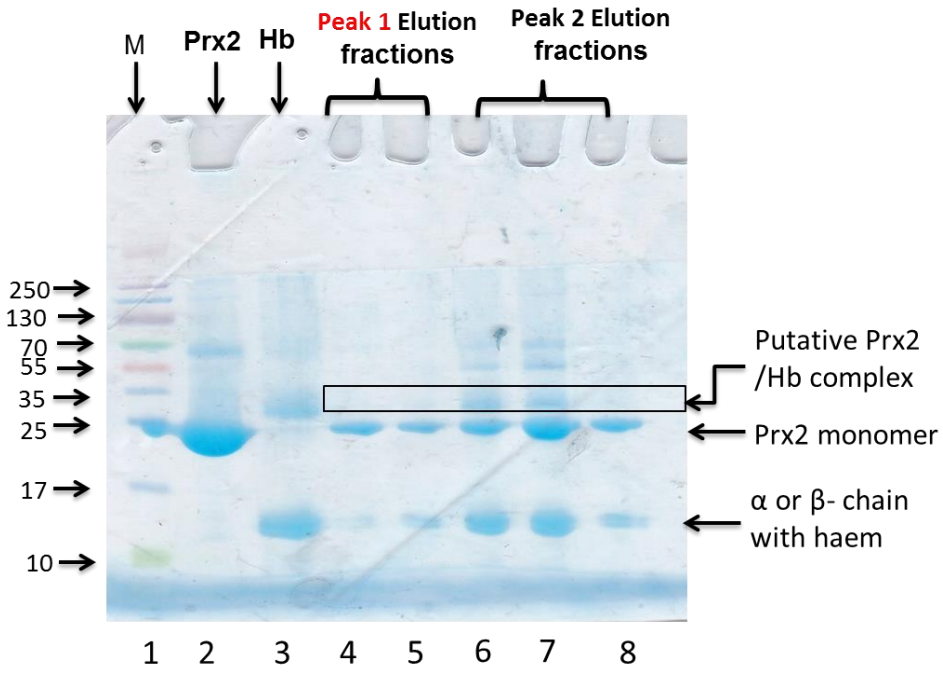

Figure 4.4. SDS-PAGE elution analysis for the S6 gel filtration column for the molar ratio incubation of one mole of hPrx2 with four moles of Hb after 24 h at 4˚C in figure 4.3 above. Different amounts of haemoglobin and Prx2, and a mixture of the two were treated under reducing conditions and revealed on 15 % SDS-PAGE. Lane1 (M), molecular weight marker, lane 2 is hPrx2 sample only; lane 3 is the Hb sample only, lanes 4 and 5 are elution samples from peak 1. Lanes 6, 7, and 8 are elution fraction samples from peak 2. The box pointed at by the arrow is the putative Prx2 / Hb complex formed.

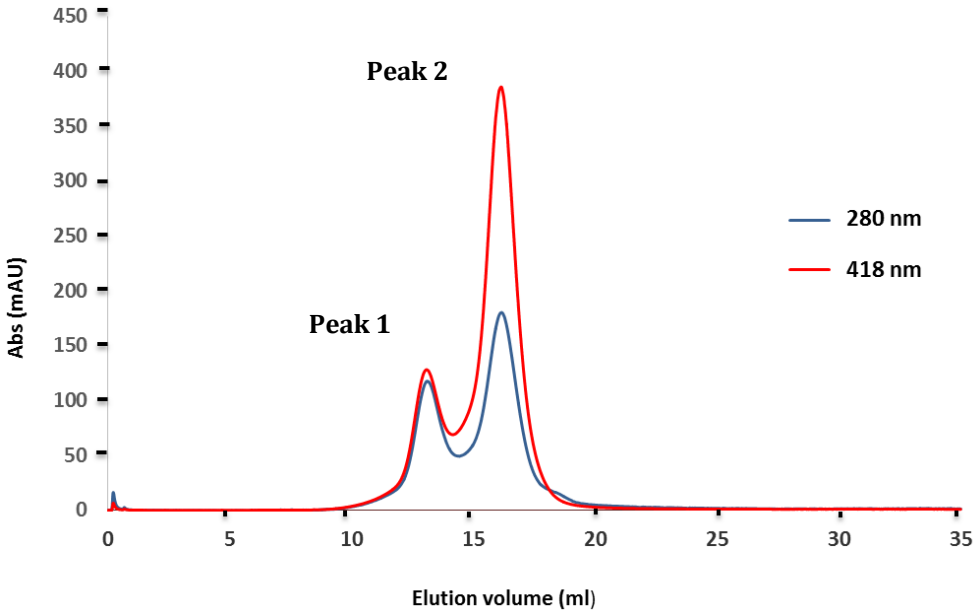

Figure 4.5 The elution profile from S6 gel filtration column for the molar ratio incubation of two moles of hPrx2 with three moles of Hb after 24 h at 4˚C.

Fractions were collected at 0.5 ml intervals throughout the elution volume. Two peaks were formed; peak 1 and peak 2. Peak 1 (280 nm) had a height of 6.8 cm and was eluted at 13.09 ml which correspond to Mr ~ 316227.8 kDa according to the calibration of the column (Fig. 4.0). Peak 2 (280 nm) had a height of 10.3 cm and was 2 eluted at 16.16 ml which correspond to Mr ~ 56234 kDa according to the calibration of the column (Fig. 4.0).

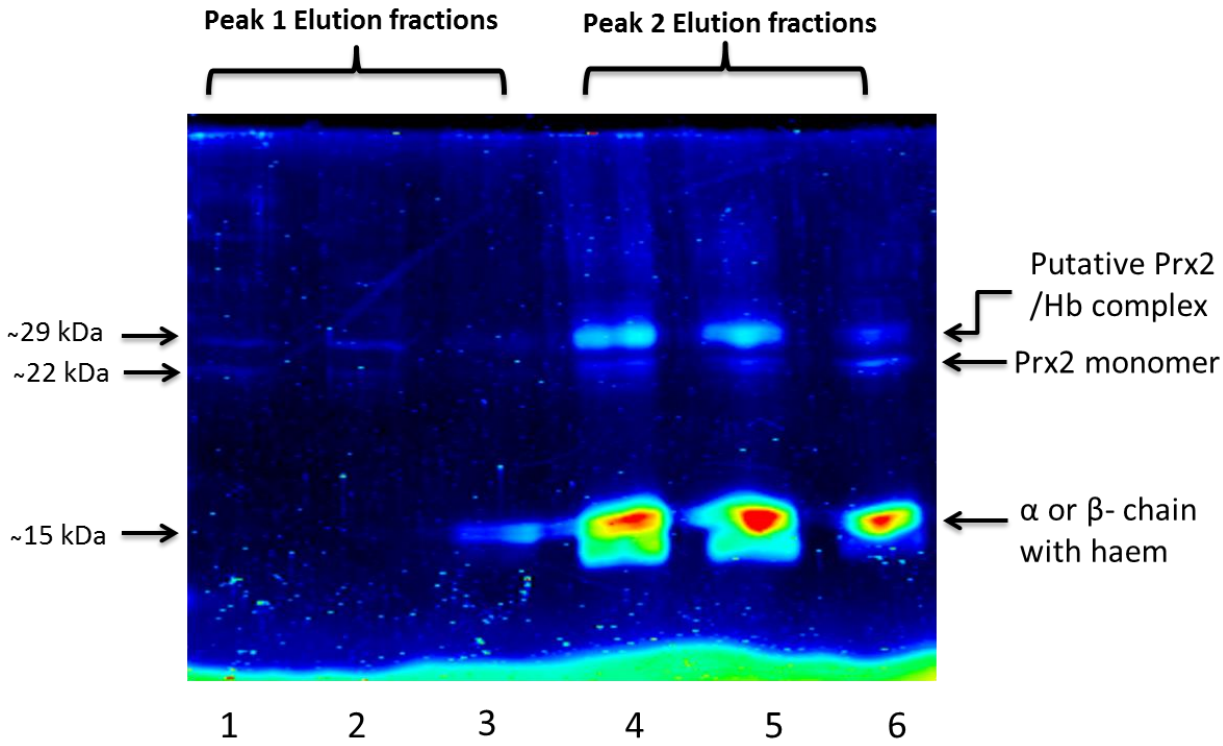

Figure 4.6 SDS-PAGE analysis for the elution on S6 gel filtration column for the molar ratio incubation of two moles of hPrx2 with three moles of Hb after 24 h at 4˚C in figure 4.5 above.

Different amounts peak (peak 1 and 2) fractions were treated under reducing conditions and revealed on 15 % SDS-PAGE. Lanes; 1, 2 and 3, are peak 1 elution fractions. Lanes; 4,5 and 6 are elution fractions from peak 2.

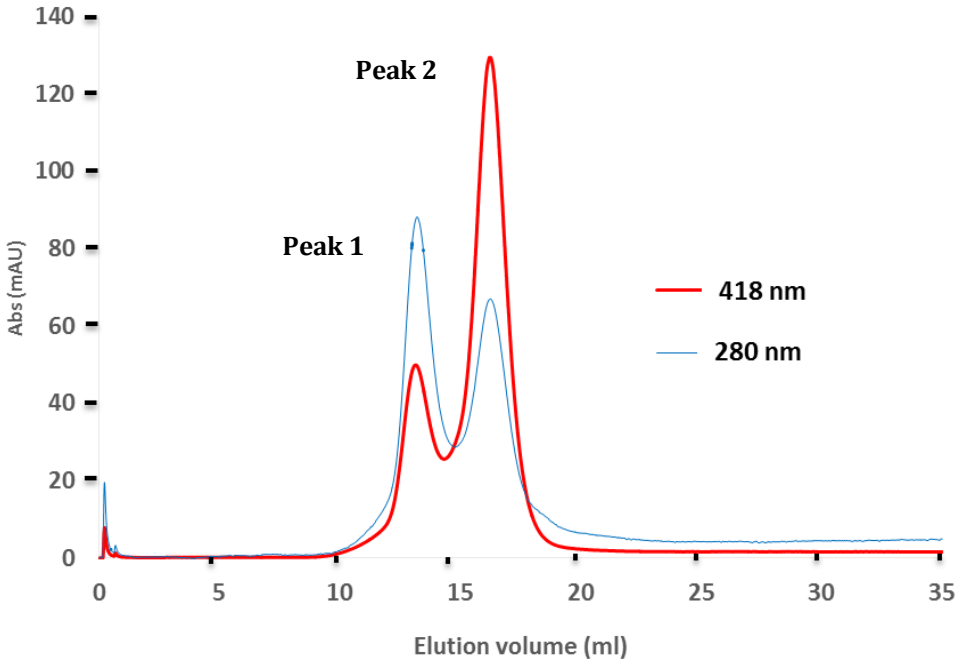

Figure 4.7. The elution profile from S6 gel filtration column for the molar ratio incubation of two moles (two decamer) of hPrx2 with one mole of Hb after 24 h at 4˚C. Fractions were collected at 0.5 ml intervals throughout the elution volume.

Two peaks were formed; peak 1 and peak 2. Peak 1 (280 nm) had a height of 15.3 cm and was eluted at 13.18 ml, which correspond to Mr ~ 281838.3 kDa according to the calibration of the column (Fig. 4.0). Peak 2 (280 nm) had a height of 11.9 cm and eluted at 16.22 ml which correspond to Mr ~ 31623 kDa according to the calibration of the column (Fig. 4.0).

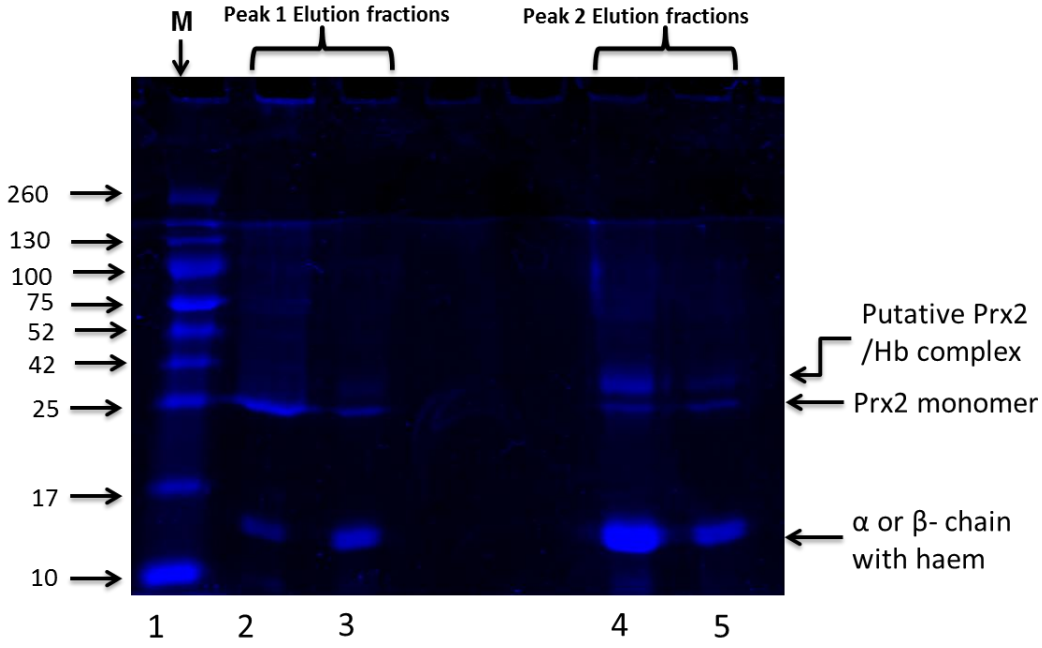

Figure 4.8. SDS-PAGE analysis for the elution on S6 gel filtration column for the molar ratio incubation of two moles of hPrx2 with one mole of Hb after 24 h at 4˚C in figure 4.7 above.

Different amounts peak (peak 1 and 2) fractions were treated under reducing conditions and revealed on 15 % SDS-PAGE. Lane 1 (M); molecular weight marker, lanes 2 and 3, are peak 1 elution fractions. Lanes; 4 and 5 are elution fractions from peak 2.

According to the calibration curve, the molecular weights of the putative Prx2/ Hb complex reported was calculated to be 29kDa and that of the pure Prx2 monomer eluted at about 22 kD as per standard curve.

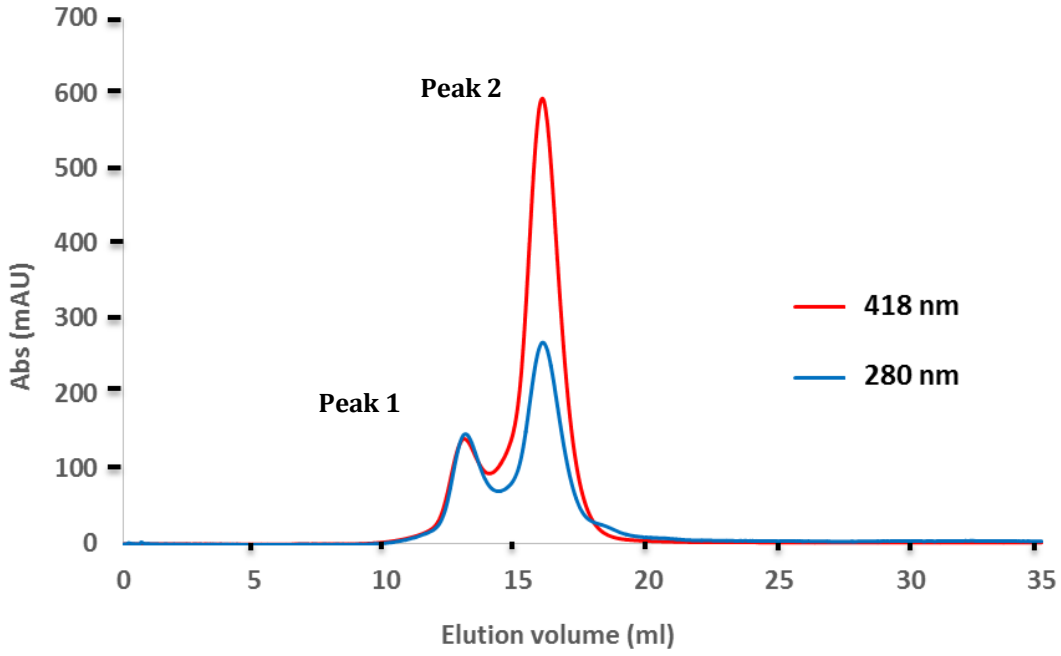

Figure 4.9. The elution profile from S6 gel filtration column for the molar ratio incubation of one mole (one decamer) of hPrx2 with two moles of Hb after 24 h at 4˚C. Fractions were collected at 0.5 ml intervals throughout the elution volume.

Two peaks were formed; peak 1 and peak 2. Peak 1 (280 nm) had a height of 5.9 cm and was eluted at 13.06 ml, which correspond to Mr ~ 257039.6 kDa according to the calibration of the column (Fig. 4.0). Peak 2 (280 nm) had a height of 10.2 cm and eluted at 16.00 ml which correspond to Mr ~ 63096 kDa according to the calibration of the column (Fig. 4.0). This elution profile provided that the two proteins were interacting due to the fact that the absorbance at 418 nm was present in both peaks.

4.3.2 hPrx2-SNO and complex formation with Hb

Next, a potential interaction of Prx2 with haem was also studied using the incubation of known concentrations of hPrx2 with known concentrations of hPrx2-GSNO.

It was hypothesised that Prx2 takes part in NO metabolism, thus facilitating its transport through RBC membrane by the formation of Prx2-SNO, which has been previously detected in different cell types (Yang and Loscalzo, 2005; Fang *et al*., 2007). It was also

suggested that the formation of a complex with Hb, is the one which facilitates NO transfer. Therefore in order to study Prx2-SNO interaction with Hb, I performed a cell-free synthesis of the S-nitrosated protein. The protocol used (Section 3.4.3.6) is a new method which is completely different from that previously validated method by our group used for the synthesis of S-nitrosoalbumin based on the use of acidified nitrite as nitrosating agent. The method used GSNO as the source of NO and this was achieved in two ways as described in section 3.4.3.6. The method was user friendly, not harsh causing denaturing of the protein, as experienced with the validated method (in section 3.4.2.4) by our group.

Once Prx2-SNO was synthesised and characterised it was possible to study its interaction with Hb by UV-vis spectrophotometry as described in Section 4.2.4. Hb (1 µM) was incubated with Prx2 (1 µM) in PBS at pH 7.4. The UV-vis absorbance of the mixture was then recorded between 220-520 nm (Figure 4.15 B). Similarly UV-vis spectra were collected for: Hb (1µM) incubated with SNOPrx2 (protein concentration was 1 µM and RSNO concentration was 15 nM) (Figure 4.15 C); Hb (1 µM) incubated.

Control scans with Prx2 alone, Hb alone and SNOPrx2 alone were run as well (Figure 4.15 A). While there were no significant changes in the UV scans of Hb when it was incubated with buffer or water, it was possible to see a decrease in intensity and a small (~1 nm) λ_{max} shift towards higher wavelengths (red shift) of the Soret band when Hb was incubated with Prx2-SNO (Figure 4.15 C). None of the same changes were observed when Hb was incubated water or buffer.

As mentioned earlier, During Prx2 purification from RBCs several fractions containing Prx2 were found to have traces of Hb. The difficulty to further purify these fractions was perhaps indicative of a complex formation between the two proteins. Recombinant hPrx2 protein sample were used to synthesize Prx-SNO samples used to monitor the protein-protein interactions. Although these data are not conclusive, as more Prx2-Hb fractions should be analysed, they provided us with a first indication of a possible hPrx2-SNO presence in the potentially in a complex with Hb.

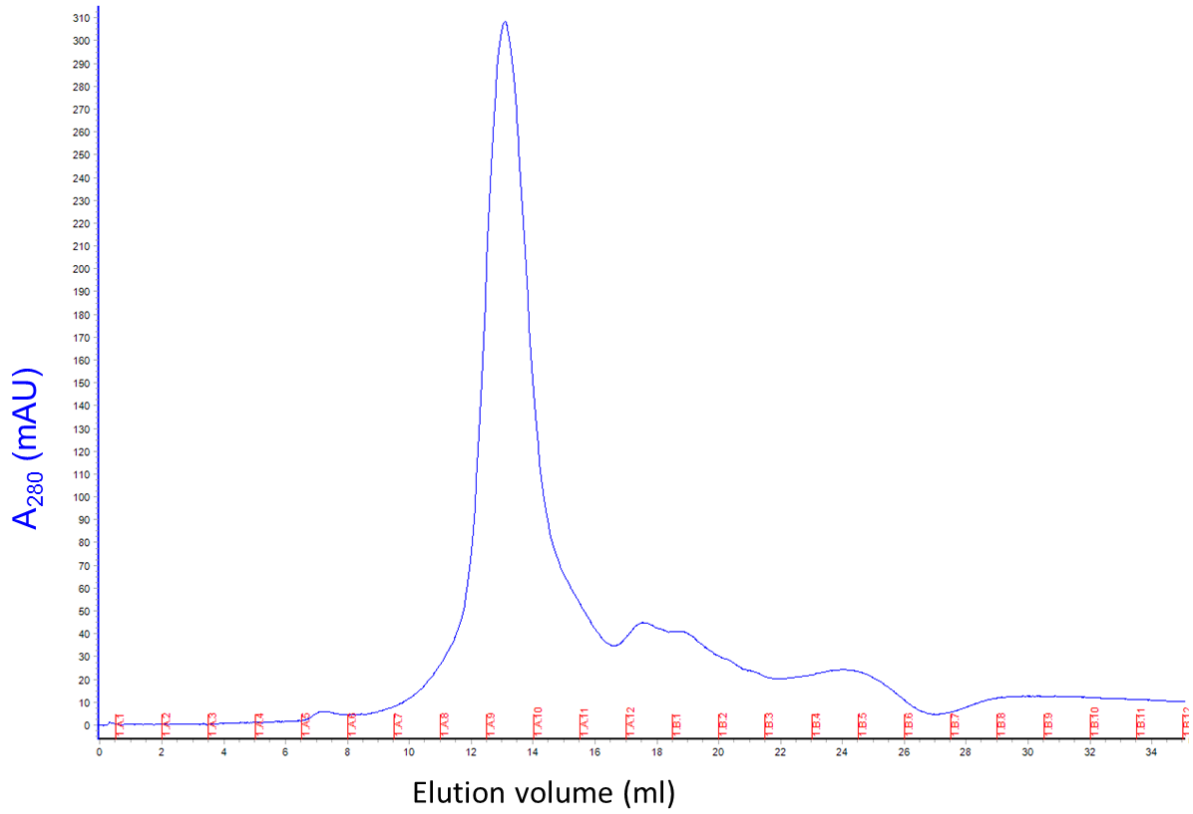

Figure 4.10. The elution profile chromatograph from S6 gel filtration column for hPrx2-GSNO protein sample after 24 h incubation at 4˚C. 500 ml of 4.5 mg/ml hPrx2-GSNO as loaded on the column and fractions of 0.5 ml were collected across the column. According to the elution profile above, hPrx2-GSNO eluted at ~ 13 ml. This elution profile acted a control for all the chromatographic study for the interactions between hPrx2-GSNO and Hb. The hPrx2-GSNO protein samples were prepared as described in material section 3.4.3.6 and loaded onto the SDS-PAGE.

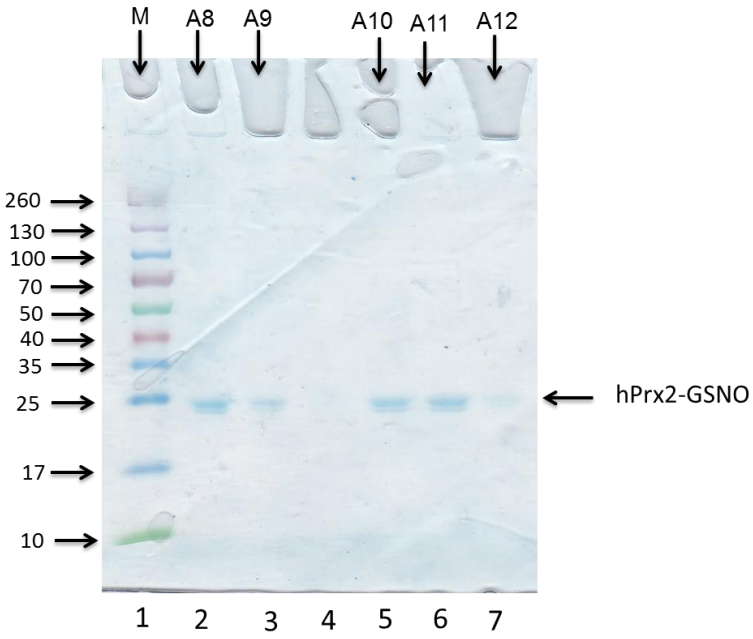

Figure 4.11. SDS-PAGE for the elution profile for the gel filtration column for hPrx2-GSNO. 10 µl of samples of fractions A8-A12 of the elute from the gel filtration (Fig. 4.10) were loaded on SDS-PAGE under reducing conditions and detected by coomassie brilliant staining. Lane 1: MW markers; lanes 2-7: S6 gel filtration column fractions A8-A12 in increasing order. The fractions were free from contaminants and had the expected size band for hPrx2 (~ 22 kDa).

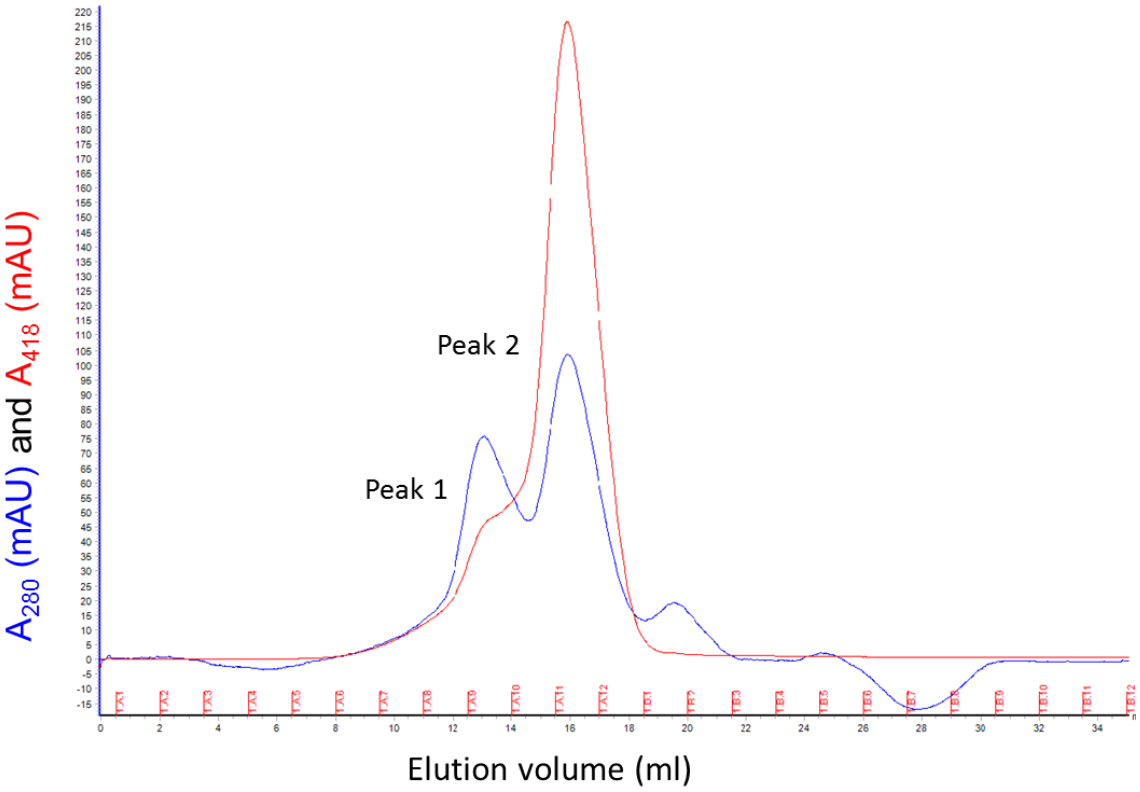

Figure 4.12 Elution profile from S6 gel filtration column for the molar ratio incubation of one mole of hPrx2-SNO with one mole of Hb after 24 h at 4˚C. peak 1 eluted at about 13 ml, peak 2 eluted at about 16.ml and peak 3 which was produced as a result of protein degradation eluted at about 20 ml. 0.5 ml fractions were collected across the column and loaded on the SDS-PAGE of protein analysis. Fractions from peak 1 and 2 were collected separately and concentrated to about 10 mg/ml for crystallographic studies.

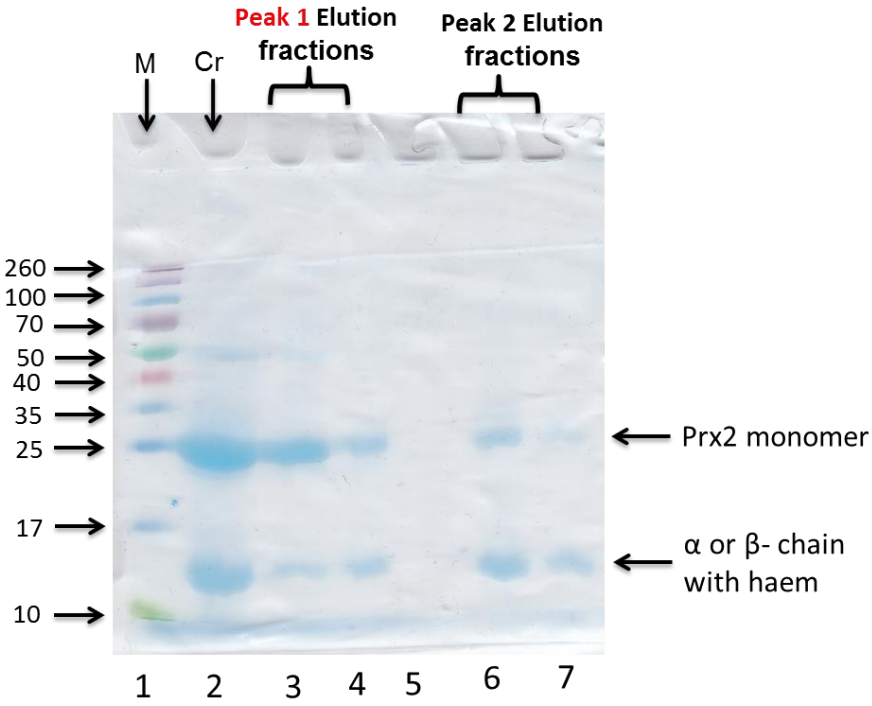

Figure 4.13. SDS-PAGE elution analysis for the S6 gel filtration column for the molar ratio incubation for 24 h at 4°C, of one mole of hPrx2-GSNO with four moles of Hb. 10 µl of each sample fractions were prepared and loaded onto the SDS-PAGE for protein analysis. Lane1 (M), molecular weight marker, lane 2 (Cr) is the crude sample mixture loaded onto the column; lanes 3 and 4 are fraction samples from peak 1 from figure 4.12. Lane 5 is an empty lane. Lanes 6 and 7 are fractions from peak 2 from figure 4.12. Both peaks (1 and s), demonstrated the presence of hPrx2 and Hb in the ratios: peak 1 contained more hPrx2 than Hb (lanes 3 and 4), while as peak 2 demonstrated to contain more Hb than hPrx2 (lanes 6 and 7).

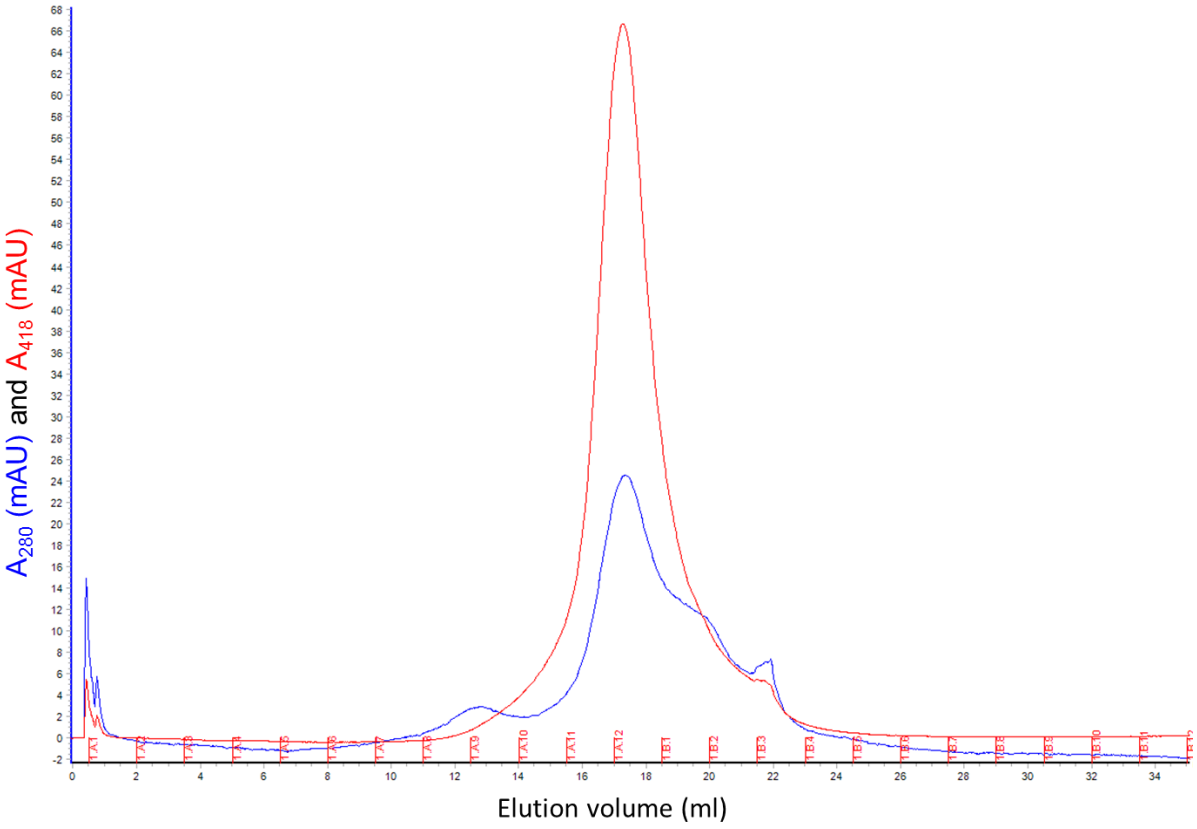

Figure 4.14 Elution profile from S6 gel filtration column for the molar ratio incubation of one mole of hPrx2-GSNO with two moles of Hb after 24 h at 4°C.

There was a shoulder of Peak~12.5 ml and peak 2 eluted at about~17ml.

4.3.3 The detection of the interactions of: hPrx2, hPrx2-SNO with Hb by UV-vis spectrophotometry

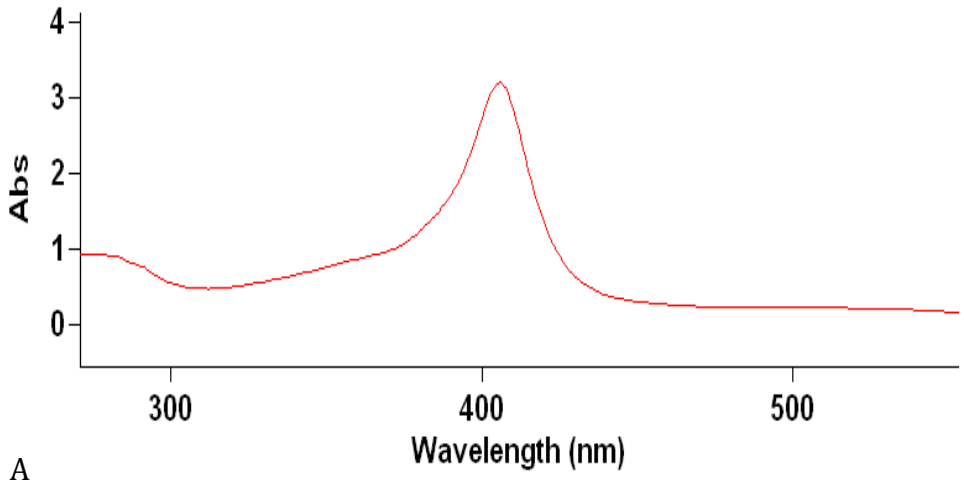

A

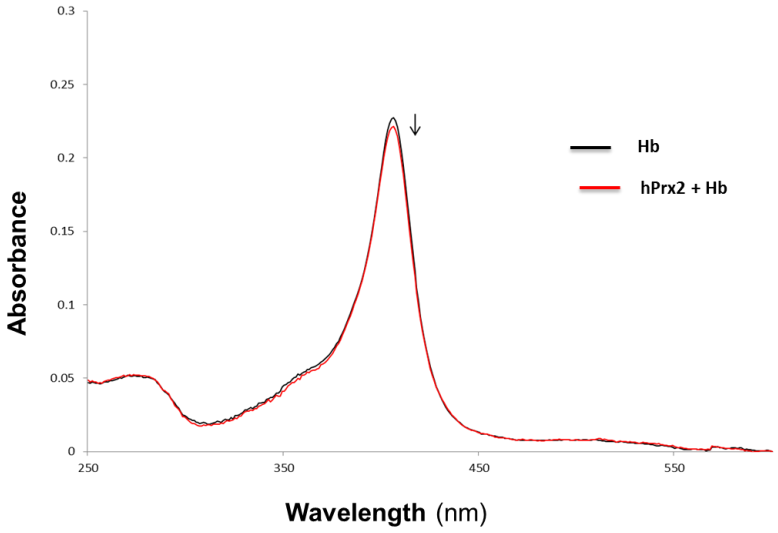

B

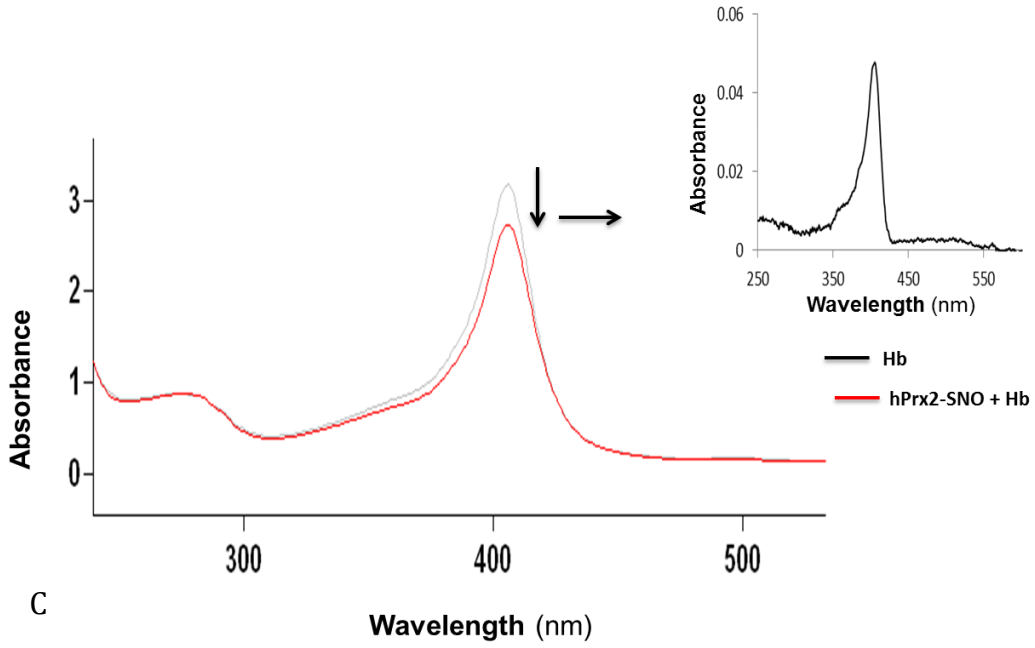

Figure 4.15. Representative UV-vis absorbance scans for: Hb mixed with water (A),hPrx2 + Hb (B) and hPrx2-SNO + Hb (C). It was possible to observe a shift of the λ_{max} of the Soret band (410 nm) towards higher wavelengths. 50 µl of 8.8 mM RSNO was incubated on ice for 10 min.

The potential interaction between Prx2 and Hb was also followed up by reducing SDS; reducing and non-reducing PAGE, followed by Western blotting. In these experiments, the same ratios as before of Prx2 and Hb, and same incubation times were used as to the size exclusion chromatography experiments.

Although haemoglobin displays pseudo-peroxidase activity (Cooper *et al*., 2008) and thus may cause chemiluminescence in the presence of enhanced chemiluminescence and H_2O_2 substrates, this phenomenon was not expected to cause major difficulties in interpreting the results of Hb Western blots probed with anti-Prx2 antibodies after considering the molecular weight of the detected bands (monomeric Prx2 is 22 kDa, while globin monomers are 15 kDa each).

A reducing SDS-PAGE of Prx2, Hb and a mixture of the two was carried out with and without subsequent immunoblotting for Prx2. The reducing SDS-PAGE (Fig. 4.9) showed that Hb migrated as monomeric and dimeric globin chains (15 and 30 kDa,

respectively) under reducing conditions. Prx2 was revealed as a 22 kDa monomer. No band shift or extra bands were present in the lane containing the mixture of Prx2 and Hb (Fig. 4.9).

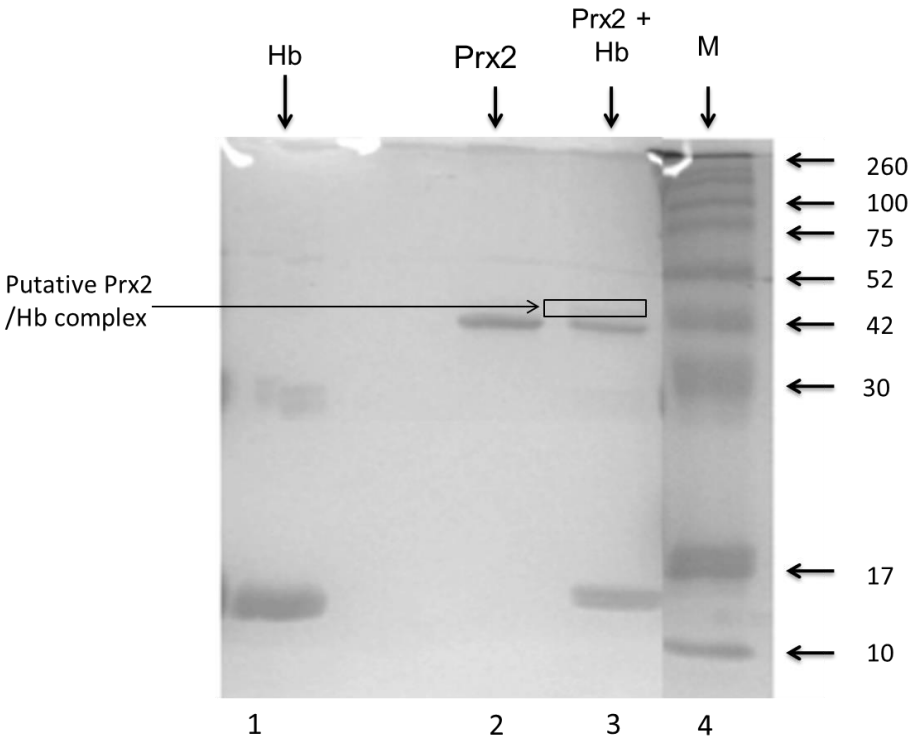

Figure 4.16. A non-reducing SDS-PAGE of Prx2, Hb and a mixture of Prx2 + Hb. Different amounts of Hb and hPrx2, and a mixture of the two were prepared and revealed on 15 % SDS-PAGE without further incubation. The bands were then visualised using Commassie staining as described in chapter 2. Known molecular weight standards (M) were used to estimate the molecular size of the protein. Lane identities: lane 1; 1.5 mg /ml (10 µl tetramer) haemoglobin (Hb); lane 2 is 5.152 mg/ml (10 µl Prx2); lane 3 is 10 µl for the mixture of 5.152 mg/ml Prx2 + 0.7488 mg/ml Hb; lane 4 is molecular weight standards (M). The arrow pointing at a box on the gel indicates the putative complex formed when hPrx2 mixed with Hb in the ratio 10:4 (one mole of hPrx2 with four moles of Hb).

Chapter 5:

Crystallization and X-ray diffraction studies of hPrx2-Hb and hPrx2-SNO complexes

5.0 Introduction

(Schroder et al., 2000) solved the structure of hPrx2. However, the structure for hPrx2-Hb and hPrx2-SNO are yet to be solved. One of aims of this research project was to try to solve the protein structures of hPrx2-Hb, in support of the hypothesis that Prx2 transports NO. A number of methodologies were involved in the isolation and purification of the native hPrx2 from RBCs. More complex methods were required for the expression of hPrx2 in *E.coli*, purification of the protein and screening of various crystallization conditions kits to find the perfect crystallization conditions for the protein.

The knowledge of the structure of a protein can provide important details about the protein's function, mechanism of action and its interaction with other molecules. The techniques of NMR or X-ray diffraction can be used to solve the three dimensional structure of protein. In order to solve protein structures by X-ray diffraction, high quality well-ordered crystals are used. The crystallization of protein is dependent on many inter-related factors. These include protein purity (homogeneity), solubility, aggregation and concentration of precipitant, additive, temperature, pH while as salt concentration are some of the other external factors. The most common precipitants are ammonium sulfate and polyethylene glycol (PEG).

Protein crystallization process can be further explained by looking at the different phase stages consisted (see figure 5.1) in the process. There are two phases of crystallization, nucleation followed by growth. Each of these stages is dependent on both protein concentration and the crystallization agent concentration. To promote either stage, supersaturation needs to occur. This is a condition where there is more protein than can be dissolved in the volume of fluid. Supersaturation leads to either a crystalline or amorphous phase when equilibrium returns. Supersaturation is induced in crystallization by introducing factors that reduce protein solubility, these including: allowing water to evaporate, changing temperatures, or adding an ionic solute (a precipitant). Protein precipitants include salts and high molecular weight PEGs. Salts bring protein out of solution by competing for the water of hydration.

In the first nucleation phase, protein molecules need to overcome an energy barrier to form a periodically ordered aggregate of a critical size that can survive in a thermodynamic sense. Nucleation can happen throughout the solution or on a solid

surface such as a dust particle or the bottom of the crystallization well. In some cases nucleation crystal growth can be induced by the addition of artificial nucleants such as horse hair. When nucleation occurs, protein is removed from solution; therefore the level of supersaturation will be reduced to the metastable phase. This allows growth to occur and reduces any further nucleation events. If the crystallization has reached equilibrium, the crystal growth will push the supersaturation further into the metastable phase. If however there is no equilibrium, the solution may remain in the nucleation phase and more nucleation events occur resulting in many small crystals.

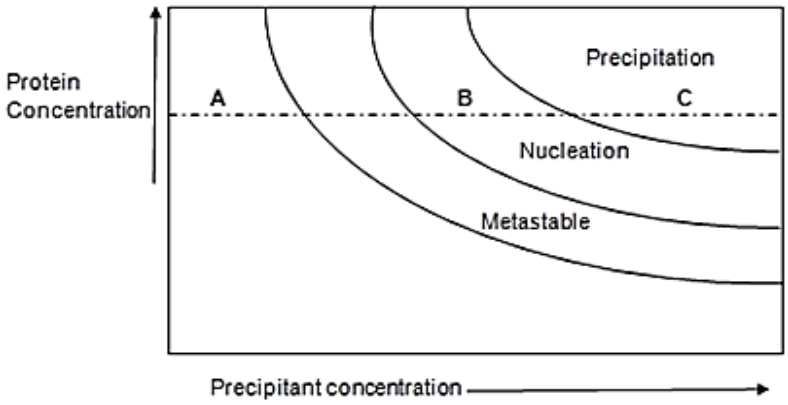

Figure 5.1 The phase diagram showing the solubility of the protein as the precipitant concentration changes. At point A the protein will stay under-saturation. At point B the protein will crystallize and the concentration of the protein in solution drops to saturation as the crystal grows. At point C the protein will precipitate out but crystals may still grow. Figure adapted from Paul (2010).

5.1 Methods of crystallization

In order to determine in which condition a protein will crystallize it is common to carry out a wide range of plate screening with a variety of conditions, commonly using commercial crystallization kits. There are several different methods of crystallisation such as microbatch and vapour-phase diffusion. Microbatch experiments are where the protein and precipitant are mixed directly under oil. In the true microbatch method there is little to no diffusion as H_2O cannot travel through the paraffin oil placed on top of the droplet (Chayen *et al*., 1992; Brumshtein *et al*., 2008). Protein crystallisation using this method requires that the precipitants concentration is correct for crystal formation. Microbatch crystallisation using Al's oil (50/50 paraffin/silicon oil mix) shows some slow diffusion of water thus increasing the concentration of precipitant and protein in the crystallisation droplet and is similar in this way to vapour diffusion.

Vapour diffusion method is based on slow equilibration between a reservoir, which contains the precipitating condition that is separated from the protein droplet mixed with a small volume of precipitant. An equilibrium state is created when water diffuses from the drop to join precipitants in the reservoir. This increase in precipitant and protein concentration within the drop can bring the protein into the super-saturation state. As protein crystals begin to grow the solution is brought into the metastable crystal growth zone.

5.2 X-ray crystallography

X-rays can be used to determine the 3D structure of protein. Usually, X-rays with a wavelength between 0.5 and 1.6 Å are used as these wavelengths are comparable to the inter atomic distances in protein crystals. They are also capable to penetrate and diffract, scatter strongly enough by the crystals. X-ray waves are shot right onto the crystal to cause a diffraction pattern, which is produced according to the different properties of the crystal. From the diffraction pattern, the three dimensional structure of the proteins is then determined.

Protein crystals are made up of a regular repeating array of unit cells, which amplify X-ray diffraction patterns. These unit cells are defined by three lengths (a, b, and c) and

by the three angles (alpha, beta, and gamma). The more unit cells present within the crystal, the stronger the resulting diffraction. The crystal is thought of being divided into a number of planes which runs through the unit cell, and those planes have various orientations and spacing running between them. A collection of numerous individual reflections (spots), make-up the diffraction pattern, with the spots corresponding to the diffraction from the crystal planes.

Bragg, 1913 (Bragg's law) illustrated the relationship between the diffraction pattern and the spacing of the crystal planes, which helps our understanding into of this mystery. Bragg's law describes the relationship between the reflection angle (θ), the distance between the planes (d) and the wavelength (λ) shown in the equation below.

$$n\lambda = 2d\sin\theta$$

Where: n is an integer, λ is the wavelength of the radiation, d is the spacing between the lattice planes and θ is the angle of incidence of the X-ray beam.

From Bragg's law, all the planes that run through the crystal are treated as mirrors that can reflect the X-rays therefore these reflections give rise to the reflection spots. X-rays might constructively add up if rays start or arrive in phase at the crystal. Constructive diffraction will occur according to Bragg's law within a crystal with two planes separated by distance (d) if the difference in path length ($2d\sin\theta$) between the waves is equal to the integer number of wavelength (figure 5.2).

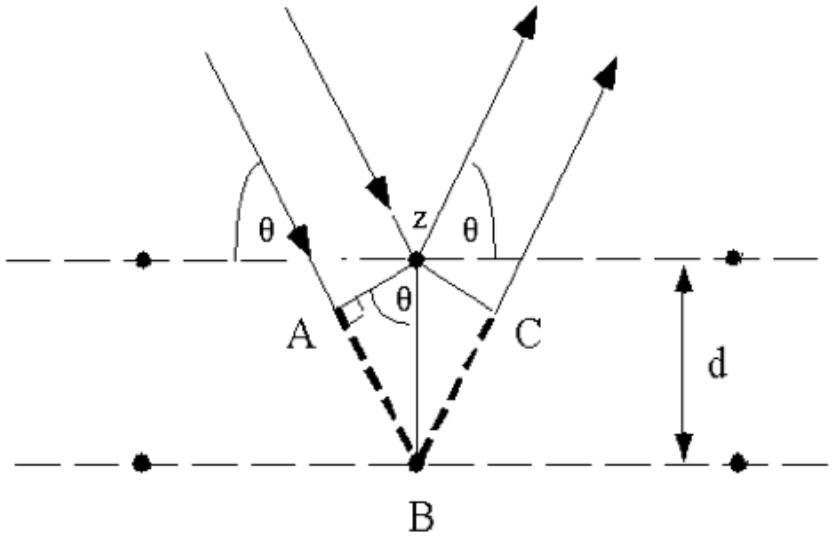

Figure 5.2 Conditions that satisfy Bragg's law. Figure adapted from Asherie (2004).

From the figure 5.2 above, we can conclude that the shorter the spacing between the crystal planes then the greater the angle of diffraction. The various lattice planes that divide the crystal across its three dimension (a, b and c) are described by a set of Miller incidences (h, k and l). A value of the reflection angle (θ) can be calculated using simple trigonometry and from this the spacing (d_{hkl}) can be calculated. Thereafter the dimensions of the unit cell can be calculated.

During data collection, it is important to rotate the crystal to obtain a diffraction pattern because for a stationary crystal only a limited number of the crystal planes will satisfy Bragg's law. Rotating the crystal allows data to be collected from all the crystal planes. This is better explained by the Ewald's sphere, which describes Bragg's law in three dimensions. In the Ewald's sphere, the crystal is placed at the centre and with a radius of $1/\lambda$. Each reciprocal lattice point has a position relative to its family of crystal planes, which are located at a vector from the crystal with a length that is inversely proportional to the d spacing (Dauter, 1999). A diffraction spot is produced if the lattice point lies on the surface of the sphere (figure 6.3). Rotating the crystal to a reciprocal lattice point, changes the point, that lie on the sphere's surface and this produces all the required reflections.

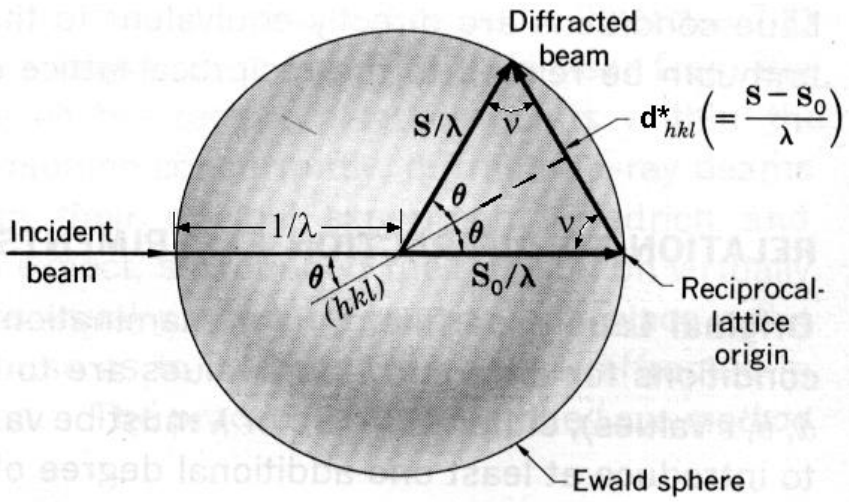

Figure 5.3 Ewald's Sphere. Figure adapted from Dauter (1999).

In the Bragg construction both the incident beam and the scattered beam are inclined to the (hkl*)* plane at an angle q making the angles of incidence and "reflection" equal. The X-ray diffraction data is used to calculate the electron density throughout the unit cell. The intensity of each spot is proportional to the amplitude of the diffracted X-ray waves. Phase information is recalculated using other methods, as it is lost during data collection. By combining the amplitude ($|F_h|$) and phase ($i\alpha h$) of the reflections a structure factor (F) can be obtained.

5.3 Materials and methods

5.3.1 Structural modelling for hPrx2 complex formation with Hb

We hypothesized Prx2 mediates the transfer of NO in RBCs; thus, Prx2 interacts with NO to form a stable complex (Prx2-NO) as described in earlier chapters. In order to fully understand how this can possibly happen, we had to come up with a structural model. Looking at all the possible proteins and molecules which might carry out the function we hypothesize for Prx2 in RBCS. The protein likely to carry the bound NO in RBCs must have at least the following features: the protein or peptide should be in abundance, the protein or peptide should be readily exchangeable (pass the NO to carrier molecules), and the interaction should be specific between NO and the carrier protein or peptide predicted. Protein disulfide-isomerase (PDI), Hb, hPrx2 and free glutathione has all the desired features making them prime candidates for NO carrier.

Folding in the cell is very critical, assisted by catalysts that speed-up protein folding and chaperones that inhibit aggregation (Buchner, 1996; Hartl and Hayer-Hartl 2002). Therefore, when the folding process does not function properly, it can be catastrophic for the cell. PDI is an enzyme in the endoplasmic reticulum (ER) in eukaryotes and the periplasm of bacteria which is responsible for the formation and breakage of disulfide bonds between cysteine residues within protein as they fold. A number of diseases are due to misfolded proteins (Thomas *et al*., 1995; Koo *et al*., 1999; Dobson, 2001), such as Alzheimer's (Harper and Lansbury, 1997),emphysema (Cabral *et al*., 2001), prion infections (DeBurman *et al*., 1997), and goiter (Kim *et al*., 1997). PDI has an active cysteine (Cys61 or Cys406 in yeast) which can interact with NO, and is readily to be transported across membrane (Fig. 5.4).

5.3.1.1 Structural modeling analysis

Structure model building was done by Dr Isupov, performed in COOT (Emsley *et al*., 2010). The final models are displayed in figures 5.4 – 5.6. The docking was done manually with already solved structures (hPrx2, Hb, and PDI) available. A number of dockings were conducted namely: (a) The Hb tetramer was stationary and decameric hPrx2 was docked to test the possible interaction between the Hb active free cysteine (Cysβ93) can transfer NO to hPrx2 free cysteine (Cys51). (b) The Hb tetramer was stationary and PDI was docked manually to test the possibility of NO transfer between Hb active free Cysβ93 and PDI free Cys61. (c) The hPrx2 decamer was stationary and PDI was docked manually to test the possibility of NO transfer between hPrx2 active free Cys51 and PDI free Cys61.

5.3.2 Co-crystallisation

5.3.2.1 Co-crystallisation of hPrx2 with Hb

Co-crystallization of hPrx2 with Hb was carried out using two approaches. The first approach was done by mixing the two proteins in various molar ratios as described in sections 4.2.3.1 – 4.2.3.6. The elution fractions from the chromatography column confirmed to contain a protein complex (via SDS-PAGE Fig.4.4, 4.6 and 4.8) were collected.

The second approach to crystallisation was when pure recombinant hPrx2 of known concentration and volume was mixed with known concentration and volume of pure Hb, mixed in a 50:50 mixture. The mixture was incubated for 24 h at 4°C. The samples were centrifuged at 15,000 x g at 4°C for 10 min before being used in crystallization trials to remove any precipitated protein.

5.3.2.2 Co-crystallisation of hPrx2 with GSNO and hPrx2-SNO with Hb

Freshly made GSNO of known concentration was incubated for 24 h at 4°C with known volume and concentrations of hPrx2. Then, the samples were centrifuged at 15,000 x g at 4°C for 10 min before being used in crystallisation trials to remove any precipitated protein.

The co-crystallisation of hPrx2-SNO with Hb was done by concentrating gel filtration fractions peak 1 and peak 2 (figure 4.12) and set them for micro batch crystallisation method procedure.

5.3.3 Crystallography

5.3.3.1 Initial crystal trials using microbatch method

Microbatch crystallization trials were set up in a Hampton 96 well plate using an Oryx 6 crystallization robot (Douglas Instruments, UK). A range of different commercial screens were used for the microbatch method. Trials were set up, screening commercial crystallization kit conditions: MDI5-C12-B Cryo 2HT-96 (Molecular Dimension Laboratories) (Appendix 7.4), Sigma 8007, Sigma 70437 (Sigma Aldrich) (Appendix 7.5 and 7.6) and JCSG plus (Molecular Dimensions Laboratories) (Appendix 7.3). The robot mixed 0.5 µl screen with 0.5 µl of protein and covered it with a drop of oil at the top (50:50 mixes of silicon oil and paraffin). Crystallization trays were left to incubate in a still 18°C incubator, checked under a microscope for any signs of crystal formation on a weekly basis. The crystallization conditions that showed successful crystal hits were repeated with optimized conditions.

5.3.3.2 Optimization of crystal trails

Crystallization is often divided into two steps. In the screening step solutions that have previously given crystals are used to find new conditions where a protein crystallizes. Then, in the *optimization* step, the resulting crystals are improved by making small changes to the crystallization conditions identified in the screening step. Different robots and crystallization approaches are used for these two steps. The screening step is often automated, while the optimization step is slow, and it is frequently carried out by hand.

Microseeding has been used routinely for optimization by a minority of crystallizers for many years (Bergfors, 2003). However this is painstaking work because you need to identify conditions where seeding is likely to work. A new approach allows microseeding to pick up entirely new conditions - conditions where crystals would not form in the absence of crystal seeds. Moreover the quality of the crystals found is generally better too. Ireton and Stoddard (2004) introduced a new approach to microseeding, where they dubbed “microseed matrix screening”. Crystal seeds were systematically added to diverse conditions as part of the optimization procedure. These conditions included ingredients that were not present in the original hits.

For example, Ireton and Stoddard identified crystallization conditions for the protein CD that contained sodium acetate in a standard screening experiment. The resulting crystals, however, could not be used to solve the structure of the protein because the mosaicity was too high. However, by seeding into conditions where the sodium acetate in the initial hit has been replaced with calcium acetate, well-diffracting crystals were grown that allowed the structure to be solved. However, D’Arcy *et al*. later changed this approach by the introduction of two practical changes, which together allowed automation: (1) seeding experiments were carried out using ordinary commercial crystallization screens. (2) Microseeding was carried out using solutions containing seeds prepared by crushing crystals using the “seed-bead” kit from Hampton Research.

In our study, conditions that produced crystal optimization were carried out using the X-step optimization software (Douglas Instruments, UK). The X-step software varies the precipitant concentrations, protein concentrations, additive concentrations and pH by +/- 30 %. The microbatch method was once again used on the Oryx 6 crystallization robot

(Douglas Instruments, UK). The droplet was covered with Al's oil (50:50 mixes of silicon oil and paraffin). The plates were stored at 18°C and regularly checked for crystals using a light microscope as described earlier.

5.3.3.3 Preparation of crystals for data collection

Crystals were frozen using a cryo-protectant (0.1 M HEPES Na salt, pH 7.5, 20% PEG 200, 10% PEG 8000, 25% Glycerol). The crystals were removed from the droplet and placed in the cryo-protectant before being frozen directly in liquid nitrogen.

5.3.4 Structure determination

5.3.4.1 Data processing

Data was processed using MOSFLM (CCP4) (Evans, 2006), SCALA (CCP4) (Weiss and Hilgenfeld, 1997) and Xia2 (CCP4) (Winn *et al*., 2011).

5.3.4.2 Phase determination

Phases were determined using the molecular replacement method performed in MOLREP (Vagin and Teplyakov, 2010).

5.4 Results

5.4.1 Co-crystallisation of hPrx2 with Hb

The purified enzyme was concentrated to ~13 mg/ml and microbatch crystallization experiments were carried out using commercial crystal screens (as in methods 5.3.2). Initial results gave crystals produced in 0.2 M sodium sulfate salt, 0.1 M sodium acetate buffer pH 4.5, in precipitants 50% v/v PEG 400 (Fig 5.7). The crystals (Fig. 5.7) were confirmed to be protein crystals but failed to diffract.

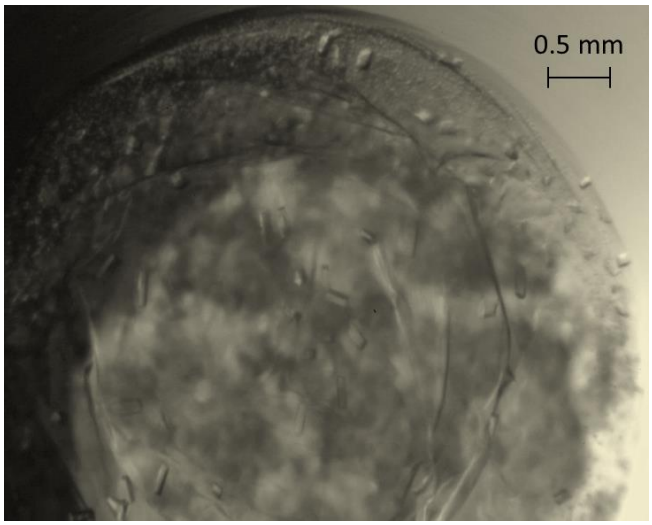

Figure 5.1 Crystals obtained by micro batch method from JCSG plus plate after two weeks incubation at 18°C under the conditions: 0.2 M sodium sulfate salt, 0.1 M sodium acetate buffer pH 4.5 and 50% v/v PEG 400.

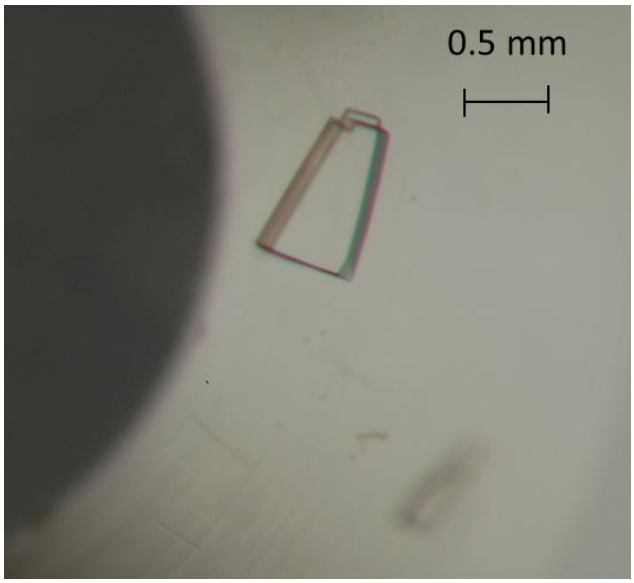

Figure 5.2 Crystal obtained by micro batch method from JCSG plus plate after two weeks incubation at 18°C under the conditions: 0.1 M PCTP buffer, with no salt at pH 9.0 and under precipitant of 25%w/v PEG 1500.

The crystals were tested to be protein crystals and they diffracted at 11 Å, but no data was collected because the resolution was not good (crystals were not good for data collection).

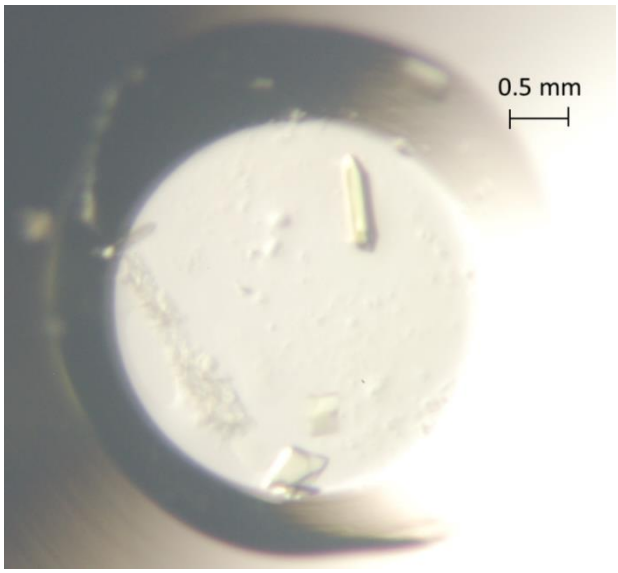

Figure 5.3 Co-crystallization of 50µl hPrx2 protein with 50µl Hb. Crystals obtained by micro batch method from JCSG plus plate after one-week incubation at 18°C under; 0.1 M PCTP buffer, with no salt at pH 7.0 and under precipitant of 25%w/v PEG 1500.

The protein diffracted at 8 Å, though it was not good enough diffraction for analysis.

5.4.2 Co-crystallization of hPrx2 with GSNO, and SNO-hPrx2 with Hb

We were able to co-crystallize hPrx2 with GSNO and SNO-hPrx2 with Hb. The protein was able to crystallize under various conditions as described in figures; 5.10, 5.11 and 5.12.

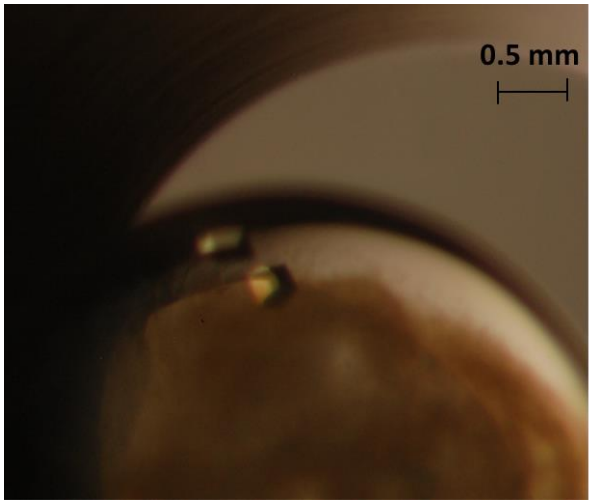

Figure 5.4 Co-crystallization hPrx2 with GSNO. Peak 1 elution fractions of figure 4.12 were concentrated to ~13 mg/ml and setup the protein solution for crystallization. Crystals were obtained by micro batch method from JCSG plus plate after one-week incubation at 18°C under; 0.2 M ammonium formate salt, with no buffer, 20 %w/v PEG 3350 and they diffracted at 7 Å.

The same protein also crystallized under two other conditions. Firstly, under 0.2 M ammonium chloride salt with no buffer, under the precipitant of 20 % w/v PEG3350. Then also under conditions; 0.2 M potassium formate salt with no buffer, under the precipitant of 20 % w/v PEG 3350. These crystals were very small, but still had the same shape as the one in figure 5.10 above.

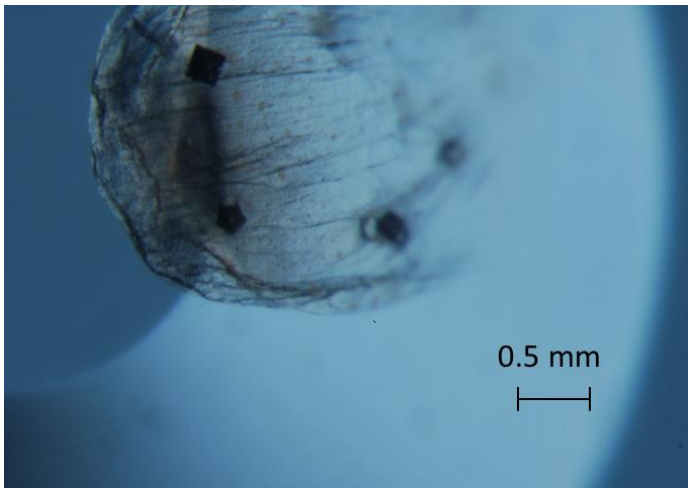

5.5 Co-crystallization hPrx2 with GSNO. Peak 2 elution fractions of figure 4.12 were concentrated to ~13 mg/ml and the protein samples were set up for crystallization as mentioned earlier. Crystals were obtained by micro batch method from JCSG plus plate after one-week incubation at 18°C under; 0.2 M ammonium phosphate monobasic salt, 0.1 M Tris buffer at pH8.5, under 50 % v/v MPD precipitant and the crystal diffracted at 7 Å.

Also there were protein crystals under the conditions: 0.2 M potassium nitrate salt, without buffer and 20 % w/v PEG 3350 precipitant. The crystals were very small and dried-out.

5.4.4 Co-crystallisation of hPrx2-SNO with Hb

Nitrosated samples of hPrx2 purified by S6 column was mixed with the S6 purified Hb (Fig. 4.1) samples in a 50:50 molar ratio. The protein sample was centrifuged before crystallization to remove any precipitated protein as mentioned previously. The protein was able to crystallise after two weeks incubation as described in figure

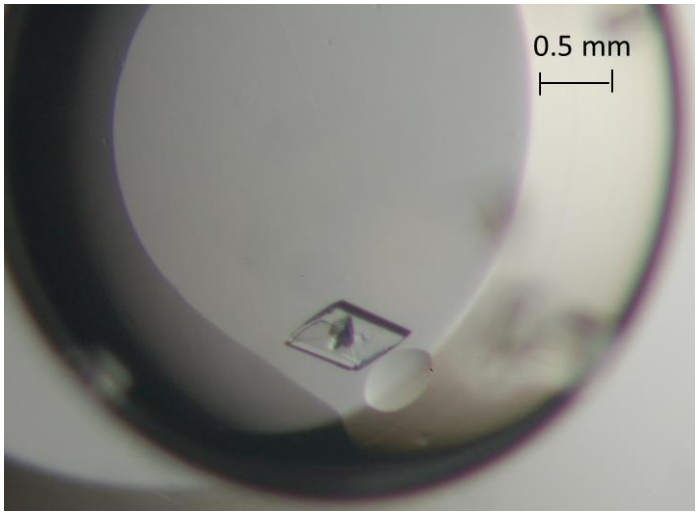

5.6 Co-crystallization hPrx2-SNO with Hb. The protein crystal was obtained by micro batch method from JCSG *plus* plate after two-weeks incubation at 18°C. The crystals appeared in the similar well conditions as observed before when hPrx2 was mixed with GSNO (Fig. 5.11) (0.2 M ammonium phosphate monobasic salt, 0.1 M Tris buffer at pH8.5, 50 % v/v MPD precipitant). The protein crystal diffracted at 6 Å with a better resolution than the one observed before.

The higher resolution dataset was collected at a wavelength of 0.97 Å, 900 frames were collected but date only extended to 6 Å resolution. The crystal was indexed in space group C2 with unit cell parameters a, b, c = 200.745, 138.602, 49.186 Å alpha (α), beta (β), and gamma (γ) = 90.0, 106.809, and 90.0°. These were different from the unit cell parameters of the already published hPrx2 structure. Optimization experiments were carried out around these conditions as described methods section 5.3.3.2, but they failed to yield any crystals.

5.4.5 Discussion

Versatile and robust methods the Differential scanning fluorimetry (DSF), was fundamental for the characterisation and identifying potential protein ligands (Geders *et al*., 2012). It was therefore an attractive method for initial screening of the stability of the synthesised SNO-Hb and Prx2-SNO via different methods of synthesis used. The use of first Boltzmann (the derivative approach) fig 3.4, to interpret the melting patterns of Prx2-SNO (Fig. 3.3) it was easy to identify the critical buffer conditions at which the stability of the protein is lost.

The two methods of modeling the thermal unfolding differ in that the Boltzmann method fits the experimental data to the Boltzmann equation, assuming a regular sigmoidal shape to the unfolding curve. In contrast, the derivative method takes the first derivative of the experimental data at each point (lower panel in Fig 3.3a), and considers the melting temperature to be the point of highest first derivative. The derivative method generally returns a higher melting temperature by around 2 - 3°C. Most proteins will return a more consistent result (*i.e.,* the standard error of the melting temperature for triplicate experiments is lower) for one of the two methods. This is usually intimately related to the precise shape of the protein-unfolding curve, and it is necessary to empirically determine the best method in each case. Where the derivative model is used, it is also important to consider multiple melting events. The data obtained from both Saville assay and chemiluminescence procedure clearly demonstrated evidence for multiple transitions, and in these cases the results were easier to interpret for the multiple melting events demonstrated.

The DSF results demonstrated the effect of pH on the stability of Hb and hPrx2 during the synthesis of SNO-Hb and Prx2-SNO. The effect of pH demonstrated a positive correlation towards the stability and synthesis of RSNO's (SNO-Hb and Prx2-SNO) via the acidified nitrite route. The lower the pH (more acidic environment e.g. pH 4.5 and below), the yields of RSNO were high but protein lost its stability (protein being denatured). At a higher pH, close to neutral pH (i.e. pH 5.6 and above), very few protein thiols were being nitrosated; hence low yields of stable SNO-Hb and Prx2-SNO were being produced. The optimum pH to synthesise a stable SNO-Hb and Prx2-SNO *via* the acidified nitrite method was found to be pH5.6 though with less yield.

During protein purification, using an anion exchange column followed by gel filtration chromatography, native human Prx2 from packed red blood cells was partially purified. Without any reducing treatment, hPrx2 was present in the haemolysate in decameric and dimeric forms, from which the decameric form was isolated. The enzymatic activity of hPrx2 was tried in this present study, but the results were inconclusive. However, it was suitable for our aims to be used as a positive control in protein-protein interaction experiments. Studying the spectral properties of purified the native hPrx2; we found that the preparation displayed a peak at 418 nm, which is indicative of the Soret band. This suggested that the purified hPrx2 was contaminated with haem or haemoglobin. Prx1 is known to interact with haem (Iwahara *et al*., 1995); we considered whether this contamination of Prx2 by haem or Hb might be due to a similar protein-protein interaction reported. Recombinant hPrx2 preparation which was free of haemoglobin was analysed using gel filtration chromatography and Western blotting was used to confirm protein-protein interaction between hPrx2 and Hb.

During Prx2 purification from RBCs several fractions containing Prx2 were found to have traces of Hb. The difficulty to further purify these fractions was perhaps indication of a complex formation between the two proteins. It was hypothesised that hPrx2 takes part in NO metabolism facilitating its transport through the RBC membrane by the formation of SNOPrx2, which has been previously detected in different cell types (Fang *et al*., 2007). We suggested that the formation of a complex with Hb might aid NO transfer. Therefore, in order to study SNOPrx2 interaction with Hb, a cell-free synthesis of the S-nitrosated protein was performed. A number of protocols (Sections 3.1-3.4) were previously validated by our group for the synthesis of S-nitrosoalbumin. The same protocols were used to synthesize the nitrosated proteins (Prx2-SNO and Hb-SNO).

During the modification, no reducing agents were required to pre-treat the protein. The S-nitrosation only occurred on the Cys residues which were already reduced and present as free –SH groups.

A robust, sensitive and reliable technique (gas-phase chemiluminescence) was needed to measure the content of RSNO present in the samples. The positive controls (GSNO and GSH+NO_2^- in HCl 1M) produced a signal resistant to sulfanilamide treatment (+ Sulf) that disappeared if the aliquots were treated with Hg^{2+} (+ Hg^{2+}), typical RSNO-

characteristics. The NO_2^- + NaSH samples produced a signal destroyed by sulfanilamide treatment, characteristic of the presence of NO_2^- alone in the sample. The addition of Hg^{2+} in the presence of sulfanilamide blocked the signal completely. Hg^{2+} converted all the RSNOs in the samples into NO_2^-, which were then blocked by sulfanilamide. The NO_2^-+ NaSH samples gave a chemiluminescent signal which was sulfanilamide-sensitive. It appeared that there was no RSNO in the samples and that the only contribution to the chemiluminescent signal was coming from the unreacted NO_2^-. The RSNO concentration amounted to 2.56 ± 1.27 µM (mean ± S.D., n=3 determination on one Prx2-Hb preparation, with a moles RSNO over moles of protein in a ratio equal to 0.02. Although these data are not conclusive, more Prx2-Hb fractions should be analysed, however, they have provided us with a first indication of a possible SNOPrx2 presence in the RBC, potentially in a complex with Hb which needs to be investigated further.

Problems were encountered with the Saville assay carried out in method section 3.4.3.1. There were high levels of colouration observed in Prx2-SNO samples treated with no Hg^{2+}. In one reaction, the absorbance at 540 nm was 0.16 absorbance units for the Hg^{2+}-treated Prx2-SNO sample, and 0.11 absorbance units for the non-Hg^{2+}-treated samples. Zhang *et al*., (1996) reported similar observations with other nitroso groups such as N-nitrosoalbumin in studies of NO release. However, the same incidence of high levels of colouration was also observed by us with standard solutions of GSNO thus making the NO release by the decomposition of Prx2-SNO by Hg^{2+} explanation to appear unlikely.

In the non-Hg^{2+}-treated samples, the high colouration might be due to the decomposition of RSNO (most commonly caused by metal ions in water) which is independent of the caused by Hg^{2+}. This problem was solved by treating all reagents with Chelex resin (metal chelator), to remove metals that might cause the decomposition of Prx-SNO leading to false readings.

The post-modification studies of hPrx2 using LC-MS/MS system produced a mixture of results. Some of the results were in agreement with the literature available about post-modification of Cys residues in proteins (the formation of cysteine sulfinic acid) (Schroder *et al*., 2000), while as others were inconclusive. The inconsistence of the results might be due the absence of repeated experiments (n=3) to report by the time of this thesis.

The peptide modification can be quantified by comparing the precursor areas of particular peptides of the same peptide but in different environment (treated or un-treated) (Tables 3.5 – 3.6). We were not able to use adopt this route because; some of the identified peptides did not have precursor areas. This was thought to be caused by the overlapping peaks, which made the system not to be able to detect the baseline of the identified peptides to calculate their precursor areas therefore, recorded with no precursor area as a result. A well thought-through system, which can stop the overlapping of peaks, would be a good starting point to monitor post-modification studies of hPrx2 using LC-MS/MS system.

Versatile and robust methods the Differential scanning fluorimetry (DSF), was fundamental for the characterisation and identifying potential protein ligands (Geders *et al*., 2012). It was therefore an attractive method for initial screening of the stability of the synthesised SNO-Hb and Prx2-SNO via different methods of synthesis used. The use of first Boltzmann (the derivative approach) fig 3.4, to interpret the melting patterns of Prx2-SNO (Fig. 3.3) it was easy to identify the critical buffer conditions at which the stability of the protein is lost.

The two methods of modeling the thermal unfolding differ in that the Boltzmann method fits the experimental data to the Boltzmann equation, assuming a regular sigmoidal shape to the unfolding curve. In contrast, the derivative method takes the first derivative of the experimental data at each point (lower panel in Fig 3.3a), and considers the melting temperature to be the point of highest first derivative. The derivative method generally returns a higher melting temperature by around 2 - 3°C. Most proteins will return a more consistent result (*i.e.,* the standard error of the melting temperature for triplicate experiments is lower) for one of the two methods. This is usually intimately related to the precise shape of the protein-unfolding curve, and it is necessary to

empirically determine the best method in each case. Where the derivative model is used, it is also important to consider multiple melting events. The data obtained from both Saville assay, chemiluminescence procedure clearly demonstrated evidence for multiple transitions, and in this case, the results were easier to interpret for the multiple melting events demonstrated.

The DSF results demonstrated the effect of pH on the stability of Hb and hPrx2 during the synthesis of SNO-Hb and Prx2-SNO. The effect of pH demonstrated a positive correlation towards the stability and synthesis of RSNO's (SNO-Hb and Prx2-SNO) via the acidified nitrite route. The lower the pH (more acidic environment e.g. pH 4.5 and below), the yields of RSNO were high but protein lost its stability (protein being denatured). At a higher pH, close to neutral pH (i.e. pH 5.6 and above), very few protein thiols were being nitrosated; hence low yields of stable SNO-Hb and Prx2-SNO were being produced. The optimum pH to synthesise a stable SNO-Hb and Prx2-SNO *via* the acidified nitrite method was found to be pH5.6 though with less yield.

During protein purification, using an anion exchange column followed by gel filtration chromatography, native human Prx2 from packed red blood cells was partially purified. Without any reducing treatment, hPrx2 was present in the haemolysate in decameric and dimeric forms, from which the decameric form was isolated. The enzymatic activity of hPrx2 was tried in this present study, but the results were inconclusive. However, it was suitable for our aims to be used as a positive control in protein-protein interaction experiments. Studying the spectral properties of purified the native hPrx2; we found that the preparation displayed a peak at 418 nm, which is indicative of the Soret band. This suggested that the purified hPrx2 was contaminated with haem or haemoglobin. Prx1 is known to interact with haem (Iwahara *et al*., 1995); we considered whether this contamination of Prx2 by haem or Hb might be due to a similar protein-protein interaction reported. Recombinant hPrx2 preparation which was free of haemoglobin was analysed using gel filtration chromatography and Western blotting was used to confirm protein-protein interaction between hPrx2 and Hb.

During Prx2 purification from RBCs several fractions containing Prx2 were found to have traces of Hb. The difficulty to further purify these fractions was perhaps indication of a complex formation between the two proteins. It was hypothesised that hPrx2 takes

part in NO metabolism facilitating its transport through the RBC membrane by the formation of SNOPrx2, which has been previously detected in different cell types (Fang *et al*., 2007). We suggested that the formation of a complex with Hb might aid NO transfer. Therefore, in order to study SNOPrx2 interaction with Hb, a cell-free synthesis of the S-nitrosated protein was performed. A number of protocols (Sections 3.1-3.4) were previously validated by our group for the synthesis of S-nitrosoalbumin. The same protocols were used to synthesize the nitrosated proteins (Prx2-SNO and Hb-SNO).

During the modification, no reducing agents were required to pre-treat the protein. The S-nitrosation only occurred on the Cys residues which were already reduced and present as free –SH groups.

A robust, sensitive and reliable technique (gas-phase chemiluminescence) was needed to measure the content of RSNO present in the samples. The positive controls (GSNO and GSH+NO_2^- in HCl 1M) produced a signal resistant to sulfanilamide treatment (+ Sulf) that disappeared if the aliquots were treated with Hg^{2+} (+ Hg^{2+}), typical RSNO-characteristics. The NO_2^- + NaSH samples produced a signal destroyed by sulfanilamide treatment, characteristic of the presence of NO_2^- alone in the sample. The addition of Hg^{2+} in the presence of sulfanilamide blocked the signal completely. Hg^{2+} converted all the RSNOs in the samples into NO_2^-, which were then blocked by sulfanilamide. The NO_2^-+ NaSH samples gave a chemiluminescent signal which was sulfanilamide-sensitive. It appeared that there was no RSNO in the samples and that the only contribution to the chemiluminescent signal was coming from the unreacted NO_2^-. The RSNO concentration amounted to 2.56 ± 1.27 µM (mean ± S.D., n=3 determination on one Prx2-Hb preparation, with a moles RSNO over moles of protein in a ratio equal to 0.02. Although these data are not conclusive, more Prx2-Hb fractions should be analysed, however, they have provided us with a first indication of a possible SNOPrx2 presence in the RBC, potentially in a complex with Hb which needs to be investigated further.

Problems were encountered with the Saville assay carried out in method section 3.4.3.1. There were high levels of colouration observed in Prx2-SNO samples treated with no Hg^{2+}. In one reaction, the absorbance at 540 nm was 0.16 absorbance units for the Hg^{2+}-treated Prx2-SNO sample, and 0.11 absorbance units for the non-Hg^{2+}-treated

samples. Zhang *et al*., (1996) reported similar observations with other nitroso groups such as N-nitrosoalbumin in studies of NO release. However, the same incidence of high levels of colouration was also observed by us with standard solutions of GSNO thus making the NO release by the decomposition of Prx2-SNO by Hg^{2+} explanation to appear unlikely.

In the non-Hg^{2+}-treated samples, the high colouration might be due to the decomposition of RSNO (most commonly caused by metal ions in water) which is independent of the caused by Hg^{2+}. This problem was solved by treating all reagents with Chelex resin (metal chelator), to remove metals that might cause the decomposition of Prx-SNO leading to false readings.

In nature, proteins do not work in isolation. Most of the proteins act as part of complexes, with small molecules or with other biological molecules. Proteins and enzymes are organised within the cell to form clusters in a dynamic and versatile ways Using nickel column chromatography followed by gel filtration chromatography, we purified recombinant hPrx2 free of haemoglobin. Using an anion exchange column followed by gel filtration chromatography, we purified native human Prx2 from RBCs. The fact that purified Prx2 from RBCs contained haemoglobin or haem, whilst purified recombinant hPrx2 when mixed with haemoglobin co-eluted together where both peaks in (Fig; 4.3, 4.5 4.7 and 4.9) contained Prx2 and Hb this was an indication that these two protein molecules might be interacting.

Therefore, this potential interaction was analysed by two means: gel filtration chromatography and SDS-PAGE followed by Western blotting. By mixing Prx2 and Hb in the ratios (10:1, 10:2, 10:4, 10:6 and 10:8) and loading the samples onto a gel filtration column - after 0 or 24 hours incubation at 4^{o}C - followed by elution in a neutral buffer, we were able to detect a small shift in peaks compared with the chromatograms of Prx2 and haemoglobin alone. When used SDS- PAGE to study protein-protein interaction, two bands found to present whereby; one corresponds to hPrx2, and the protein band, which corresponds to Hb. Also, on Western blots carried out in conjunction with native PAGE, extra bands were detected depending on the incubation time of the mixture. Clear band shifts were visible on the blot of all mixture ratios but

more with 1:1 and 1:4 mixtures of Prx2 and haemoglobin. When incubating for 72 hrs, a band shift was not detectable on the blot of all ratio mixtures of Prx2 and haemoglobin.

The complex formation binding stoichiometry results are based upon the elution volumes from a calibrated gel filtration column. Size-exclusion chromatography separates a protein based on its Stokes radius (Irvine, 2001), which is based on the molecular weight and shape. Prx has been seen to elute at the volume expected for the mass of the decameric state of the protein despite its toroidal shape. The binding of Hb to the decameric hPrx2 is assumed to not affect the overall shape on complex formation.

Therefore, it appears that the incubation time had a crucial influence on the interaction between Prx2 and haemoglobin. Incubation times that were either too short (0 min) or too long (72 hrs) did not lead to complex formation. An incubation time of approximately 24 hr at 4^{o}C seemed optimal - this was employed in all Prx2-Hb interaction experiments we tried.

Although these preliminary data support the hypothesis that Prx2 and haemoglobin are able to interact and form complexes, our experiments suggest that this complex formation is very sensitive to experimental conditions and more work will need to be done to establish the nature and the role of this interaction.

Previous work on the crystallization and complex formation of hPrx2 was done with human oxidoreductase sulfiredoxin hSrx. No work has been done on the complex formation between hPrx2 with Hb, and SNO-hPrx2 with Hb. The complex formation results were based upon the elution volumes from a calibrated Superose 6 gel filtration column Size-exclusion chromatography (Fig. 3.7) separates a protein based on iits Stokes radius (Irvine, 2001), which is based on the molecular weight and shape. Prx2 has been seen to elute at the volume expected for the mass of the decameric state of the protein despite its toroidal shape. The binding of NO or Hb to hPrx2 assumed did not affect the overall shape on complex formation.

The findings reported are novel. The crystal structure of the decameric form of hPrx2 from RBCs was previously studied, and structure determined to 1.7 Å resolution at the University of Exeter, PDB: 1QMV (Schroder *et al*., 2000). The toroid structure of hPrx2 is formed from five dimer unities (Fig. 1.12). The active site of hPrx2 has two active

sites per homodimer and that the CysP in all of the active sites of the decamer is present in the sulfinic acid form (Schroder *et al*., 2000). As part of the mechanism of this enzyme, the peroxidatic cysteine (Cys51) forms an intermolecular disulfide bond with the resolving cysteine (Cys172) from another monomer (Wood *et al*., 2003b). The peroxidatic cysteine (Cys51) is highly sensitive and gets oxidised very easily by oxidising agents such as oxygen, H_2O_2, sulphur dioxide (SO_2), HNO_3. The interchanging oxidation state of the peroxidatic cysteine, caused to obtain a mixture of oligomeric state of the hPrx2 enzyme; decameric and dimeric form (Fig. 2.4) (wood *et al*., 2002b). It is thought that, the formation of the disulfide led to the breakdown of the dimer-dimer interface as shown by Schroder *et al*., ending up producing five homodimers (Schroder *et al*., 2000). Due to sensitivity of the cysteine residues in the active site of hPrx2, a reasonable portion of protein was found to be oxidised (Fig. 2.4). However, we do not know the exact amount of the protein that was oxidised, we can only just estimate that 25% of the hPrx2 cysteines were oxidised.

Conditions in which the protein was able to get 'super-saturation' (protein being brought out of solutions) by the precipitants of the crystallization conditions were established, and the protein was stable in those conditions. The optimisation attempt failed to yield crystals; this might be because of some other uncontrollable variables such as room temperature and humidity, which might be different from the prior crystal preparation dishes. More optimisation attempts around the crystallisation conditions where; hPrx2 was co-crystallised with Hb, and hPrx2 co-crystallised with GSNO are needed to be carried out. Failure to obtain better crystals for data collection through optimisation method, crystal soaking is an alternative approach to be considered.

Chapter 6:

Summary and future work

The work reported in this thesis has described the investigation into the native and recombinant human erythrocyte Prx2 characterisation, and interaction the counterpart proteins and other micro-molecules. The thesis objectives with respect to the isolation of pure Prx2 from RBCs, to complete the interaction studies of native hPrx2 and Hb, this was not achieved due the problems faced as discussed in section 2.6. Purification of recombinant hPrx2 was successfully achieved using two chromatographic steps, the nickel affinity chromatography and the gel filtration chromatography. Attempts to investigate the interactions between NO, Hb and hPrx2, (to determine whether there is a transfer which involves transnitrosation) where nitrosated haemoglobin (SNO-Hb) and hPrx2 transfer NO as described in equation 1.31 was done using recombinant hPrx2 samples. In addition, dimer hPrx2 / SNO-hPrx2 have been extracted directly from recombinant hPrx2. Purified proteins were subjected to characterisation as follows:

6.1 Structure characterisation

Studies on Prx2 have been focused on human erythrocyte native Prx2 so far (Schroder *et al.,* 2000), where as in this project both native Prx2 and erythrocyte recombinant Prx2 were characterised and compared to each other. The secondary and tertiary structures were studied by X-ray crystallography; the quaternary structure was investigated by gel filtration chromatography, native gel electrophoresis and dynamic light scattering.

The characterisation of secondary and tertiary structures by use of X-ray crystallography was comparatively successful. The crystallisation of hPrx2 in different space group and cell parameters; a, b, c and α, β and γ was achieved from those reported in (Schroder *et al.,* 2000). However, we don't know if this will affect the conformation similarity despite difference in space group spacing and cell parameters. Although we know this was a different protein used (His-tag protein), the results were inconclusive we do not know whether we crystallised hPrx2-His-tag or hPrx2 complex.

Additionally, the presence of the His-tag we do not know if it affected the oligomeric state of the recombinant hPrx2 we can only speculate.

The quaternary structure of hPrx2 and the post-modified protein SNO-hPrx2 were characterised by use of gel filtration chromatography. Elution characterisation of recombinant hPrx2 showed the same elution profile with native hPrx2 predominantly decameric form, whereas modified SNO-hPrx2 was eluted in predominantly in dimeric rather than decameric form. The addition of GSNO to the growths medium during the over-expression of hPrx2 in *E.coli* denoted that this factor affects the oligomeric state of hPrx2 protein as high lightened in figure 3.5 and figure 3.8 in chapter 3. The crystallisation trials for SNO-hPrx2 were successful, but the protein crystals were too small for data collection.

Although one might suggest that, the contaminations of Hb and hPrx2 experienced was caused by co-elution of the two other than protein-protein interactions. However, in this project, the SDS-PAGE and the gel filtration chromatography analysis showed that the two proteins were interacting.

SDS-PAGE analysis of native hPrx2 and recombinant hPrx2 using non reducing loading buffer showed that disulfide states were found partially in decameric eluted fractions (Fig 2.4). However, we are not sure if similar results would be present in the post-modified hPrx2 (hPrx2-SNO) samples.

6.2 Characterisation of protein stability

The enzyme (hPrx2) has been cloned and recombinant protein over-expressed in *E. coli* as described in section 2.4.2, while the native protein was isolated from RBCs as described in section 2.4.1. The comparison of different hPrx2 and Hb variants showed that SNO-hPrx2 samples especially formed by addition of GSNO to the protein samples were the most stable variants in structure. It maintained a single decamer form for longer storage times than the other variants and showed less aggregation at -20 ˚C.

Both native and recombinant hPrx2 showed a good solubility resulting in no aggregation during the concentration. The storage of these proteins for two weeks at 4 ˚C showed no degradation detectable on SDS-PAGE analysis.

The expansion of work relating to NO and protein *S*-nitrosation over recent years has led to some very intriguing and promising areas of research. Although the vast majority of the studies explored functional aspects of *S*-nitrosation on specific proteins, the development of mass spectrometry-based approaches (Dennehy *et al*., 2006; Leonard *et al*., 2009; Held and Gibson 2012) has enabled studies that hold excellent promise in providing proteome-wide information for the structural and functional biology of *S*-nitrosation. Acquisition of endogenous *S*-nitrosocysteine Prx2 proteomes will also facilitate investigations on the issues that still remain uncertain, such as the biochemical mechanisms of *S*-nitrosocysteine (SNO-hPrx2) formation, the mechanisms of denitrosation, the effects on protein stability, the structural elements that may govern selective *S*-nitrosation, and the molecular mechanisms by which protein *S*-nitrosation regulates protein function and location.

6.3 Characterisation of protein-protein interaction

Attempts were made to test the complex formation between hPrx2 and Hb and other post-modified hPrx2 (SNO-Prx2). Owing the importance of purity for protein-protein interaction and complex formation, recombinant hPrx2 protein samples were used. Where by, all impurities such as nucleic acids were removed and the absorption spectra for the proteins were obtain to determine the A_{260} /A_{280} ratio. The relative protein confirmations were monitored using UV-vis spectrometry and their isoelectric points were determined for both native and recombinant samples.

Different biological and biochemical techniques such as; denaturing and native gel electrophoresis, were used to investigate complex formation. During this project, different methods and conditions were used to find any interaction or complex formation either transient or permanent interaction between hPrx2 and Hb. The experimental trials were successful; it was impossible to get pure hPrx2 from RBCs as highlighted in figure 2.6, Hb tetramer (~ 56 kDa), co-eluted with decameric hPrx2 (~ 250 kDa). From SDS-PAGE for the gel filtration chromatography for native hPrx2, both bands; the hPrx2 band and the β and α chines of Hb were present (Fig. 2.7).

6.4 Future work

6.4.1 Synthesis and stability of SNO-Hb and SNO-hPrx2

One of the future works proposed is: after the nitrosation hPrx2 protein thiols to use a biotin-labeling reaction to measure the amount of protein thiols being modified in the process. Proteins can be biotinylated chemically or enzymatically. Chemical biotinylation utilises various conjugation chemistries to yield nonspecific biotinylation of amines, carboxylates, sulfhydryls and carbohydrates (e.g., NHS-coupling gives biotinylation of any primary amines in the protein). When a biotin-containing sample is added, the biotin binds strongly to avidin and displaces the weakly bound 2-(4-hydroxyozobenzene) benzoic acid assay (HABA) resulting in a decrease in absorbance relative to the amount of HABA displaced

6.4.2 Protein-protein interactions between: hPrx2, NO, Hb and SNO-hPrx2

Our preliminary data appeared to support the hypothesis that Prx2 interacts with haemoglobin. However, the results were inconclusive further experiments will be necessary to confirm the hypothesis and to provide more information on the existence of a Prx2-Hb interaction.

The conditions of incubation of hPrx2 and Hb appeared to influence the experimental outcome. Therefore, the mixture of hPrx2 and Hb should be studied using different incubation times, molar ratios and temperature. Crucially, our experiments were performed at 4^{o}C, but this low temperature may have influenced the slow interaction of the two proteins to for form a complex as expected. It would be more relevant to perform these experiments at a human body temperature (37^{o}C).

Moreover, we did not chemically reduce hPrx2 and Hb before the reactions. However, this might also have a crucial influence on the interaction. Therefore, these molecules should be reduced with either DTT and then used in experiments after dialysis or nitrosate hPrx2 in RBCs before opening the cells. It may also be of interest to observe the effect on the interaction of providing reducing equivalents for hPrx2 in the same reaction mixture.

Also more sensitive techniques such as surface Plasmon resonance (SPR), to test for the protein-protein interactions would be ideal technique to explorer. SPR spectroscopy is an optical technique that can be used without radio or other labelling of the components of a complex provided that one of the partners can be immobilised to a solid support. The SPR effect is based on changes in the refractive index of solutions nearby the immobilised surface. The technique is extremely sensitive (Stockley and Persson, 2009). The SPR technique will provide an opportunity to measure bimolecular interactions in real time with a high degree of sensitivity. SPR biosensors have been widely used in a variety of assays, including specificity, concentration measurement, kinetics, and affinity thermodynamic parameters (Jason-Moller *et al*., 2006). SPR has been also applied in different fields. Examples include food analysis, proteomics, immunogenicity and drug discovery (Torreri *et al*., 2005).

6.4.3 Crystallization, X-ray diffraction and complex formation studies

The crystallization work described can be taken forward in several ways using further crystallization trials, X-ray diffraction studies and more molecular modelling experiments. Also the complex formation (protein-protein interactions) of hPrx2 with Hb and SNO-hPrx2 with Hb can be improved by changing the soaking procedures. Soaking hPrx2 crystals for a longer period either in pure Hb protein solution or in SNO-hPrx2 purified and concentrated protein solutions. In this study, due to the low resolution of the X-ray data collected and the lack of full occupancy of the active site of hPrx2, it was not possible to have X-ray crystals of hPrx2-Hb and [SNO-hPrx2] Hb. However, by knowing the exact location of the active sites of the enzyme and the binding site pockets from the modeling analysis, we can try and experiment the effects of alkalinity at the binding pockets.

One crystallization method with various conditions was tried to obtain the protein crystals reported in this chapter in a complex form; an attempt to crystalise a native form crystals of hPrx2-Hb is recommended. Further crystallization trials could be continued using different crystallisation methods such as hanging drop and microseeding (crystal seeding) method, also to try more other crystallization conditions to obtain crystals that diffract at higher resolutions. This could potentially give further insights into the

speculated interaction between hPrx2 and Hb, to explain the transnitrosation mechanism between hPrx2 and Hb.

Therefore, the work presented in this thesis may be developed further in a number of directions. So far, experimental methods could not achieve the desired complex formation between hPrx2 variants and Hb, and other post-modified proteins under the conditions studied to observe transient or permanent interactions. It is suggested to optimise the conditions by subjecting the proteins to mutation or truncation or using chemical cross linkers to stabilise the interactions for possible crystal formation. Some of the above mentioned techniques have been used before for Prx1 complex formation with Srx by Johnson and colleagues. Another direction which would be worthy of further study is prediction of hPrx2 – Hb (protein –protein interactions) is to expand on the computational methods tried. It is possible to investigate interaction of hPrx2 with relevant counterpart proteins by protein-protein docking. Trying some several other computer programs available for this purpose like PatchDock, 3D-Dock Suite, and ZDOCK.

6.4.4 Structural modelling analysis

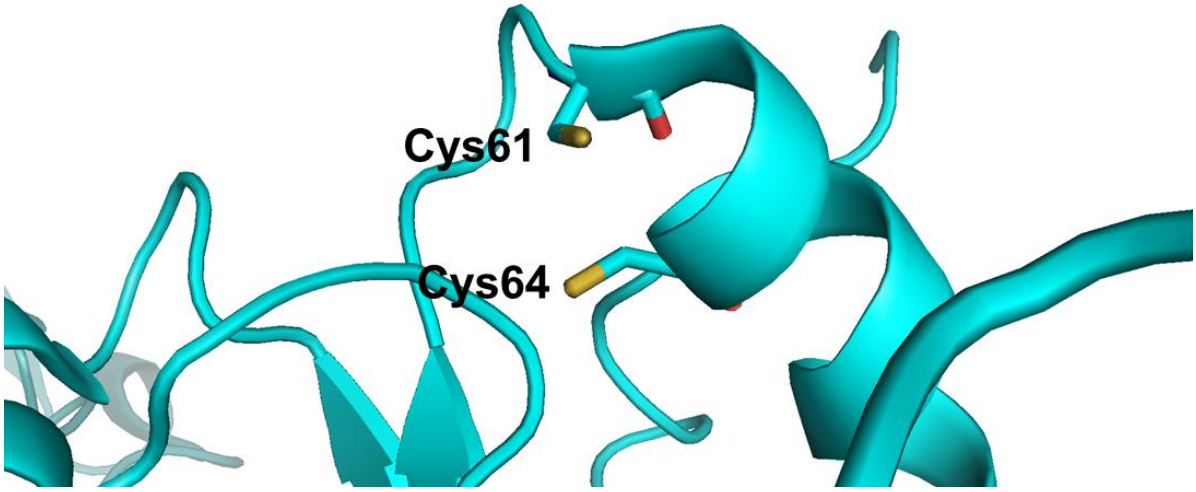

Figure 6.1 Cartoon representative of the putative site of S-nitrosation in PDI. The cysteines found in the active site are marked Cys61 and Cys64 (figure created using PlyMol Schrödinger, Inc. and model building was done in COOT (Emsley *et al*., 2010) by Dr Isupov.

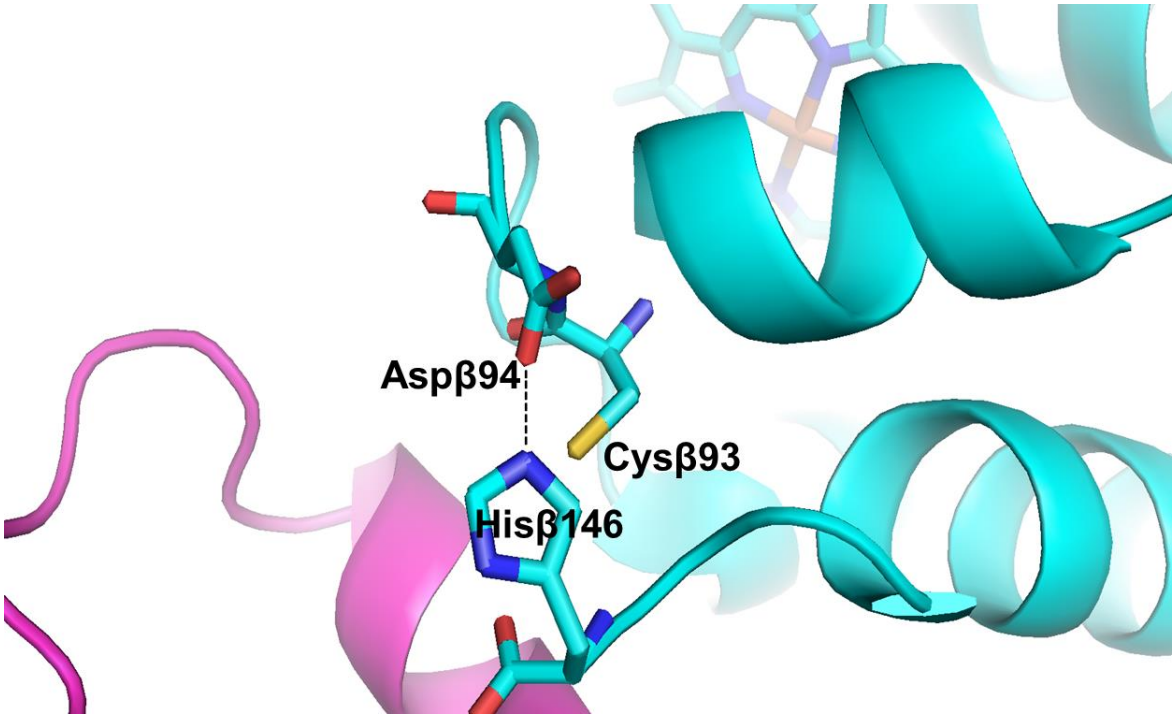

Figure 6.2 Cartoon representative of the putative site of S-nitrosation in Hb. On the protein surface, Hisβ146 makes a salt bridge with Hβisβ146 thus shielding Cysβ93 from solvent. The picture is coloured according to secondary structure, showing β-sheets (pink), α-helices (blue) and loop region in blue. The figure was created using PlyMol Schrödinger, Inc. and modelling was done by Dr Isupov using, coot software (Emsley *et al.*, 2010).

The active site cysteine (Cysβ93) is shielded from access by large molecules, but molecules like N_2O_3 (which have ability to break the salt bridge) can still access the active Cysβ93 to form Cys-NO.

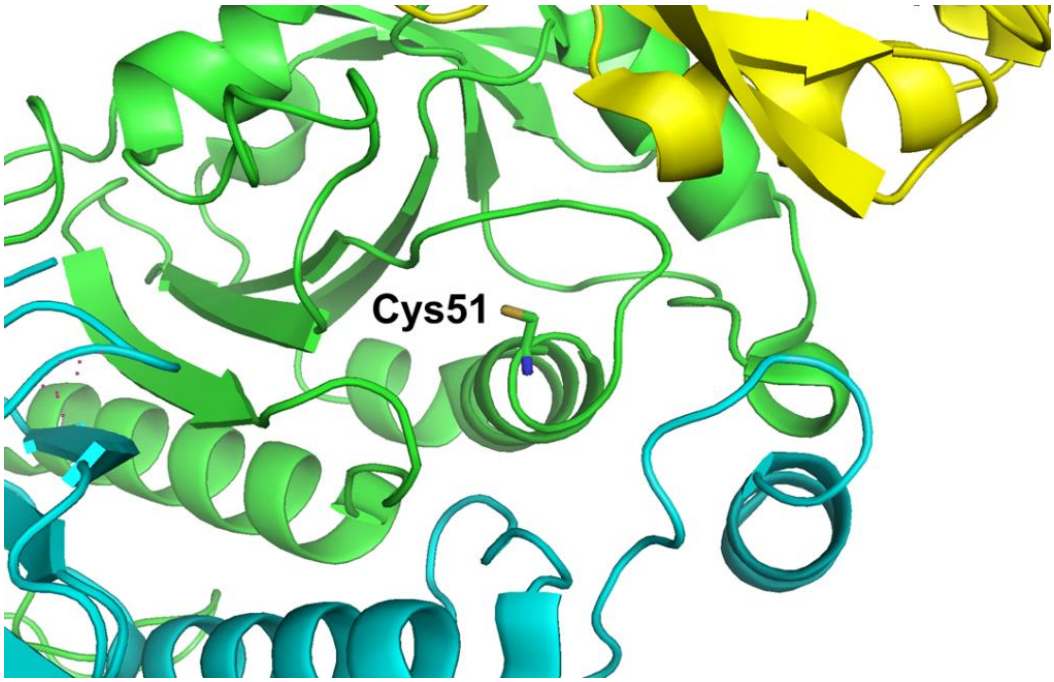

Figure 6.3 Cartoon representative of the putative site of S-nitrosation in hPrx2. The picture is coloured according to secondary structure, showing β-sheets (yellow), α-helices (green) and loop region in blue. Cys51 is barred in a hole which marks it hard to be accessed by attacking proteins and residues. The figure was created using PlyMol Schrödinger, Inc. and modelling was done by Dr Isupov using, coot software (Emsley *et al*., 2010).

In oxidised form, the sulfinic acid group of the active-site (Cys51) makes a salt bridge with Arg 127 helping to stabilize the decameric structure (Wood *et al*., 2003a).

As mentioned in section 5.2, the protein or residue which is likely to carry the bound NO in RBCs should be in abundance, Hb Cysβ93 appears to be the best candidate for the long term NO accumulation and transport. Both hPrx2 and PDI can be intermediate carriers, but not long term. The second cysteine (resolving Cys172 in Prx2) is likely to attack the Cys-NO with the release of NO and disulphide formation.

When Hisβ146 of Hb makes a salt bridge with Aspβ94, it shields Cysβ93 in the Hb active site but NO can still attack this Cys to form Cys-NO. Any further protein or smaller molecule NO carriers that might attack the active cysteine in the active site (Cysβ93) can do so when the salt bridge is broken (higher pH) or switched away by interacting with the attacking protein or smaller molecules.

Two structures of human Prx2 were looked at in disulfide form and in overoxidised form (pdb 1qmv). Although Cys51 has nearby Arg127 which could get involved in breaking the salt bridge in Hb, this arginine does not appear to move with Cys51. Movement of Cys51 between the two positions does not appear to expose it enough for the direct attack onto Hb Cysβ93-NO. No charged residues are positioned along its trajectory, which could facilitate the displacement of the shielding salt bridge of Hb. Therefore, for Prx2Cys51 to be involved in NO transport, the latter should be diffused to the Prx active site or brought by an intermediate carrier such as glutathione.

When protein disulphide isomerase (PDI) was looked at using the yeast analogue structure (pdb 2b5e), had several thioredoxin-like domains; two of which retain thioredoxin-like pair of cysteines. These have exposed cysteine residue poised for attack onto modified cysteine-NO (Cys-NO).

In conclusion, provided that diffusion or glutathione carry NO within RBC both PDI and Prx2 can be medium-term NO carriers. However, if a direct attack onto Cysβ93-NOHb by protein Cys residue is required for the NO transfer PDI is a significantly more likely candidate as it has exposed cysteine residue and a nearby charged residue to break salt bridge shield.

Chapter 7:

Appendix

7.1 Appendix 1: molecular protein ladder used

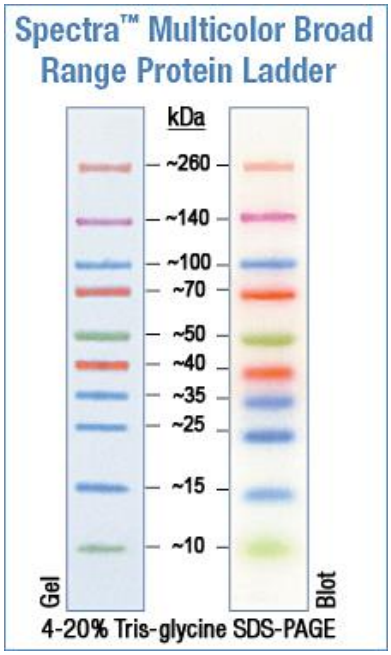

7.2 Appendix 2: Analysis of bands from SDS-PAGE shown in Fig 2.2, the report shows all the significant identifications ($p<0.05$) resulting from a Mascot search of the MALDI MS data against the NCBI Human database.

Search Type	Combined MS/MS		
Search Result	MALDI_NCBI_Hsapiens_Mascot_2014-09-26 15:57:24		
Protein 1:	catalase [Homo sapiens]		
Accession:	gi|4557014	**Score:**	521.48
Database:	NCBInr	**MW [kDa]:**	59.70
Seq. Coverage [%]:	21.40 %	**pI:**	6.90
		No. of Peptides:	9
Modification(s):	Carbamidomethyl, Oxidation		

```
          10         20         30         40         50         60         70         80         90        100        110        120
MADSRDPASD QMQHWKEQRA AQKADVLTTG AGNPVGDKLN VITVGPRGPL LVQDVVFTDE MAHFDRERIP ERVVHAKGAG AFGYFEVTHD ITKYSKAKVF EHIGKKTPIA VRFSTVAGES

         130        140        150        160        170        180        190        200        210        220        230        240
GSADTVRDPR GFAVKFYTED GNWDLVGNNT PIFFIRDPIL FPSFIHSQKR NPQTHLKDPD MVWDFWSLRP ESLHQVSFLF SDRGIPDGHR HMNGYGSHTF KLVNANGEAV YCKFHYKTDQ

         250        260        270        280        290        300        310        320        330        340        350        360
GIKNLSVEDA ARLSQEDPDY GIRDLFNAIA TGKYPSWTFY IQVMTFNQAE TFPFNPFDLT KVWPHKDYPL IPVGKLVLNR NPVNYFAEVE QIAFDPSNMP PGIEASPDKM LQGRLFAYPD

         370        380        390        400        410        420        430        440        450        460        470        480
THRHRLGPNY LHIPVNCPYR ARVANYQRDG PMCMQDNQGG APNYYPNSFG APEQQPSALE HSIQYSGEVR RFNTANDDNV TQVRAFYVNV LNEEQRKRLC ENIAGHLKDA QIFIQKKAVK

         490        500        510        520        530
NFTEVHPDYG SHIQALLDKY NAEKPKNAIH TFVQSGSHLA AREKANL
```

Cmpd.	No. of Cmpds.	m/z meas.	Δ m/z [ppm]	z	Rt [min]	Score	P	Range	Sequence	Modification
	1	2189.0790	4.30	1		76.6	0	48-66	R.GPLLVQDVVFTDEMAHFDR.E	
	1	2205.0825	8.19	1		62.3	0	48-66	R.GPLLVQDVVFTDEMAHFDR.E	Oxidation: 14
	1	2518.2119	3.23	1		115.2	0	136-156	K.FYTEDGNWDLVGNNTPIFFIR.D	
	1	1528.8013	-9.49	1		79.6	0	157-169	R.DPILFPSFIHSQK.R	
	1	1292.6068	-3.77	1		45.7	0	253-263	R.LSQEDPDYGIR.D	
	1	1119.5452	-11.61	1		34.2	0	355-363	R.LFAYPDTHR.H	
	1	1812.9021	-10.62	1		64.5	0	366-380	R.LGPNYLHIPVNCPYR.A	Carbamidomethyl: 12
	1	1493.6968	-0.71	1		34.4	0	432-444	R.FNTANDDNVTQVR.A	
	1	1481.7172	-14.23	1		73.3	0	445-456	R.AFYVNVLNEEQR.K	

Protein 2:	aldehyde dehydrogenase 1 [Homo sapiens]		
Accession:	gi|2183299	**Score:**	232.61
Database:	NCBInr	**MW [kDa]:**	54.80
Seq. Coverage [%]:	13.60 %	**pI:**	6.30
		No. of Peptides:	5

```
10        20        30        40        50        60        70        80        90        100       110       120
MSSSGTPDLP VLLTDLKIQY TKIFINNEWH DSVSGKKFPV FNPATEEELC QVEEGDKEDV DKAVKAARQA FQIGSPWRTM DASERGRLLY KLADLIERDR LLLATMESMN GGKLYSNAYL
130       140       150       160       170       180       190       200       210       220       230       240
SDLAGCIKTL RYCAGWADKI QGRTIPIDGN FFTYTRHEPI GVCGQIIPWN FPLVMLIWKI GPALSCGNTV VVKPAEQTPL TALHVASLIK EAGFPPGVVN IVPGYGPTAG AAISSHMDID
250       260       270       280       290       300       310       320       330       340       350       360
KVAFTGSTEV GKLIKEAAGK SNLKRVTLEL GGKSPCIVLA DADLDNAVEF AHHGVFYHQG QCCIAASRIF VEESIYDEFV RRSVERAKKY ILGNPLTPGV TQGPQIDKEQ YDKILDLIES
370       380       390       400       410       420       430       440       450       460       470       480
GKKEGAKLEC GGGPWGNKGY FVQPTVFSNV TDEMRIAKEE IFGPVQQIMK FKSLDDVIKR ANNTFYGLSA GVFTKDIDKA ITISSALQAG TVWVNCYGVV SAQCPFGGFK MSGNGRELGE
490       500       510
YGFHEYTEVK TVTVKISQKN S
```

Cmpd.	No. of Cmpds.	m/z meas.	Δ m/z [ppm]	z	Rt [min]	Score	P	Range	Sequence	Modification
	1	1189.6128	1.26	1		18.9	0	69-78	R.QAFQIGSPWR.T	
	1	1544.7519	-14.52	1		58.6	0	144-156	R.TIPIDGNFFTYTR.H	
	1	1645.7859	-15.17	1		54.7	0	309-321	R.IFVEESIYDEFVR.R	
	1	1989.9405	1.52	1		57.4	0	379-395	K.GYFVQPTVFSNVTDEMR.I	
	1	1589.7667	-18.31	1		45.0	0	421-435	R.ANNTFYGLSAGVFTK.D	

Protein 3:	thiol-specific antioxidant protein [Homo sapiens]		
Accession:	gi|438069	**Score:**	41.13
Database:	NCBInr	**MW [kDa]:**	21.80
Seq. Coverage [%]:	8.60 %	**pI:**	6.83

```
10        20        30        40        50        60        70        80        90        100       110       120
MASGNARIGK PAPDFKATAV VDGAFKEVKL SDYKGKYVVL FFYPLDFTFV CPTEIIAFTT VKRTSAKLGC EVLGVSVDSQ FTHLAWINTP RKEGGLGPLN IPLLADVTRR LSEDYGVLKN
130       140       150       160       170       180       190       200
DEGIAYRGLF IIDGKGVLRQ ITVNDLPVGR SVDEALRLVQ AFQYTDEHGE VCPAAWKPGR DTIKPNVDDS KEYFSKHN
```

Cmpd.	No. of Cmpds.	m/z meas.	Δ m/z [ppm]	z	Rt [min]	Score	P	Range	Sequence	Modification
	1	1734.9420	-18.91	1		41.1	0	93-109	K.EGGLGPLNIPLLADVTR.R	

MS results for SDS-PAGE (gel band 2

Protein 2:	Chain A, Structure Of Haemoglobin In The Deoxy Quaternary State With Ligand Bound At The Alpha Haems		
Accession:	gi|229751	**Score:**	208.50
Database:	NCBInr	**MW [kDa]:**	15.10

```
10        20        30        40        50        60        70        80        90        100       110       120
VLSPADKTNV KAAWGKVGAH AGEYGAEALE RMFLSFPTTK TYFPHFDLSH GSAQVKGHGK KVADALTNAV AHVDDMPNAL SALSDLHAHK LRVDPVNFKL LSHCLLVTLA AHLPAEFTPA
130       140       150
VHASLDKFLA SVSTVLTSKY R
```

Cmpd.	No. of Cmpds.	m/z meas.	Δ m/z [ppm]	z	Rt [min]	Score	P	Range	Sequence	Modification
	1	1529.7319	-1.60	1		114.2	0	17-31	K.VGAHAGEYGAEALER.M	
	1	1833.8868	-2.78	1		94.3	0	41-56	K.TYFPHFDLSHGSAQVK.G	

MS results for SDS-PAGE (gel band 2)

Search Type	Combined MS/MS		
Search Result	MALDI_NCBI_Hsapiens_Mascot_2014-09-26 15:57:24		
Protein 1:	thiol-specific antioxidant protein [Homo sapiens]		
Accession:	gi|438069	**Score:**	50.59
Database:	NCBInr	**MW [kDa]:**	21.80
Seq. Coverage [%]:	8.60 %	**pI:**	6.83
		No. of Peptides:	1

```
10        20        30        40        50        60        70        80        90        100       110       120
MASGNARIGK PAPDFKATAV VDGAFKEVKL SDYKGKYVVL FFYPLDFTFV CPTEIIAFTT VKRTSAKLGC EVLGVSVDSQ FTHLAWINTP RKEGGLGPLN IPLLADVTRR LSEDYGVLKN
130       140       150       160       170       180       190       200
DEGIAYRGLF IIDGKGVLRQ ITVNDLPVGR SVDEALRLVQ AFQYTDEHGE VCPAAWKPGR DTIKPNVDDS KEYFSKHN
```

Cmpd.	No. of Cmpds.	m/z meas.	Δ m/z [ppm]	z	Rt [min]	Score	P	Range	Sequence	Modification
	1	1735.0393	37.14	1		50.6	0	93-109	K.EGGLGPLNIPLLADVTR.R	

MS results for SDS-PAGE (gel band 2)

Search Type	Combined MS/MS		
Search Result	MALDI_NCBI_Hsapiens_Mascot_2014-09-26 15:57:24		
Protein 1:	unnamed protein product [Homo sapiens]		
Accession:	gi|29446	**Score:**	580.07
Database:	NCBInr	**MW [kDa]:**	16.00
Seq. Coverage [%]:	65.30 %	**pI:**	7.13
		No. of Peptides:	7
Modification(s):	Carbamidomethyl, Oxidation		

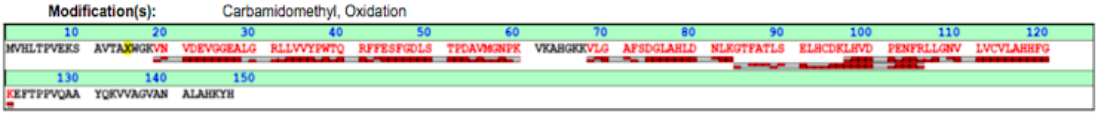

Cmpd.	No. of Cmpds.	m/z meas.	Δ m/z [ppm]	z	Rt [min]	Score	P	Range	Sequence	Modification
	1	1314.6694	3.46	1		60.1	0	19-31	K.VNVDEVGGEALGR.L	
	1	1274.7281	1.95	1		61.5	0	32-41	R.LLVVYPWTQR.F	
	1	2074.9011	-20.03	1		139.1	0	42-60	R.FFESFGDLSTPDAVMGNPK.V	Oxidation: 15
	1	1669.8656	-15.08	1		91.5	0	68-83	K.VLGAFSDGLAHLDNLK.G	
	1	2586.2687	10.87	1		98.2	1	84-105	K.GTFATLSELHCDKLHVDPENFR.L	Carbamidomethyl: 11
	1	1126.5701	5.41	1		49.5	0	97-105	K.LHVDPENFR.L	
	1	1776.9813	-7.26	1		80.1	0	106-121	R.LLGNVLVCVLAHHFGK.E	Carbamidomethyl: 8

7.3 Appendix 3:

Crystal screen JCSG-*plus* HT-96 (Molecular Dimensions Laboratories)

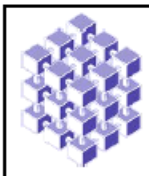

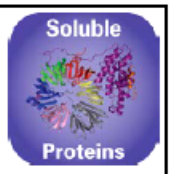

JCSG-*plus* HT-96 **Wells A1- D12** **MD1–40**

Well #	Conc.	Salt	Conc.	Buffer	pH	Conc.	Precipitant
A1	0.2 M	Lithium sulfate	0.1 M	Sodium acetate	4.5	50 % w/v	PEG 400
A2		None	0.1 M	Sodium citrate	5.5	20 % w/v	PEG 3000
A3	0.2 M	Ammonium citrate dibasic		None		20 % w/v	PEG 3350
A4	0.02 M	Calcium chloride dihydrate	0.1 M	Sodium acetate	4.6	30 % v/v	MPD
A5	0.2 M	Magnesium formate dihydrate		None		20 % w/v	PEG 3350
A6	0.2 M	Lithium sulfate	0.1 M	Phosphate/citrate	4.2	20 % w/v	PEG 1000
A7		None	0.1 M	CHES	9.5	20 % w/v	PEG 8000
A8	0.2 M	Ammonium formate		None		20 % w/v	PEG 3350
A9	0.2 M	Ammonium chloride		None		20 % w/v	PEG 3350
A10	0.2 M	Potassium formate		None		20 % w/v	PEG 3350
A11	0.2 M	Ammonium phosphate monobasic	0.1 M	Tris	8.5	50 % v/v	MPD
A12	0.2 M	Potassium nitrate		None		20 % w/v	PEG 3350
B1	0.8 M	Ammonium sulfate	0.1 M	Citrate	4.0		None
B2	0.2 M	Sodium thiocyanate		None		20 % w/v	PEG 3350
B3		None	0.1 M	BICINE	9.0	20 % w/v	PEG 6000
B4		None	0.1 M	HEPES	7.5	10 % w/v	PEG 8000
						8 % v/v	Ethylene glycol
B5		None	0.1 M	Sodium cacodylate	6.5	40 % v/v	MPD
						5 % w/v	PEG 8000
B6		None	0.1 M	Phosphate/citrate	4.2	40 % v/v	Ethanol
						5 % w/v	PEG 1000
B7		None	0.1 M	Sodium acetate	4.6	8 % w/v	PEG 4000
B8	0.2 M	Magnesium chloride hexahydrate	0.1 M	Tris	7.0	10 % w/v	PEG 8000
B9		None	0.1 M	Citrate	5.0	20 % w/v	PEG 6000
B10	0.2 M	Magnesium chloride hexahydrate	0.1 M	Sodium cacodylate	6.5	50 % v/v	PEG 200
B11	1.6 M	Sodium citrate tribasic dihydrate pH 6.5		None			None
B12	0.2 M	Potassium citrate tribasic monohydrate		None		20 % w/v	PEG 3350
C1	0.2 M	Sodium chloride	0.1 M	Phosphate/citrate	4.2	20 % w/v	PEG 8000
C2	1.0 M	Lithium chloride	0.1 M	Citrate	4.0	20 % w/v	PEG 6000
C3	0.2 M	Ammonium nitrate		None		20 % w/v	PEG 3350
C4		None	0.1 M	HEPES	7.0	10 % w/v	PEG 6000
C5	0.8 M	Sodium phosphate monobasic monohydrate	0.1 M	Sodium HEPES	7.5		None
	0.8 M	Potassium phosphate monobasic		None			
C6		None	0.1 M	Phosphate/citrate	4.2	40 % v/v	PEG 300
C7	0.2 M	Zinc acetate dihydrate	0.1 M	Sodium acetate	4.5	10 % w/v	PEG 3000
C8		None	0.1 M	Tris	8.5	20 % v/v	Ethanol
C9		None	0.1 M	Sodium/potassium phosphate	6.2	25 % v/v	1,2-Propandiol
						10 %v/v	Glycerol
C10		None	0.1 M	BICINE	9.0	10 % w/v	PEG 20,000
						2 % v/v	1,4-Dioxane
C11	2.0 M	Ammonium sulfate	0.1 M	Sodium acetate	4.6		None
C12		None		None		10 % w/v	PEG 1000
						10 % w/v	PEG 8000
D1		None		None		24 % w/v	PEG 1500
						20 % v/v	Glycerol
D2	0.2 M	Magnesium chloride hexahydrate	0.1 M	Sodium HEPES	7.5	30 % v/v	PEG 400
D3	0.2 M	Sodium chloride	0.1 M	Sodium/potassium phosphate	6.2	50 % v/v	PEG 200
D4	0.2 M	Lithium sulfate	0.1 M	Sodium acetate	4.5	30 % w/v	PEG 8000
D5		None	0.1 M	HEPES	7.5	70 % v/v	MPD
D6	0.2 M	Magnesium chloride hexahydrate	0.1 M	Tris	8.5	20 % w/v	PEG 8000
D7	0.2 M	Lithium sulfate	0.1 M	Tris	8.5	40 % v/v	PEG 400
D8		None	0.1 M	Tris	8.0	40 % v/v	MPD
D9	0.17 M	Ammonium sulfate		None		25.5 % w/v	PEG 4000
						15 % v/v	Glycerol
D10	0.2 M	Calcium acetate hydrate	0.1 M	Sodium cacodylate	6.5	40 % v/v	PEG 300
D11	0.14 M	Calcium chloride dihydrate	0.07 M	Sodium acetate	4.6	14 % v/v	2-Propanol
						30 % v/v	Glycerol
D12	0.04 M	Potassium phosphate monobasic		None		16 % w/v	PEG 8000
						20 % v/v	Glycerol

3

Molecular Dimensions

Soluble Proteins

JCSG-*plus* HT-96 Wells E1 – H12 MD1–40

Well #	Conc.	Salt	Conc.	Buffer	pH	Conc.	Precipitant
E1	1.0 M	Sodium citrate tribasic dihydrate	0.1 M	Sodium cacodylate	6.5		None
E2	2.0 M	Ammonium sulfate	0.1 M	Sodium cacodylate	6.5		None
	0.2 M	Sodium chloride					
E3	0.2 M	Sodium chloride	0.1 M	HEPES	7.5	10 % v/v	2-Propanol
E4	1.26 M	Ammonium sulfate	0.1 M	Tris	8.5		None
	0.2 M	Lithium sulfate					
E5		None	0.1 M	CAPS	10.5	40 % v/v	MPD
E6	0.2 M	Zinc acetate dihydrate	0.1 M	Imidazole	8.0	20 % w/v	PEG 3000
E7	0.2 M	Zinc acetate dihydrate	0.1 M	Sodium cacodylate	6.5	10 % v/v	2-Propanol
E8	1.0 M	Ammonium phosphate dibasic	0.1 M	Sodium acetate	4.5		None
E9	1.6 M	Magnesium sulfate heptahydrate	0.1 M	MES	6.5		None
E10		None	0.1 M	BICINE	9.0	10 % w/v	PEG 6000
E11	0.16 M	Calcium acetate hydrate	0.08 M	Sodium cacodylate	6.5	14.4 % w/v	PEG 8000
						20 % v/v	Glycerol
E12		None	0.1 M	Imidazole	8.0	10 % w/v	PEG 8000
F1	0.05 M	Cesium chloride	0.1 M	MES	6.5	30 % v/v	Jeffamine® M-600
F2	3.2 M	Ammonium sulfate	0.1 M	Citrate	5.0		None
F3		None	0.1 M	Tris	8.0	20 % v/v	MPD
F4		None	0.1 M	HEPES	7.5	20 % v/v	Jeffamine® M-600
F5	0.2 M	Magnesium chloride hexahydrate	0.1 M	Tris	8.5	50 % v/v	Ethylene glycol
F6		None	0.1 M	BICINE	9.0	10 % v/v	MPD
F7	0.8 M	Succinic acid pH 7.0		None			None
F8	2.1 M	DL-Malic acid pH 7.0		None			None
F9	2.4 M	Sodium malonate dibasic monohydrate pH 7.0		None			None
F10	1.1 M	Sodium malonate dibasic monohydrate	0.1 M	HEPES	7.0	0.5 % v/v	Jeffamine® ED-2003
F11	1.0 M	Succinic acid	0.1 M	HEPES	7.0	1 % w/v	PEG 2000 MME
F12		None	0.1 M	HEPES	7.0	30 % v/v	Jeffamine® M-600
G1		None	0.1 M	HEPES	7.0	30 % v/v	Jeffamine® ED-2003
G2	0.02 M	Magnesium chloride hexahydrate	0.1 M	HEPES	7.5	22 % w/v	Poly(acrylic acid sodium salt) 5100
G3	0.01 M	Cobalt(II) chloride hexahydrate	0.1 M	Tris	8.5	20 % w/v	Polyvinylpyrrolidone
G4	0.2 M	TMAO	0.1 M	Tris	8.5	20 % w/v	PEG 2000 MME
G5	0.005 M	Cobalt(II) chloride hexahydrate	0.1 M	HEPES	7.5	12 % w/v	PEG 3350
	0.005 M	Cadmium chloride hemi(pentahydrate)					
	0.005 M	Magnesium chloride hexahydrate					
	0.005 M	Nickel(II) chloride hexahydrate					
G6	0.2 M	Sodium malonate dibasic monohydrate		None		20 % w/v	PEG 3350
G7	0.1 M	Succinic acid		None		15 % w/v	PEG 3350
G8	0.15 M	DL-Malic acid		None		20 % w/v	PEG 3350
G9	0.1 M	Potassium thiocyanate		None		30 % w/v	PEG 2000 MME
G10	0.15 M	Potassium bromide		None		30 % w/v	PEG 2000 MME
G11	2.0 M	Ammonium sulfate	0.1 M	BIS-Tris	5.5		None
G12	3.0 M	Sodium chloride	0.1 M	BIS-Tris	5.5		None
H1	0.3 M	Magnesium formate dihydrate	0.1 M	BIS-Tris	5.5		None
H2	1.0 M	Ammonium sulfate	0.1 M	BIS-Tris	5.5	1 % w/v	PEG 3350
H3		None	0.1 M	BIS-Tris	5.5	25 % w/v	PEG 3350
H4	0.2 M	Calcium chloride dihydrate	0.1 M	BIS-Tris	5.5	45 % v/v	MPD
H5	0.2 M	Ammonium acetate	0.1 M	BIS-Tris	5.5	45 % v/v	MPD
H6	0.1 M	Ammonium acetate	0.1 M	BIS-Tris	5.5	17 % w/v	PEG 10,000
H7	0.2 M	Ammonium sulfate	0.1 M	BIS-Tris	5.5	25 % w/v	PEG 3350
H8	0.2 M	Sodium chloride	0.1 M	BIS-Tris	5.5	25 % w/v	PEG 3350
H9	0.2 M	Lithium sulfate	0.1 M	BIS-Tris	5.5	25 % w/v	PEG 3350
H10	0.2 M	Ammonium acetate	0.1 M	BIS-Tris	5.5	25 % w/v	PEG 3350
H11	0.2 M	Magnesium chloride hexahydrate	0.1 M	BIS-Tris	5.5	25 % w/v	PEG 3350
H12	0.2 M	Ammonium acetate	0.1 M	HEPES	7.5	45 % v/v	MPD

Abbreviations: Bis Tris; Bis-(2-hydroxyethyl)imino-tris(hydroxymethyl)methane, **CAPS**; N-Cyclohexyl-3-aminopropanesulfonic acid, **CHES**; 2-(N-Cyclohexylamino)ethane Sulfonic Acid, **HEPES**; 2-(4-(2-Hydroxyethyl)-1-piperazinyl)ethanesulfonic Acid, **Na HEPES**; 2-(4-(2-Hydroxyethyl)-1-piperazinyl)ethanesulfonic Acid Sodium Salt, **MES**; 2-(N-morpholino)ethanesulfonic acid, **MPD**; 2,4-methyl pentanediol, **PEG**; Polyethylene glycol (2K, 6K , 8K and 10K correspond to the molecular weight, in thousands of Daltons, of PEG), **TMAO**: Trimethylamine N-oxide, **Tris**; 2-Amino-2-(hydroxymethyl)propane-1,3-diol.

N.B. Jeffamine ED-2001 has been superseded with Jeffamine ED-2003. Polyvinylpyrolidone K15 is called Polyvinylpyrolidine.

7.4 Appendix 4:

Crystal screen MDI5-C12-B_Cryo 2HT-96 (Molecular Dimensions Laboratories)

EB-C12-B

Well	Precipitation Reagent	Buffer	Salt	
A1	40% (v/v) MPD	100 mM Sodium phosphate dibasic/ Citric acid pH 4.2		
A2	40% (v/v) Ethylene glycol	100 mM Sodium acetate/ Acetic acid pH 4.5		
A3	50% (v/v) PEG 200	100 mM Sodium citrate/ Citric acid pH 5.5		
A4	40% (v/v) PEG 300	100 mM HEPES/ Sodium hydroxide pH 7.5	200 mM Sodium chloride	
A5	40% (v/v) PEG 400	100 mM Sodium citrate/ Citric acid pH 5.5	200 mM Magnesium chloride	
A6	40% (v/v) PEG 600	100 mM Sodium cacodylate/ Hydrochloric acid pH 6.5	200 mM Calcium acetate	
A7	40% (v/v) Reagent alcohol	100 mM Tris base/ Hydrochloric acid pH 8.5	50 mM Magnesium chloride	
A8	35% (v/v) 2-Ethoxyethanol	100 mM Sodium cacodylate/ Hydrochloric acid pH 6.5		
A9	35% (v/v) 2-Propanol	100 mM Sodium phosphate dibasic/ Citric acid pH 4.2		
A10	45% (v/v) Glycerol	100 mM Imidazole/ Hydrochloric acid pH 8.0		
A11	35% (v/v) MPD	100 mM Tris base/ Hydrochloric acid pH 8.5	200 mM Ammonium sulfate	
A12	50% (v/v) Ethylene glycol	100 mM Sodium acetate/ Acetic acid pH 4.5	5% (w/v) PEG 1000	
B1	30% (v/v) PEG 200	100 mM MES/ Sodium hydroxide pH 6.0	5% (w/v) PEG 3000	
B2	20% (v/v) PEG 300	100 mM Sodium phosphate dibasic/ Citric acid pH 4.2	200 mM Ammonium sulfate	10% (v/v) Glycerol
B3	50% (v/v) PEG 400	100 mM CHES/ Sodium hydroxide pH 9.5	200 mM Sodium chloride	
B4	30% (v/v) PEG 600	100 mM MES/ Sodium hydroxide pH 6.0	5% (w/v) PEG 1000	10% (v/v) Glycerol
B5	40% (v/v) 1,2-Propanediol	100 mM HEPES/ Sodium hydroxide pH 7.5		
B6	35% (v/v) 2-Ethoxyethanol	100 mM Imidazole/ Hydrochloric acid pH 8.0	50 mM Calcium acetate	
B7	35% (v/v) 2-Propanol	100 mM Tris base/ Hydrochloric acid pH 8.5		
B8	30% (v/v) 1,2-Propanediol	100 mM Sodium citrate/ Citric acid pH 5.5	20% (v/v) MPD	
B9	40% (v/v) 1,2-Propanediol	100 mM Sodium acetate/ Acetic acid pH 4.5	50 mM Calcium acetate	
B10	40% (v/v) Ethylene glycol	100 mM Sodium phosphate dibasic/ Potassium phosphate monobasic pH 6.2		
B11	40% (v/v) MPD	100 mM Tris base/ Hydrochloric acid pH 7.0	200 mM Ammonium sulfate	
B12	40% (v/v) PEG 400	100 mM Sodium phosphate dibasic/ Potassium phosphate monobasic pH 6.2	200 mM Sodium chloride	
C1	30% (v/v) PEG 200	100 mM Tris base/ Hydrochloric acid pH 8.5	200 mM Ammonium phosphate dibasic	
C2	40% (v/v) PEG 300	100 mM CHES/ Sodium hydroxide pH 9.5	200 mM Sodium chloride	
C3	30% (v/v) PEG 400	100 mM CAPS/ Sodium hydroxide pH 10.5	500 mM Lithium sulfate	10% (v/v) Glycerol
C4	30% (v/v) PEG 600	100 mM HEPES/ Sodium hydroxide pH 7.5	50 mM Lithium sulfate	10% (v/v) Glycerol
C5	40% (v/v) PEG 300	100 mM CHES/ Sodium hydroxide pH 9.5	200 mM Sodium citrate tribasic	
C6	35% (v/v) 2-Ethoxyethanol	100 mM Sodium citrate/ Citric acid pH 5.5		
C7	40% (v/v) 1,2-Propanediol	100 mM Sodium citrate/ Citric acid pH 5.5	5% (w/v) PEG 1000	
C8	40% (v/v) 1,2-Propanediol	100 mM CHES/ Sodium hydroxide pH 9.5	200 mM Sodium citrate tribasic	
C9	25% (v/v) 1,2-Propanediol	100 mM Imidazole/ Hydrochloric acid pH 8.0	200 mM Zinc acetate	10% (v/v) Glycerol
C10	40% (v/v) MPD	100 mM Imidazole/ Hydrochloric acid pH 8.0	200 mM Magnesium chloride	
C11	40% (v/v) Ethylene glycol	100 mM HEPES/ Sodium hydroxide pH 7.5	5% (w/v) PEG 3000	
C12	50% (v/v) PEG 200	100 mM Tris base/ Hydrochloric acid pH 7.0	50 mM Lithium sulfate	
D1	40% (v/v) PEG 300	100 mM Sodium cacodylate/ Hydrochloric acid pH 6.5	200 mM Calcium acetate	
D2	40% (v/v) PEG 400	100 mM Tris base/ Hydrochloric acid pH 8.5	200 mM Lithium sulfate	
D3	40% (v/v) PEG 600	100 mM Sodium phosphate dibasic/ Citric acid pH 4.2		
D4	40% (v/v) Reagent alcohol	100 mM Sodium phosphate dibasic/ Citric acid pH 4.2	5% (w/v) PEG 1000	
D5	25% (v/v) 1,2-Propanediol	100 mM Sodium phosphate dibasic/ Citric acid pH 4.2	5% (w/v) PEG 3000	10% (v/v) Glycerol
D6	40% (v/v) Ethylene glycol	100 mM Tris base/ Hydrochloric acid pH 7.0		
D7	50% (v/v) Ethylene glycol	100 mM Tris base/ Hydrochloric acid pH 8.5	200 mM Magnesium chloride	
D8	50% (v/v) PEG 200	100 mM Sodium cacodylate/ Hydrochloric acid pH 6.5	200 mM Zinc acetate	
D9	20% (v/v) PEG 300	100 mM Tris base/ Hydrochloric acid pH 8.5	5% (w/v) PEG 8000	10% (v/v) Glycerol
D10	40% (v/v) PEG 400	100 mM MES/ Sodium hydroxide pH 6.0	5% (w/v) PEG 3000	
D11	50% (v/v) PEG 400	100 mM Sodium acetate/ Acetic acid pH 4.5	200 mM Lithium sulfate	
D12	40% (v/v) PEG 600	100 mM Imidazole/ Hydrochloric acid pH 8.0	200 mM Zinc acetate	

Well	Precipitation Reagent	Buffer	Salt	
E1	40% (v/v) MPD	100 mM Sodium cacodylate/ Hydrochloric acid pH 6.5		5% (w/v) PEG 8000
E2	50% (v/v) PEG 200	100 mM CHES/ Sodium hydroxide pH 9.5		
E3	40% (v/v) Ethylene glycol	100 mM Sodium phosphate dibasic/ Citric acid pH 4.2	200 mM Ammonium sulfate	
E4	40% (v/v) PEG 400	100 mM HEPES free acid/ Sodium hydroxide pH 7.5	200 mM Calcium acetate	
E5	40% (v/v) PEG 300	100 mM Tris base/ Hydrochloric acid pH 7.0		5% (w/v) PEG 1000
E6	30% (v/v) PEG 600	100 mM Sodium cacodylate/ Hydrochloric acid pH 6.5	1000 mM Sodium chloride	10% (v/v) Glycerol
E7	40% (v/v) Reagent alcohol	100 mM Tris base/ Hydrochloric acid pH 7.0		
E8	35% (v/v) 2-Ethoxyethanol	100 mM Sodium phosphate dibasic/ Potassium phosphate monobasic pH 6.2	200 mM Sodium chloride	
E9	35% (v/v) 2-Propanol	100 mM Imidazole/ Hydrochloric acid pH 8.0	50 mM Zinc acetate	
E10	40% (v/v) 1,2-Propanediol	100 mM Sodium acetate/ Acetic acid pH 4.5		
E11	25% (v/v) 1,2-Propanediol	100 mM Sodium phosphate dibasic/ Potassium phosphate monobasic pH 6.2		10% (v/v) Glycerol
E12	40% (v/v) 1,2-Propanediol	100 mM Sodium citrate tribasic/ Citric acid pH 5.5	200 mM Sodium chloride	
F1	35% (v/v) MPD	100 mM Sodium cacodylate/ Hydrochloric acid pH 6.5	50 mM Zinc acetate	
F2	40% (v/v) Ethylene glycol	100 mM Imidazole/ Hydrochloric acid pH 8.0	200 mM Calcium acetate	
F3	50% (v/v) PEG 200	100 mM Sodium phosphate dibasic/ Potassium phosphate monobasic pH 6.2	200 mM Sodium chloride	
F4	20% (v/v) PEG 300	100 mM Imidazole/ Hydrochloric acid pH 8.0	1000 mM Ammonium sulfate	10% (v/v) Glycerol
F5	50% (v/v) PEG 400	100 mM MES/ Sodium hydroxide pH 6.0		
F6	40% (v/v) PEG 300	100 mM Sodium phosphate dibasic/ Citric acid pH 4.2		
F7	40% (v/v) PEG 600	100 mM Sodium acetate/ Acetic acid pH 4.5	200 mM Magnesium chloride	
F8	50% (v/v) Ethylene glycol	100 mM CHES/ Sodium hydroxide pH 9.5	500 mM Potassium sodium tartrate	
F9	35% (v/v) 2-Ethoxyethanol	100 mM Tris base/ Hydrochloric acid pH 8.5	200 mM Lithium sulfate	
F10	35% (v/v) 2-Propanol	100 mM Sodium cacodylate/ Hydrochloric acid pH 6.5	200 mM Magnesium chloride	
F11	30% (v/v) 1,2-Propanediol	100 mM HEPES free acid/ Sodium hydroxide pH 7.5		20% (v/v) PEG 400
F12	25% (v/v) 1,2-Propanediol	100 mM Tris base/ Hydrochloric acid pH 8.5	200 mM Magnesium chloride	10% (v/v) Glycerol
G1	40% (v/v) MPD	100 mM CAPS/ Sodium hydroxide pH 10.5		
G2	40% (v/v) Ethylene glycol	100 mM MES/ Sodium hydroxide pH 6.0	200 Zinc acetate	
G3	50% (v/v) PEG 200	100 mM Tris base/ Hydrochloric acid pH 7.0		
G4	40% (v/v) PEG 300	100 mM Imidazole/ Hydrochloric acid pH 8.0	200 Zinc acetate	
G5	30% (v/v) PEG 400	100 mM HEPES free acid/ Sodium hydroxide pH 7.5	5% (w/v) PEG 3000	10% (v/v) Glycerol
G6	40% (v/v) PEG 600	100 mM Sodium citrate tribasic/ Citric acid pH 5.5		
G7	40% (v/v) PEG 600	100 mM CHES/ Sodium hydroxide pH 9.5		
G8	35% (v/v) 2-Propanol	100 mM Sodium acetate/ Acetic acid pH 4.5		
G9	45% (v/v) Glycerol	100 mM Sodium cacodylate/ Hydrochloric acid pH 6.5	200 mM Calcium acetate	
G10	25% (v/v) 1,2-Propanediol	100 mM Tris base/ Hydrochloric acid pH 7.0	200 mM Ammonium sulfate	10% (v/v) Glycerol
G11	40% (v/v) MPD	100 mM Sodium citrate tribasic/ Citric acid pH 5.5		
G12	50% (v/v) PEG 200	100 mM Sodium cacodylate/ Hydrochloric acid pH 6.5	200 mM Magnesium chloride	
H1	50% (v/v) Ethylene glycol	100 mM Imidazole/ Hydrochloric acid pH 8.0		
H2	40% (v/v) PEG 400	100 mM Sodium acetate/ Acetic acid pH 4.5		
H3	30% (v/v) PEG 600	100 mM Tris base/ Hydrochloric acid pH 7.0	500 mM Ammonium sulfate	10% (v/v) Glycerol
H4	40% (v/v) MPD	100 mM CHES/ Sodium hydroxide pH 9.5		
H5	50% (v/v) Ethylene glycol	100 mM HEPES free acid/ Sodium hydroxide pH 7.5	200 mM Lithium sulfate	
H6	30% (v/v) PEG 200	100 mM Sodium acetate/ Acetic acid pH 4.5	100 mM Sodium chloride	
H7	40% (v/v) PEG 400	100 mM Imidazole/ Hydrochloric acid pH 8.0		
H8	35% (v/v) MPD	100 mM Sodium acetate/ Acetic acid pH 4.5		10% (v/v) Glycerol
H9	40% (v/v) PEG 300	100 mM Sodium acetate/ Acetic acid pH 4.5	200 mM Sodium chloride	
H10	30% (v/v) PEG 200	100 mM CAPS/ Sodium hydroxide pH 10.5	200 mM Ammonium sulfate	
H11	50% (v/v) PEG 200	100 mM HEPES free acid/ Sodium hydroxide pH 7.5		
H12	50% (v/v) PEG 200	100 mM Sodium phosphate dibasic/ Citric acid pH 4.2	200 mM Sodium chloride	

7.5 Appendix 5: Sigma 82009 crystal screen (Sigma Aldrich)

SIGMA

82009 Crystallization Basic Kit for Proteins Observation Sheet

Sample description: _____ Date: _____
concentration: _____ Incubation Temperature: _____
buffer: _____ Reservoir Volume: _____
1 Drop contains : Crystallization Reagent_____ul Sample_____ul Additive (name)_____(volume)_____ul

	precipitate without birefringent and edges	precipitates shows birefringent or has edges
1 drop is clear	3 mostly clear drop	7 spherulites or small structures maybe edges
2 drop contains non-protein particles	4 fully precipitated dark colour	8 crystal grown 1 D
	5 gelatinous protein precipitate	9 crystal grown 2 D
	6 phase separation	10 crystal grown 3 D

No.	Fluka No.	Reagent composition	Date:	Date:	Date:	Date:	Date:
1.	89754	Ca-chloride 0.02M, Na-acetate (pH 4.6) 0.1M, 2-Methyl-2,4-pentanediol 30%					
2.	78016	K-,Na-tartrate 0.4M					
3.	77104	NH_4-dihydrogenphosphate 0.4M					
4.	84653	TRIS-HCl (pH 8.5) 0.1M, NH_4-sulfate 2.0M					
5.	77103	Na-citrate 0.2M, HEPES Na-salt (pH 7.5) 0.1M, 2-Methyl-2,4-pentanediol 30%					
6.	78760	Mg-chloride 0.2M, TRIS-HCl (pH 8.5) 0.1M, PEG 4000 30%					
7.	70114	Na-cacodylate (pH 6.5) 0.1M, Na-acetate 1.4M					
8.	85887	Na-citrate 0.2M, Na-cacodylate (pH 6.5) 0.1M, 2-Propanol 30%					
9.	73374	NH_4-acetate 0.2M, Na-citrate (pH 5.6) 0.1M, PEG 4000 30%					
10.	76028	NH_4-acetate 0.2M, Na-acetate (pH 4.6) 0.1M, PEG 4000 30%					
11.	78993	Na-citrate (pH 5.6) 0.1M, NH_4-dihyrogenphosphate 1.0M					
12.	73682	Mg-chloride 0.2M, HEPES Na-salt (pH 7.5) 0.1M, 2-Propanol 30%					
13.	76018	Na-citrate 0.2M, TRIS-HCl (pH 8.5) 0.1M, PEG 400 30%					
14.	79052	Ca-chloride 0.2M, HEPES Na-salt (pH 7.5) 0.1M, PEG 400 28%					
15.	86686	NH_4-sulfate 0.2M, Na-cacodylate (pH 6.5) 0.1M, PEG 8000 30%					
16.	86445	HEPES Na-salt (pH 7.5) 0.1M, Li-sulfate 1.5M					
17.	89786	Li-sulfate 0.2M, TRIS-HCl (pH 8.5) 0.1M, PEG 4000 30%					
18.	88518	Mg-acetate 0.2M, Na-cacodylate pH (6.5) 0.1M, PEG 8000 20%					
19.	88512	NH_4-acetate 0.2M, TRIS-HCl (pH 8.5) 0.1M, 2-Propanol 30%					
20.	82406	NH_4-sulfate 0.2M, Na-acetate (pH 4.6) 0.1M, PEG 4000 25%					
21.	87924	Mg-acetate 0.2M, Na-cacodylate (pH 6.5) 0.1M, 2-Methyl-2,4-pentanediol 30%					
22.	88543	Na-acetate 0.2M, TRIS-HCl (pH 8.5) 0.1M, PEG 4000 30%					
23.	73642	Mg-chloride 0.2M, HEPES Na-salt (pH 7.5) 0.1M, PEG 400 30%					
24.	92644	Ca-chloride 0.2M, Na-acetate (pH 4.6) 0.1M, 2-Propanol 20%					
25.	70377	Imidazole (pH 6.5) 0.1M, Na-acetate 1M					
26.	88530	NH_4-acetate 0.2M, Na-citrate (pH 5.6) 0.1M, 2-Methyl-2,4-pentanediol 30%					
27.	92465	Na-citrate 0.2M, HEPES Na-salt (pH 7.5) 0.1M, 2-Propanol 20%					
28.	96345	Na-acetate 0.2M, Na-cacodylate pH (6.5) 0.1M, PEG 8000 30%					
29.	93268	HEPES Na-salt (pH 7.5) 0.1M, K-,Na-tartrate 0.8M					
30.	71907	NH_4-sulfate 0.2M, PEG 8000 30%					
31.	80677	NH_4-sulfate 0.2M, PEG 4000 30%					
32.	76399	NH_4-sulfate 2M					
33.	73932	Na-formiate 4M					
34.	76728	Na-acetate (pH 4.6) 0.1M,Na-formiate 2M					
35.	71835	HEPES Na-salt (pH 7.5) 0.1M, K-dihydrogenphosphate 0.8M, Na-dihydrogenphosphate 0.8M					
36.	80526	TRIS-HCl (pH 8.5) 0.1M, PEG 8000 8%					
37.	77436	Na-acetate (pH 4.6) 0.1M, PEG 4000 8%					
38.	73931	HEPES Na-salt (pH 7.5) 0.1M, Na-citrate 1.4M					
39.	80346	HEPES Na-salt (pH 7.5) 0.1M, PEG 400 2%, NH_4-sulfate 2.0M					
40.	73933	Na-citrate (pH 5.6) 0.1M, 2-Propanol 20%, PEG 4000 20%					
41.	80565	HEPES Na-salt (pH 7.5) 0.1M, 2-Propanol 10%, PEG 4000 20%					
42.	80806	K-dihydrogenphosphate 0.05M, PEG 8000 20%					
43.	78225	PEG 1500 30%					
44.	73934	Mg-formiate 0.2M					
45.	82409	Zn-acetate 0.2M, Na-cacodylate (pH 6.5) 0.1M, PEG 8000 18%					
46.	91113	Ca-acetate 0.2M, Na-cacodylate (pH 6.5) 0.1M, PEG 8000 18%					
47.	91633	Na-acetate (pH 4.6) 0.1M, NH_4-sulfate 2.0M					
48.	85934	TRIS-HCl (pH 8.5) 0.1M, NH_4-dihydrogenphosphate 2.0M					
49.	91114	Li-sulfate 1.0M, PEG 8000 2%					
50.	88862	Li-sulfate 0.5M, PEG 8000 15%					

7.6 Appendix 6: Sigma 70437 crystal screen (Sigma Aldrich)

SIGMA

70437 Crystallization Extension Kit for Proteins Observation Sheet

Sample description: _____ Date: _____
concentration: _____ Incubation Temperature: _____
buffer: _____ Reservoir Volume: _____
1 Drop contains : Crystallization Reagent_____ul Sample_____ul Additive (name)_____(volume)_____ul

1 drop is clear
2 drop contains non-protein particles

precipitate without birefringent and edges
3 mostly clear drop
4 fully precipitated dark colour
5 gelatinous protein precipitate
6 phase separation

precipitates shows birefringent or has edges
7 spherulites or small structures maybe edges
8 crystal grown 1 D
9 crystal grown 2 D
10 crystal grown 3 D

No.	Fluka No.	Name	Date:	Date:	Date:	Date:	Date:
1.	88716	Na-chloride 2M, PEG 6000 10%					
2.	83935	Na-chloride 0.5M, Mg-chloride 0.01M, CTAB 0,01M					
3.	72526	Ethylene glycol 25%					
4.	75691	Dioxane 35%					
5.	70293	NH_4-sulfate 2M, 2-Propanol 5%					
6.	95514	Imidazole (pH 7.0) 1M					
7.	93593	PEG 1000 10%, PEG 8000 10%					
8.	92982	Na-chloride 1.5M, Ethanol 10%					
9.	93471	Na-chloride 2M, Na-acetate (pH 4.6) 0.1M					
10.	93714	Na-chloride 0.2M, Na-acetate (pH 4.6) 0.1M, 2-Methyl-2,4-pentanediol 30%					
11.	96346	Co-chloride 0.01M, Na-acetate (pH 4.6) 0.1M, 1,6-Hexanediol 1M					
12.	95958	Cd-chloride 0.1M, Na-acetate (pH 4.6) 0.1M, PEG 400 30%					
13.	92913	NH_4-sulfate 0.2M, Na-acetate (pH 4.6) 0.1M, PEG MME 2000 30%					
14.	96765	K-,Na-tartrate 0.2M, NH_4-sulfate 2M, Na-citrate (pH 5.6) 0.1M					
15.	92347	Li-sulfate 1M, NH_4-sulfate 0.5M, Na-citrate (pH 5.6) 0.1M					
16.	94832	Na-chloride 0.5M, Na-citrate (pH 5.6) 0.1M, Polyethylenimin 2%					
17.	94839	Na-citrate (pH 5.6) 0.1M, tert.-Butanol 35%					
18.	71228	Fe(III)-chloride 0.01M, Na-citrate (pH 5.6) 0.1M, Jeffamine M-600 10%					
19.	80557	Na-citrate (pH 5.6) 0.1M, 1,6-Hexanediol 2.5M					
20.	80094	Mg-sulfate 1.6M, MES (pH 6.5) 0.1M					
21.	77583	Na-chloride 2M, Ka-,Na- dihydrogenphosphate each 0.1M, MES (pH 6.5) 0.1M					
22.	79975	MES (pH 6.5) 0.1M, PEG 20'000 12%					
23.	80095	NH_4-sulfate 1.6M, MES (pH 6.5) 0.1M, Dioxane 10%					
24.	72873	Cs-chloride 0.05M, MES (pH 6.5) 0.1M, Jeffamine M-600 30%					
25.	72874	Co-chloride 0.01M, NH_4-sulfate 1.8M, MES (pH 6.5) 0.1M					
26.	79688	NH_4-sulfate 0.2M, MES (pH 6.5) 0.1M, PEG MME 5000 30%					
27.	74616	Zn-sulfate 0.01M, MES (pH 6.5) 0.1M, PEG MME 550 25%					
28.	73894	Na-citrate (pH 6.5) 1.6M					
29.	80386	NH_4-sulfate 0.5M, HEPES Na-salt (pH 7.5) 0.1M, 2-Methyl-2,4-pentanediol 30%					
30.	80060	HEPES Na-salt (pH 7.5) 0.1M, 2-Methyl-2,4-pentanediol 5%, PEG 6000 10%					
31.	79976	HEPES Na-salt (pH 7.5) 0.1M, Jeffamine M-600 20%					
32.	79687	NH_4-sulfate 1.6M, Na-chloride 0.1M, HEPES Na-salt (pH 7.5) 0.1M					
33.	91476	NH_4-formate 2.0M, HEPES Na-salt (pH 7.5) 0.1M					
34.	89718	Na-acetate 1.0M, Cd-sulfate 0.05M, HEPES Na-salt (pH 7.5) 0.1M					
35.	86953	HEPES Na-salt (pH 7.5) 0.1M, 2-Methyl-2,4-pentanediol 70%					
36.	82238	Na-chloride 4.3M, HEPES Na-salt (pH 7.5) 0.1M					
37.	90196	HEPES Na-salt (pH 7.5) 0.1M, Ethylene glycol 8%, PEG 8000 10%					
38.	82217	HEPES Na-salt (pH 7.5) 0.1M, PEG 10'000 20%					
39.	82208	Mg-chloride 0.2M, TRIS-HCl (pH 8.5) 0.1M, 1,6-Hexanediol 3.4M					
40.	86261	TRIS-HCl (pH 8.5) 0.1M, tert.-Butanol 25%					
41.	81935	Li-sulfate 1M, Ni(II)-chloride 0.01M, TRIS-HCl (pH 8.5) 0.1M					
42.	82237	NH_4-sulfate 1.5M, TRIS-HCl (pH 8.5) 0.1M, Glycerol 12%					
43.	80925	NH_4-phosphate 0.2M, TRIS-HCl (pH 8.5) 0.1M, 2-Methyl-2,4-pentanediol 50%					
44.	88438	TRIS-HCl (pH 8.5) 0.1M, Ethanol 20%					
45.	88439	Ni(II)-chloride 0.01M, TRIS-HCl (pH 8.5) 0.1M, PEG MME 2000 20%					
46.	91229	Na-chloride 0.1M, Bicine (pH 9.0) 0.1M, PEG MME 550 20%					
47.	95633	Mg-chloride 2M, Bicine (pH 7.5) 0.1M					
48.	80106	Bicine (pH 9.0) 0.1M, Dioxane 2%, PEG 20'000 10%					
49.	79924	Mg-chloride 0.1 M, TRIS-HCl (pH 8.5) 0.1M, PEG 20'000 15%					
50.	80105	PEG 20'000 20 %					

Chapter 8:

References

Abdiche, Y, Malashock, D, Pinkerton, and Pons, J. (2008) Determinating kinetics and affinities of protein interactions using parallel real-time label-free biosensor, the Octet. *Anal Biochem*, **377**: 209-217.

Adrian V, Stephanie A.L, and Ernesto F (1990) Characterization of protein-protein interactions by isothermal titration calorimetry. Methods in Molecular Biology, **261**: 35-54.

Alberts B (1998**)** The cell as a collection of protein machines: preparing the next generation of molecular biologists. *Cell*, **92**: 291-294

Alberts B, Bray D, Lewis J, Raff M, Roberts K and Watson J (1994) Molecular Biology of the Cell. *Garland New York*, 3rd *edition***, pp** 1361.

Alderton W.K, Cooper, C.E and Knowles, R.G (2001) Nitric oxide synthases: structure, function and inhibition. *Biochem J*, **357**: 593–615

Alessandro M, Phillip S, Franco T, Mariarita B, Maria E, Daniela S, Antonella P, Angela S, and Lucia D (2010) Peroxiredoxin-2 expression is increased in β-thalassemic mouse red cells but is displaced from the membrane as marker of oxidative stress. *Free Radical Bio Med*, **3**: 457-466.

Allen *R.C.* (1980) Electrophoresis **I**: *32- 37*.

Alving K,Weitzberg E, and Lundberg JM (1993) Increased amount of nitric oxide in exhaled air of asthmatics. *Eur Respir J* **6**: 1368-1370.

Amelle DR and Stamler JS (1995) NO^+, NO^- donation by S-nitrosothiol: implications for regulation of physiological function by S-nitrosylation and acceleration of disulfide formation. *Arch Biochem Biophys* **318**:279-285.

Amirmansour C, Vallance P, Bogle RG (1999) Tyrosine nitration in blood occurs with increasing nitric oxide concentration. *Br J Pharmacol*, **3**: 788-794.

Andras D and Igor A (2001) Detection of Multiple Protein Conformational Ensembles in Solution via Deconvolution of Charge-State Distributions in ESI MS. *American Chemical Society*, **73**: 4763-4773.

Bai Y (2015) Detecting protein-protein interactions by gel filtration chromatography. *Methods Mol Biol*. **1278**:223-232.

Barnett D, McAninly J and Williams D. (1994) Transnitrosation between nitrosothiols and thiols. *J. Chem.* **2**: 1131−1133.

Bayden A.S, Yakovlev V.A, Graves P.R, Mikkelsen R.B, Kellogg G.E, (2011) Factors influencing protein tyrosine nitration – structure-based predictive models, *Free Radical Biology & Medicin.* **50**: 749-762.

Bonaventura C, Ferruzzi G, Tesh S, and Stevens R.D (1999) *J. Biol Chem.* **274:**24742-24748.

Borland C, (1991) Endothelium in control, *Br. Heart J.* **272:** 405.

Broniowska, K.A. and Hogg N (2012) The chemical biology of *S*-nitrosothiols. *Antioxid. Redox. Signal,* **17**, 969–980.

Bryan NS, Rassaf T, Maloney RE, Rodriguez CM, Saijo F, Rodriguez JR and Feelisch M (2004) Cellular targets and mechanisms of nitros(yl) action: an insight into their nature and kinetics in vivo. *Proc Natl Acad Sci* USA 101:4308-4313

Bryan NS, Rassaf T, Maloney RE, Rodriguez CM, Saijo F, Rodriguez JR and Feelisch M (2005) Nitrite is a signaling molecule and regulator of gene expression in mammalian tissues. *Nat Chem Biol* **1**:290-297.

Buchner J (1996) Supervising the fold: functional principles of molecular chaperones. *FASEB J,* **10**: 10-19.

Buerk DG (2007) Nitric oxide regulation of microvascular oxygen. Antioxid Redox Signal 9:829-843

Buerk DG (2007) Nitric oxide regulation of microvascular oxygen. *Antioxide Redox Signal* **9**:829-843.

Butler A.R, Megson I.L, Wright P.G (1998) Diffusion of nitric oxide and scavenging by blood in the vasculature. *Biochem. Biophys.Acta* **1425**:168–176.

Cabral C.M, Liu Y and Sifers R.N (2001) Dissecting glycoprotein quality control in the secretory pathway. *Trends Biochem Sci*, **26**:619-624.

Cannon RO3rd, Schechter AN, Panza JA, Ognibene FP, Pease-Fye ME, Waclawiw MA, Shelhamer JH, Gladwin MT (2001) Effects of inhaled nitric oxide on regional blood flow are consistent with intravascular nitric oxide delivery. *J Clin Invest* **108**: 279–287.

Cassoly R and Gibson Q.H (1975) Conformation, co-operativity and ligand-binding in human hemoglobin. *J. Mol.Biol*. **91**:301–313.

Ceron. P.I, Cremonez. D.C, Bendhack. L.M and Tedesco. A.C (2001) The relaxation induced by S-nitroso-glutathione and S-nitroso-N-acetylcysteine in rat aorta is not related to nitric oxide production. J.Pharmacol Exp Ther, 298:686-694.

Chae HZ, Chung SJ, Rhee SG (1994) *J Biol Chem* **269**:27670–27678.
Chem **266**:18964 –18968.

Chin HJ and Chen YC (2012) Reactive nitrogen oxide species-induced post-translational modifications in human hemoglobin and the association with cigarette smoking. *Anal Chem* **18**: 7881-7890.

Choi YB, Tenneti L, Le DA, Ortiz J, Bai G, Chen HS, Lipton SA (2000) *Nat*
Chou KC (1989) Low-frequency resonance and cooperativity of hemoglobin. *Trends Biochem. Sci*. **14**: 212–223.

Christen S, Cattin I, Knight I. A, Winyard P. G, Blum J.W and Elsasser T. K (2007) Plasma S-nitrosothiol status in neonatal calves: ontogenetic association with tissue-specific S-nitrosylation and nitric oxide synthase. *Expt Biol Medi,* **233**: 309-322.

Chung KK, Thomas B, Li X, Pletnikova O, Troncoso JC, Marsh L, Dawson VL, Dawson TM (2004) *Science* **304**:1328 –1331.

Coin J.T and Olson J.S (1979) Rate of oxygen up-take by human red blood cells. *J. Biol. Chem*. **254**:1178–1190.

Cook J.K, Kim S.Y, Teague D, Krisha M.C, Pacelli R, Mitchell J.B, Wink D.A (1996) Convenient colorimetric and fluorometric assay for S-nitrosothiols. *Anal Biochem*, **238**: 150-158.

Cortese-Krott M and Malte Kelm, (2014) Endothelial nitric oxide synthase in red blood cells: key to a new erythrocrine function *Redox Biol* **2**: 251-258.

Cortese-Krott, Rodriguez-Mateos A, Sansone R, Kuhnle G, Thasian-Sivarajah S, Krenz T, Horn P, Krisp C, Wolters D Heib C Kroncke K, Hogg N Feelisch M and Kelm (2012) Human red blood cells at work: identification and visualization of erythrocytic eNOS activity in health and disease. *Blood* **20**: 4229-4237.

Cosby K, Partovi KS, Crawford JH, Patel RP, Reiter CD, Martyr S, Yang BK, Waclawiw MA, Zolos G, Xu X, Huang KT, Shields H, Kim-Shapiro DB, Schechter AN, Cannon RO and Gladwin MT (2003) Nitrite reducation to nitric oxide by deoxyhaemoglobin vasodilates the human circulation. *Nat Med* **9**:1498-1505.

Cullen D.C, Brown R.G.W and Lowe, C.R (1987) Detection of immuno-complex formation via surface plasmon resonance on gold-coated diffraction gratings. *Biosensors* **3**:211-225.

Cvekl A, Sax C.M, Bresnick E.H and Piatigorsky J (1994) A complex array of positive and negative elements regulates the chicken alpha A-crystallin gene: involvement of Pax-6, USF, CREB and/or CREM, and AP-1 proteins**.** *American Society for microbiology*

Datta B, Tufnell-Barrett T, Bleasdale R, Jones C, Beeton I, Paul V, Frenneaux M, James P. Red blood cell nitric oxide as an endocrine vasoregulator: a potential role in congestive heart failure.*Circulation*. In press.

David A.W, Raymond W.N, John F.D, Danae C, Ingeborg H, George W.C, Francoise L, Jacques L John A.C, Murali C.K, William G.D and James B.M (1994) reaction kinetics for nitrosation of cysteine and glutathione in aerobic nitric oxide solutions at neutral pH. Insight into the fate and physiological effect of intermediates generated in the NO/O_2 reaction. *Chem. Res. Toxicol* **7**: 519-525.

David F. Waugh (1954) Protein-protein interactions. Advances in protein chemistry. **9**:

325-437.

DeBurman S.K, Raymond G.J, Caughey B and Lindquist S (1997) Chaperone-supervised conversion of prion protein to its protease-resistant form. *Proc. Natl. Acad. Sci. USA*, **94**:13938-13943.

Dennehy M. K, Richards K. A., Wernke G. R, Shyr Y and Liebler D. C. (2006) Cytosolic and nuclear protein targets of thiol-reactive electrophiles. *Chem. Res. Toxicol.* **19**: 20–29.

Dicks A and William D (1996), Generation of nitric oxide from S-nitrosothiols using protein-bound Cu2+ sources. *Current Biology* **8***:* 655-659*.*

Dobson C.M, (2001) Protein folding and its links with human disease. *Biochem Soc*., 68: 1-26.

Doyle M P, Hoekstra J W (1981) *J Inorg Biochem* **14**: 351–358.

Doyle M.P and Hoekstra J.W (1981) Oxidation of nitrogen oxides by bound dioxygen in hemoproteins. *J. Inorg.Biochem*. **14**:351–358.

Duranski MR, Greer J, Dejam A, Jaganmohan S, Hogg N, Langston W, Patel RP, Yet SF, Wang X, Kevil CG, Gladwin MT, Lefer DJ (2005) Cytoprotective effects of nitrite during in vivo ischemia-reperfusion of the heart and liver. J *Clin Invest* **115**: 1232-1240.

Duranski MR, Greer JJ, Dejam A, Jaganmohan S, Hogg N, Langston W, Patel RP, Yet SF, Wang X, Kevil CG, Gladwin MT and Lefer DJ (2005) Cytoprotective effects of nitrite during in vivo ischemia-reperfusion of the heart and liver. *J Clin Invest* **115**: 1232-1240.

Dykhuizen RS, Masson J, McKnight G, Mowat AN, Smith LM and Benjamin N (1996) Plasma nitrate concentration in infective gastroenteritis and inflammatory bowel disease. *Gut* **39**: 393-395.

Eich R F, Li T, Lemon D D, Doherty D H, Curry S R, Aitken J F, Mathews A J, Johnson K A, Smith R D, Phillips G N Jr, Olson J S (1996) *Biochemistry* **35**: 6976–6983.

EichR.F, Li,T.S, Lemon D.D, Doherty D.H, Curry S.R, Aitken J.F, Mathews A.J, Johnson K.A, Smith R.D, Phillips G.N, and Olson J.S (1996) Mechanism of NO-induced oxidation of myoglobin and hemoglobin. *Biochemistry* **35**: 6976–6983.

EM, Zhang Z, Masliah E, et al. (2004) *Proc Natl Acad Sci* U*SA* **101**:10810 –10814.
Emery C.J (1995) Vasodilation action of the S-nitrosothiol, SNAP, in rat isolated perfused lung. Physiol Res, **44**:19-24.

Emsley P, Lohkamp B, Scott WG and Cowtan K (2010) Features and development of Coot. *Acta Crystallogr D Biol Crystal*logr **66**: 486-501.

Fang Jianguo, Nakamura Tomohiro, Cho Dong-Hyung, Gu Zezong and Lipton Stuart (2007) S-nitrosylation of peroxiredoxin 2 promotes oxidative stress-induced neuronal cell death in Parkinson's disease. *PNAS***, 140:**18742 -18747.

Fields S and Song O.K (1989) The yeast two-hybrid system. *Nature*, **340**: 243-246.

Ford P.C, Wink D.A, Stanbury D.M (1993) Autoxidation kinetics of aqueous nitric oxide. *FEBS Lett* **326**:1-3.

Foster, M.W., Mchachon, T.J, and Stamler, J.S (2003) S-nitrosylation in health and disease. Trend Mol Med, 9:160-168

Freyer, M. W., Lewis, E. A. (2008) Isothermal titration calorimetry: experimental design, data analysis, and probing macromolecules / ligand binding and kinetic interaction. *Methods Cell Biol***. 84**: 79-113.

Galley HF, Webster NR (2004) Physiology of the endothelium. *Br J Anaesth*. **93**: 105 – 13

Gallyas F (197 1) Acta Morphol. *Acad. Sci. Hung*, **19**: 57-7I.

Gandley R.E, Taylor R.N, Tyurin V.A, Huang W, Arroyo A, Daftary A, Harger G, Jiang J, Pitt B, Hubel C.A and Kagan V.E (2005) S-nitrosoalbumin-mediated relaxation is enhanced by ascorbate and copper: effects in pregnancy and preeclampsia plasm. *Hypertension*, **45**: 21-27.

Geders T. W, Gustafson K, Finzel, B. C (2012) Use of differential scanning florimetry to optimize the purication and crystallization of PLP-dependent enzyme. *Acta Crystallogr Sect F Struct Biol Cryst Commun*. **68**: 596-600.

Geoffrey H and Allen M (2006) Analytical ultracentrifugation for the study of protein association and assembly. *Current Opinion in Chem. Bio*, **10**: 430-436.

Giraldez RR, Panda A, Xia Y, Sanders SP and Zweier JL (1997) Decreased nitric oxide synthase activity causes impaired endothelium-dependant relaxation in the postischemic heart. *J Biol Chem* **272**:21420-21426.

Giustarini .D, Milzani. A, Dalle-Donne.I and Rossi. R. (2007) Detection of S-nitrosathiols in biological fluids. J Chromatogr B, 851: 124-139.

Giustarini D, Milzani S, Colombo R, Dalle-Donne I and Rossi R (2003) Nitric oxide and *S*-nitrosothiols in human blood. *Clinica Chemica Acta* **330**, 85−98.

Giustarini D, Milzani A, Dalle-Donne I, and Rossi R, (2007) Detection of S-nitrosothiols in biological fluid: A comparison of among the most widely applied methodologies. *Bio Chem*, **851**: 124-139.

Giustarini. D, Milzani. A, Dalle-Donne. I and Rossi. R (2007) Detection of S-nitrosothiols in biological fluids. J Chromatogr B, 851:124-139.

Gladwin M T, Ognibene F P, Shelhamer J H, Pease-Fye M E, Noguchi C T, Rodgers G P, Schechter A N(2001) *Free Radical Res* **35**:175–180.
Gladwin MT (2005), Nitrite as an intrinsic signaling molecule. *Nat Chem Bio* **1**: 245-246.

Gladwin MT, Totzeck M, Hendgen-Cotta U, Luedike P, Berenbrink M, Klare J, Steinhoff H, Semmler D, Shiva S, Williams D, Kipar A, Vet.habil M, Schrader J, Kelm M, Cossins A, and Rassaf T, (2012) Nitrite Regulates Hypoxic Vasodilation *via* Myoglobin–Dependent Nitric Oxide Generation. PMC **3**: 325-334.

Godber BL, Doel JJ, Sapkota Gp, Blake DR, Steven CR, Eisenthal R and Harrison R (2000) Reduction of nitrite to nitric oxide catalysed by xanthine oxidoreductase. J Biol Chem 275:7757-7763.

Golemis E.A, and Adams P.D (2005) Protein-Protein Interactions. A Molecular Cloning *Manual Edn 2, Cold Spring Harbor Laboratory Press.*

Gow A.J and Stamler J.S (1998) *Nature* (London) **391**: 169-173.

Gow A.J, Luchsinger B.P, Pawloski J.R, Singel D.J, and Stamler J.S (1999) *Proc. Natl. Acad. Sci. USA* **96**:9027-9032.

Gow.A, Buerk .D.G, and Ischiropoulos.H (1997) A novel reaction mechanism for the formation of s-nitrosothiols in vival. J. Bio Chem, 272:2841-2845.

Greenwood N.N, and Earnshaw A (1984) Chemistry of the Elements. *Pergamon Press New York*, **pp** 508-527.

Guevara, J, Johnston, D. A, Ramagali, L. S., Martin B. A, Capetillo S and Rodriquez L. V (1982) Electrophoresis. **3**: 197-205.

Gupta. S, Moreland. R. B, Munarriz. R, Daley. J, Goldstein. I and SaenzDe Tejada. I (1995) Possible role of Na(+)-K(+)-ATPase in the regulation of human corpus cavernosum smooth muscle contractility by nitric oxide. *Br J Pharmacol*, **116**:2201-2206.

H, Liddington R, Zhang D, (2007) *Neuron* **53**: 53 – 64.

Han T.H and Liao J.C (2005) Erythrocyte nitric oxide transport reduced by a sub-membrane cytoskeletal barrier. *Biochim. Biophys.Acta* **1723**: 135–142.

Harris J.R (1969). Some negative contrast staining features of a protein from erythrocyte ghosts. *J. Mol. Biol*, **46**:329-335.

Harper J.D, Lansbury P.T (1997) Models of amyloid seeding in Alzheimer's disease and scrapie: mechanistic truths and physiological consequences of the time-dependent solubility of amyloid proteins. *Annual Rev. Biochem*, **66:** 385-407.

Hartl F.U, Hayer-Hartl M (2002) Molecular chaperones in the cytosol: from nascent chain to folded protein. *Science, **295***: 1852-1858.

Held J. M., Gibson B. W. (2012) Regulatory control or oxidative damage? Proteomic approaches to interrogate the role of cysteine oxidation status in biological processes. *Mol. Cell. Proteomics* **11**: R111.013037.

Herold S and Rock G (2005) Mechanistic studies of S-nitrosothiols formation by NO / O2 and NO / methaemoglobin. *Arch Biophys*, **436**: 386-396.

Herold S, Exner M, Nauser T (2001) Kinetic and mechanistic studies of the NO mediated oxidation of oxymyoglobin and oxyhemoglobin. *Biochemistry* **40**: 3385–3395

Herold S, Exner M, Nauser T(2001) *Biochemistry* **40**:3385–3395.

Herold. S and Rock. G (2005) Mechanistic studies of S-nitrosothiol formation by NO/O_2 and NO/ methemoglobin. Arch Biochem Biophys, **436**: 386-396.

Herrick A.L (2005) Pathogenesis of Raynaud's phenomenon. *Rheumatology Oxford*, **44**: 587–96.

Heslop R.B, and Jones K (1976) Inorganic Chemistry, *Elsevier, Amsterdam* **pp** 424-432.

Hess D, Matsumoto A, Nudelman R, Stamler JS (2001) *Nat Cell Biol*

Hess DT, Matsumoto A, Kim SO, Marshall HE, Stamler JS (2005) Nat Rev *Mol Cell Biol* **6**: 150 –166.

Hilde J, Xiong L, Lauren A, Guido M, and Qun H (2009) Dynamic Light Scattering as a Powerful Tool for Gold Nanoparticle Bio-conjugation and Biomolecular Binding Studies. *Analytical Chemistry*, **81**: 9425-9432.

Hogg N (1999) The kinetics of S-transnitrosation - a reversible second –order reaction. *Anal Biochem* **272**: 257-262.

Hogg N (2000) Biological chemistry and clinical potential of S-nitrosothiols. *Free Radical Biol Med,* **28**: 1478–86.

Hogg N (2002) The biochemistry and physiology of S-nitrosothiols. *Annu Rev Pharmacol Toxicol*, **42**: 585–600.

Hord NG, Tang Y and Bryan NS (2009) Food sources of nitrate and nitrites : the physiologic context for potential health benefits. *Am J Clin Nutr* **90**:1-9.

Huang K T, Han T H, Hyduke D R, Vaughn M W, Van Herle H, Hein T W, Zhang C, Kuo L, Liao J C(2001) *Proc Natl Acad Sci USA* **98**: 11771–11776.

Huang K.T, Han T.H, Hyduke D.R, Vaughn M.W, VanHerle H, Hein T.W, Zhang C.H, Kuo L, and Liao J.C (2001) Modulation of nitric oxide bioavailability by erythrocytes. *Proc.Natl.Acad.Sci.USA* **98**: 11771–11776.

Huang PL (2009) eNOS, metabolic syndrome and cardiovascular diseases. *Trends Endocrinol Metab* **20**: 295-302.

Hughes M. N (1999) Relationship between nitric oxide, nitroxyl ion, nitrosonium cation and peroxynitrite. *Biochim Biophys Acta*, **1411**: 263-272.

Ignarro L J, Byrns R E, Buga G M, Wood K S(1987) *Circ Res* **61**:866–879.
In vivo transfer of nitric oxide between a plasma protein-bound reservoir and low molecular weight thiols. Scharfstein, J.S, Keaney, J.F. Jr, Slivka, A, Welch, G.N, Vita, J.A, Stamler J.S Loscalzo, and J. *J. Clin. Invest* **1994**, *94*, 1432–1439.

Insights into regulatory, cytotoxic, and cytoprotective mechanisms of nitric oxide. Wink, D.A. and Mitchell, J.B. Chemical biology of nitric oxide: *Free Radic. Biol. Med* **1998**, *25*, 434–456.
Ishima, Y., Hiroyama, S., Kragh-Hansen, U., Maruyama, T., Sawa, T., Akaike,
Jacob C, Holme A.L and Fry F.H, (2004). The sulfinic acid switch in proteins. *Org. Biochem*. **2**:1953-1956.

Jacob L, Marc S.L and Peter S (2002) Modern analytical ultracentrifugation in protein science. *Protein Science,* **11**: 2067-2079.

Jaffrey SR, Erdjument-Bromage H, Ferris CD, Tempst P, Snyder SH (2001)
Jakubowski Henry (2013) Chemical reactivity of amino acid side chains. (College of St. Benedict / St. John's University) USA

Jan C.D, Patrick H.B, Brent B, Hiroshi Y, Ettore A, Lawrence E.S and Peter S, (2007) Studying multisite binary and ternary protein interactions by global analysis of

isothermal titration calorimetry data in SEDPHAT: Application to adaptor protein complexes in cell signaling. *Protein Science*, **16**: 30-42.

Jeffers A, Gladwin M.T, and Kim-Shapiro D.B (2006) Computation of plasma hemoglobin nitric oxide scavenging in hemolytic anemias, *Free Radic. Biol. Med*. **41**:1557–1565.

Jensen, Frank B (2009) The dual roles of red blood cells in tissue oxygen delivery: oxygen carriers and regulators of local blood flow. *Journal of Experimental Biology*. **212**:3387–3393.

Jia L, Bonaventura C, Bonaventura J, Stamler JS (1996) S-nitrosohaemoglobin: a dynamic activity of blood involved in vascular control. Nature. **380**: 221–226.

Jiri H (2008) Surface Plasmon Resonance Sensors for Detection of Chemical and Biological Species. *Chem. Rev*, **106**:462-493.

Jiri H, Sinclair S, and Gunter G (1999) Surface plasmon resonance sensors: review

Jon O. Lundberg, Eddie Weitzberg & Mark T. Gladwin (2008) Therapeutic opportunities for inorganic nitrite. *Nature Reviews Drug Discovery* **7**:156-167.

Joshi, M. S., Ferguson, T. B., Jr., Han, T. H., Hyduke, D. R., Liao, J. C., Rassaf, T., Bryan, N., Feelisch, M. & Lancaster, J. R., Jr. (2002) *Proc. Natl. Acad. Sci. USA* **99,** in press.

Jourd'heuil, D, Hallen. K, Feelisch. M and Grisham M.B (2000) Dynamic state of *S*-nitrosothiols in human plasma and whole blood. *Free Radic. Biol. Med **28*:**409–417.

Julian V, Xuecui G and Juergen k (2004) Identification of protein-protein interactions using *in vivo* cross-linking and mass spectrometry. *Proteomics*, **4**: 3845-3854.

Kai T, T. & Otagiri, M (2010). One-step preparation of S-nitrosated human

Kalyanaraman B (2004) Nitrated lipids: a class of cell –signaling molecules. *Proc Natl Acad Sci USA*, **101**: 11527-11528

Katsumi H, Nishikawa M, Yamsshita F and Hashida M (2004) Physicochemical tissue distribution and vasodilation characteristics of nitrosated serum albumin: delivery of nitric *in vivo*. *J Pharm Sci,* **93**: 2343-2352.

Kavdia M, Tsoukias N.M, and Popel A.S, (2002) Model of nitric oxide diffusion in an arteriole: impact of hemoglobin-based blood substi- tutes, *Am. J. Physiol. Heart Circ. Physiol*. **282:** H2245–H2253.

Kelm M (1999) Nitric oxide metabolism and breakdown. *Biochim Biophys Acta* **1411**:273-289.

Kelm M (1999) Nitric oxide metabolism and breakdown. *Biochom Biophys Acta* **1411**:273-289.

Kelm M, Dahmann R, Wink D, Feelisch F, (1997) The nitric oxide-superoxide assay: insight into the biological chemistry of O2 / NO-interaction. *J Bio. Chemistry.* **272**:9922-9932.

Kelm M, Feelisch T, Deussen A, Motz W, Strauer B.E, (1995) Role of nitric oxide in the regulation of coronary vascular tone in heart from hypertensive rate. **25** 186-193.

Kelm M, Schafer S, Dahmann R, Dolu B, Perings S, Decking U, Schrader J, Strauer B.E (1997) Nitric oxide induced contractile dysfunction of reduction is related to a reduction in myocardial energy generation C*ardiovasc Res.* **36**:185-193.

Kelm M, Schrader J, (1990) Control of coronary vascular tone by nitric oxide, *Cire. Res* **66**:1561-1575.

Kelm Malte, Feelich Martin, Krebber Thomas, Deuben Andreas, Motz Wolfgang, Strauer Bodo (1995) Role of nitric oxide in the regulation of coronary vascular tone in hearts from hypertensive rats. *Hyper jour* **25**:186-193.

Kevil CG, Kolluru GK, Pattillo CB and Giordano T (2011) Inorganic nitrite therapy: historical perspective and future directions. *Free Radic Bio Med* **51**:576-593.

Kharitonov V.G, Sundquist A.R, and Sharma V.S (1995) Kinetics of nitrosation of thiols by nitric oxide in the presence of oxygen. *J Biol Chem,* **270:** 28158-28164.

Kim P.S, O.Y Kwon O.Y, and Arvan P (1996) An endoplasmic reticulum storage disease causing congenital goiter with hypothyroidism. *Cell Biol J*, **133**: 517-527.

Kirsch M, Fuchs A and De Groot H (2003) Regiospecific nitrosation of N-terminal blocked tryptophan derivatives of N_2O_3 at physiological pH. *J Bio Chem*, **278**: 11931-11936.

Kirsch Michael, Lehnig Manfred, Korth Hans-Gert, sustmann Reiner and Groot Herbert (2001) Inhibition of proxynitrite-induced nitration of tyrosine by glutathione in the presence of carbon dioxide through both radical repair and peroxynitrite formation. *Chem.European* J, **7**: 3313-3320.

Kleinbongard P, Dejam A, Lauer T, Rassaf T, Schindler A, Picker O, Scheeren T, Godecke A, Schrader J, Schulz R, Heusch G, Schaub GA, Bryan NS, Feelish M and Kelm M (2003) Plasma nitrite reflects constitutive nitric oxide synthase activity in mammals. *Free Radic Bio Med* **35**: 790-796.

Kolberg.M, Bleifuss.G, Sjoberg.B.M, Graslund.A, Lubitz.W, Lendzian.F and Lassmann.G (2002) Generation and electron paramagnetic resonance spin trapping detection of thiyl radicals in model proteins and in the R1 subunit of E.coli ribonucleotide reductase. Arch Biochem Biophys, 397:57-68.

Koo E.H, Lansbury P.J, Kelly J.W (1999) Amyloid diseases: abnormal protein aggregation in neurodegeneration. *Proc. Natl. Acad. Sci. USA*, **96**: 9989-9990.

Kosaka H and Seiyama A (1997) *Nat. Med,* **3**:456-459.

Kwak. Y, Jones. K. A, Warner. D.O and Perkins. W. J (2006) Prolonged relaxation consistent with persistent soluble guanylyl cyclase activation in canine pulmonary artery following brief treatment with nitric oxide donors. Life Sci, 79:201-209.

Labeling strategy for site-specific identification of the *s*-nitrosoproteome. Chen Y.J, Ku W.C, Lin P.Y, Chou HC, Khoo K.H, and Chen Y.J. *J. Proteome Res* **2010**, *9*, 6417–6439.

Laemmli, (I 970) *Nature*, 227: 680-685.

Lancaster J.R (1994) Simulation of the diffusion and reaction of endogenously produced nitric oxide. *Proc. Natl Acad. Sci. USA* **91**:8137-8141

Lancaster JR (1994) Stimulation of the diffusion and reaction of endogeneous produced nitric oxide. *Proceedings of the National Academy of Science* USA **91**:8137-1841.

Leonard S. E, Reddie K. G and Carroll K. S. (2009) Mining the thiol proteome for sulfenic acid modifications reveals new targets for oxidation in cells. *ACS Chem. Biol*. **4**: 783–799.

Liao J C, Hein T W, Vaughn M W, Huang K T, Kuo L(1999) *Proc Natl Acad Sci USA* **96**:8757–8761

Liao J.C, Hein T.W, Vaughn M.W, Huang K.T, Kuo L (1999) Intravascular flow decreases erythrocyte consumption of nitric oxide. *Proc. Natl.Acad.Sci.USA* **96**:8757–8761.

Lipton SA (2006) *Nature* **441**:513 – 517.

Liu X, Miller M J, Joshi M S, Sadowska-Krowicka H, Clark D A, Lancaster J R Jr(1998) *J Biol Chem* **273**:18709–18713.

Liu X, Miller MJ, Joshi MS, Thomas DD and Lancaster JR (1998) Accelerated reaction of nitric oxide with oxygen within the hydrophobic interior of biological membranes. Proc Nat Aced Sci USA 95:2175-2179.

Liu X.P, Miller M.J.S, Joshi M.S, Sadowska-Krowicka H, Clark D.A and Lancaster J.R (1998) Diffusion-limited reaction of free nitric oxide with erythrocytes. **J.** *Biochem*. **273**:18709–18713.

Liu X.P, Samouilov A, Lancaster J.R and Zweier J.L (2002) Nitric oxide up take by erythrocytes is primarily limited by extracellular diffusion not membrane resistance. *J. Biochem*. **277**:26194–26199.

Lodish H, Arnold B, Lawrence S, Paul M, David B, and Darnell J (2000) Molecular Cell Biology. *New York 4th edition*, **pp** 1272.

Longford. E, Brown. A.S, Wainwright. R, De Belder. A, Thomas. M.R, Smith. R, Radomski. M.W, Martin. J and Moncada. S (1994) Inhibition of platelet activity by S-nitrosoglutathione during coronary angioplasty. Lancet, 344:1458-1460.

Luisa B. Maia and José J. G. Moura (2011) Nitrite reduction by xanthine oxidase family enzymes: a new class of nitrite reductase. Journal of Biological inorganic Chemistry, **16**: 443-460.

Lundberg JO, Weitzberg E, Cole JA and Benjamin N (2004) Nitrate, bacteria and human health. *Nat Rev Microbiol* **2**:593-602.

Lundberg JO, Weitzberg E, Gladwin MT (2008), The nitrate-nitrite-nitric oxide pathway in physiology and therapeutics. *Nat Rev Drug Discov* **7**:156–167.

Lundberg JO, Weitzberg. E and Gladwin MT (2008) The nitrate-nitrite-nitric oxide pathway In physiology and therapeutics. Nat Rev Drug Disco **7**:156 – 167.

Machha A and Schechter AN (2011) Dietary nitrite and nitrate: a review of potential mechanisms of cardiovascular benefits*. Eur J Nutr*.

Majmudar J and Martin B (2014) Strategies for profiling native S-nitrosylation. *Biopolymers* **2**: 173-179.

Manta Bruno, Hugo Martin, Denicola Ana, and Ortiz Cecilia (2008) The peroxidase and peroxynitrite reductase activity of human erythrocyte peroxiredoxin 2. *Biochem and Biophysics*, **2**: 146-154.

Mark T. Gladwin, Harold Raat, Sruti Shiva, Cameron Dezfulian, Neil Hogg, Daniel B. Kim-Shapiro, and Rakesh P. Patel (2006) Nitrite as a vascular endocrine nitric oxide reservoir that contributes to hypoxic signaling, cytoprotection and vasodilation. J Physiol Heart Circ

Marshall HE, Hess DT, Stamler JS (2004) *Proc Natl Acad Sci USA* **101**:8841–

Maton, Anthea; Jean Hopkins; Charles William McLaughlin; Susan Johnson; Maryanna Quon Warner; David LaHart; Jill D. Wright (1993). *Human Biology and Health*. Englewood Cliffs, New Jersey, USA: Prentice Hall. ISBN 0-13-981176-1.

McMahon TJ, Moon RE, Luschinger BP, Carraway MS, Stone AE, Stolp BW, Gow AJ, Pawloski JR, Watke P, Singel DJ, Piantadosi CA, Stamler JS (2002) Nitric oxide in the human respiratory cycle. *Nat Med*, **8**: 711–717.

Meigs JB, O'Donnell CJ, Tofler GH (2006) Hemostatic markers of endothelial dysfunction and risk of incident type 2 diabetes: the Framingham offspring study. *Diabetes*, **55**:530–7

Merril C. R, Goldman D, Sedman, S. A., and Ebert M. H (1981) *Science* **211:** 1437-1438.

Methodologies for the characterization, identification and quantification of *S*-nitrosylated proteins. Foster, M.W.. *Biochim. Biophys. Acta* **2011**, *1820*, 675–683.

Miersch.S and Mutus. B (2005) Protein s-nitosation: biochemistry and characterization of protein protein thiol –NO interactions as cellular signals. Clin Biochem: 38:777-791.

Mike P W and Michael J S (2010) Protein-protein interactions. *Biochem Society Transactions*, **4**: 875-878.

Millar TM, Stevens CR, Benjamin N, Eisenthal R, Harrison R and Blake DR (1998) Xanthine oxidoreductase catalyses the reduction of nitrates and nitrite to nitric oxide under hypoxic conditions. *FEBS Lett*, **427**:225-228.

Minghui G, Junyan Ji, and Fred E (2000) Signature-peptide approach to detecting proteins in complex mixtures. *Journal of Chromatography* A, **870**:295-313.

Misato K, Makiko Y, and Masayasu I (1996) Role of ascorbic acid in the metabolism of S-nitroso-glutathione. FEBS Letters **2**: 149-152.

Mitchell DA, Marletta MA, (2005) Thioredoxin catalyzes the S-nitrosation of the caspase-3 active site cysteine. *Nat Chem Biol* **1**: 154 –158.

Modin A, Bjorne H, Herulf M, Alving K, Weitzberg E, and Lundberg JO (2001) Nitrite-derived nitric oxide: a possible mediator of acidic-metabolic vasodilation. *Acta Physiol Scand* **171**:9-16.

Moncada S and Erusalimsky JD (2002) Does nitric oxide modulate mitochondrial energy generated and apoptosis? *Nat Rev Mol Cell Bio* **3**: 214-220

Moncada S and Higgs EA (2006) The discovery of nitric oxide and its role in vascular biology. Br. J Pharmacol **147**: S193-201.

Moncada S, Radomski M, and Palmer R, (2002) Endothelium-derived relaxing factor: Identification as nitric oxide and role in the control of vascular tone and platelet function. *Biochem Phar* **37**:2495-2501.

Moore RB, Mankad MV, Shriver SK, Mankad VN, Plishker GA (1991) *J Biol*
Murad F (1986) Cyclic guanosine monophosphate as a mediator of vasodilation. *Journal of Clinical Investigation* **78**:1-5.

Murshudov G.N, Vagin A.A, and Dodson E.J (1997). Refinement of macromolecular structures by the maximum-likelihood method. *Acta Crystallogr. D. Biol. Crystallogr.* **53**:240-255.
Nagababu E, MohantyJ J.G, Friedman J.S, and Rifkind J.M (2013) Role of peroxiredoxin-2 in protecting RBCs from hydrogen peroxide-induced oxidative stress. *Free Radical*, **47**: 164-171.

Nagababu E, Ramsamy S, Abernethy DR and Rifkind JM (2003) Active nitric oxide produced in red cell under hypoxic conditions by deoxyhaemoglobin-mediated nitrite reduction. *J Biol Chem* **278**:46349-46356.

Nat Cell Biol **3**:193 –197.

Neal G, Paschalis D, Margarita T, Karthik R and Harry I (2013) Regulation of protein function and signaling by reversible cysteine *S*-nitrosylation. *J Biol. Chem.* **37**:26473-460261.

Nedospasov A, Rafikov R, Beda N and Nudler R (2000) An autocatalytic mechanism of protein nitrosylation. *Proc Natl Aced Sci USA,* **97**: 13543-13548.

Nedospasov A, Rafikov R, Beda N, and Nudler E (2000) An autocatalytic mechanism of protein nitrosation. *Proc Natl Acad Sci USA*, **97**: 13543-13548.
Neurosci **3**:15 – 21.

Nitric oxide circulates in mammalian plasma primarily as an *S*-nitroso adduct of serum albumin. Stamler, J.S, Jaraki. O, Osborne. J, Simon. D.I, Keaney. J, Vita. J, Singel. D, Valeri. C.R, and Loscalzo. J. *Proc. Natl. Acad. Sci. USA* **1992**, **89**, 7674–7677.

Nitric oxide, superoxide, and peroxynitrite: The good, the bad, and ugly. Beckman, J.S, and Koppenol, W.H. *J. Physiol* **1996**, *271*, C1424–C1437.

Nitrosothiol reactivity profiling identifies *S*-nitrosylated proteins with unexpected stability. Paige J.S, Xu. G, Stancevic B, and Jaffrey S.R. *Chem. Biol* **2008**, *15*, 1307–1316.

Noble D.R and Williams D.L.H (2000) Structure-reactivity studies of the Cu2+ catalysed decomposition of four S-nitrosothiols based around the S-nitrosocystein /S-nitrosoglutathione structure*. Nitric Oxide*, **4**: 392-398.

Oae Shigeru, Kim Yong, Fukushima Daikichi and Shinhama, Koichi (1978) New syntheses of thionitrites and their chemical reactivities. J. Bio-Org Chem. **9** 913-917

Orie. N.N, Vallance. P, Jones. D.P and Moore. K.P (2005) S-nitrosoalbumin carriers a thiol-labile pool of nitric oxide, which causes vasodilation in the rat. Am JPhysiol Heart Circ Physiol, 289:H916-926.

Palmer R M, Ferrige A G, Moncada S(1987) *Nature (London)* **327**:524–52
Palmerini C.A, Saccardi C, Arienti G, and Palombari R (2002) Formation of nitrosothiols from gasous nitric oxide at pH 7.4. *J Biochem Mol Toxicol*, **16**: 135-139.

Pantoliano, M. W., *et al*.(2001) High-density miniaturized thermal shift assays as a general strategy for drug discovery. *J Biomol Screen*, **6**: 429-440.

Patel R.P, Hogg N, Spencer N.Y, Kalyanaraman B, Matalon S and Darley-Usmar V.M (1999) *J. Biol. Chem***. 274**: 15487-15492.

Patel RP, Hogg N, Spencer NY, Kalyanaraman B, Matalon S, Darley-Usmar VM, (1999) Biochemical characterization of human S-nitrosohemoglobin: effects on oxygen binding and and transnitrosation. *J Biol Chem* **274**:15487–15492.

Paula H, Stephan K and Edouard S.P (2012) Size-exclusion chromatography for the analysis of protein bio therapeutics and their aggregates. *Methods Mol Biol* **35**: 2923-2950.

Pawloski JR, Hess DT, Stamler JS (2001) Export by red blood cells of nitric oxide bioactivity. *Nature,* **409**: 622–626.

Phizicky E.M and Fields S (1995) Protein-protein interactions: methods for detection and analysis *Microbial Rev*, **59**: 94-123.

Prakash A Nemade and Raj Pardasani (2015) SVM model to predict Human death domain protein-protein interactions based on amino acid composition. **8**:14 -25.

Rassaf T, Flogel U, Drexhage C, Hendgen-Cotta U, Kelm M and Schrader J (2007) Nitrite reductase function of deoxymyoglobine: oxygen sensor and regulator of cardiac energetics and function. Cir Res **100**:1749-1754.

Rassaf T, Kleinbongard P, Preik M, Dejam A, Gharini P, Lauer T, (2002) Plasma nitrosothiols contribute to the systemic vasodilator effects of intravenously applied NO. *Circ Res*; 91:470– 7.

Reiter C.D, Wang X, J.E. Tanus-Santos J.E, Hogg N, Cannon R.O, Schechter A.N, Gladwin M.T (2002) Cell-free hemoglobin limits nitric oxide bioavailability in sickle-cell disease *Nat. Med*. **8**:1383 –1389.

Richardson RS, Leigh JS, Wagner PD and Noyszewski EA (1999) Cellular PO2 as a determinant of maximal mitochondrial oxygen consumption in trained human skeletal muscle. *J Appl Physiol* **87**:325-331.

Rossi R, Lusini L, Giannerini F, Giustarini D, Lungarella G, Di Simplicio P, (1997) A method to study kinetics of transnitrosation with nitrosoglutathione: reactions with hemoglobin and other thiols. *Anal Biochem* **254**: 215–220.

Rotem engelman, Pnina Weisman-shomer, Tamar Ziv, Jianqiang Xu, Elias S. J and Moran Benhar (2013) Multilevel Regulation of 2-Cys Peroxiredoxin Reaction Cycle by *S*-Nitrosylation. *J Biol Chem* **16**: 11312-1132

Samouilov, A. & Zweier, J. L. (1998). Development of chemiluminescence-based methods for specific quantitation of nitrosylated thiols. *Anal Biochem,* **258,** 322-30.

Saville B (1958) A scheme for the colorimentric determination of microgram amounts of thiols. *Analyst*, **83**: 670-672.

Schrammel. A, Grorren.A, Schmidt.K, Pfeiffer. S, and Mayer.B (2003) S-nitrosotion of glutathione by nitric oxide, peroxynitrite and NO /O2- free radical Bio Med, 34:1078-1088.

Scorza G, Pietraforte D, and Minetti, M (1997) Role of ascorbate and protein thiols in the release of nitric oxide from S-nitroso-albumin and S-nitroso-glutathione in human plasma Free Radical Biology & Medicine 4: 633-642

Seeley K.W, S.M. Stevens S.M, (2012) Investigation of local primary structure effects on peroxynitrite-mediated tyrosine nitration using targeted mass spectrometry, *J Proteomics.* **75**: 1691-700.

Sensors and Actuator B: chemical, **54**:3-15.

serum albumin with high biological activities. *Nitric Oxide,* **23:** 121-127.

Shishido S.M, Seabra A.B, Loh W and Ganzarolli De Oliveira M (2003) Thermal and photochemical nitric oxide release from S-nitrosothiols incorporated in Pluronic F127 gel: potential uses for local and controlled nitric oxide release. *Biomaterials*, **24**: 3543-3553.

Shiva S, Huang Z, Grubina R, Sun J, Ringwood LA, MacArthur PH, Xu X, Murphy E, Darley-Usmar VM and Gladwin MT (2007) Deoxymyoglobin is a nitrite reductase that generates nitric oxide and regulates mitochondrial respiration. *Circ Res* **100**:654-661.

Shiva S, Huang Z, Grubina R, Sun J, Ringwood LA, MacRrthur PH, Xu X, Murphy E, Darley-Usmar VM and Gladwin MT (2007) Deoxymyoglobin is a nitrite reductase that generate nitric oxide andregulates mitochondrial respiration. *Circ Res* **100**:654-5661.

Shiva S, Wang X, Rigwood LA, Xu X, Yaditskaya S, Annavajjhala V, Miyajima H, Hogg N, Harris ZL and Gladwin MT (2006) Ceruloplasin is a NO oxidase and nitrite synthase that determines endocrine NO homeostasis. *Nat Chem Biol* **2**:486-493.

Sies H (1991) Oxidative stress: from basic research to clinical application, *Am J. Med*. **91**:31S-38S.

Souza J.M, Daikhin E, Yudkoff M, Raman C.S, Ischiropoulos H, (1999) Factors determining the selectivity of protein tyrosine nitration. *Archives of Biochemistry* and *Biophysics.* **2**: 169-178.

Spiegelhalder B, Eisenbrand G and Preussmann R (1976) Influence of dietary nitrate on nitrite content of human saliva: possible relevance to in vivo formation of N-nitroso compounds. *Food Cosmet Toxicol* 1**4**:545-548.

Spiegelhalder B, Eisenbrand G and Preussmann R (1976) Influence of dietary nitrate on nitrite content of human saliva: possible relevance to in vivo formation of N-nitroso compounds. *Food Cosmet Toxically*, **14**: 545-548.

Ssu-Han, Shih-Jiuan Chiu, and The-Min Hu (2012) Superoxide Dismutatase as a Novel Macromolecular Nitric Oxide Carrier: Preparation and characterization. *J.Mol Sci*, **13**:13985-14001.

Stamler J.S, Jia L, Eu J.P, McMahon T.J, Demchenko I.T, Bonaventura J, Gernert K, and Piantadosi C.A (1997) *Science* **276**: 2034-2037.

Stamler Js (1994) Redox signalling: nitrosylation and related targets interactions of nitric oxide. *Cell* **78**:931-936.

Stamler JS, Jaraki O, Osborne J, Simon DI, Keaney J, Vita J (1992) Nitric oxide circulates in mammalian plasma primarily as an S-nitroso adduct of serum albumin. *Proc Natl Acad Sci USA*, **89**:7674– 7677.

Stamler JS, Simon DI, Osborne JA, Mullins ME, Jaraki O, Michel T, Singel DJ, Loscalzo J (1992) S-nitrosylation of proteins with nitric oxide: synthesis and characterization of biologically active compounds. *Proc Natl Acad Sci U S A*, **89**: 444–448.

Stamler JS, Singel DJ, Loscalzo J (1992). Biochemistry of nitric oxide and its redox activated forms. *Science*; **258**: 1898– 1902.

Stamler. J .S, Jaraki. O, Osborne. J, Simon. D. I, Keaney. J, Vita. J, Singel. D, Valeri. C. R and Loscalzo. J (1992a) Nitric oxide circulate in mammalian plasma primarily as an S-nitroso adduct of serum albumin Proc Natl Acad Sci USA, 89:7674-7677.

Stamler. J. S, Simon. D. I, Jaraki. O, Osborne. J. A, Francis. S, Mullins. M Singel. D and Loscalzo. J (1992b) S-nitosylation of tissue-type plasminogen-activator confers vasodilatory and antiplatelet properties on the enzyme. Proc *Natl Acad Sci USA*, **89**:8087-8091.

Stone,J.R., (2004) An assessment of proposed mechanisms for sensing hydrogen peroxide in mammalian systems. *Arch. Biochem. Biophys* **422**:119-124.

Structural profiling of endogenous *S*-nitrosocysteine residues reveals unique features that accommodate diverse mechanisms for protein *S*-nitrosylation. Doulias P.T, Greene, J.L, Greco T.M, Tenopoulou M. Seeholzer, S.H, Dunbrack R.L, and Ischiropoulos. H. *Proc. Natl. Acad. Sci. USA* **2010**, *107*, 16958–16963.

Stubauer G, Giuffre A and Sarti P (1999) Mechanism of S-nitrosothiol formation and degradation mediated by copper ions. *J. Biochem*, **274**: 28128-28133.

Stuehr DJ, Santolini J, Wang ZQ, Wei CC and Adak S (2004) Update on mechanism and catalytic regulation in the NO synthases. *J Bio Chem* **279**:36167-36170.

Swift H. R and William D. L. H (1997) Decomposition of S-nitrosothiols by mercury (II) and silver salts. *J. Chem. Soc., Perkin Trans*, **2**: 1933-1935.

Takahashi H, Shin Y, Cho SJ, Zago WM, Nakamura T, Gu Z, Ma Y, Furukawa

The SNO-proteome: Causation and classifications. Seth, D and Stamler J.S. *Curr. Opin. Chem. Biol* **2011**, *15*, 129–136.

Thomas P.J, Qu B.H, Pedersen P.L, (1995) Defective protein folding as a basis of human disease. *Trends Biochem. Sci*, **20**: 456-459.

Thomas, D.D, and Jourd'heuil D. (2012) *S*-nitrosation: Current concepts and new developments. *Antioxid. Redox. Signal*, **17**: 934–936.

Torres Filho I.P, Spiess B.D, Barbee R.W, Ward K.R, Oldenhof J, and Pittman R.N (2005) Systemic responses to hemodilution after transfusion with stored blood and with a hemoglobin-based oxygen carrier, *Anesth. Analg*. **100**: 912–920.

Tosatto S.C, Bosello F, Fogolari P, Mauri A, Roveri S, Toppo L, Flohe F, Ursini, and Maiorino M (2008) The catalytic site of glutathione peroxidases. *Antioxid. Redox. Signal*. **10**: 1515-1526.

Travis. M.D, Hoque A, Bates. J. N and Lewis. S. J (2000) Blocked of voltage sensitive Ca^{2+} - channels markedly diminishes nitric oxide – but not L-S-nitrosocysteine or endothelium dependent vasodilation *in vivo*. Eur J Pharmacol, **408**: 289-298.

Tullett J.M, Rees D.D, Shuker D.E.G and Gescher A (2001) Lack of correlation between the observed stability and pharmacological properties of S-nitroso derivatives of glutathione and cysteine-related peptides. *Biochem Pharmacol*, **62**: 1239-1247.

Uehara T, Nakamura T, Yao D, Shi ZQ, Gu Z, Ma Y, Masliah E, Nomura Y,
Van faasen EE, Bahrami S, Feelisch M, Hogg N, Kelm M, K-m-Shapiro DB, Kozlov AV, Li H, Lundberg JO, Mason R, Nohl H, Rassaf T, Samouilov A, Slama-Schwok A, Shiva S, Vanin AF, Weitzberg E, Zweier J, Gladwin MT (2009) Nitrite as regulator of hypoxic signaling in mammalian physiology. *Med Rev* **29**: 683-741.

Van Kessel et al. (2003) "2.4 Proteins – Natural Polyamides." Chemistry 12. Toronto: Nelson, p. 122.

Vanin A.F, Muller B, Alencer J.L, Lobysheva L, Nepveu F and Stoclet J.C (2002) Evidence that intrinsic iron but not intrinsic copper determines S-nitrosocysteine decomposition in buffer solution. *Nitric Oxide*, **7**: 194-209.

Vaughn M.W, Huang K.T, Kuo L and Liao J.C (2000) Erythrocytes possess an intrinsic barrier to nitric oxide consumption. *J. Biochem.* **275**:2342–2348.

Vaughn M.W, Huang K.T, Kuo L and Liao J.C, (2001) Erythrocyte consumption of nitric oxide: competition experiment and model analysis. *Nitric Oxide* **5**:18–31.

Vaughn M.W, Kuo L, and Liao J.C (1998) Effective diffusion distance of nitric oxide in the microcirculation. Am. *J.Physiol.HeartCirc.Physiol*. **43**: H1705–H1714.

Veves A, Akbari CM, and Primavera J (1998) Endothelial dysfunction and the expression of endothelial nitric oxide synthetase in diabetic neuropathy, vascular disease, and foot ulceration. *Diabetes* **47**:457–63.

Vivoli, M, Novak, H. R, Littlechild, J. A, Harmer, N. J (2014) Determination of Protein-ligand Interactions Using Differential Scanning Fluorimetry. *J. Vis. Exp.* **91**.

Wang P. G, Xian M, Tang X, Wu X, Wen Z, Cai T, Janczuk A (2002) Nitric oxide donors: chemical activities and biological applications. *Chem. Rev,* **102**: 1091-1134.

Wang. X, Tanus-Santos. J. E, Reiter. C. D, Dejam. A, Shiva. S, Smith. R. D, Hogg. N and Gladwin. M. T (2004) Biological activity of nitric oxide in the plasmatic compartment. Proc Natl Acad Sci USA, **101**: 11477-11482.

Well J.H, 2004. Amino Acids, Peptides, Proteins, Structures and Important Properties. General Biochemistry, sixth edition. New Age International Ltd, *New Delhi, India, pp*. 1–16.

Williams D.L.H (1996) S-nitrosothiols and role of metal ions in decomposition to nitric oxide. *Methods enzymol*, **268**: 299-308.

Williams D.L.H (1999) the chemistry of S-nitrosothiols. *Acc. Chem. Res*, **32**: 869-876.
Williams D.L.H (2004) Nitrosation reactions and the chemistry of nitric oxide, London UK, Elsevier.

Williams D.L.H (2004) Nitrosation reactions and the chemistry of nitric oxide. London, UK, Elsevier.

Winn MD, Ballard CC, Cowtan KD, Dodson EJ, Emsley P, Evans PR, Keegan RM, Krissinel EB, Leslie AG, McCoy A, McNicholas SJ, Murshudov GN, Pannu NS, Potterton EA, Powell HR, Read RJ, Vagin A and Wilson KS. (2011) Overview of the CCP4 suite and current developments. *Acta Crystallogr D Biol Crystallogr*. **67**: 235-242.

Wolzt M, MacAllister R. J, Davis D, Feelisch M, Moncada S, Vallance P and Hobbs A.J (1999) *J. Biol Chem*. **274:** 28983-28990.

Wolzt M, MacAllister RJ, Davis D, Feelisch M, Moncada S, Vallance P, Hobbs AJ (1999) Biochemical characterization of S-nitrosohemoglobin: mechanisms underlying synthesis, NO release and biological activity. *J Biol Chem*. **274**: 28983–28990.

Xiong L, Qiu D, Lauren A, Janelle C, Genevieve K Jianhua Z, Hui C, and Qun H (2008) A One-Step Homogeneous Immunoassay for Cancer Biomarker Detection Using Gold Nanoparticle Probes Coupled with Dynamic Light Scattering. *Journal of the American Chemical Society*, **130**: 2780-2782.

Yang, Y and Loscalzo, J (2005) S-nitrosoprotein formation and localization in endothelial cells. *Proc Natl Acad Sci USA*, **102**: 117-22.

Yao D, Gu Z, Nakamura T, Shi ZQ, Ma Y, Gaston B, Palmer LA, Rockenstein
Ying-Hao H, Sun-Uk K, Tae-Ho K, Dong-Seok L, Doo-Sang P, Eui-Jeon W, Sang Y, Bo Yeon, Sue G,(2012) Peroxiredoxin II is essential for preventing hemolytic anemia from oxidative stress through maintaining hemoglobin stability. Biochem and Biophysical Research, 3: 427-432.

Yonetani T, Tsuneshige A, Zhou Y, and Chen X (1998) *J. Biol. Chem* **273**: 20323-20333.

Ysart G, Miller P, Barrett G, Farrington D, Lawrance P, and Harrison N (1999) Dietary exposures to nitrate in the UK. *Food addit Cotam* **16**:521-532.

Ze-Young P and David H (2001) Identification of individual proteins in complex protein mixtures by high-resolution, high-mass-accuracy MALDI TOF-Mass Spectrometry analysis of In-solution thermal denaturation/enzymatic digestion. *Anal. Chem*. **73**: 2558-2564.

Zhang Y, Hogg N (2005) S-nitrosothiols: cellular formation and transport. *Free Radical Biol Med*, **38**: 831–8.

Zweier JL, Wang P, Samouilov A and Kuppusamy (1995) Enzyme-independent formation of nitric oxide in biological tissues. *Nat Med* **1**: 804-809.